Title
The SWI/SNF complex regulates splicing outcomes to determine cell fate in response to environmental cues in Saccharomyces cerevisiae

Author
Venkataramanan, Srivats

Publication Date
2017

Peer reviewed|Thesis/dissertation

UNIVERSITY OF CALIFORNIA

Los Angeles

The SWI/SNF complex regulates splicing outcomes to determine cell fate in response to environmental cues in *Saccharomyces cerevisiae*

A dissertation submitted in partial satisfaction

of the requirements for the degree Doctor of Philosophy

in Molecular, Cell and Developmental Biology

by

Srivats Venkataramanan

2017

ABSTRACT OF THE DISSERTATION

The SWI/SNF complex regulates splicing outcomes to determine cell fate in response to environmental cues in *Saccharomyces cerevisiae*.

by

Srivats Venkataramanan

Doctor of Philosophy in Molecular, Cell and Developmental Biology

University of California, Los Angeles, 2017

Professor Tracy L. Johnson, Chair

Despite its relatively streamlined genome, there are important examples of regulated RNA splicing in *Saccharomyces cerevisiae*. Here we show crucial roles for the chromatin remodeling complex SWI/SNF in splicing regulation in response to environmental changes. Nutrient-dependent downregulation of Snf2, the ATPase subunit of SWI/SNF, regulates downregulation of ribosomal protein genes (RPGs). RPGs are intron-enriched, and are highly transcribed. We show that their downregulation causes spliceosome redistribution from this abundant class of intron-containing RNAs to transcripts containing non-canonical splice-signals, which otherwise have poor affinity for the spliceosome.

Meiosis in *S. cerevisiae* is a response to prolonged starvation, involving regulated transcription and splicing of meiosis-specific transcripts. Splicing of a subset of these relies upon the meiosis-specific splicing activator Mer1. We find that SWI/SNF affects meiotic splicing in multiple ways. First, meiosis-specific downregulation of Snf2 leads to RPG

downregulation and spliceosome redistribution to Mer1-regulated transcripts. Secondly, Mer1 expression is SWI/SNF dependent—Snf2 is poised at the *MER1* promoter, and timing of Snf2 downregulation in relation to acetylation states of both itself and its target genomic loci allows coordination between these mechanisms. Hence, the SWI/SNF complex directs regulated meiotic splicing in *S. cerevisiae*. Furthermore, Snf2 itself is subject to precise regulation in response to cellular needs via several novel modes of RNA processing and regulation, as well as control of protein acetylation and turnover. This multi-level coordinated regulation orchestrates activity and targets of splicing programs as a cellular adaptive strategy in response to environmental stresses.

We also report roles for the SWI/SNF complex in respiration, partially via splicing regulation. Nutrient-dependent decrease in Snf2 leads to increase in *PTC7* splicing, due to RPG downregulation and spliceosome redistribution. The spliced *PTC7* transcript encodes a mitochondrial phosphatase regulator of Coenzyme Q_6 (CoQ_6) biosynthesis, a mitochondrial redox-active lipid essential for respiration, and increased *PTC7* splicing increases CoQ_6 levels. Contrastingly, the nonspliced *PTC7* isoform encodes a protein repressing CoQ_6 biosynthesis via as-yet-unknown mechanisms. These findings establish a novel role for SWI/SNF in the transition of yeast cells from fermentative to respiratory metabolism. Overall, the SWI/SNF complex regulates cellular stress responses by redirecting energy from translation to specialized splicing programs.

The dissertation of Srivats Venkataramanan is approved.

Douglas L. Black

Jeffrey A. Long

Tracy L. Johnson, Committee Chair

University of California, Los Angeles

2017

To my parents,

who set me upon the path;

and my wife,

who keeps me on it.

TABLE OF CONTENTS **PAGE**

LIST OF FIGURES **PAGE**

LIST OF TABLES **PAGE**

LIST OF SUPPLEMENTARY FIGURES **PAGE**

LIST OF ABBREVIATIONS

S. cerevisiae	*Saccharomyces cerevisiae*
DNA	deoxyribonucleic acid
RNA	ribonucleic acid
mRNA	messenger RNA
pre-mRNA	precursor mRNA
snRNA	small nuclear RNA
snRNP	small nuclear ribonucleoprotein
5'SS	5' splice site
BP	branch point
3'SS	3' splice site
ICG	intron-containing gene
RPG	ribosomal protein gene
ORF	open reading frame
uORF	upstream ORF
m^6A	N^6 - methyladenosine
SWI/SNF	SWItch/Sucrose Non-Fermentable
gDNA	genomic DNA
CoQ_6	Coenzyme Q_6

ACKNOWLEDGEMENTS

The corpus of work represented in this dissertation would not have been possible without the help of many people. First and foremost, I would like to thank my supervisor and mentor, Dr. Tracy Johnson. Her patience, encouragement and guidance have helped me become a better scientist. She has taught me the value of both unbridled enthusiasm as well as measured temperance, each in its own measure, each at its own time. Without her, none of the work in this dissertation would be possible, and for that, I am forever grateful. I would also like to thank the members of my committee, Dr. Douglas Black, Dr. Jeffrey Long, and Dr. Utpal Banerjee for their guidance and insightful discussions throughout the course of my time at UCLA. I would also like to extend my gratitude to all the faculty and staff, both at UCLA and UCSD for believing in me, and supporting me throughout my Ph.D.

I would be remiss if I failed to thank the members of the Johnson lab, past and present. Ever present for productive and insightful scientific conversation, patient with my various idiosyncrasies; they have been in equal measure fierce critics and staunch support. Their contributions have improved the science presented within this dissertation, as well as seen me through what has at times been a long and arduous process. Special mentions must go out to Azad, who mentored and guided me when I first joined the lab; Stephen for all the help with bioinformatics and being a patient teacher/sounding board and Anoop, for being the kind of undergraduate mentee most only dream of having the opportunity to interact with.

Chapters 5 and 6 of this dissertation are the result of a thoroughly enjoyable and extremely fruitful collaboration with the laboratory of Dr. Catherine Clarke. I would like to thank

all the members in the lab, and especially Agape Awad and Dr. Clarke herself for countless invaluable scientific discussions and the opportunity to work with them.

I would also like to extend my gratitude to Dr. Amander Clark, for providing me with a wonderfully enjoyable teaching opportunity, as well as for insightful discussions regarding the work in this dissertation.

As a graduate student, I have received financial support from the Philip J. Whitcome Graduate Fellowship from the Molecular Biology Interdepartmental Ph.D. Program at UCLA, as well as a UCLA Graduate Division Dissertation Year Fellowship. Funding from the National Institutes of Health Grant GM085474 to Tracy Johnson supported the research presented in this work.

The process of completing a Ph.D. is a long and arduous one. Along the way, I have been grateful for the support and friendship of many. My classmates at UCSD, a.k.a. 'The Honey Badgers', were the greatest group of friends anyone could ever ask for, and more help than they probably realize to a barely-out-of-college young man halfway across the world from any place he might reasonably call home. I am also immensely grateful to the community at UCLA, faculty, staff and students alike, for welcoming me warmly when I was a transplant, and for all their support through the years.

I would like to also thank my parents, Sriranjini V Ramanan and R Venkataramanan. They bore me, raised me, supported me, taught me, and loved me, through trials and tribulations. My debt to them can never truly be repaid.

Most importantly, I would like to thank my best friend, companion, and wife, Lauren Neves. She has constantly been my source of strength both within and outside the lab. We have

together laughed, cried, gorged ourselves, adventured, traveled and much more. This dissertation is as much her labor of love as mine.

Reprint of publications

- Neves, L. T., Douglass, S., Spreafico, R., Venkataramanan, S., Kress, T. L. and Johnson, T. L. (2017) 'The histone variant H2A.Z promotes efficient cotranscriptional splicing in S. cerevisiae', ***Genes & Development***, 31(7), pp. 702–717. doi: 10.1101/gad.295188.116.

  Chapter 2 is a reprint of this publication. I contributed to the bioinformatics work indicated in Figure 4. I am grateful to all of my co-authors and Cold Spring Harbor Lab Press for allowing me to include a reprint of this chapter.

- Venkataramanan, S., Douglass, S., Galivanche, A.R. & Johnson, T.L. "The chromatin remodeling complex SWI/SNF regulates splicing of meiotic transcripts in *S. cerevisiae."* ***Nucleic Acids Research***, 45 (13): 7708-7721, doi:10.1093/nar/gkx373.

  Chapter 3 is a reprint of this publication. I gratefully acknowledge all of the authors on this paper, and Oxford University Press for allowing me to include a reprint of this chapter.

- Awad, A.*, Venkataramanan, S.*, Nag, A., Galivanche, A.R., Bradley, M., Neves, L.T., Douglass, S., Clarke, C. & Johnson, T.L. "The SWI/SNF complex regulates Coenzyme

Q6 (CoQ6) synthesis and the metabolic shift to respiration in *Saccharomyces cerevisiae* via regulation of splicing." ***Journal of Biological Chemistry*****,** 292**,** 14851-14866. doi:10.1074/jbc.M117.798397.

* - indicates co-first authorship.

Chapter 5 is a reprint of this publication. I am grateful to Dr. Catherine Clarke for the opportunity to collaborate on this work, to all of the authors on this paper, and to the American Society for Biochemistry and Molecular Biology for allowing me to include a reprint of this chapter.

VITA

EDUCATION

2006-2011 ..... B. Tech/M.Tech in Biotechnology (minor in Chemistry);
Indian Institute of Technology Madras, Chennai, India.

PUBLICATIONS

- Venkataramanan, S., Douglass, S., Galivanche, A.R. & Johnson, T.L. (2017) "The chromatin remodeling complex SWI/SNF regulates splicing of meiotic transcripts in *S. cerevisiae."* ***Nucleic Acids Research***, 45 (13): 7708-7721, doi:10.1093/nar/gkx373.

- Neves, L. T., Douglass, S., Spreafico, R., Venkataramanan, S., Kress, T. L. and Johnson, T. L. (2017) "The histone variant H2A.Z promotes efficient cotranscriptional splicing in S. cerevisiae", ***Genes & Development***, 31(7), pp. 702–717. doi: 10.1101/gad.295188.116.

- Awad, A.*, Venkataramanan, S.*, Nag, A., Galivanche, A.R., Bradley, M., Neves, L.T., Douglass, S., Clarke, C. & Johnson, T.L. (2017) "The SWI/SNF complex regulates Coenzyme Q6 (CoQ6) synthesis and the metabolic shift to respiration in *Saccharomyces cerevisiae* via regulation of splicing." ***Journal of Biological Chemistry*****,** 292**,** 14851-14866. doi:10.1074/jbc.M117.798397.

  * indicates co-first authorship.

CONFERENCE TALKS

- **Molecular Biology Institute 2017 Annual Retreat and Research Conference:** "The SWI/SNF complex regulates splicing outcomes to determine cell fate in response to environmental cues."

- **Gordon Research Seminar 2016: Post-Transcriptional Gene Regulation:** "The SWI/SNF complex is a regulator of stress-responsive pre-mRNA splicing in *S. cerevisiae*."

- **Rustbelt RNA Meeting 2015:** "The SWI/SNF complex is a master regulator of meiotic splicing in *S. cerevisiae*."

- **Molecular Biology Institute 2015 Annual Retreat and Research Conference:** "The SWI/SNF complex is a master regulator for gametogenesis in *S. cerevisiae* via regulation of splicing."

- **Molecular Cell and Developmental Biology Annual Research Conference 2014:** "Regulation of splicing by chromatin remodeler Snf2 is important for *S. cerevisiae* entry into meiosis."

CONFERENCE POSTERS

- **Molecular Cell and Developmental Biology Annual Research Conference 2016** "The SWI/SNF complex regulates Coenzyme Q6 (CoQ6) synthesis and the metabolic shift to respiration in *Saccharomyces cerevisiae* via regulation of splicing."

- **Gordon Research Conference: Post-Transcriptional Gene Regulation** "The SWI/SNF complex is a master regulator for gametogenesis in *S. cerevisiae* via regulation of splicing."

- **Gordon Research Seminar: Post-Transcriptional Gene Regulation** "The SWI/SNF complex is a master regulator for gametogenesis in *S. cerevisiae* via regulation of splicing."

- **Molecular Biology Institute 2016 Annual Retreat and Research Conference** "The SWI/SNF complex is a key regulator of stress-responsive splicing modulation in S. cerevisiae."

- **American Society for Biochemistry and Molecular Biology 2016** "The SWI/SNF complex is a key regulator of stress-responsive splicing modulation in S. cerevisiae."

- **Molecular Cell and Developmental Biology Annual Research Conference 2015** "The SWI/SNF complex is a master regulator for gametogenesis in *S. cerevisiae* via regulation of splicing."

- **International Genetically Engineered Machine competition (iGEM) 2009** (Team IIT Madras): PLASMID - Plasmid Locking Assembly for Sustaining Multiple Inserted DNA.

- **Steenbock Symposium 2009 (University of Wisconsin, Madison)** "Understanding the mechanisms of Puf5p mediated translational repression in *S. cerevisiae."*

FELLOWSHIPS AND AWARDS

- **Dissertation Year Fellowship**, University of California, Los Angeles.

- **Whitcome Pre-doctoral Fellowship in Molecular Biology**, Molecular Biology Institute, University of California, Los Angeles.

- **Best Poster Award:** Molecular Biology Institute 2016 Annual Retreat and Research Conference.

- **Best Thematic Poster Award (Chromatin Structure and Transcription Regulation)**: American Society for Biochemistry and Molecular Biology 2016.

- **The Khorana Program for Scholars, 2009**; a joint initiative by The University of Wisconsin-Madison (UW), the Department of Biotechnology (DBT), the Government of India, and Indo-US Science and Technology Forum (IUSSTF).

- **GE Foundation Scholar-Leader Program scholarship** for India in 2009.

CHAPTER 1

Background – Splicing, chromatin and the SWI/SNF chromatin-remodeling complex.

A detailed view of spliceosome assembly and pre-mRNA splicing

Eukaryotic pre-mRNAs are transcribed by RNA polymerase II and often contain one or more intervening, non-coding regions, known as introns. During splicing, the introns are excised, and the exons are ligated together (Figure 1.1). While introns are generally poorly conserved, they are demarcated by specific sequences: the 5' splice site (5'SS), the branch point (BP), and the 3' splice site (3'SS). This process of pre-mRNA splicing is central to proper gene expression and is catalyzed by the spliceosome. This macromolecular assembly consists of five highly conserved small nuclear ribonucleoprotein complexes (snRNPs) that catalyze the two transesterification reactions (also referred to as the two steps) required for excising the intron, as well as two Mg^{2+} ions that stabilize the components. In the first step, the BP adenosine attacks the 5' SS, creating an intron lariat and releasing the 5' exon. The 5' exon then attacks the 3' SS in the second step, thereby releasing the intron and ligating the two exons. Among the further numerous accessory proteins are DExD/H-family proteins that perform ATP hydrolysis for accurate recognition of splicing signals and catalysis. Structural studies have confirmed that most of the proteins in the yeast spliceosome have a conserved counterpart in humans, although humans do have a variety of additional proteins (Fabrizio et al., 2009). The biochemical and genetic tractability of yeast, as well as its conservation with humans, render the yeast spliceosome an important resource for understanding its mechanistic activity during the splicing reaction. The conservation of the splicing machinery across eukaryotes means that conclusions drawn about the yeast spliceosome largely remain consistent across metazoan spliceosomes.

Removal of an intron and ligation of exons requires numerous step-wise interactions between the pre-mRNA, snRNPs, and other spliceosomal proteins. Dynamic interactions between the pre-mRNA and snRNPs are critical to splicing because they define the intron's

boundaries and catalyze the two necessary transesterification reactions. The spliceosome undergoes numerous rearrangements during the process of the splicing reaction to form a series of complexes that are given different names to distinguish them (Figure 1.2). First, the A complex forms when the U1 snRNP binds the intronic 5'SS and the U2 snRNP binds the intronic BP (forming the bulged branch helix) in a base-pairing dependent manner. U1 and U2 come in close proximity and bind the U4/U6.U5 tri-snRNP to form complex B, the fully assembled, yet catalytically-inactive, spliceosome. The B^{act} complex (the activated, but not catalytically competent, spliceosome) requires rearrangement of the snRNAs; U6 replaces U1 at the 5'SS, and the U4/U6 duplex unwinds, thereby releasing U1 and U4 from the spliceosome. Finally, the 5'SS and BP are brought within close proximity to form the B* complex, the catalytically competent spliceosome. At this point, two consecutive transesterification reactions can occur. In the first step, the 2' hydroxyl group of a BP adenosine attacks the phosphodiester bond between the last nucleotide of the exon and the first nucleotide of the 5'SS, thus forming the intron lariat and releasing the first exon, forming complex C. The catalytic center is then rearranged in a U5-dependent manner, bringing the 5' and 3' exons in close proximity, forming complex C*, and allowing the second step of splicing to occur. During the second step, the free 3' hydroxyl of exon 1 attacks the phosphodiester bond between the last nucleotide of the 3'SS and the first nucleotide of the downstream exon, leading to ligation of the two exons and removal of the intron lariat. The spliced RNA is released from the spliceosome to form the intron lariat spliceosome complex (Lapointe et al.). Finally, the spliceosome is disassembled from the excised intron lariat and the components are recycled, thus allowing more splicing reactions to occur.

The two transesterification reactions that make up pre-mRNA splicing are carried out via metal ion catalysis and rely on two Mg^{2+} ions in the catalytic core of the spliceosome

(Sontheimer et al., 1997). Precise arrangement of the snRNAs and Mg^{2+} ions is required to form the catalytic core, which then remains unchanged through the first and second steps of splicing (Galej et al., 2016, Fica et al., 2017). The snRNAs bring the 5'SS, BP, and 3'SS into close proximity and position the two Mg^{2+} ions (M1 and M2) that stabilize the necessary atoms of the pre-mRNA. M1 stabilizes the incoming nucleophile for each transesterification reaction (first step: the 2' hydroxyl of the BP bulge adenosine; second step: the 3'hydroxyl of the 5' exon's). M2 stabilizes the leaving group (first step: the 3' hydroxyl of the 5' exon; second step: 3' hydroxyl of the lariat) (Steitz and Steitz, 1993, Fica et al., 2014, Galej et al., 2016). A triplex formed by the U6 tertiary structure holds these Mg2+ ions in place. This framework within the catalytic core comprises of a U6 internal stem loop flanked by two antiparallel U2/U6 helices I and II. Helix I is interrupted by a two-residue bulge in the U2 snRNA, splitting it into helix Ia and Ib (Luukkonen and Seraphin, 1998a, Luukkonen and Seraphin, 1998b). In *S. cerevisiae*, residues 59-61 of the U6 snRNA form helix 1B and are immediately upstream of the U6 ISL. These residues form base triple interactions with two nucleotides of U2 upstream of helix Ia, and a single bulged uracil nucleotide in the U6 ISL, thereby forming the U6 triplex. In addition to the catalytic core, the branch helix and U5 stem loop I form important RNA components around the active site. The BP and U2 snRNA base pair to make the branch helix, which ensures the BP is in proximity to the catalytic core. Also, the sequence upstream of the U6 triplex nucleotides base pair to the 5'SS. The U5 stem loop I holds the region of the 5' exon just upstream of the 5'SS in place. The first step involves the formation of a 2'-5' ester linkage between the hydroxyl groups of the bulged base in the BP, and the first nucleotide of the intron. This linkage, as well as the free 3' hydroxyl of the last base of the upstream exon, are held in place immediately after branching, contributing to the reversibility of the splicing reaction (Tseng and Cheng, 2008,

Galej et al., 2016). The highly conserved Prp8 protein is an integral component of the U5 snRNP that has roles in both steps of splicing and is hypothesized to stabilize U5 connections with exons. In purified activated spliceosomes, Prp8 directly cross-links with U2, U5 and U6 snRNAs and pre-mRNA, placing it in position to bring the components of the active site together (Li et al., 2013).

Prp8 contains an RNase H-like (RH) domain, which has two conformations: the "closed" RH domain conformation promotes the first step of splicing, while second "open" conformation binds a single Mg+2 ion and promotes the second step (Galej et al., 2013, Schellenberg et al., 2013). Between the first and second transesterification steps, the RH domain is significantly reoriented, likely as a result of the action of the Prp16 DEAH-box helicase. Prp8 RH domain reorientation is closely tracked by that of the branch helix, which is initially stabilized by Cwc25 and Yju2 in its pre-first step configuration, and then by Prp17 and Cef1 in the pre-second step configuration (Fica et al., 2017, Galej et al., 2016). Complex rearrangements at the catalytic center are necessary for the second step and final release of the mRNA and spliceosome (Figure 1.3). These rearrangements require the activities of numerous proteins, including several DExH/D family helicases, the Nineteen Complex (NTC) and NTC-related proteins (NTR), and Prp8, the most conserved protein in the spliceosome (Grainger and Beggs, 2005). Briefly, the action of Prp16 rotates the branch helix away from the catalytic core, a motion that hinges around a single adenine base between helix Ia and the branch helix. This motion also clears Cwc25, Yju2 and Isy1 from the active site, allowing sequential binding of Slu7, Prp18 and DEAH-box helicase Prp22 which promotes movement of the U5 snRNP and entry of the 3'SS (Tseng et al., 2010, Fica et al., 2017). This rearrangement forms the C* complex in which the second step occurs rapidly in an ATP-independent manner (Mayas et al., 2006). Once the exons

are ligated, Prp22 (another DEAH-box helicase) releases the mRNA from the spliceosome in an ATP-dependent manner. Prp22 ejects the mRNA and disrupts the U5 snRNP interactions in the spliceosome, and the NTR complex is then recruited to the spliceosome (Wagner et al., 1998, Schwer and Gross, 1998, Aronova et al., 2007, Chen et al., 2012). Among other proteins, the NTR complex contains Prp43, a DEAH-box helicase that eventually disassembles the spliceosome and releases the lariat intron along with U2, U5 and U6 snRNAs from the spliceosome (Arenas and Abelson, 1997, Fourmann et al., 2013).

Regulated pre-mRNA splicing in *Saccharomyces cerevisiae.*

The process of pre-mRNA splicing serves to greatly expand the information encoded within the genome of eukaryotes. In addition to diversifying the proteome, pre-mRNA splicing provides an effective checkpoint for the regulation of gene expression. This regulation might be achieved through various mechanisms, such as the introduction of premature termination codons (PTCs) targeting the transcript for nonsense-mediated degradation, altering the stability and/or translation efficiency of transcripts via differential usage of UTRs.

In metazoans, the vast majority of pre-mRNAs contain multiple introns and are therefore subject to a variety of alternative splicing patterns such as cassette-exon inclusion or skipping, mutually exclusive exons, intron retention, and alternative 5' or 3' splice site choice (Pan et al., 2008, Wang et al., 2008). Multiple mechanisms that regulate alternative splicing and splice site choice have been demonstrated, including but not limited to splice site strength (consensus and accessibility), tissue or developmental stage specific trans-acting factors, differential recruitment of spliceosomal components by chromatin-associated adaptor proteins, and polymerase kinetics (Warf and Berglund, 2010, Allemand et al., 2008).

Although the components of the spliceosome and the mechanism of pre-mRNA splicing is conserved from yeast to humans, only ~300 of the ~6500 protein coding genes within the *Saccharomyces cerevisiae* genome are known to contain introns. Despite this relative paucity of introns within the yeast genome, intron-containing genes are extremely highly transcribed in yeast, and contribute to ~30% of all transcripts at any given time in a yeast cell (Manuel Ares et al., 1999, Warner, 1999). In addition, there are numerous examples of regulated alternative splicing in yeast, and these have been shown to be important for general cellular fitness as well as specialized processes such as meiotic differentiation (Venkataramanan et al., 2017, Johnson and Vilardell, 2012). Given the conservation of the process of pre-mRNA splicing, study of the diverse mechanisms and contexts of these regulated splicing events provide valuable insight towards understanding gene regulation across eukaryotes.

For example, the splicing of *YRA1* and *DBP2* transcripts in *S. cerevisiae* are autoregulated by their own respective gene products. *YRA1* encodes a component of the RNA export machinery that couples mRNA export and 3' end processing via its interactions with Mex67 and Pcf11 (Johnson et al., 2011). Yra1 inhibits the splicing of the *YRA1* pre-mRNA by enhancing the rapid export of the intron-retaining pre-mRNA prior to the first step of splicing, thus forming an autoregulatory negative feedback loop (Dong et al., 2007, Rodriguez-Navarro et al., 2002b). This autoregulation of *YRA1* splicing requires specific features of the transcript architecture: 1) a long 5' exon (285 nucleotides); 2) a large intron (776 nucleotides) and 3) a non-canonical BP sequence (GACUAAC – UACUAAC is canonical) (Dong et al., 2010, Dong et al., 2007, Preker and Guthrie, 2006). Deletion of the *YRA1* intron renders the cells temperature-sensitive, demonstrating the importance of splicing regulation in cell viability (Dong et al., 2007, Preker and Guthrie, 2006, Rodriguez-Navarro et al., 2002b). This is likely due to a

disruption of the negative feedback loop and an excess of Yra1 in the cell, which causes significant DNA damage, telomere instability and senescence like phenotype (Gavalda et al., 2016).

DBP2 encodes for a DEAD-box RNA helicase implicated in mRNA decay, suppression of transcription from cryptic initiation sites, as well as rRNA processing (Bond et al., 2001). The *DBP2* transcript contains the longest intron (1002 nucleotides) identified in yeast to date, and its splicing is negatively regulated by the Dbp2 protein in a manner reminiscent of *YRA1* (Barta and Iggo, 1995). However, the precise mechanism of Dbp2 mediated splicing regulation remains unknown. Dbp2 has been shown to function as a co-transcriptional RNA chaperone and promotes mRNP assembly, and it has been proposed that co-transcriptional action of Dbp2 on the *DBP2* intron could lead to premature termination or cleavage of the nascent transcript (Ma et al., 2013). Interestingly, Yra1 has been shown to interact with, and oppose the helicase activity of Dbp2 on nascent transcripts, thereby also helping guide the formation of mRNPs (Ma and Tran, 2015). The striking similarity between the regulatory mechanisms of *YRA1* and *DBP2*, which in turn function coordinately to guide co-transcriptional RNP assembly raises interesting questions regarding their co-evolution.

Besides autoregulatory loops such as the one described above, alternative splicing in *S. cerevisiae* has been shown to diversify the proteome. One such example is *SRC1,* which encodes an integral inner nuclear membrane protein that localizes to sub-telomeric genes (Grund et al., 2008, Rodriguez-Navarro et al., 2002a). *SRC1* contains a single intron with two alternative, overlapping 5' splice sites. Utilization of the downstream 5'SS results in the translation of a longer protein that spans the nuclear membrane twice, whereas splicing at the upstream 5′-splice site results in a truncated protein that spans the nuclear membrane only once and has

significantly reduced activity. It has been proposed that truncated *SRC1* has a unique cellular function, since it is specifically enriched in the G2 phase of the cell cycle in a Hub1 dependent manner (Mishra et al., 2011). However, as yet, no distinct function for the shorter form of Src1 has been identified.

There are other examples on productive alternative splicing in yeast, where alternatively spliced isoforms of a transcript produce different protein products with distinct functions. Recently, the *FES1* transcript was shown to undergo alternative splicing at its 3' end giving rise to two distinct proteins with different C-termini (Gowda et al., 2016). Fes1 is an Hsp70 nucleotide exchange factor that is essential for the ubiquitin-mediated degradation of chaperone associated mis-folded proteins. Competition between polyadenylation and splicing results in a dominant protein isoform (Fes1S) from the unspliced transcript, with the polyadenylation site within the putative intron; and a novel, less abundant protein isoform (Fes1L) from the spliced transcript (Gowda et al., 2016). Fes1L localizes to the nucleus, whereas Fes1S is largely cytoplasmic, consistent with the two protein isoforms having distinct functions (Gowda et al., 2016). While the exact biological role of Fes1L is as yet unknown (it is not required for misfolded protein degradation in the nucleus), the conservation of the intron amongst yeast species speaks to its functionality.

Another example of alternative splicing resulting in isoforms that localize to different cellular compartments is *PTC7.* The spliced *PTC7* transcript codes for a mitochondrial localized PP2C type phosphatase ($Ptc7_S$) that dephosporylates Coq7, and promotes Coenzyme Q_6 (CoQ_6) biosynthesis (Martin-Montalvo et al., 2013, Juneau et al., 2009). Retention of the intron of the *PTC7* transcript results in a longer isoform ($Ptc7_{NS}$) that localizes to the nuclear membrane due to a single transmembrane helix encoded for by the intron, and whose molecular function

remains unknown (Juneau et al., 2009). However, we recently demonstrated that $Ptc7_{NS}$ has a repressive effect of CoQ_6 biosynthesis (Awad et al., 2017).

While the generation of two protein isoforms from the *PTC7* transcript relies upon the intron not having a premature termination codon, most introns are in fact not conducive to read through translation. There are instances in which the regulation of splicing of such introns has been shown to be important for gene regulation and overall fitness in *S. cerevisiae.* The *SUS1* transcript encodes for a small protein component of both the SAGA and TREX complexes, thereby potentially coordinating transcription and nuclear export of RNA. The *SUS1* transcript is unusual amongst *S. cerevisiae* genes in that it contains two introns, the first of which possesses a non-consensus 5' SS (GUAUGA) and BP (UACUGAC). The first intron of *SUS1* is retained under stress conditions such as heat shock or nutrient stress. This intron-retained transcript retains the ability to produce a small, truncated peptide, and while no biological role for this peptide has yet been identified, recent results have suggested that regulation of *SUS1* splicing is critical for proper export of mRNA, as well as H2B ubiquitination (Hossain et al., 2011, Hossain et al., 2009).

More recently, it has been shown that inefficient splicing of the *GCR1* transcript leads to the production of a distinct Gcr1 protein isoform from the intron-retained transcript via a non-canonical translation initiation mechanism from within the intron. This Gcr1 isoform has a distinct N-terminus from the canonical protein (which is produced from the spliced *GCR1* transcript), and the combination of the two isoforms is required for systems-level control of glycolytic gene expression in *S. cerevisiae* (Hossain et al., 2016). *SUS1* and *GCR1* are examples of diversification of the yeast proteome via regulated intron-retention.

With these examples of alternative splicing regulation, it is clear that yeast have retained the ability to control gene expression through the removal of introns. This suggests that the genes containing introns may reveal important insights into splicing regulatory mechanisms and the pathways they control. In fact, the largest energy investment of the cell is disproportionately under the control of pre-mRNA splicing in yeast. Although yeast only possess ~300 introns, ~90 of them are within the ~130 annotated ribosomal protein genes (RPGs), the most highly expressed class of messages within the cell (Manuel Ares et al., 1999, Warner, 1999). Since most of what the yeast cell does at any point in time is translate new proteins, and most of the mRNA in the yeast cell encodes for RPGs, their regulation at the level of splicing is highly significant. Moreover, while *S. cerevisiae* has undergone a massive intron-loss event in its evolutionary history, the fact that the RPGs have retained their introns is unlikely to be random (Hooks et al., 2014). In fact, deletion of some RPG introns in yeast leads to decreased fitness or adaptation to environmental stress (Parenteau et al., 2011, Parenteau et al., 2008). It has recently been demonstrated that the architecture of RPGs is optimized for robust and efficient ribosome production (Reuveni et al., 2017). It therefore stands to reason that the preponderance of introns within RPGs also serves significant regulatory functions, perhaps via a variety of mechanisms.

An example of RPG regulation via a negative feedback loop at the level of splicing is *RPL30.* Excess Rpl30 protein binds to a stem loop structure within the *RPL30* pre-mRNA that includes the 5'SS, and inhibits its splicing (Macias et al., 2008). This stem loop strongly resembles the natural Rpl30 binding site in helix 34 of 25S rRNA (Vilardell et al., 2000). A newly translated Rpl30 peptide can therefore either bind to the precursor rRNA and promote ribosome biogenesis, or bind to its own transcript and repress its own synthesis. This provides an elegant mechanism of titration between the protein and RNA components of the ribosome based

on its relative affinities to the two RNA platforms. Notably, Rpl30 binding to its pre-mRNA still permits U1 recognition of the 5'SS, but blocks binding of the U2 snRNP, likely by disrupting an interaction between the U1 and U2 snRNPs (Bragulat et al., 2010).

A number of introns are found in RPGs with paralogs, and cross-regulation between paralogs is another important mechanism of splicing regulation amongst RPGs in yeast. For instance, Rps14 protein binds to a stem–loop structure in *RPS14B* pre-mRNA, inhibiting it's splicing and leading to its rapid degradation (Fewell and Woolford, 1999). Consistent with this, *RPS14B* transcripts are spliced very slowly and inefficiently whereas *RPS14A* behaves like most other RPG transcripts (Wallace and Beggs, 2017). Similar paralog dependent splicing inhibition has also been described for *RPS9A* (whose splicing is inhibited specifically by the protein product from *RPL9B*) and *RPL22B* (whose splicing is inhibited by Rpl22) (Petibon et al., 2016, Gabunilas and Chanfreau, 2016). While the purpose of these modes of regulation remain unknown, it is likely that they provide the yeast cell with a mechanism to modulate the transcription of RPGs and processing of rRNA to stoichiometric levels. It has also been suggested that paralog inhibition serves to buffer the fitness of the yeast cell from potential detrimental effects of integration of the paralog protein product (when they differ) into the ribosome, raising the intriguing possibility that the mechanisms described help regulate the specialization of ribosomes in response to specific conditions (Gabunilas and Chanfreau, 2016, Petibon et al., 2016).

The overwhelming enrichment of introns in a single functional class of co-regulated genes (RPGs) raises other intriguing possible mechanisms of splicing regulation. Since the spliceosome is a limiting component in the yeast cell, highly abundant intron-containing RPG transcripts serve as a sink for the spliceosome, sequestering them away from other, sub-optimal

introns (Munding et al., 2013). Downregulating the transcription of these RPGs therefore relieves the competition for the spliceosome and allows for the efficient splicing of other, otherwise poorly spliced pre-mRNAs. This trans-competition amongst pre-mRNAs within the yeast cell for the spliceosome has important regulatory implications, particularly in the splicing of meiotic transcripts in yeast. The downregulation of RPGs in response to nutrient deprivation that initiates the meiotic transcription program in yeast is critical for the efficient splicing of numerous meiotic ICGs. Consistent with this, meiotic ICGs that are vegetatively expressed remain unspliced (Munding et al., 2013).

Interestingly, the gene structure of RPGs in *S. cerevisiae* allows for their coordinate transcriptional regulation. The target of rapamycin complex I (TORC1) plays a key role in the co-regulation of RPGs (Loewith and Hall, 2011). Transcription of most RPGs requires the binding of general regulatory factor Repressor Activator Protein 1 (Rap1) to binding sites located between ~400 and ~200 bp upstream of the transcription start site (TSS) (Lascaris et al., 1999, Knight et al., 2014). Rap1 alters chromatin structure and recruits Forkhead Like transcription factor Fhl1 to the RPG promoters. Fhl1 has two co-factors; the co-activator Ifh1 and the co-repressor Crf1. Under favorable growth conditions, the activity of TOR retains Crf1 in the cytoplasm, allowing Fhl1 to recruit Ifh1 and activate RPG transcription. Under unfavorable growth conditions, Crf1 gets phosphorylated and relocalizes to the nucleus, displacing Ifh1 and associating with Fhl1 to repress RPG transcription (Martin et al., 2004). A recent ChIP-seq analysis in *S. cerevisiae* highlighted the involvement of HMG-like protein Hmo1 in transcription of about half of the RPGs, demonstrating that while RPGs are co-regulated, the intricacies of the mechanisms of regulation are not fully understood (Knight et al., 2014).

Furthermore, meiosis boasts the only developmental specific splicing factor identified in yeast to date, Mer1 (Engebrecht and Roeder, 1990, Spingola and Ares, 2000). Mer1 is expressed specifically during meiosis, at which time it activates the splicing of four Mer1-responsive introns (*MER2, MER3, SPO22* and *AMA1*), collectively called the Mer1 regulon (Munding et al., 2010). Mer1 enhances the splicing of these pre-mRNAs through its interaction with a conserved intronic enhancer sequence, and is critical for the progression of meiosis (Spingola and Ares, 2000). Meiosis is a critical program for the long-term survival of *S. cerevisiae* under conditions of nutrient deprivation, and its reliance on splicing regulation underlines the crucial nature of this gene regulatory process in yeast.

Co-transcriptional splicing and chromatin.

In vitro studies of splicing demonstrate that spliceosome assembly and the catalytic reactions of splicing are not absolutely dependent on transcription, yet there is now ample evidence that most splicing is at least initiated co-transcriptionally. In yeast, recognition of the 5' SS is co-transcriptional and BP recognition has been shown to be influenced by the state of the chromatin (Kotovic et al., 2003). Additionally, not only does spliceosome assembly take place co-transcriptionally, but also although most co-transcriptional splicing begins when the 3'SS clears the Pol II exit channel, catalysis is also completed very shortly thereafter (Carrillo Oesterreich et al., 2016, Wallace and Beggs, 2017). Furthermore, in mammalian systems, most splicing appears to be completed while the nascent RNA is still tethered to chromatin via RNA polymerase II (Pandya-Jones et al., 2013, Bhatt et al., 2012, Brody et al., 2011). Because the highly complex process of generating the catalytically active spliceosome, which involves numerous snRNP recruitment and rearrangement steps, occurs in such proximity to the

chromatin, there is ample potential for regulation by the chromatin environment and crosstalk between the processes of transcription and splicing.

The diverse mechanisms of co-transcriptional regulation of pre-mRNA splicing fall broadly under two non-mutually exclusive categories: recruitment and kinetics (reviewed in (Saldi et al., 2016)). In the first, a combination of the structure of the chromatin environment around a given gene, the transcription factors involved in the regulation of expression of the gene, and the CTD of the elongating RNA polymerase serves to recruit a cohort of RNA processing factors to the site of transcription. The specific splicing factors recruited and the relative affinities of recruitment of different splicing factors varies depending on the characteristics of the environment described above, resulting in differential splicing outcomes. The second model is one in which transcription exposes cis-regulatory sequences within the RNA at a certain rate, providing trans-effector factors a 'window of opportunity' to bind to the RNA and execute their function. An upstream regulatory 'event' (a combination of cis-element and trans-factor) therefore has a temporal advantage over a competing downstream one, the magnitude of which is determined by the rate at which the RNA is being transcribed. It is important to emphasize that the two models are inextricably linked, with the chromatin environment heavily influencing the rate of transcription, and vice versa.

Nucleosome positioning, composition and post-transcriptional marks on histones have all been shown to have profound effects on splicing outcomes. Nucleosomes are relatively enriched in exonic regions of the genome compared to introns (Schwartz et al., 2009, Tilgner et al., 2009). Further, exon-positioned nucleosomes are enriched for specific post-transcriptional histone modifications (H3K27me1, me2, and me3, H3K36me3, H3K79me1, H4K20me1) (Kolasinska-Zwierz et al., 2009, Andersson et al., 2009, Dhami et al., 2010, Spies et al., 2009, Huff et al.,

2010, Hon et al., 2009, Nahkuri et al., 2009); whereas intronic nucleosomes are enriched for other histone modifications (H2BK5me1, H2Bub1, H3K4me1, and me2, H3K9me1, H3K79me1, me2, and me3) (Dhami et al., 2010, Huff et al., 2010). While the roles of the majority of these histone modifications in splicing remain as yet unknown, and are the subject of active investigations, the interactions of several of them with the splicing machinery and the downstream splicing outcomes have been characterized. For instance, H3K4me3, which is enriched around transcription start sites, has been shown to recruit the U2 snRNP via interactions with readers such as Chd1 or Sgf29 and consequently, enhance splicing efficiency for promoter-proximal introns (Sims et al., 2007, Vermeulen et al., 2010, Luco et al., 2010, Shilatifard, 2008). Other examples include the association of histone H3 and H4 hyperacetylation with exon skipping, likely due to a decrease in the nucleosomal kinetic barrier upon acetylation and a corresponding increase in the rate of transcription (Zhou et al., 2011, Sharma et al., 2014, Bintu et al., 2012, Schor et al., 2009); and H3K36me3, which binds MRG15, which in turn recruits a splicing regulator PTB to chromatin (Luco et al., 2010); as well as several more (reviewed in (Saldi et al., 2016)).

Post-translational modifications on histones are not the only mechanism by which chromatin influences splicing. The landscape of chromatin is further expanded by the existence of variant histones such as H2A.Z, H3.3 and macroH2A. H3.3K36me is specifically recognized by the BS69 chromatin reader, which in turn physically interacts with the U5 snRNP, suggesting that histone variant might also have regulatory roles in splicing (Guo et al., 2014). We have demonstrated the role of one such variant, H2A.Z, in Chapter 2 of this dissertation (Neves et al., 2017). H2A.Z has also been shown to bind SF3B1, a component of the U2 snRNP, in mammals (Fujimoto et al., 2012).

In addition to the regulatory potential of histone modifications and variant histones, the nucleosome itself forms a major structural barrier to the elongating polymerase (although the energetic magnitude of the barrier depends on histone modifications) (Bintu et al., 2012). Recently, the importance of nucleosome positioning in regulating splicing outcomes has been demonstrated. Well-positioned nucleosomes caused increased pol II pausing near alternative exons that are preferentially included in certain breast-cancer cells (Iannone et al., 2015). Depletion of histones in colon carcinoma cells caused increased intron retention, likely due to elevated pol II transcription rates (Jimeno-Gonzalez et al., 2015). Furthermore, splice sites (both 5' and 3') are very strongly correlated with pause sites for RNA polymerase (as measured by NET-Seq), via an underlying mechanism that is as yet incompletely understood (Mayer et al., 2015, Nojima et al., 2015). However, these observations make amply clear that nucleosome positioning influences splicing outcomes.

How, then, are nucleosome positions upon the DNA template determined? While potential sequence determinants remain unknown, positioning of nucleosomes within chromatin is achieved largely via the help of chromatin-modifying enzymes. Chromatin modifying enzymes can influence splicing both by modifying the kinetic barriers to the polymerase and thereby altering transcription rates, as well as by acting as intermediaries in the recruitment model. The enzymes themselves are responsive to histone modifications. For instance, H2Bub1 cooperates with FACT and SWI/SNF to mobilize nucleosomes within genes at which it is enriched, promoting faster transcription (Fuchs et al., 2014, Pavri et al., 2006, Shema-Yaacoby et al., 2013). The SWI/SNF complex, which is detailed in the following sections, is also responsive to H3K9ac, a histone mark laid down by the histone acetyltransferase Gcn5 (Ruiz-Garcia et al., 1997, Dutta et al., 2014). Gcn5, and indeed H3 acetylation, has been demonstrated to be

important for the recruitment of the U2 snRNP, as well as rearrangements within the spliceosome (Gunderson et al., 2011, Gunderson and Johnson, 2009).

The SWI/SNF chromatin-remodeling complex

The archetype of chromatin modifying enzymes is the ATP-dependent SWI/SNF complex (Dutta et al., 2017). Originally identified in yeast in screens for mating type switching and sucrose fermentation, the SWI/SNF complex is a large, conserved, multi-subunit complex that is targeted to genomic loci by post-translational modifications (such as acetylation) on histone tails (Neigeborn and Carlson, 1984, Stern et al., 1984). ATP hydrolysis by the catalytic subunit (Snf2 in yeast) leads to disruption of the contacts between the histone core of the nucleosome and the DNA, resulting in either sliding of the nucleosome along the DNA strand, or complete eviction of the nucleosome, rendering the DNA strand accessible to transcription factors (Liu et al., 2017). The precise molecular mechanism of remodeling is still the subject of considerable investigation, and numerous potential models have been proposed (Kadoch et al., 2016, Liu et al., 2011, Liu et al., 2017).

While the overall architecture of the SWI/SNF complex is remarkably conserved across all eukaryotes, the subunit composition demonstrates increasing variability along an evolutionary timescale (Euskirchen et al., 2012, Tang et al., 2010). The interchangeable nature of the individual components of the complex leads to increased combinatorial complex polymorphism, diversity and specialization, allowing for tissue or developmental-stage specific response and regulation of chromatin (Kadoch and Crabtree, 2015). For instance, in yeast, the RSC complex is closely related to the canonical SWI/SNF complex and shares some auxiliary subunits such as the actin related proteins Arp7 and Arp9, but has a different ATPase subunit, Sth1 (Cairns et al.,

1996). In Drosophila, two distinct SWI/SNF complexes, BAP and PBAP share a common ATPase subunit, BRM/Brahma. In addition, they share numerous other core components, including some that are absent in yeast (Tang et al., 2010). In humans, the BAF complex has been found to contain either of two ATPases, BRG1 or hBRM in a context-dependent manner, whereas the PBAF complex only contains BRG1. There are over 100 distinct theoretical SWI/SNF complexes possible in humans by combinatorial subunit rearrangement, and many of them have been identified in specific tissue type and/or developmental contexts (Kadoch and Crabtree, 2015). For instance, embryonic stem (ES) cells contain a specialized SWI/SNF complex that includes BRG1 as the ATPase, BAF155 and BAF60A as auxiliary subunits, and a novel, specific subunit, BRD7 (Kaeser et al., 2008, Ho et al., 2009). SWI/SNF dependent transcriptional repression has been demonstrated to be crucial in regulating ES pluripotency (Zhang et al., 2014).

The remarkable diversity of SWI/SNF complexes renders them particularly susceptible to cell-type specific mutations, and in fact, greater than 20% of all human tumors show mutations in at least one member of a SWI/SNF complex (Biegel et al., 2014). For example, approximately 50% of ovarian carcinomas demonstrate inactivating mutations in a single allele of BAF250A (Swi1 in yeast) (Jones et al., 2010, Wiegand et al., 2010). The diversity of the complexes render them vulnerable targets for mutations causing malignancy (Helming et al., 2014). Often, combined complex dosage can partially compensate for individual mutations in cells, rendering them viable, but severely misregulated (Smith-Roe and Bultman, 2013). In addition, seemingly core mutations can manifest in a tissue-specific phenotype, as in the case of the ATPase subunit BRG1, which is mutated in >90% of all small cell ovarian cancers but in <5% of lung cancers (Ramos et al., 2014, Roberts et al., 2000, Smith-Roe and Bultman, 2013).

The susceptibility of SWI/SNF complexes to oncogenic mutations is at least in part due to its role in interacting with transcription factors in a dynamic, regulated and cell-type specific manner to regulate tissue specific transcription and therefore, cell fate. There are numerous described cases in which cellular transcriptional response to an environmental cue is dependent on SWI/SNF remodeling. For instance, SWI/SNF is specifically recruited to, and is required for expression of, muscle-specific genes by p38 dependent phosphorylation of BAF60, sometime after its enzymatic activation by MKK6 (Simone et al., 2004). Numerous surfaces within the SWI/SNF complex serve as interaction sites for hormone receptors, serving as specific and essential co-activators. The interaction of glucocorticoid receptor (GR) with a face made up of parts of BAF250, BAF60a and BAF57 is essential for activation of GR responsive genes. Vitamin D receptor (VDR) heterodimers bind with BAF60a to influence transcription, estrogen and androgen receptors incteract with BAF57, and so forth (Koszewski et al., 2003, Belandia et al., 2002, Link et al., 2005). The SWI/SNF complex has also been implicated in the control of cell cycle, specifically in the exit from G1 and S phase, in conjunction with Rb protein and histone deacetylases (Zhang et al., 2000). We recently showed that dynamic acetylation of a component of the SWI/SNF complex is crucial for meiosis in yeast (detailed in Chapter 3) (Venkataramanan et al., 2017). Interestingly, post-translational modifications of SWI/SNF have previously also been described in controlling the progression of mitosis in metazoan cells (Sif et al., 1998, Muchardt et al., 1996).

SWI/SNF complex in splicing

The SWI/SNF complex has previously been demonstrated to have effects on pre-mRNA splicing. Not only does the complex affect the rate of the polymerase by mobilizing nucleosomes

and thus affect the kinetics of splicing, it also directly interacts with splicing factors (Patrick et al., 2015, Waldholm et al., 2011, Yu et al., 2014, Batsche et al., 2006). Depletion of components of SWI/SNF complexes has been shown to alter patterns of splicing. Furthermore, although the effects of BRM on splicing correlates with altered polymerase pausing, these effects were demonstrated to be independent of its ATPase activity, and thus, its enzymatic role in chromatin remodeling (Batsche et al., 2006, Yu et al., 2014). It has been hypothesized that the role of BRM in splicing is via its incorporation onto nascent RNPs during transcription, and subsequent recruitment of splicing factors (Tyagi et al., 2009). Also, as previously mentioned, the SWI/SNF complex is responsive to histone modifications like H2Bub1 and H3K9ac that have previously been shown to influence spliceosome assembly and rearrangements, opening up the possibility that members of the complex could form a bridge between chromatin and the spliceosome.

In Chapters 3 and 5, we demonstrate a novel role for the SWI/SNF complex in determining splicing outcomes in yeast, via regulation of competition for the limiting spliceosome (Venkataramanan et al., 2017). The SWI/SNF complex directs cellular resources to specialized splicing programs in response to environmental stress, in order for the yeast cell to be able to adapt. It should be noted that, while this does not preclude other roles for SWI/SNF complexes in splicing, the role that we describe for Snf2 in reconfiguring the splicing landscape is well conserved over 20 million years of evolution and is likely to inform our understanding of the role of competition in splicing regulation across eukaryotes.

Acknowledgements

I would like to thank Dr. Erin Wissink for her help with the figures within this chapter.

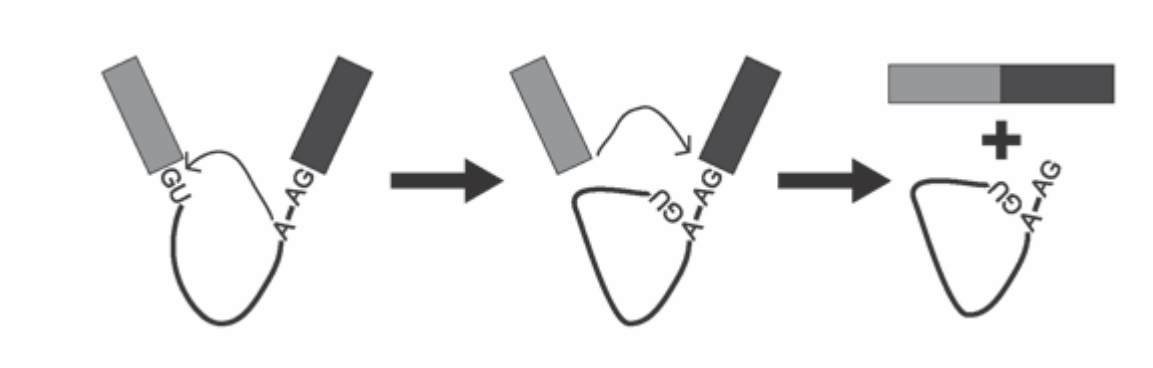

Figure 1.1. Two transesterification reactions. In the first step of splicing, the branchpoint adenosine (underlined here within the consensus BP sequence: UACUAAC) attacks the 5' splice site, forming an intron lariat. In the second step, the 5' exon's –OH attacks the 3' splice site, which fully removes the intron and ligates the exons together**.**

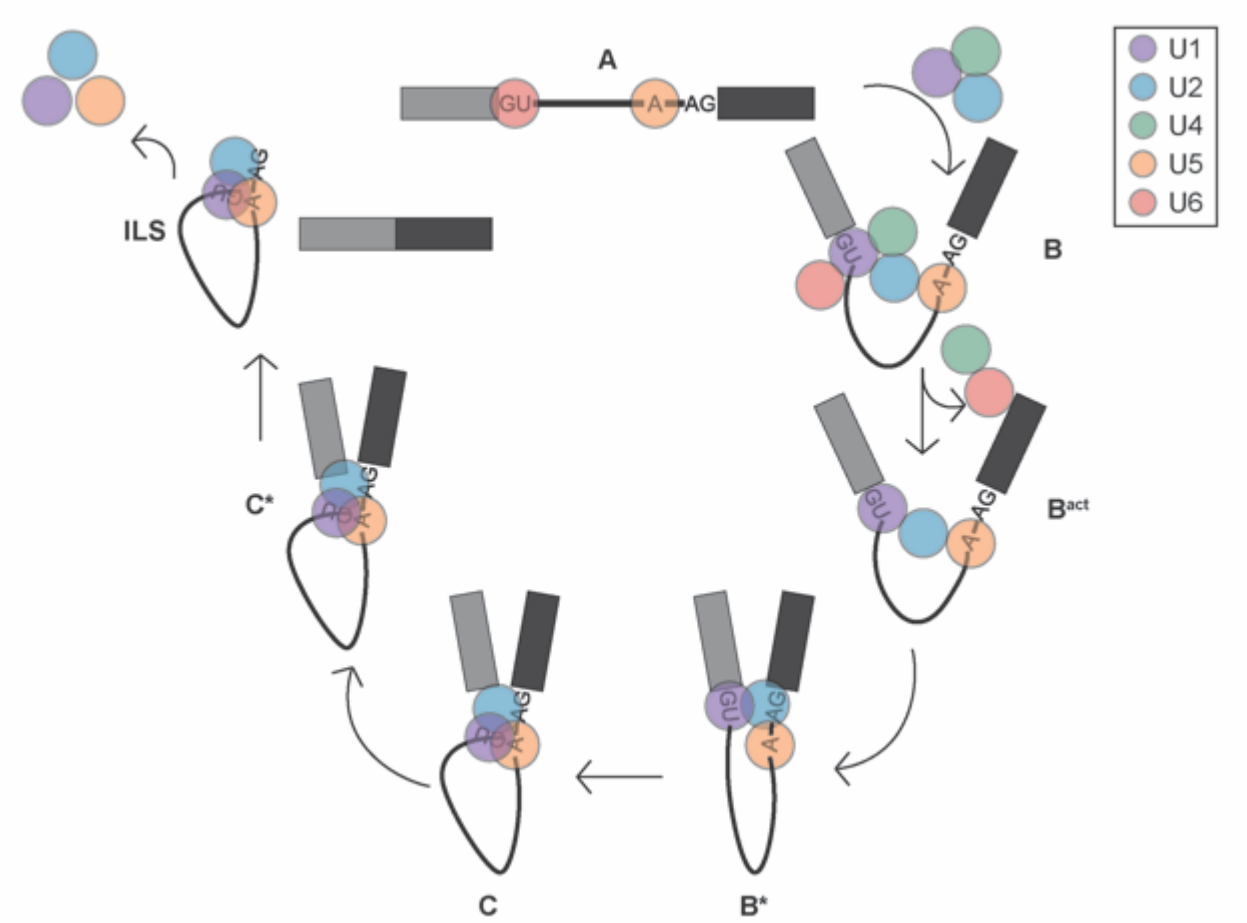

Figure 1.2. The role of snRNAs in splicing. U1 and U2 assemble co-transcriptionally by binding to the 5' SS and BP, respectively, forming the A complex. They recruit the tri-snRNP, forming the B complex. U1 and U4 then leave the spliceosome, and U6 replaces U1 at binding the 5' SS, forming the B^{act} complex. The B* complex has rearrangements that promote the first transesterification reaction (complex C). The C* complex then has rearrangements that promote the second transesterification reaction. The resulting products are the ligated exons and the ILS, from which the spliceosome is disassembled.

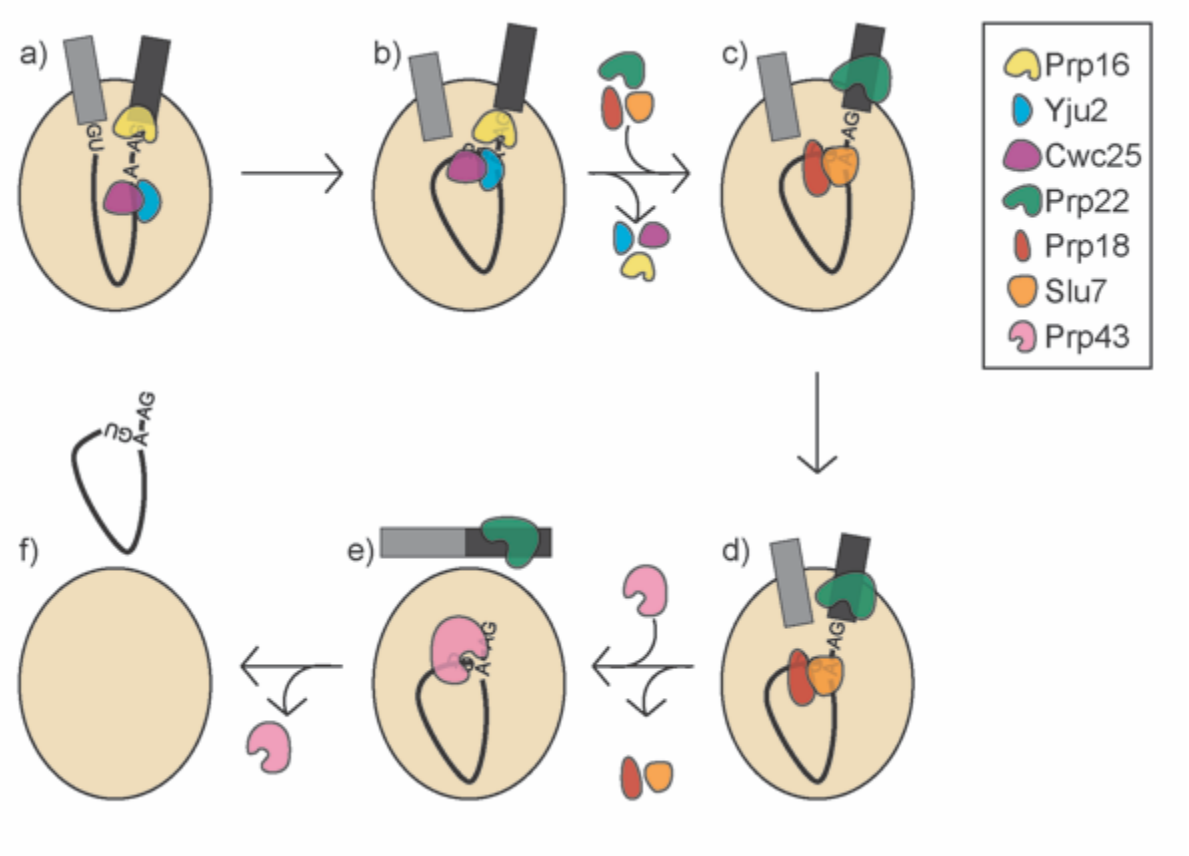

Figure 1.3. Protein re-arrangements at the spliceosome active site. Prp16, Yju2, and Cwc25 are present at the spliceosome before the first transesterification reaction (a). After the first step completes, Prp16 removes Yju2, Cwc25, and itself from the spliceosome (b). The second-step factors Prp22, Prp18, and Slu7 are then able to bind the spliceosome (c) and cause rearrangements that promote the second transesterification reaction (d). After the second step completes, Prp22 enables the ligated exons to vacate the spliceosome (e). Prp43 then catalyzes spliceosome disassembly (e, f).

References

Allemand, E., Batsche, E. & Muchardt, C. 2008. Splicing, transcription, and chromatin: a menage a trois. *Curr Opin Genet Dev,* 18**,** 145-51.

Andersson, R., Enroth, S., Rada-Iglesias, A., Wadelius, C. & Komorowski, J. 2009. Nucleosomes are well positioned in exons and carry characteristic histone modifications. *Genome Res,* 19**,** 1732-41.

Arenas, J. E. & Abelson, J. N. 1997. Prp43: An RNA helicase-like factor involved in spliceosome disassembly. *Proceedings of the National Academy of Sciences,* 94**,** 11798-11802.

Aronova, A., Bacikova, D., Crotti, L. B., Horowitz, D. S. & Schwer, B. 2007. Functional interactions between Prp8, Prp18, Slu7, and U5 snRNA during the second step of pre-mRNA splicing. *RNA,* 13**,** 1437-1444.

Awad, A. M., Venkataramanan, S., Nag, A., Galivanche, A. R., Bradley, M. C., Neves, L., Douglass, S., Clarke, C. F. & Johnson, T. L. 2017. Chromatin-remodeling SWI/SNF complex regulates coenzyme Q6 synthesis and a metabolic shift to respiration in yeast. *Journal of Biological Chemistry*.

Barta, I. & Iggo, R. 1995. Autoregulation of expression of the yeast Dbp2p 'DEAD-box' protein is mediated by sequences in the conserved DBP2 intron. *EMBO J,* 14**,** 3800-8.

Batsche, E., Yaniv, M. & Muchardt, C. 2006. The human SWI/SNF subunit Brm is a regulator of alternative splicing. *Nat Struct Mol Biol,* 13**,** 22-9.

Belandia, B., Orford, R. L., Hurst, H. C. & Parker, M. G. 2002. Targeting of SWI/SNF chromatin remodelling complexes to estrogen-responsive genes. *EMBO J.,* 21**,** 4094-4103.

Bhatt, D. M., Pandya-Jones, A., Tong, A. J., Barozzi, I., Lissner, M. M., Natoli, G., Black, D. L. & Smale, S. T. 2012. Transcript dynamics of proinflammatory genes revealed by sequence analysis of subcellular RNA fractions. *Cell,* 150**,** 279-90.

Biegel, J. A., Busse, T. M. & Weissman, B. E. 2014. SWI/SNF chromatin remodeling complexes and cancer. *Am. J. Med. Genet. C Semin. Med. Genet.,* 166C**,** 350-366.

Bintu, L., Ishibashi, T., Dangkulwanich, M., Wu, Y. Y., Lubkowska, L., Kashlev, M. & Bustamante, C. 2012. Nucleosomal elements that control the topography of the barrier to transcription. *Cell,* 151**,** 738-49.

Bond, A. T., Mangus, D. A., He, F. & Jacobson, A. 2001. Absence of Dbp2p alters both nonsense-mediated mRNA decay and rRNA processing. *Mol Cell Biol,* 21**,** 7366-79.

Bragulat, M., Meyer, M., Macias, S., Camats, M., Labrador, M. & Vilardell, J. 2010. RPL30 regulation of splicing reveals distinct roles for Cbp80 in U1 and U2 snRNP cotranscriptional recruitment. *RNA,* 16**,** 2033-41.

Brody, Y., Neufeld, N., Bieberstein, N., Causse, S. Z., Bohnlein, E. M., Neugebauer, K. M., Darzacq, X. & Shav-Tal, Y. 2011. The in vivo kinetics of RNA polymerase II elongation during co-transcriptional splicing. *PLoS Biol,* 9**,** e1000573.

Cairns, B. R., Lorch, Y., Li, Y., Zhang, M., Lacomis, L., Erdjument-Bromage, H., Tempst, P., Du, J., Laurent, B. & Kornberg, R. D. 1996. RSC, an essential, abundant chromatin-remodeling complex. *Cell,* 87**,** 1249-1260.

Carrillo Oesterreich, F., Herzel, L., Straube, K., Hujer, K., Howard, J. & Neugebauer, K. M. 2016. Splicing of Nascent RNA Coincides with Intron Exit from RNA Polymerase II. *Cell,* 165**,** 372-81.

Chen, H. C., Tseng, C. K., Tsai, R. T., Chung, C. S. & Cheng, S. C. 2012. Link of NTR-Mediated Spliceosome Disassembly with DEAH-Box ATPases Prp2, Prp16, and Prp22. *Molecular and Cellular Biology,* 33**,** 514-525.

Dhami, P., Saffrey, P., Bruce, A. W., Dillon, S. C., Chiang, K., Bonhoure, N., Koch, C. M., Bye, J., James, K., Foad, N. S., Ellis, P., Watkins, N. A., Ouwehand, W. H., Langford, C., Andrews, R. M., Dunham, I. & Vetrie, D. 2010. Complex exon-intron marking by histone modifications is not determined solely by nucleosome distribution. *PLoS One,* 5**,** e12339.

Dong, S., Jacobson, A. & He, F. 2010. Degradation of YRA1 Pre-mRNA in the cytoplasm requires translational repression, multiple modular intronic elements, Edc3p, and Mex67p. *PLoS Biol,* 8**,** e1000360.

Dong, S., Li, C., Zenklusen, D., Singer, R. H., Jacobson, A. & He, F. 2007. YRA1 autoregulation requires nuclear export and cytoplasmic Edc3p-mediated degradation of its pre-mRNA. *Mol Cell,* 25**,** 559-73.

Dutta, A., Gogol, M., Kim, J. H., Smolle, M., Venkatesh, S., Gilmore, J., Florens, L., Washburn, M. P. & Workman, J. L. 2014. Swi/Snf dynamics on stress-responsive genes is governed by competitive bromodomain interactions. *Genes Dev,* 28**,** 2314-30.

Dutta, A., Sardiu, M., Gogol, M., Gilmore, J., Zhang, D., Florens, L., Abmayr, S. M., Washburn, M. P. & Workman, J. L. 2017. Composition and Function of Mutant Swi/Snf Complexes. *Cell Rep,* 18**,** 2124-2134.

Engebrecht, J. & Roeder, G. S. 1990. MER1, a yeast gene required for chromosome pairing and genetic recombination, is induced in meiosis. *Mol Cell Biol,* 10**,** 2379-89.

Euskirchen, G., Auerbach, R. K. & Snyder, M. 2012. SWI/SNF Chromatin-remodeling Factors: Multiscale Analyses and Diverse Functions. *J. Biol. Chem.,* 287**,** 30897-30905.

Fabrizio, P., Dannenberg, J., Dube, P., Kastner, B., Stark, H., Urlaub, H. & Luhrmann, R. 2009. The evolutionarily conserved core design of the catalytic activation step of the yeast spliceosome. *Mol Cell,* 36**,** 593-608.

Fewell, S. W. & Woolford, J. L., Jr. 1999. Ribosomal protein S14 of Saccharomyces cerevisiae regulates its expression by binding to RPS14B pre-mRNA and to 18S rRNA. *Mol Cell Biol,* 19**,** 826-34.

Fica, S. M., Mefford, M. A., Piccirilli, J. A. & Staley, J. P. 2014. Evidence for a group II intron-like catalytic triplex in the spliceosome. *Nat Struct Mol Biol,* 21**,** 464-71.

Fica, S. M., Oubridge, C., Galej, W. P., Wilkinson, M. E., Bai, X. C., Newman, A. J. & Nagai, K. 2017. Structure of a spliceosome remodelled for exon ligation. *Nature*.

Fourmann, J. B., Schmitzova, J., Christian, H., Urlaub, H., Ficner, R., Boon, K. L., Fabrizio, P. & Luhrmann, R. 2013. Dissection of the factor requirements for spliceosome disassembly and the elucidation of its dissociation products using a purified splicing system. *Genes Dev,* 27**,** 413-28.

Fuchs, G., Hollander, D., Voichek, Y., Ast, G. & Oren, M. 2014. Cotranscriptional histone H2B monoubiquitylation is tightly coupled with RNA polymerase II elongation rate. *Genome Res,* 24**,** 1572-83.

Fujimoto, S., Seebart, C., Guastafierro, T., Prenni, J., Caiafa, P. & Zlatanova, J. 2012. Proteome analysis of protein partners to nucleosomes containing canonical H2A or the variant histones H2A.Z or H2A.X. *Biol Chem,* 393**,** 47-61.

Gabunilas, J. & Chanfreau, G. 2016. Splicing-Mediated Autoregulation Modulates Rpl22p Expression in Saccharomyces cerevisiae. *PLoS Genet,* 12**,** e1005999.

Galej, W. P., Oubridge, C., Newman, A. J. & Nagai, K. 2013. Crystal structure of Prp8 reveals active site cavity of the spliceosome. *Nature,* 493**,** 638-43.

Galej, W. P., Wilkinson, M. E., Fica, S. M., Oubridge, C., Newman, A. J. & Nagai, K. 2016. Cryo-EM structure of the spliceosome immediately after branching. *Nature,* 537**,** 197-201.

Gavalda, S., Santos-Pereira, J. M., Garcia-Rubio, M. L., Luna, R. & Aguilera, A. 2016. Excess of Yra1 RNA-Binding Factor Causes Transcription-Dependent Genome Instability, Replication Impairment and Telomere Shortening. *PLoS Genet,* 12**,** e1005966.

Gowda, N. K., Kaimal, J. M., Masser, A. E., Kang, W., Friedlander, M. R. & Andreasson, C. 2016. Cytosolic splice isoform of Hsp70 nucleotide exchange factor Fes1 is required for the degradation of misfolded proteins in yeast. *Mol Biol Cell,* 27**,** 1210-9.

Grainger, R. J. & Beggs, J. D. 2005. Prp8 protein: at the heart of the spliceosome. *RNA,* 11**,** 533-57.

Grund, S. E., Fischer, T., Cabal, G. G., Antunez, O., Perez-Ortin, J. E. & Hurt, E. 2008. The inner nuclear membrane protein Src1 associates with subtelomeric genes and alters their regulated gene expression. *J Cell Biol,* 182**,** 897-910.

Gunderson, F. Q. & Johnson, T. L. 2009. Acetylation by the transcriptional coactivator Gcn5 plays a novel role in co-transcriptional spliceosome assembly. *PLoS Genet,* 5**,** e1000682.

Gunderson, F. Q., Merkhofer, E. C. & Johnson, T. L. 2011. Dynamic histone acetylation is critical for cotranscriptional spliceosome assembly and spliceosomal rearrangements. *Proc Natl Acad Sci U S A,* 108**,** 2004-9.

Guo, R., Zheng, L., Park, J. W., Lv, R., Chen, H., Jiao, F., Xu, W., Mu, S., Wen, H., Qiu, J., Wang, Z., Yang, P., Wu, F., Hui, J., Fu, X., Shi, X., Shi, Y. G., Xing, Y., Lan, F. & Shi, Y. 2014. BS69/ZMYND11 reads and connects histone H3.3 lysine 36 trimethylation-decorated chromatin to regulated pre-mRNA processing. *Mol Cell,* 56**,** 298-310.

Helming, K. C., Wang, X. & Roberts, C. W. M. 2014. Vulnerabilities of mutant SWI/SNF complexes in cancer. *Cancer Cell,* 26**,** 309-317.

Ho, L., Ronan, J. L., Wu, J., Staahl, B. T., Chen, L., Kuo, A., Lessard, J., Nesvizhskii, A. I., Ranish, J. & Crabtree, G. R. 2009. An embryonic stem cell chromatin remodeling complex, esBAF, is essential for embryonic stem cell self-renewal and pluripotency. *Proc. Natl. Acad. Sci. U. S. A.,* 106**,** 5181-5186.

Hon, G., Wang, W. & Ren, B. 2009. Discovery and annotation of functional chromatin signatures in the human genome. *PLoS Comput Biol,* 5**,** e1000566.

Hooks, K. B., Delneri, D. & Griffiths-Jones, S. 2014. Intron evolution in Saccharomycetaceae. *Genome Biol Evol,* 6**,** 2543-56.

Hossain, M. A., Claggett, J. M., Edwards, S. R., Shi, A., Pennebaker, S. L., Cheng, M. Y., Hasty, J. & Johnson, T. L. 2016. Posttranscriptional Regulation of Gcr1 Expression and Activity Is Crucial for Metabolic Adjustment in Response to Glucose Availability. *Mol. Cell,* 62**,** 346-358.

Hossain, M. A., Claggett, J. M., Nguyen, T. & Johnson, T. L. 2009. The cap binding complex influences H2B ubiquitination by facilitating splicing of the SUS1 pre-mRNA. *RNA,* 15**,** 1515-27.

Hossain, M. A., Rodriguez, C. M. & Johnson, T. L. 2011. Key features of the two-intron Saccharomyces cerevisiae gene SUS1 contribute to its alternative splicing. *Nucleic Acids Res,* 39**,** 8612-27.

Huff, J. T., Plocik, A. M., Guthrie, C. & Yamamoto, K. R. 2010. Reciprocal intronic and exonic histone modification regions in humans. *Nat Struct Mol Biol,* 17**,** 1495-9.

Iannone, C., Pohl, A., Papasaikas, P., Soronellas, D., Vicent, G. P., Beato, M. & ValcaRcel, J. 2015. Relationship between nucleosome positioning and progesterone-induced alternative splicing in breast cancer cells. *RNA,* 21**,** 360-74.

Jimeno-Gonzalez, S., Payan-Bravo, L., Munoz-Cabello, A. M., Guijo, M., Gutierrez, G., Prado, F. & Reyes, J. C. 2015. Defective histone supply causes changes in RNA polymerase II

elongation rate and cotranscriptional pre-mRNA splicing. *Proc Natl Acad Sci U S A,* 112**,** 14840-5.

Johnson, S. A., Kim, H., Erickson, B. & Bentley, D. L. 2011. The export factor Yra1 modulates mRNA 3' end processing. *Nat Struct Mol Biol,* 18**,** 1164-71.

Johnson, T. L. & Vilardell, J. 2012. Regulated pre-mRNA splicing: the ghostwriter of the eukaryotic genome. *Biochim Biophys Acta,* 1819**,** 538-45.

Jones, S., Wang, T.-L., Shih, I.-M., Mao, T.-L., Nakayama, K., Roden, R., Glas, R., Slamon, D., Diaz, L. A., Jr., Vogelstein, B., Kinzler, K. W., Velculescu, V. E. & Papadopoulos, N. 2010. Frequent mutations of chromatin remodeling gene ARID1A in ovarian clear cell carcinoma. *Science,* 330**,** 228-231.

Juneau, K., Nislow, C. & Davis, R. W. 2009. Alternative splicing of PTC7 in Saccharomyces cerevisiae determines protein localization. *Genetics,* 183**,** 185-194.

Kadoch, C., Copeland, R. A. & Keilhack, H. 2016. PRC2 and SWI/SNF Chromatin Remodeling Complexes in Health and Disease. *Biochemistry,* 55**,** 1600-14.

Kadoch, C. & Crabtree, G. R. 2015. Mammalian SWI/SNF chromatin remodeling complexes and cancer: Mechanistic insights gained from human genomics. *Sci Adv,* 1**,** e1500447.

Kaeser, M. D., Aslanian, A., Dong, M.-Q., Yates, J. R., 3rd & Emerson, B. M. 2008. BRD7, a novel PBAF-specific SWI/SNF subunit, is required for target gene activation and repression in embryonic stem cells. *J. Biol. Chem.,* 283**,** 32254-32263.

Knight, B., Kubik, S., Ghosh, B., Bruzzone, M. J., Geertz, M., Martin, V., Denervaud, N., Jacquet, P., Ozkan, B., Rougemont, J., Maerkl, S. J., Naef, F. & Shore, D. 2014. Two distinct promoter architectures centered on dynamic nucleosomes control ribosomal protein gene transcription. *Genes Dev,* 28**,** 1695-709.

Kolasinska-Zwierz, P., Down, T., Latorre, I., Liu, T., Liu, X. S. & Ahringer, J. 2009. Differential chromatin marking of introns and expressed exons by H3K36me3. *Nat Genet,* 41**,** 376-81.

Koszewski, N. J., Henry, K. W., Lubert, E. J., Gravatte, H. & Noonan, D. J. 2003. Use of a modified yeast one-hybrid screen to identify BAF60a interactions with the Vitamin D receptor heterodimer. *J. Steroid Biochem. Mol. Biol.,* 87**,** 223-231.

Kotovic, K. M., Lockshon, D., Boric, L. & Neugebauer, K. M. 2003. Cotranscriptional Recruitment of the U1 snRNP to Intron-Containing Genes in Yeast. *Molecular and Cellular Biology,* 23**,** 5768-5779.

Lapointe, C. P., Stefely, J. A., Jochem, A., Hutchins, P. D., Wilson, G. M., Kwiecien, N. W., Coon, J. J., Wickens, M. & Pagliarini, D. J. 2017. Post-Transcriptional Control of Coenzyme Q Biosynthesis Revealed by Transomic Analysis of the RNA-Binding Protein Puf3p. *bioRxiv*.

Lascaris, R. F., Mager, W. H. & Planta, R. J. 1999. DNA-binding requirements of the yeast protein Rap1p as selected in silico from ribosomal protein gene promoter sequences. *Bioinformatics,* 15**,** 267-77.

Li, X., Zhang, W., Xu, T., Ramsey, J., Zhang, L., Hill, R., Hansen, K. C., Hesselberth, J. R. & Zhao, R. 2013. Comprehensive in vivo RNA-binding site analyses reveal a role of Prp8 in spliceosomal assembly. *Nucleic Acids Res,* 41**,** 3805-18.

Link, K. A., Burd, C. J., Williams, E., Marshall, T., Rosson, G., Henry, E., Weissman, B. & Knudsen, K. E. 2005. BAF57 governs androgen receptor action and androgen-dependent proliferation through SWI/SNF. *Mol Cell Biol,* 25**,** 2200-15.

Liu, N., Balliano, A. & Hayes, J. J. 2011. Mechanism(s) of SWI/SNF-induced nucleosome mobilization. *Chembiochem,* 12**,** 196-204.

Liu, X., Li, M., Xia, X., Li, X. & Chen, Z. 2017. Mechanism of chromatin remodelling revealed by the Snf2-nucleosome structure. *Nature,* 544**,** 440-445.

Loewith, R. & Hall, M. N. 2011. Target of rapamycin (TOR) in nutrient signaling and growth control. *Genetics,* 189**,** 1177-201.

Luco, R. F., Pan, Q., Tominaga, K., Blencowe, B. J., Pereira-Smith, O. M. & Misteli, T. 2010. Regulation of alternative splicing by histone modifications. *Science,* 327**,** 996-1000.

Luukkonen, B. G. & Seraphin, B. 1998a. Genetic interaction between U6 snRNA and the first intron nucleotide in Saccharomyces cerevisiae. *RNA,* 4**,** 167-80.

Luukkonen, B. G. & Seraphin, B. 1998b. A role for U2/U6 helix Ib in 5' splice site selection. *RNA,* 4**,** 915-27.

Ma, W. K., Cloutier, S. C. & Tran, E. J. 2013. The DEAD-box protein Dbp2 functions with the RNA-binding protein Yra1 to promote mRNP assembly. *J Mol Biol,* 425**,** 3824-38.

Ma, W. K. & Tran, E. J. 2015. Measuring helicase inhibition of the DEAD-box protein Dbp2 by Yra1. *Methods Mol Biol,* 1259**,** 183-97.

Macias, S., Bragulat, M., Tardiff, D. F. & Vilardell, J. 2008. L30 binds the nascent RPL30 transcript to repress U2 snRNP recruitment. *Mol Cell,* 30**,** 732-42.

Manuel Ares, J., Grate, L. & Pauling, M. H. 1999. An handful of intron-containing genes produces the lion's share of yeast mRNA. *RNA,* 5**,** 1138-1139.

Martin, D. E., Soulard, A. & Hall, M. N. 2004. TOR regulates ribosomal protein gene expression via PKA and the Forkhead transcription factor FHL1. *Cell,* 119**,** 969-79.

Martin-Montalvo, A., Gonzalez-Mariscal, I., Pomares-Viciana, T., Padilla-Lopez, S., Ballesteros, M., Vazquez-Fonseca, L., Gandolfo, P., Brautigan, D. L., Navas, P. & Santos-Ocana, C. 2013.

The phosphatase Ptc7 induces coenzyme Q biosynthesis by activating the hydroxylase Coq7 in yeast. *J Biol Chem,* 288**,** 28126-37.

Mayas, R. M., Maita, H. & Staley, J. P. 2006. Exon ligation is proofread by the DExD/H-box ATPase Prp22p. *Nature Structural & Molecular Biology,* 13**,** 482-490.

Mayer, A., Iulio, J. D., Maleri, S., Eser, U., Vierstra, J., Reynolds, A., Sandstrom, R., Stamatoyannopoulos, J. A. & Churchman, L. S. 2015. Native elongating transcript sequencing reveals human transcriptional activity at nucleotide resolution. *Cell,* 161**,** 541-554.

Mishra, S. K., Ammon, T., Popowicz, G. M., Krajewski, M., Nagel, R. J., Ares, M., Jr., Holak, T. A. & Jentsch, S. 2011. Role of the ubiquitin-like protein Hub1 in splice-site usage and alternative splicing. *Nature,* 474**,** 173-8.

Muchardt, C., Reyes, J. C., Bourachot, B., Leguoy, E. & Yaniv, M. 1996. The hbrm and BRG-1 proteins, components of the human SNF/SWI complex, are phosphorylated and excluded from the condensed chromosomes during mitosis. *EMBO J,* 15**,** 3394-402.

Munding, E. M., Igel, A. H., Shiue, L., Dorighi, K. M., Trevino, L. R. & Ares, M., Jr. 2010. Integration of a splicing regulatory network within the meiotic gene expression program of Saccharomyces cerevisiae. *Genes Dev,* 24**,** 2693-704.

Munding, E. M., Shiue, L., Katzman, S., Donohue, J. P. & Ares, M. 2013. Competition between Pre-mRNAs for the Splicing Machinery Drives Global Regulation of Splicing. *Mol. Cell,* 51**,** 338-348.

Nahkuri, S., Taft, R. J. & Mattick, J. S. 2009. Nucleosomes are preferentially positioned at exons in somatic and sperm cells. *Cell Cycle,* 8**,** 3420-4.

Neigeborn, L. & Carlson, M. 1984. Genes affecting the regulation of SUC2 gene expression by glucose repression in Saccharomyces cerevisiae. *Genetics,* 108**,** 845-58.

Neves, L. T., Douglass, S., Spreafico, R., Venkataramanan, S., Kress, T. L. & Johnson, T. L. 2017. The histone variant H2A.Z promotes efficient cotranscriptional splicing in S. cerevisiae. *Genes Dev.,* 31**,** 702-717.

Nojima, T., Gomes, T., Grosso, A. R., Kimura, H., Dye, M. J., Dhir, S., Carmo-Fonseca, M. & Proudfoot, N. J. 2015. Mammalian NET-Seq Reveals Genome-wide Nascent Transcription Coupled to RNA Processing. *Cell,* 161**,** 526-40.

Pan, Q., Shai, O., Lee, L. J., Frey, B. J. & Blencowe, B. J. 2008. Deep surveying of alternative splicing complexity in the human transcriptome by high-throughput sequencing. *Nat Genet,* 40**,** 1413-5.

Pandya-Jones, A., Bhatt, D. M., Lin, C. H., Tong, A. J., Smale, S. T. & Black, D. L. 2013. Splicing kinetics and transcript release from the chromatin compartment limit the rate of Lipid A-induced gene expression. *RNA,* 19**,** 811-27.

Parenteau, J., Durand, M., Morin, G., Gagnon, J., Lucier, J. F., Wellinger, R. J., Chabot, B. & Elela, S. A. 2011. Introns within ribosomal protein genes regulate the production and function of yeast ribosomes. *Cell,* 147**,** 320-31.

Parenteau, J., Durand, M., Veronneau, S., Lacombe, A. A., Morin, G., Guerin, V., Cecez, B., Gervais-Bird, J., Koh, C. S., Brunelle, D., Wellinger, R. J., Chabot, B. & Abou Elela, S. 2008. Deletion of many yeast introns reveals a minority of genes that require splicing for function. *Mol Biol Cell,* 19**,** 1932-41.

Patrick, K. L., Ryan, C. J., Xu, J., Lipp, J. J., Nissen, K. E., Roguev, A., Shales, M., Krogan, N. J. & Guthrie, C. 2015. Genetic interaction mapping reveals a role for the SWI/SNF nucleosome remodeler in spliceosome activation in fission yeast. *PLoS Genet,* 11**,** e1005074.

Pavri, R., Zhu, B., Li, G., Trojer, P., Mandal, S., Shilatifard, A. & Reinberg, D. 2006. Histone H2B monoubiquitination functions cooperatively with FACT to regulate elongation by RNA polymerase II. *Cell,* 125**,** 703-17.

Petibon, C., Parenteau, J., Catala, M. & Elela, S. A. 2016. Introns regulate the production of ribosomal proteins by modulating splicing of duplicated ribosomal protein genes. *Nucleic Acids Res,* 44**,** 3878-91.

Preker, P. J. & Guthrie, C. 2006. Autoregulation of the mRNA export factor Yra1p requires inefficient splicing of its pre-mRNA. *RNA,* 12**,** 994-1006.

Ramos, P., Karnezis, A. N., Craig, D. W., Sekulic, A., Russell, M. L., Hendricks, W. P. D., Corneveaux, J. J., Barrett, M. T., Shumansky, K., Yang, Y., Shah, S. P., Prentice, L. M., Marra, M. A., Kiefer, J., Zismann, V. L., McEachron, T. A., Salhia, B., Prat, J., D'Angelo, E., Clarke, B. A., Pressey, J. G., Farley, J. H., Anthony, S. P., Roden, R. B. S., Cunliffe, H. E., Huntsman, D. G. & Trent, J. M. 2014. Small cell carcinoma of the ovary, hypercalcemic type, displays frequent inactivating germline and somatic mutations in SMARCA4. *Nat. Genet.,* 46**,** 427-429.

Reuveni, S., Ehrenberg, M. & Paulsson, J. 2017. Ribosomes are optimized for autocatalytic production. *Nature,* 547**,** 293-297.

Roberts, C. W., Galusha, S. A., McMenamin, M. E., Fletcher, C. D. & Orkin, S. H. 2000. Haploinsufficiency of Snf5 (integrase interactor 1) predisposes to malignant rhabdoid tumors in mice. *Proc. Natl. Acad. Sci. U. S. A.,* 97**,** 13796-13800.

Rodriguez-Navarro, S., Igual, J. C. & Perez-Ortin, J. E. 2002a. SRC1: an intron-containing yeast gene involved in sister chromatid segregation. *Yeast,* 19**,** 43-54.

Rodriguez-Navarro, S., Strasser, K. & Hurt, E. 2002b. An intron in the YRA1 gene is required to control Yra1 protein expression and mRNA export in yeast. *EMBO Rep,* 3**,** 438-42.

Ruiz-Garcia, A. B., Sendra, R., Pamblanco, M. & Tordera, V. 1997. Gcn5p is involved in the acetylation of histone H3 in nucleosomes. *FEBS Lett,* 403**,** 186-90.

Saldi, T., Cortazar, M. A., Sheridan, R. M. & Bentley, D. L. 2016. Coupling of RNA Polymerase II Transcription Elongation with Pre-mRNA Splicing. *J Mol Biol,* 428**,** 2623-35.

Schellenberg, M. J., Wu, T., Ritchie, D. B., Fica, S., Staley, J. P., Atta, K. A., LaPointe, P. & MacMillan, A. M. 2013. A conformational switch in PRP8 mediates metal ion coordination that promotes pre-mRNA exon ligation. *Nat Struct Mol Biol,* 20**,** 728-34.

Schor, I. E., Rascovan, N., Pelisch, F., Allo, M. & Kornblihtt, A. R. 2009. Neuronal cell depolarization induces intragenic chromatin modifications affecting NCAM alternative splicing. *Proc Natl Acad Sci U S A,* 106**,** 4325-30.

Schwartz, S., Meshorer, E. & Ast, G. 2009. Chromatin organization marks exon-intron structure. *Nat Struct Mol Biol,* 16**,** 990-5.

Schwer, B. & Gross, C. 1998. Prp22, a DExH-box RNA helicase, plays two distinct roles in yeast pre-mRNA splicing. *The EMBO Journal,* 17**,** 9.

Sharma, A., Nguyen, H., Geng, C., Hinman, M. N., Luo, G. & Lou, H. 2014. Calcium-mediated histone modifications regulate alternative splicing in cardiomyocytes. *Proc Natl Acad Sci U S A,* 111**,** E4920-8.

Shema-Yaacoby, E., Nikolov, M., Haj-Yahya, M., Siman, P., Allemand, E., Yamaguchi, Y., Muchardt, C., Urlaub, H., Brik, A., Oren, M. & Fischle, W. 2013. Systematic identification of proteins binding to chromatin-embedded ubiquitylated H2B reveals recruitment of SWI/SNF to regulate transcription. *Cell Rep,* 4**,** 601-8.

Shilatifard, A. 2008. Molecular implementation and physiological roles for histone H3 lysine 4 (H3K4) methylation. *Curr Opin Cell Biol,* 20**,** 341-8.

Sif, S., Stukenberg, P. T., Kirschner, M. W. & Kingston, R. E. 1998. Mitotic inactivation of a human SWI/SNF chromatin remodeling complex. *Genes Dev,* 12**,** 2842-51.

Simone, C., Forcales, S. V., Hill, D. A., Imbalzano, A. N., Latella, L. & Puri, P. L. 2004. p38 pathway targets SWI-SNF chromatin-remodeling complex to muscle-specific loci. *Nat. Genet.,* 36**,** 738-743.

Sims, R. J., 3rd, Millhouse, S., Chen, C. F., Lewis, B. A., Erdjument-Bromage, H., Tempst, P., Manley, J. L. & Reinberg, D. 2007. Recognition of trimethylated histone H3 lysine 4 facilitates the recruitment of transcription postinitiation factors and pre-mRNA splicing. *Mol Cell,* 28**,** 665-76.

Smith-Roe, S. L. & Bultman, S. J. 2013. Combined gene dosage requirement for SWI/SNF catalytic subunits during early mammalian development. *Mamm. Genome,* 24**,** 21-29.

Sontheimer, E. J., Sun, S. & Piccirilli, J. A. 1997. Metal ion catalysis during splicing of premessenger RNA. *Nature,* 388**,** 801-5.

Spies, N., Nielsen, C. B., Padgett, R. A. & Burge, C. B. 2009. Biased chromatin signatures around polyadenylation sites and exons. *Mol Cell,* 36**,** 245-54.

Spingola, M. & Ares, M., Jr. 2000. A yeast intronic splicing enhancer and Nam8p are required for Mer1p-activated splicing. *Mol Cell,* 6**,** 329-38.

Steitz, T. A. & Steitz, J. A. 1993. A general two-metal-ion mechanism for catalytic RNA. *Proc Natl Acad Sci U S A,* 90**,** 6498-502.

Stern, M., Jensen, R. & Herskowitz, I. 1984. Five SWI genes are required for expression of the HO gene in yeast. *J Mol Biol,* 178**,** 853-68.

Tang, L., Nogales, E. & Ciferri, C. 2010. Structure and function of SWI/SNF chromatin remodeling complexes and mechanistic implications for transcription. *Prog. Biophys. Mol. Biol.,* 102**,** 122-128.

Tilgner, H., Nikolaou, C., Althammer, S., Sammeth, M., Beato, M., Valcarcel, J. & Guigo, R. 2009. Nucleosome positioning as a determinant of exon recognition. *Nat Struct Mol Biol,* 16**,** 996-1001.

Tseng, C.-K. & Cheng, S.-C. 2008. Both catalytic steps of nuclear pre-mRNA splicing are reversible. *Science,* 320**,** 1782-1784.

Tseng, C. K., Liu, H. L. & Cheng, S. C. 2010. DEAH-box ATPase Prp16 has dual roles in remodeling of the spliceosome in catalytic steps. *RNA,* 17**,** 145-154.

Tyagi, A., Ryme, J., Brodin, D., Ostlund Farrants, A. K. & Visa, N. 2009. SWI/SNF associates with nascent pre-mRNPs and regulates alternative pre-mRNA processing. *PLoS Genet,* 5**,** e1000470.

Venkataramanan, S., Douglass, S., Galivanche, A. R. & Johnson, T. L. 2017. The chromatin remodeling complex Swi/Snf regulates splicing of meiotic transcripts in Saccharomyces cerevisiae. *Nucleic Acids Research*.

Vermeulen, M., Eberl, H. C., Matarese, F., Marks, H., Denissov, S., Butter, F., Lee, K. K., Olsen, J. V., Hyman, A. A., Stunnenberg, H. G. & Mann, M. 2010. Quantitative interaction proteomics and genome-wide profiling of epigenetic histone marks and their readers. *Cell,* 142**,** 967-80.

Vilardell, J., Yu, S. J. & Warner, J. R. 2000. Multiple functions of an evolutionarily conserved RNA binding domain. *Mol Cell,* 5**,** 761-6.

Wagner, J. D. O., Jankowsky, E., Company, M., Pyle, A. M. & Abelson, J. 1998. The DEAH-box protein PRP22 is an ATPase that mediates ATP-dependent mRNA release from the spliceosome and unwinds RNA duplexes. *The EMBO Journal,* 17**,** 12.

Waldholm, J., Wang, Z., Brodin, D., Tyagi, A., Yu, S., Theopold, U., Farrants, A. K. & Visa, N. 2011. SWI/SNF regulates the alternative processing of a specific subset of pre-mRNAs in Drosophila melanogaster. *BMC Mol Biol,* 12**,** 46.

Wallace, E. W. J. & Beggs, J. D. 2017. Extremely fast and incredibly close: cotranscriptional splicing in budding yeast. *RNA,* 23**,** 601-610.

Wang, E. T., Sandberg, R., Luo, S., Khrebtukova, I., Zhang, L., Mayr, C., Kingsmore, S. F., Schroth, G. P. & Burge, C. B. 2008. Alternative isoform regulation in human tissue transcriptomes. *Nature,* 456**,** 470-6.

Warf, M. B. & Berglund, J. A. 2010. Role of RNA structure in regulating pre-mRNA splicing. *Trends Biochem Sci,* 35**,** 169-78.

Warner, J. R. 1999. The economics of ribosome biosynthesis in yeast. *Trends Biochem. Sci.,* 24**,** 437-440.

Wiegand, K. C., Shah, S. P., Al-Agha, O. M., Zhao, Y., Tse, K., Zeng, T., Senz, J., McConechy, M. K., Anglesio, M. S., Kalloger, S. E., Yang, W., Heravi-Moussavi, A., Giuliany, R., Chow, C., Fee, J., Zayed, A., Prentice, L., Melnyk, N., Turashvili, G., Delaney, A. D., Madore, J., Yip, S., McPherson, A. W., Ha, G., Bell, L., Fereday, S., Tam, A., Galletta, L., Tonin, P. N., Provencher, D., Miller, D., Jones, S. J. M., Moore, R. A., Morin, G. B., Oloumi, A., Boyd, N., Aparicio, S. A., Shih, I.-M., Mes-Masson, A.-M., Bowtell, D. D., Hirst, M., Gilks, B., Marra, M. A. & Huntsman, D. G. 2010. ARID1A mutations in endometriosis-associated ovarian carcinomas. *N. Engl. J. Med.,* 363**,** 1532-1543.

Yu, S., Waldholm, J., Bohm, S. & Visa, N. 2014. Brahma regulates a specific trans-splicing event at the mod(mdg4) locus of Drosophila melanogaster. *RNA Biol,* 11**,** 134-45.

Zhang, H. S., Gavin, M., Dahiya, A., Postigo, A. A., Ma, D., Luo, R. X., Harbour, J. W. & Dean, D. C. 2000. Exit from G1 and S phase of the cell cycle is regulated by repressor complexes containing HDAC-Rb-hSWI/SNF and Rb-hSWI/SNF. *Cell,* 101**,** 79-89.

Zhang, X., Li, B., Li, W., Ma, L., Zheng, D., Li, L., Yang, W., Chu, M., Chen, W., Mailman, R. B., Zhu, J., Fan, G., Archer, T. K. & Wang, Y. 2014. Transcriptional repression by the BRG1-SWI/SNF complex affects the pluripotency of human embryonic stem cells. *Stem Cell Reports,* 3**,** 460-474.

Zhou, H. L., Hinman, M. N., Barron, V. A., Geng, C., Zhou, G., Luo, G., Siegel, R. E. & Lou, H. 2011. Hu proteins regulate alternative splicing by inducing localized histone hyperacetylation in an RNA-dependent manner. *Proc Natl Acad Sci U S A,* 108**,** E627-35.

CHAPTER 2

The histone variant H2A.Z promotes efficient co-transcriptional splicing in *Saccharomyces cerevisiae.*

The histone variant H2A.Z promotes efficient cotranscriptional splicing in *S. cerevisiae*

Lauren T. Neves,[1,2] Stephen Douglass,[1] Roberto Spreafico,[3] Srivats Venkataramanan,[1] Tracy L. Kress,[4] and Tracy L. Johnson[1,5]

[1]Department of Molecular, Cell, and Developmental Biology, University of California at Los Angeles, Los Angeles, California, 90095 USA; [2]Graduate Program in Molecular Biology Interdepartmental Program, University of California at Los Angeles, Los Angeles, California 90095, USA; [3]Institute for Quantitative and Computational Biosciences, University of California at Los Angeles, Los Angeles, California 90095, USA; [4]Department of Biology, The College of New Jersey, Ewing, New Jersey 08628, USA; [5]Molecular Biology Institute, University of California at Los Angeles, Los Angeles, California 90095, USA

In eukaryotes, a dynamic ribonucleic protein machine known as the spliceosome catalyzes the removal of introns from premessenger RNA (pre-mRNA). Recent studies show the processes of RNA synthesis and RNA processing to be spatio–temporally coordinated, indicating that RNA splicing takes place in the context of chromatin. H2A.Z is a highly conserved histone variant of the canonical histone H2A. In *Saccharomyces cerevisiae*, H2A.Z is deposited into chromatin by the SWR-C complex, is found near the 5′ ends of protein-coding genes, and has been implicated in transcription regulation. Here we show that splicing of intron-containing genes in cells lacking H2A.Z is impaired, particularly under suboptimal splicing conditions. Cells lacking H2A.Z are especially dependent on a functional U2 snRNP (small nuclear RNA [snRNA] plus associated proteins), as H2A.Z shows extensive genetic interactions with U2 snRNP-associated proteins, and RNA sequencing (RNA-seq) reveals that introns with nonconsensus branch points are particularly sensitive to H2A.Z loss. Consistently, H2A.Z promotes efficient spliceosomal rearrangements involving the U2 snRNP, as H2A.Z loss results in persistent U2 snRNP association and decreased recruitment of downstream snRNPs to nascent RNA. H2A.Z impairs transcription elongation, suggesting that spliceosome rearrangements are tied to H2A.Z's role in elongation. Depletion of disassembly factor Prp43 suppresses H2A.Z-mediated splice defects, indicating that, in the absence of H2A.Z, stalled spliceosomes are disassembled, and unspliced RNAs are released. Together, these data demonstrate that H2A.Z is required for efficient pre-mRNA splicing and indicate a role for H2A.Z in coordinating the kinetics of transcription elongation and splicing.

[*Keywords*: H2A.Z; HTZ1; RNA processing; Swr1; budding yeast; chromatin; pre-mRNA splicing]

Supplemental material is available for this article.

Received December 19, 2016; revised version accepted March 27, 2017.

Eukaryotic genes are comprised of coding sequences (exons) interrupted by intervening sequences (introns). Introns are removed from the newly synthesized RNA by a large macromolecular machine known as the spliceosome. The spliceosome is a dynamic ribonucleoprotein complex made up of five highly structured small nuclear RNAs (snRNAs) and over a hundred associated proteins and catalyzes intron removal through a series of precisely coordinated rearrangements of its five snRNPs (snRNA plus associated proteins).

While RNA synthesis and RNA splicing have been traditionally analyzed as biochemically distinct reactions, many studies have demonstrated that these processes are spatially and temporally coordinated. There is ample evidence to show that the spliceosome recognizes splice sites within nascent premessenger RNA (pre-mRNA) while the RNA polymerase II (RNAPII) is actively transcribing the DNA template (Beyer and Osheim 1988, 1991; Bauren and Wieslander 1994; Bauren et al. 1996; Huang and Spector 1996; Maniatis and Reed 2002). Chromatin immunoprecipitation (ChIP) studies (in yeast and metazoans) show that spliceosome components are recruited to specific sequence signals (splice sites) in the pre-mRNA while still associated with the transcription complex (Kotovic et al. 2003; Gornemann et al. 2005; Lacadie and Rosbash 2005; Listerman et al. 2006).

Corresponding author: tljohnson@ucla.edu
Article is online at http://www.genesdev.org/cgi/doi/10.1101/gad.295188.116.

Recently, it has been shown that not only spliceosome recruitment but also catalysis and completion of splicing occur while the nascent RNA is associated with actively transcribing polymerase (Oesterreich et al. 2016). Support for temporal coordination of these two processes also comes from evidence showing that changes in transcription elongation rate can alter splicing efficiency and splice site selection (de la Mata et al. 2003; Howe et al. 2003; Fong et al. 2014; Oesterreich et al. 2016).

Due to the proximity of the splicing complex to the DNA synthesis machinery, splicing takes place within the context of not only transcription but also chromatin, the array of nucleosomes made up of DNA wrapped around eight histone proteins. Nucleosomes are well positioned within genes and have been found to occupy exons more frequently than introns (Schwartz et al. 2009; Amit et al. 2012), suggesting that nucleosomes help demarcate exons at the DNA level. Perturbations to chromatin organization have been linked to widespread changes in splicing, and post-translational modifications of individual histone proteins can influence splicing (for review, see Naftelberg et al. 2015). Particularly in budding yeast, monoubiquitylation of histone H2B and methylation of H3K36 by Set2 each promotes efficient splicing and is required for efficient cotranscriptional recruitment of splicing factors to the nascent mRNA (Moehle et al. 2012; Sorenson et al. 2016). Additionally, we showed that acetylation of H3 by Gcn5 is important for spliceosome assembly and downstream rearrangements (Gunderson and Johnson 2009; Gunderson et al. 2011).

In addition to the core histone proteins H2A, H2B, H3, and H4, a number of variant histones, such as H2A.Z, H3.3, and macroH2A, have also been characterized. A recent study identified a chromatin reader, BS69, that preferentially recognizes trimethylation of the histone variant H3.3 on Lys36 and physically interacts with the U5 snRNP (Guo et al. 2014), forming a physical link between the chromatin and the spliceosome, suggesting that both histones and histone variants may influence splicing. H2A.Z, encoded by *HTZ1* in *Saccharomyces cerevisiae*, is the only histone variant found across all eukaryotes. While H2A.Z and H2A share ~60% sequence similarity, H2A.Z is almost 90% conserved across species from yeast to humans (for review, see Zlatanova and Thakar 2008), suggesting that the variant carries out an important and conserved function in the cell, distinct from H2A. Unlike the four canonical histones, which are incorporated into chromatin at the time of DNA replication, H2A.Z can be inserted throughout the cell cycle (for review, see Zlatanova and Thakar 2008). The SWR-C remodeling complex catalyzes the displacement of the H2A/H2B dimer in the chromatin in exchange for an H2A.Z/H2B dimer. SWR-C recognizes the nucleosome-free region (NFR) surrounding the transcription start site (TSS) of genes and deposits H2A.Z in nucleosomes flanking the NFR (Ranjan et al. 2013). H2A.Z is well positioned in the chromatin as, although it is found in only 5% of nucleosomes, it is present in ~65% of all *S. cerevisiae* genes, typically at the +1 and −1 nucleosomes around the TSS (Guillemette et al. 2005; Raisner et al. 2005).

H2A.Z has been shown to play an important role in the regulation of transcription initiation and gene expression (Subramanian et al. 2015). In yeast, H2A.Z interacts genetically with a number of transcription factors (TFs) (Wan et al. 2009), and, in mammals, H2A.Z is necessary for recruitment of pioneer TFs (Li et al. 2012). In vitro experiments demonstrate that H2A.Z is less stably associated with DNA and therefore is more susceptible to release from the chromatin (Zhang et al. 2005). As the +1 nucleosome poses a transcriptional barrier to RNAPII, H2A.Z may promote transcription initiation by decreasing the nucleosome barrier and promoting RNAPII progression (Zhang et al. 2005; Weber et al. 2014). Studies in yeast also indicate a role in the regulation of transcription elongation, as H2A.Z genetically interacts with elongation factors Spt5 and Dst1 (Malagon et al. 2004; Santisteban et al. 2011). Moreover, H2A.Z has been found to promote transcription elongation in both yeast and mammalian cells (Santisteban et al. 2011; Rudnizky et al. 2016).

Based on the connections between transcription and pre-mRNA splicing as well as H2A.Z's role in transcriptional regulation, we performed genetic analysis of interactions between *HTZ1* and genes encoding nonessential splicing factors and showed that when any major component of the spliceosome, particularly the U2 snRNP, is compromised, the cell becomes dependent on the presence of H2A.Z. Furthermore, H2A.Z is required for efficient splicing of a subset of intron-containing genes (ICGs). This pool of genes is enriched in introns containing a branch point (BP) sequence that deviates from the highly conserved consensus sequence. Interestingly, although H2A.Z is found primarily in close proximity to the TSS, we observed H2A.Z enrichment near the BP of many ICGs. When H2A.Z is deleted, proper spliceosome rearrangements are compromised, and this is coincident with altered RNA polymerase elongation that occurs in the absence of H2A.Z. Depletion of the spliceosome disassembly factor Prp43 in cells lacking H2A.Z enhances splicing of introns, particularly of introns with nonconsensus BP sequences. These results reveal an important role for the highly conserved H2A.Z histone variant in coordinating elongation with spliceosome assembly.

Results

Cells with mutant spliceosomes are dependent on H2A.Z

In order to characterize interactions between H2A.Z and genes encoding factors involved in splicing, a targeted genetic screen was performed to identify interactions between *htz1*Δ and null alleles of nonessential splicing factors. Deletion of the genes encoding the U2 snRNP factors Msl1, Lea1, or Snu17 combined with deletion of *HTZ1* confers synthetic lethality (Fig. 1A). Msl1 and Lea1 are yeast homologs of the human proteins U2A′/B″ and bind a conserved stem–loop in the U2 snRNA (Tang et al. 1996). Snu17, which has been shown to associate with the U2 snRNP, is required for the release of the U1 snRNP after the addition of the U4/U6.U5 tri-snRNP and progression through the first catalytic step of splicing

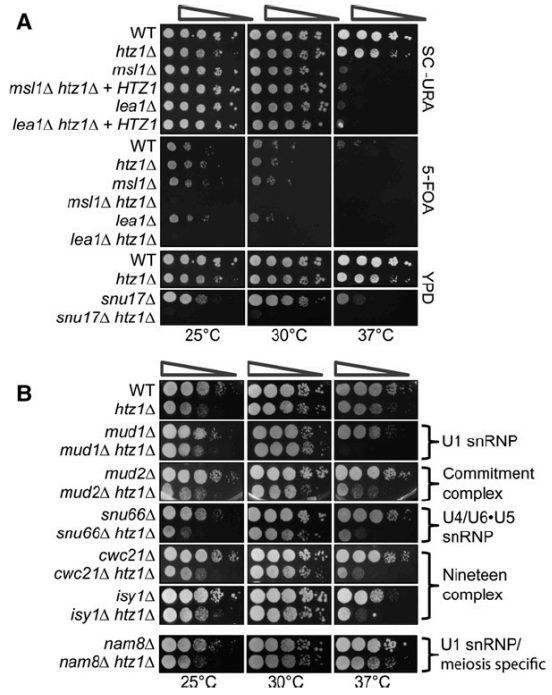

Figure 1. The histone variant H2A.Z is necessary for an optimal splicing environment. (*A*) Serial dilution assay of U2 snRNP double mutants *msl1Δ htz1Δ*, *lea1Δ htz1Δ*, and *snu17Δ htz1Δ*. For the *msl1Δ* and *lea1Δ* growth assay, cells were transformed with empty pRS316 *URA* plasmid (wild type [WT], *htz1Δ*, *msl1Δ*, and *lea1Δ*) or pRS316 containing *HTZ1* (*msl1Δ htz1Δ* and *lea1Δ htz1Δ*). Cells were grown at 30°C in SC–URA selective liquid medium until the desired OD_{600} was obtained. Cells were spotted as a 10-fold dilution onto SC–URA plates or 5-FOA plates to select for loss of the plasmid. Plates were incubated for 2 d for SC–URA plates or 4 d for 5-FOA plates at 25°C, 30°C, or 37°C. For *snu17Δ*, cells were grown at 30°C in YPD liquid medium until the desired OD_{600} was obtained. Cells were spotted as a 10-fold dilution onto YPD plates and incubated for 2 d at 25°C, 30°C, or 37°C. (*B*) Serial dilution assay of double mutants, *mud1Δ htz1Δ*, *mud2Δ htz1Δ*, *snu17Δ htz1Δ*, *snu66Δ htz1Δ*, *cwc21Δ htz1Δ*, *isy1Δ htz1Δ*, and *nam8Δ htz1Δ*. Cells were grown at 30°C in YPD liquid medium until the desired OD_{600} was obtained. Cells were spotted as a 10-fold dilution onto YPD plates and incubated for 2 d at 25°C, 30°C, or 37°C.

(Gottschalk et al. 2001). Snu17 is also a component of the retention and splicing (RES) complex, which is important for nuclear retention of unspliced pre-mRNA. This indicates that cells lacking H2A.Z are dependent on intact U2 snRNP.

Splicing is a highly dynamic process with thermal-sensitive RNA–RNA and RNA–protein interactions. We suspected that if H2A.Z affects splicing factor recruitment and/or rearrangements of the spliceosome, then perturbations in temperature could reveal additional genetic interactions between *HTZ1* and genes encoding splicing factors. To identify these interactions, we repeated our targeted genetic screen under growth temperatures that are suboptimal (37°C and 25°C). This analysis revealed genetic interactions between *HTZ1* and genes encoding components of every major spliceosomal complex (Fig. 1B). Slow growth phenotypes in many of the double mutants are exacerbated at higher temperatures, indicating that H2A.Z may be important for stabilizing spliceosomal complexes and/or rearrangements, especially in destabilizing conditions such as thermal stress. A notable exception is Nam8, a U1-associated factor that is particularly important for meiosis-specific splicing (Fig. 1B, bottom; Spingola and Ares 2000). Together, these genetic interactions indicate that a mutant spliceosome—and especially a compromised U2 snRNP—is particularly sensitive to the absence of H2A.Z in the chromatin.

H2A.Z is required for optimal splicing of a subset of ICGs

In order to determine whether deletion of H2A.Z affects splicing, we used RNA sequencing (RNA-seq) to analyze the effect of *HTZ1* deletion genome-wide. We compared the splicing efficiency of ICGs in wild-type and *htz1Δ* cells (Fig. 2A, left). Ribosomal protein genes (RPGs), which account for roughly one-third of all ICGs, show little to no change in splicing efficiency upon deletion of H2A.Z (Fig. 2A). However, H2A.Z is required for optimal splicing of a subset of ICGs with distinct properties. Notably, among non-RPGs, introns with nonconsensus BP sequences have a significantly stronger splicing defect than those with consensus BP sequences ($P = 0.018$) (Fig. 2A, right). In yeast, the highly conserved canonical BP sequence is UACUAAC, while the sequences most affected by *HTZ1* deletion contain the sequences that differ at the +1 position of the BP sequence: GACUAAC (5), AACUAAC (5), and CACUAAC (4). Neither nonconsensus 5′ splice site (5′SS) nor 3′ splice site (3′SS) sequences show this significantly enhanced dependence on H2A.Z for optimal splicing compared with non-RPG introns with consensus splice sites (Supplemental Fig. S1A, left), reinforcing the connection between H2A.Z and the U2 snRNP, which directly base-pairs with the BP sequence.

We and others have shown previously that defects in splicing are often masked by the rapid turnover of misspliced and unspliced transcripts (Hossain et al. 2011; Kawashima et al. 2014). To determine whether rapid turnover of misspliced transcripts masks splicing defects that occur in *htz1Δ* cells, we performed RNA-seq analysis in cells lacking *HTZ1* in combination with deletion of genes encoding cytoplasmic degradation pathway proteins Xrn1 or Upf1. Xrn1 is a 3′–5′ exonuclease (Larimer and Stevens 1990), and Upf1 is an ATP-dependent RNA helicase involved in nonsense-mediated decay (Ono et al. 2005). Genome-wide profiles of splicing efficiency in *htz1Δ* cells in the degradation mutant background are similar to the wild-type background profile (Fig. 2A,B, left). However, the subset of genes whose splicing is most strongly affected by deletion of *HTZ1* is larger, and splicing defects are often stronger in the degradation mutant backgrounds than the wild-type background, likely because unspliced transcripts are stabilized in the absence of Xrn1 or Upf1 (Fig. 2B). In both the *xrn1Δ* and *upf1Δ* mutant backgrounds, a

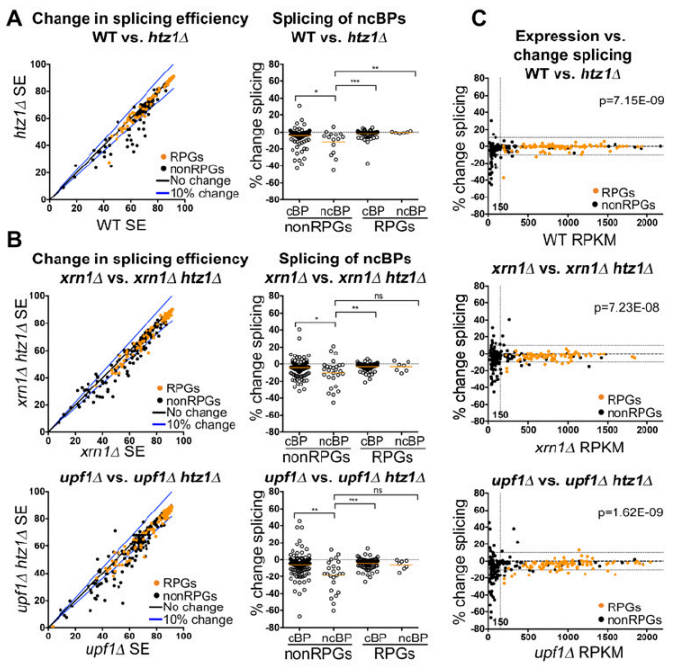

Figure 2. H2A.Z is required for optimal splicing of a subset of ICGs. (*A*, *left*) Distribution in splicing efficiencies of all ICGs upon deletion of *HTZ1*, represented as an *X*–*Y* plot. RPGs are denoted in orange. (*Right*) Distribution of changes in splicing in groups of ICGs characterized by RPGs or non-RPGs and consensus or nonconsensus BPs. (*B*, *left*) Distribution in splicing efficiencies of all ICGs upon deletion of *HTZ1* in either *xrn1*Δ (*top*) or *upf1*Δ (*bottom*) cells, represented as an *X*–*Y* plot. RPGs are denoted in orange. (*Right*) Distribution of changes in splicing in groups of ICGs characterized by RPGs or non-RPGs and consensus or nonconsensus BPs. *P*-values were determined by Mann-Whitney. (*C*) Distribution of changes in splicing efficiency upon deletion of *HTZ1* compared with reads per kilobase per million mapped reads (RPKM) in wild-type (*top*), *xrn1*Δ (*middle*), and *upf1*Δ (*bottom*) cells. The vertical dotted line represents RPKM of 150. The horizontal lines represent 10% change in splicing efficiency. Genes with an RPKM ≤150 are enriched in genes with ≥10% splicing defect (χ^2 test; *P*-values are indicated). (cBP) Consensus BP; (ncBP) nonconsensus BP; (ns) not significant; (*) *P*-value < 0.05; (**) *P*-value < 0.01; (***) *P*-value < 0.001.

significant majority of RPGs exhibits a <5% change in splicing when *HTZ1* is deleted ($P = 0.023$ and $P = 0.032$, respectively). Similar to the wild-type background, the subset of genes whose splicing is most strongly affected in *htz1*Δ is characterized by non-RPGs with nonconsensus BP sequences (Fig. 2B, right; Supplemental Fig. S1A).

RNA-seq analysis revealed 91 ICGs with a splice defect (≥10%) upon deletion of *HTZ1* in at least one background (wild type, *xrn1*Δ, or *upf1*Δ) (Supplemental Fig. S1B). This pool of genes is enriched in introns containing nonconsensus BPs (24 of 91 introns; $P = 0.003$). Of these 91 genes, 23 genes showed decreased splicing in both degradation mutant backgrounds, and 52 genes showed decreased splicing in only the *xrn1*Δ or *upf1*Δ background. It is clear that these degradation pathways can overlap, but there may be additional signals that help determine which pathway is used to remove specific unspliced transcripts.

H2A.Z is deposited in the chromatin in place of the canonical histone H2A. Swr1, a Swi2/Snf2-related ATPase, catalyzes this exchange (Krogan et al. 2003; Kobor et al. 2004; Mizuguchi et al. 2004). Similarly to *HTZ1*, *SWR1* interacts with genes encoding early splicing factors (Supplemental Fig. S2A). Loss of Swr1 leads to a global decrease in H2A.Z occupancy and loss of H2A.Z enrichment at promoters (Mizuguchi et al. 2004; Zhang et al. 2005; Sadeghi et al. 2011). We therefore asked whether Swr1 has effects on splicing similar to those of H2A.Z. To address this question, splicing efficiency of ICGs was analyzed in *swr1*Δ, *swr1*Δ *xrn1*Δ, and *swr1*Δ *upf1*Δ background cells (Supplemental Fig. S2B). Similar to H2A.Z, Swr1 appears to be important for optimal splicing of a subset of genes. Additionally, there is considerable overlap between the splicing efficiency in *swr1*Δ and *htz1*Δ cells (Supplemental Fig. S2C). While a number of genes display better splicing in *swr1*Δ cells as compared with *htz1*Δ cells, these affected genes are, for the most part, the same genes affected by H2A.Z loss (Supplemental Fig. S2D). While loss of Swr1 leads to decreased H2A.Z occupancy at promoters, it does not completely eliminate the H2A.Z in the chromatin, as Swr1-independent H2A.Z incorporation has been observed (Sadeghi et al. 2011). Residual H2A.Z in the chromatin likely accounts for the moderated splice defect in *swr1*Δ as compared with *htz1*Δ cells. Together, these results suggest that the effect of Swr1 on splicing is likely due to its role in H2A.Z exchange.

H2A.Z occupancy is reported to be negatively correlated to transcription and has been implicated in regulating gene expression (Santisteban et al. 2000; Zhang et al. 2005). We therefore asked whether defects in splicing correlate with gene expression. ICGs with strong splicing defects also have relatively low expression (reads per kilobase per million mapped reads [RPKM] <150) in the wild-type or degradation mutant background (Fig. 2C). We considered the possibility that this correlation was due to a bias in our sequencing results or filtering process. To ensure that the results are not due to an artifact of the sequencing data, we analyzed genes that did not pass the minimum-read filter threshold (Supplemental Fig. S3A). We found that changes in splicing of these genes are evenly distributed between increased and decreased splicing efficiency, demonstrating that our filters effectively removed noise and that there was no significant selection bias (Supplemental Fig. S3B). If splicing defects observed in ICGs with low expression are due to stochastic variation, we would expect the distribution of genes with

increased or decreased splicing efficiency to be the same in our filtered data and in the noise. However, we found that lowly expressed ICGs are significantly enriched in genes that have ≥10% decrease in splicing upon loss of H2A.Z as compared with the noise ($P << 0.01$ in all backgrounds) (Fig. 2C).

RT–PCR analysis confirms that genes with nonconsensus splice sites are particularly sensitive to loss of H2A.Z

In order to verify the RNA-seq results, RT–PCR was used to assess the splicing of a pool of candidate genes. Since unspliced pre-mRNA is targeted by both Xrn1 and Upf1 in ways that mask H2A.Z's effect on splicing, we decided to focus on two groups of genes: (1) genes that show intron accumulation in the wild-type, *xrn1*Δ, and *upf1*Δ backgrounds (eight genes) (Supplemental Fig. S1B) and (2) genes that show intron accumulation in both the *xrn1*Δ and *upf1*Δ cell backgrounds (15 genes) (Supplemental Fig. S1B). Of these 23 genes, nine contain introns with at least one nonconsensus splice site (Fig. 3A, in orange).

RT–PCR confirmed the decreased splicing of all eight genes in group 1 in the presence and absence of H2A.Z in wild-type, *xrn1*Δ, and *upf1*Δ cells (Fig. 3B,C). We examined the splicing intermediates of the two-intron gene *SUS1*, whose splicing has been well characterized (Hossain et al. 2009, 2011). *SUS1* is unique not only because it is one of the 10 yeast genes that contain multiple introns but also because its first intron contains both a nonconsensus 5′SS and BP sequence (Fig. 3A). Upon deletion of *HTZ1*, there is modest accumulation of *SUS1* pre-

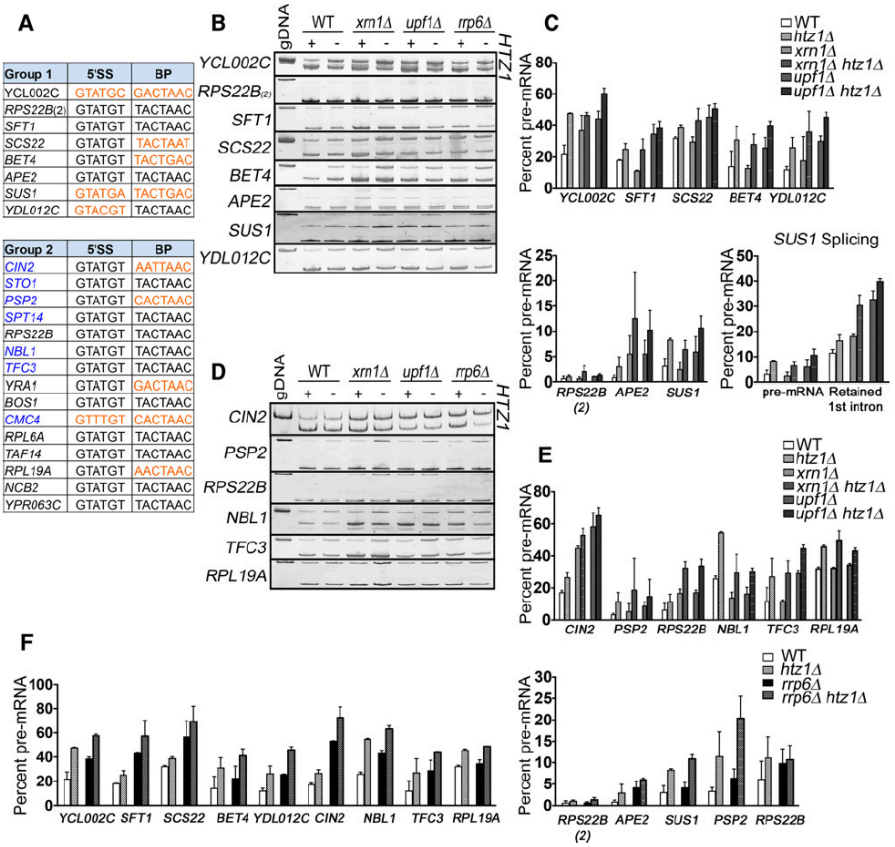

Figure 3. RT–PCR analysis confirms that genes with nonconsensus splice sites are particularly sensitive to loss of H2A.Z. (*A*) Group 1 consists of ICGs whose splicing decreases by ≥10% in the wild-type, *xrn1*Δ, and *upf1*Δ backgrounds. Group 2 consists of ICGs whose splicing decreases by ≥10% in the *xrn1*Δ and *upf1*Δ backgrounds. Genes that did not pass the minimum-read filter in the wild-type background are denoted in blue. Nonconsensus splice sites are denoted in orange. (*RPS22B*) 5′ untranslated region (UTR) intron; (*RPS22B_2*) coding region intron. (*B*) Analysis of group 1 genes by RT–PCR in wild-type, *xrn1*Δ, and *upf1*Δ cells ±*HTZ1*. Products were analyzed on 6% PAGE gels (8% for *SUS1*). Pre-mRNA size is indicated by genomic DNA size. (*C*) Quantification of group 1 RT–PCR unspliced (pre-mRNA) products. (*Bottom right*) Quantification of *SUS1* pre-mRNA and splicing intermediate containing only the second *SUS1* intron. (*D*) Analysis of group 2 genes by RT–PCR in wild-type, *xrn1*Δ, and *upf1*Δ cells ±*HTZ1*. Products were analyzed on 6% PAGE gels. Pre-mRNA size is indicated by genomic DNA size. (*E*) Quantification of group 2 RT–PCR unspliced products. (*F*) Quantification of group 1 and group 2 RT–PCR unspliced products in *rrp6*Δ cells ±*HTZ1*. Quantification graphs represent the average of two independent experiments, and error bars represent the standard deviation (SD). (gDNA) Genomic DNA.

mRNA and strong accumulation of partially spliced (first intron retained) mRNA (Fig. 3C, bottom right). Due to its weak splice sites, the first intron of *SUS1* is more susceptible to H2A.Z loss.

Of the 15 genes in group 2, seven genes did not pass our minimum-read filter in the wild-type cells and were not included in the RNA-seq analysis (Fig. 3A, in blue). It is possible that deletion of *HTZ1* causes decreased splicing of these introns in the wild-type background as well. We therefore used RT–PCR to confirm *htz1*Δ-related splicing defects in group 2 genes in wild-type, *xrn1*Δ, and *upf1*Δ cells (Fig. 3D,E). As expected, upon *HTZ1* deletion, these genes have decreased splicing in not only the degradation mutant background but also the wild-type background.

In a recent report, H2A.Z has been shown to act coordinately with the nuclear exosome, particularly the Rrp6 subunit, to control RNA expression and turnover (Rege et al. 2015). Rrp6 is a 3′–5′ exonuclease that has been implicated in the turnover of unspliced transcripts (Bousquet-Antonelli et al. 2000; Sayani and Chanfreau 2012). To determine whether the nuclear exosome is important for clearing the cell of unspliced transcripts that arise in *htz1*Δ cells, we used RT–PCR to analyze the splicing of our candidate genes in the presence and absence of H2A.Z in *rrp6*Δ cells (Fig. 3F). Deletion of *RRP6* alone results in increased pre-mRNA and, similar to *XRN1* and *UPF1* deletion, stabilizes many unspliced transcripts in *htz1*Δ cells, indicating that the nuclear exosome is important for clearing erroneous unspliced transcripts that arise in *htz1*Δ cells.

Because we found interactions between H2A.Z and components of every major spliceosome complex (Fig. 1A,B), we also examined splicing of our candidate genes in viable double mutants lacking H2A.Z and U1 snRNP factor Mud1 or nineteen complex (NTC) factor Isy1. Consistent with our genetic analyses, deletion of *HTZ1* enhances splicing defects of *mud1*Δ and *isy1*Δ cells (Supplemental Fig. S4A). Intriguingly, while splicing of most intron-containing RPGs is unaffected by *HTZ1* deletion alone, when H2A.Z loss is combined with deletion of splicing factor components, RPG splicing is defective (Supplemental Fig. S4B,C). Most intron-containing RPGs have consensus BP sequences (93%) and are efficiently spliced (Fig. 2A). Thus, it appears that, in general, H2A.Z deletion negatively affects splicing, but this effect is less obvious when splicing is robust. Moreover, these data indicate that H2A.Z generally affects the process of splicing, but BP recognition is particularly susceptible to changes in the splicing environment such that splicing of introns containing nonconsensus BP sequences is inefficient in *htz1*Δ cells even under otherwise optimal conditions.

H2A.Z-mediated splicing defects are not due to changes in spliceosome availability

H2A.Z is reported to be involved in transcriptional regulation and gene expression (Santisteban et al. 2000; Zhang et al. 2005). We therefore considered the possibility that the splicing effect of *HTZ1* deletion was due to altered transcription of a gene involved in splicing. However, RNA-seq analysis shows no significant change in the expression of genes encoding general splicing factors (Chen and Cheng 2012) or spliceosomal snRNAs (Supplemental Table S1; Supplemental Fig. S5A).

It also has been shown that competition between RNAs for spliceosome components alters splicing efficiency. Specifically in *S. cerevisiae*, due to the large number of intron-containing RPGs, perturbations to RPG expression alter the availability of the spliceosome to non-RPG pre-mRNAs (Munding et al. 2013). Therefore, up-regulation of RPG expression could lead to a decrease in splicing of non-RPGs. However, this is not the case, as the RNA-seq results show no significant change in expression of RPGs (Supplemental Fig. S5B).

H2A.Z is enriched around splice sites

H2A.Z is enriched around the TSS of the majority of yeast genes, typically in the +1 and −1 nucleosome flanking the NFR (Ranjan et al. 2013; Gu et al. 2015). However, recent reports indicate that, in *Drosophila*, H2A.Z also demarcates exon boundaries (Weber et al. 2010), while, in humans, a histone variant highly related to H2A.Z is enriched near BPs of introns (Tolstorukov et al. 2012). This suggested to us that H2A.Z's effects on splicing may be a direct result of H2A.Z's positioning relative to splicing-specific gene features in yeast. Using previously published ChIP-seq (ChIP combined with high-throughput sequencing) data (Gu et al. 2015), we confirmed that H2A.Z occupies the nucleosomes flanking the TSS of most ICGs (Fig. 4A,B, left). Additionally, H2A.Z is well positioned over, or just upstream of, the BP sequence and the 3′SS of many ICGs (Fig. 4B). At this point, it is unclear what the mechanism of this increased occupancy of H2A.Z is at particular intron sequences, but it follows a trend similar to other histone enrichment patterns within introns (for review, see Brown et al. 2012; Saldi et al. 2016). In parallel studies in *Schizosaccharomyces pombe*, this pattern of H2A.Z enrichment around splicing signals is also observed (Nissen et al. 2017).

A number of studies found that RPGs are deplete of H2A.Z-containing nucleosomes (Raisner et al. 2005; Zhang et al. 2005; Ranjan et al. 2013; Gu et al. 2015). Consistent with these studies, we observed low H2A.Z occupancy at the TSS, BP sequence, and 3′SS of intron-containing RPGs (Fig. 4A,C). Recently, it has been shown that the preinitiation complex is required for H2A.Z eviction from the chromatin during active transcription (Tramantano et al. 2016). Because RPGs are highly transcribed genes, it is possible that ChIP-seq experiments cannot capture H2A.Z occupancy in these genes due to rapid nucleosome turnover. In fact, depletion of components of the transcription machinery leads to H2A.Z accumulation in RPGs (Tramantano et al. 2016), demonstrating that, although steady-state levels are low, H2A.Z is present in RPGs and could contribute to their efficient splicing (Supplemental Fig. S4).

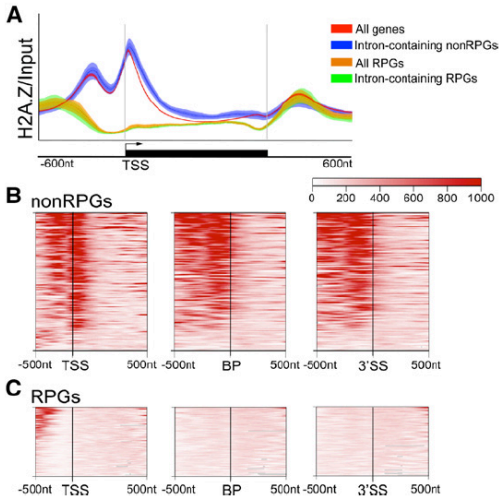

Figure 4. H2A.Z is well positioned near splice sites in non-RPGs. (*A*) H2A.Z ChIP-seq occupancy over input across the transcribed region and 600 nucleotides (nt) upstream of and downstream from the TSS and transcription stop site of all genes, all ICGs, all RPGs, intron-containing RPGs, and intron-containing non-RPGs. Lines represent the average fold enrichment of two biological replicates and 95% CI. The *Y*-axis represents 0–1000 mapped ChIP reads normalized to input. Analysis of data from Gu et al. (2015). (*B*) Hierarchical clustering of H2A.Z-binding profiles of intron-containing non-RPGs around TSSs or splice sites, oriented gene-directionality. (*Left*) Five-hundred nucleotides upstream of and 1000 nt downstream from the TSS. The vertical line indicates the TSS. Five-hundred nucleotides upstream of and 500 nt downstream from the BP sequence (*middle*) or 3′SS (*right*). $n = 147$. Introns found in the 5′ UTR were excluded. (*C*) Hierarchical clustering of H2A.Z-binding profiles of intron-containing RPGs around TSSs or splice sites, oriented gene-directionality. (*Left*) Five-hundred nucleotides upstream of and 1000 nt downstream from the TSS. The vertical line indicates the TSS. Five-hundred nucleotides upstream of and 500 nt downstream from the BP sequence (*middle*) or 3′SS (*right*). $n = 88$. Introns found in the 5′ UTR were excluded. Analysis of data by Gu et al. (2015), including an average of two biological replicates.

Cotranscriptional U2 snRNP rearrangement and downstream recruitment profiles are defective in the absence of H2A.Z

Cotranscriptional recruitment of the spliceosome to the nascent pre-mRNA has been shown to occur in a predictable and stepwise fashion (Kotovic et al. 2003; Gornemann et al. 2005; Lacadie and Rosbash 2005; Tardiff and Rosbash 2006). When spliceosomal rearrangements are perturbed, a lag in snRNP disengagement can be observed (Gornemann et al. 2005; Lacadie and Rosbash 2005; Tardiff and Rosbash 2006). Our previous studies demonstrated that histone acetylation patterns affect the recruitment of the U2 snRNP and alter spliceosomal rearrangements (Gunderson and Johnson 2009; Gunderson et al. 2011). Because ICGs containing nonconsensus BPs were enriched in our RNA-seq analysis and because we observed genetic interactions between *HTZ1* and several components of the U2 snRNP, we first analyzed U2 snRNP recruitment to nascent mRNA. We specifically examined the recruitment of Msl1, the U2B homolog, to two genes with H2A.Z occupancy upstream of the ORF (*ECM33* and *YCL002C)* and one gene deplete of H2A.Z occupancy (*RPL13A)* (Fig. 5A; Gu et al. 2015). The pattern of splicing factor recruitment to *ECM33* has been reported previously (Gornemann et al. 2005; Gunderson and Johnson 2009; Gunderson et al. 2011). *YCL002C* has a nonconsensus 5′SS and BP, and deletion of *HTZ1* leads to a splicing defect in this gene (Figs. 3B, 5B). While deletion of *HTZ1* results in no significant change in the recruitment of Msl1 to the selected genes, there is increased Msl1 enrichment at primer set 4 of *ECM33* and primer set 5 of *YCL002C* (Fig. 5D). This persistent U2 snRNP association suggests decreased U2 snRNP dissociation, and similar occupancy profiles have been interpreted as a defect in spliceosomal rearrangements (Gunderson et al. 2011). Surprisingly, *RPL13A* shows no significant increase in Msl1 in the gene body (Fig. 5D, right). Total protein levels of Msl1 or its interaction partner, Lea1, are unaffected by deletion of *HTZ1* (Supplemental Fig. S6A). This result indicates that H2A.Z's presence in the chromatin is important for the spliceosomal rearrangements that involve the U2 snRNP.

The observed Msl1 recruitment profiles, along with the results from our targeted genetic screen and RNA-seq analysis, suggest a specific role for H2A.Z in U2 snRNP function and/or rearrangements involving the U2 snRNP. However, it is possible that deletion of *HTZ1* acts more generally upon cotranscriptional recruitment or rearrangements of all snRNPs. To determine whether H2A.Z affects events upstream of U2 snRNP recruitment, we examined the recruitment of the U1 snRNP component Prp42 to *ECM33*, *YCL002C*, and *RPL13A*. Deletion of *HTZ1* does not affect Prp42 recruitment profiles to any of our candidate genes (Fig. 5E), suggesting that H2A.Z likely affects spliceosomal rearrangements that occur after U1 snRNP release. Total protein levels of Prp42 are unchanged by loss of H2A.Z (Supplemental Fig. S6B).

We predicted that, because of the stepwise cotranscriptional recruitment of splicing factors, association of splicing factors recruited to the nascent mRNA after U2 snRNP would be negatively impacted by loss of H2A.Z. In fact, there is decreased association of the U5 snRNP representative protein Snu114 with all candidate genes in the absence of *HTZ1* (Fig. 5F). While we observed no change in U2 snRNP occupancy at *RPL13A*, U5 snRNP occupancy is markedly decreased (Fig. 5F). This is consistent with our RT–PCR results in which H2A.Z loss exacerbates RPG splicing defects when the spliceosome is compromised (Supplemental Fig. S4C). H2A.Z likely affects spliceosome dynamics at all ICGs, but, because splicing of RPGs is particularly robust, spliceosome rearrangements do not rely as heavily on H2A.Z's presence in healthy cells. Decreased Snu114 occupancy cannot be attributed to changes in protein expression (Supplemental Fig. S6C). These results suggest that loss of H2A.Z increases the association of the U2 snRNP and reduces the

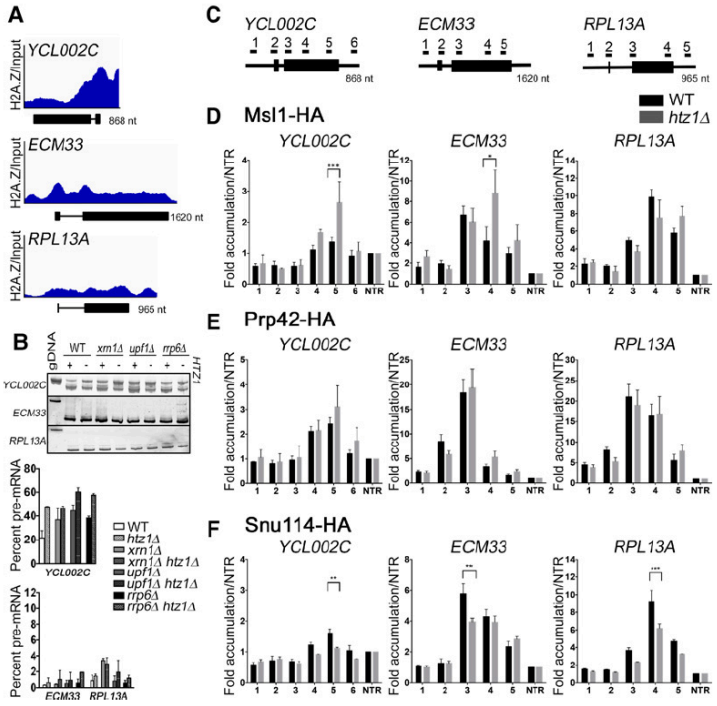

Figure 5. Cotranscriptional U2 snRNP recruitment is defective in the absence of H2A.Z. (*A*) Integrative Genome Viewer track view of H2A.Z occupancy over input by ChIP-seq across the ORF of *YCL002C* (*top*), *ECM33* (*middle*), and *RPL13A* (*bottom*). The *Y*-axis represents 0–1000 mapped ChIP reads normalized to input. A schematic of each gene is included *below* each occupancy profile. Analysis of data from Gu et al. (2015). (*B*, *top*) Analysis of *YCL002C*, *ECM33*, and *RPL13A* genes by RT–PCR in the presence and absence of *HTZ1*. Products were analyzed on 6% PAGE gels. Pre-mRNA size is indicated by genomic DNA size. (*Bottom*) Quantification of RT–PCR products. Graphs represent the average of two independent experiments, and error bars represent the SD. (*C*) Schematic of ICGs *YCL002C*, *ECM33*, and *RPL13A*. Underlined numbers represent amplicons generated by each primer set used in this experiment. (*D*) Occupancy of Msl1 at each region of *YCL002C* (*left*), *ECM33* (*middle*), or *RPL13A* (*right*) relative to the nontranscribed region in wild type or *htz1*Δ. Graphs represent the average of six (wild type) or three (*htz1*Δ) independent experiments, and error bars represent the standard error of the means (SEM). *P*-values for each primer set were determined by Student's *t*-test. Significant values are indicated. (*E*) Occupancy of Prp42 at each region candidate gene relative to the nontranscribed region in wild type or *htz1*Δ. Graphs represent the average of four independent experiments, and error bars represent the SEM. *P*-values for each primer set were determined by Student's *t*-test. No significant values were found. (*F*) Occupancy of Snu114 at each region of candidate genes relative to the nontranscribed region in wild type or *htz1*Δ. Graphs represent the average of three independent experiments, and error bars represent the SEM. *P*-values for each primer set were determined by Student's *t*-test. Significant values are indicated. (gDNA) Genomic DNA. (*) *P*-value < 0.01; (**) *P*-value < 0.001; (***) *P*-value < 0.0001.

association of downstream splicing factors. These results are consistent with a role for H2A.Z in efficient spliceosomal rearrangements.

RNAPII kinetics are altered upon loss of H2A.Z

Because we found that H2A.Z is enriched around splice sites of many ICGs, it is possible that H2A.Z promotes splicing through physical interactions with the spliceosome, perhaps through a chromatin-associated adaptor protein. Indeed, such physical interactions between splicing factors and histones have been reported (Sims et al. 2007; Luco et al. 2010), and, in humans, it has been reported that H2A.Z weakly binds the SF3B complex (Tolstorukov et al. 2012). However, we found no direct interactions between H2A.Z and tested splicing factors (Prp43, Snu66, Prp4, Lea1, Msl1, Snu114, and Cus1) (data not shown).

Cotranscriptional splicing is spatially and temporally linked to transcription, and therefore changes in RNAPII elongation rates and pausing can perturb the precisely timed rearrangements of the spliceosome and alter splicing outcomes (de la Mata et al. 2003; Howe et al. 2003; Carrillo Oesterreich et al. 2010). As H2A.Z has roles in the regulation of both transcription initiation and elongation, we considered the possibility that H2A.Z helps coordinate the processes of transcription and splicing (Santisteban et al. 2000, 2011; Zhang et al. 2005; Wan et al. 2009; Li et al. 2012; Weber et al. 2014; Subramanian et al. 2015; Rudnizky et al. 2016).

In order to determine whether loss of H2A.Z affects RNAPII kinetics in such a way that it could alter spliceosome rearrangements, we first examined the recruitment of Rpb3, the large subunit of RNAPII, to *YCL002C*, *ECM33*, and *RPL13A*. While Rpb3 recruitment to the promoter is unchanged in *htz1*Δ cells, Rpb3 occupancy through the gene body of *ECM33* and *RPL13A* is decreased in *htz1*Δ cells compared with wild-type cells (25%–31% decrease for locations 2–5) (Fig. 6B). We observed a small but consistent decrease of Rpb3 occupancy in *YCL002C* (11%–16% decrease for all locations) (Fig. 6B, left). *YCL002C* is a lowly expressed gene with generally low Rpb3 occupancy, and we believe that this makes it difficult to resolve the differences in polymerase enrichment. In order to determine whether changes in RNAPII occupancy are specific to ICGs or are a general outcome of *HTZ1* deletion, we examined Rpb3 recruitment to an intronless gene, *PMA1*. We found that, similar to the candidate ICGs, Rpb3 occupancy is reduced in *PMA1* upon *HTZ1* deletion (17%–36% decrease for all locations) (Fig. 6B, right). Unlike *ECM33* and *RPL13A*, Rpb3 occupancy is decreased at primer set 1 of *PMA1*. This could be due to primer set 1 amplifying a region just downstream from the TSS. However, this may also indicate decreased Rpb3 recruitment to the promoter of *PMA1* in

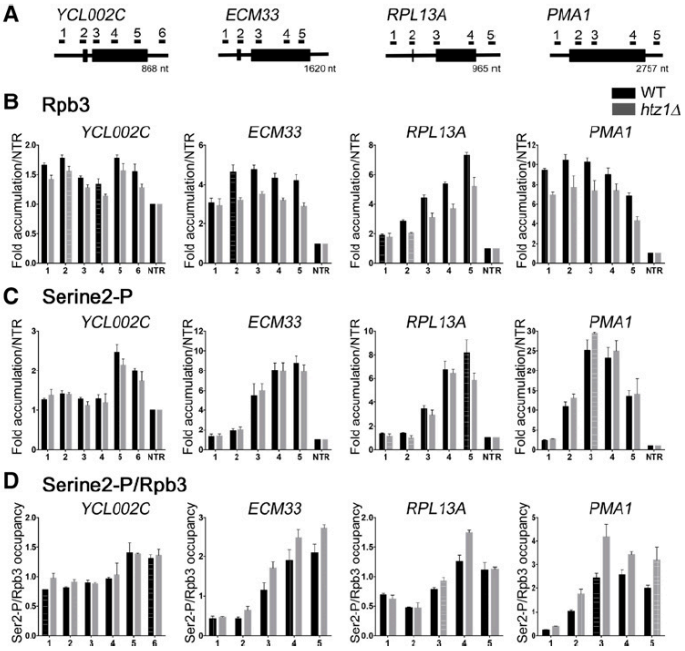

Figure 6. RNAPII elongation kinetics are altered in the absence of H2A.Z. (*A*) Schematic of ICGs *YCL002C*, *ECM33*, and *RPL13A* and intronless gene *PMA1*. (*B*) Occupancy of Rpb3 at each region of *YCL002C* (*left*), *ECM33* (*middle left*), *RPL13A* (*middle right*), or *PMA1* (*right*) relative to the nontranscribed region in wild type or *htz1*Δ. Graphs represent the average of three independent experiments, and error bars represent the SEM. (*C*) Ser2 phosphorylation state of the RNAPII C-terminal domain at each region of candidate genes relative to the nontranscribed region in wild type or *htz1*Δ. Graphs represent the average of three independent experiments, and error bars represent the SEM. (*D*) Ser2 phosphorylation state (from *C*) normalized to Rpb3 (from *B*) occupancy at each region of candidate genes.

*htz1*Δ cells. Total protein levels of Rpb3 are unchanged by loss of H2A.Z (Supplemental Fig. S6D). These results indicate that loss of H2A.Z reduces RNAPII occupancy and influences transcription elongation. While additional changes such as polymerase pausing or processivity cannot be ruled out, decreased RNAPII occupancy in *htz1*Δ cells likely reflects slowed transcription elongation. Not only does slow elongation correlate with decreased RNAPII occupancy (Mason and Struhl 2005; Garcia et al. 2010, 2012; Malik et al. 2017), but H2A.Z deletion has been shown previously to lead to a decreased rate of elongation in both yeast and mammalian cells (Santisteban et al. 2011; Rudnizky et al. 2016). Therefore, our results are consistent with past findings that H2A.Z promotes efficient transcription elongation and that H2A.Z deletion leads to changes likely including, but not limited to, slow elongation rate.

RNAPII contains a unique C-terminal domain (CTD) consisting of sequence repeats that are phosphorylated in a predictable manner during transcription elongation. Typically, the polymerase is hypophosphorylated at the promoter and, upon initiation, becomes phosphorylated at Ser5. Ser5 phosphorylation (Ser5-P) declines near the 3′ end of the transcript in favor of Ser2-P (Komarnitsky et al. 2000; Alexander et al. 2010). This dynamic phosphorylation has been implicated in regulating transcription elongation kinetics, and Ser2-P in particular is a hallmark of the elongating polymerase (for review, see Hsin and Manley 2012). Because perturbations to CTD phosphorylation reflect changes in active elongation (Garcia et al. 2010; Allepuz-Fuster et al. 2014; Davidson et al. 2014), we analyzed Ser2-P states on our candidate genes. Although *HTZ1* deletion results in decreased RNAPII occupancy across candidate genes, there is increased Ser2-P on polymerases bound to the 3′ ends of *ECM33*, *RPL13A*, and *PMA1* in *htz1*Δ cells (Fig. 6C,D). Because polymerase occupancy of *YCL002C* is low compared with other candidate genes, we were not able to observe small changes in Ser2-P on this gene (Fig. 6C,D, left). We found that Ser2-P begins to accumulate earlier toward the 5′ end in the gene bodies of *YCL002C*, *ECM33*, and *PMA1* in *htz1*Δ cells as compared with wild-type cells (Supplemental Fig. S7B). These findings are similar to past studies that have shown that transcription elongation defects correlate with increased Ser2-P (Garcia et al. 2010, 2012), Hence, it appears that increased pausing or slower elongation in cells lacking H2A.Z may allow Ser2-P accumulation earlier in transcription.

Deletion of a general elongation factor exacerbates H2A.Z-mediated splice defects and affects U2 snRNP recruitment profiles

We suspected that if H2A.Z affects splicing via its role in transcription elongation, we might be able to observe functional interactions between H2A.Z and elongation factors. Consistent with this, we observed slow growth in cells lacking both H2A.Z and the general elongation factor Dst1 (TFIIS) (Supplemental Fig. S8A). Dst1 promotes elongation and prevents backtracking of stalled polymerase elongation complexes (for review, see Freedman et al. 2013). In the absence of Dst1, RNAPII elongation is compromised, and polymerase pause sites are altered, particularly under transcriptional stress (Mason and Struhl 2005; Churchman and Weissman 2011). Intriguingly, deletion of Dst1 can also negatively affect splicing and

lead to aberrant intron retention (Lacadie et al. 2006; Carey 2015). While loss of Dst1 alone does not decrease splicing of our candidate genes, deletion of *DST1* in *htz1*Δ cells exacerbates H2A.Z-mediated splice defects, and we observed increased pre-mRNA levels in double mutants (Supplemental Fig. S8B). The *SUS1* splicing intermediate that retains the nonconsensus first intron, but not the unspliced pre-mRNA, accumulates in *dst1*Δ *htz1*Δ cells, suggesting that, similar to *htz1*Δ, splicing of introns with nonconsensus BP sequences is particularly affected in the double mutant (Supplemental Fig. S8B, right).

Deletion of Dst1 not only decreases polymerase processivity (Mason and Struhl 2005) but was also found, in a genome-wide study, to decrease RNAPII occupancy by 1.6-fold, on average, compared with wild-type cells (Ghavi-Helm et al. 2008). Because Dst1 loss exacerbates splicing defects in *htz1*Δ cells and generally decreases RNAPII occupancy, we asked whether Dst1 could affect spliceosome rearrangements similar to H2A.Z. Consistent with our observations in *htz1*Δ cells, enrichment of the U2 snRNP factor Msl1 is increased at *YCL002C* in *dst1*Δ cells (Supplemental Fig. S8D, left). While Dst1 and H2A.Z likely affect transcription elongation in different ways, this supports a model in which elongation defects can lead to changes in U2 snRNP occupancy patterns.

Depletion of disassembly factor Prp43 can suppress H2A.Z-mediated splice defects

Our findings that H2A.Z affects spliceosome rearrangements and transcription elongation suggest that the kinetics of transcription and splicing are well coordinated. We suspect that, in the absence of H2A.Z, spliceosome kinetics are disrupted by changes in transcription elongation, and stalled spliceosomes are disassembled while pre-mRNA is released. Prp43 is a DEAH-box helicase that has functions in ribosome biogenesis as well as spliceosome disassembly (Arenas and Abelson 1997; Leeds et al. 2006). Prp43 not only catalyzes disassembly upon completion of splicing (Arenas and Abelson 1997) but can also disassemble spliceosomes when splicing is slowed (Koodathingal et al. 2010; Koodathingal and Staley 2013). Intriguingly, deletion of *HTZ1* suppresses the growth defect of *prp43*^{DAmP} cells (Fig. 7A). In this strain, the 3′ untranslated region (UTR) of *PRP43* is disrupted with an antibiotic resistance cassette, which leads to decreased RNA expression (Supplemental Fig. S9A). Surprisingly, despite the severe growth defect, we did not observe a significant splicing defect for our candidate genes when Prp43 expression was decreased (Fig. 7B). This suggests that the Prp43 functions outside of splicing are significant contributors to the growth defect of *prp43*^{DAmP} cells. Interestingly, decreased Prp43 partially suppresses the splicing defect observed in *htz1*Δ cells, indicating that spliceosome disassembly is at least partially responsible for pre-mRNA accumulation in cells lacking H2A.Z (Fig. 7B; Supplemental Fig. S9B). We next analyzed splicing genome-wide to determine to what extent Prp43 depletion suppresses H2A.Z-mediated splice defects. Splicing is largely unaffected by Prp43 depletion alone; however,

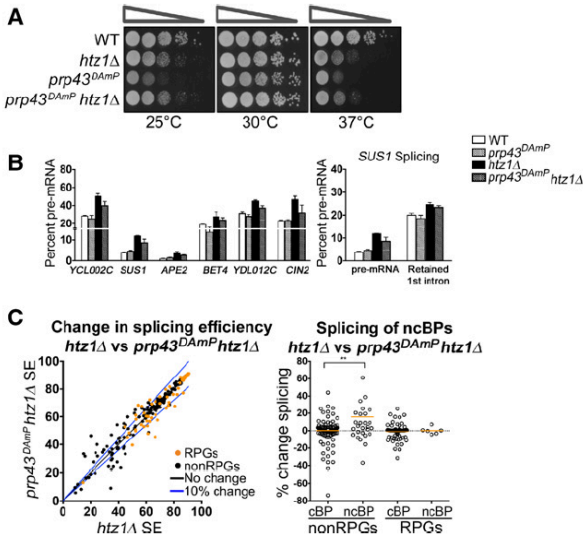

Figure 7. Decreased spliceosome disassembly can suppress H2A.Z-mediated splice defects. (*A*) Serial dilution assay of double mutant *prp43*^{DAmP} *htz1Δ*. Cells were grown at 30°C in YPD + G418 liquid medium until the desired OD_{600} was obtained. Cells were spotted as a 10-fold dilution onto YPD + G418 plates and incubated for 2 d at 25°C, 30°C, or 37°C. (*B*, *left*) Quantification of pre-mRNA of candidate genes by RT–PCR in wild-type and *prp43*^{DAmP} cells ±*HTZ1*. (*Right*) Quantification of *SUS1* RT–PCR pre-mRNA and splicing intermediate containing only the second *SUS1* intron. Quantification graphs represent the average of two to three independent experiments, and error bars represent the SD. (*C*, *left*) Distribution in splicing efficiencies of all ICGs upon deletion of *HTZ1* in *prp43*^{DAmP} cells, represented as an *X*–*Y* plot. RPGs are denoted in orange. (*Right*) Distribution of changes in splicing in groups of ICGs characterized by RPGs or non-RPGs and consensus or nonconsensus BPs. (cBP) Consensus BP; (ncBP) nonconsensus BP. (**) *P*-value < 0.01.

there are subsets of ICGs whose splicing efficiency increases or decreases in *prp43*^{DAmP} cells, suggesting gene-specific sensitivity to Prp43 depletion (Supplemental Fig. S9C). Consistent with the results shown in Figure 7B, we found that Prp43 depletion in *htz1*Δ cells improves splicing in a subset of ICGs (Fig. 7C left). The pool of genes in which splicing is most improved by Prp43 depletion (≥10%) is significantly enriched with introns containing a nonconsensus BP ($P = 0.005$). Additionally, among non-RPGs, splicing of introns containing a nonconsensus BP sequence is significantly more improved by Prp43 depletion than splicing of those with consensus BP sequences ($P = 0.01$) (Fig. 7C right). Consistent with our observations in *htz1*Δ cells, introns with nonconsensus BPs are more sensitive to Prp43 depletion than those with nonconsensus 5′SSs or 3′SSs (Supplemental Fig. S9D). Together, these data suggest that when rearrangements involving the U2 snRNP are defective or slowed in *htz1*Δ cells, decreased disassembly may allow more time for spliceosome rearrangements to occur.

Overall, these results are consistent with a model in which compromised elongation leads to a splicing defect.

In the case of *htz1*Δ, this defect contributes to defects in U2 snRNP rearrangements and downstream snRNP recruitment. Prp43 is able to recognize and disassemble spliceosomes with defective rearrangement, leading to the release of unspliced pre-mRNA in *htz1*Δ cells. While genes with robust splicing are refractory to these changes in the kinetics of spliceosome rearrangements, those with weak splice sites are unable to splice efficiently. These results highlight an important, albeit underappreciated, feature of cotranscriptional splicing: Compromised transcription elongation does not necessarily provide a "window of opportunity" to resolve splicing defects, but rather, kinetics of transcription elongation and splicing are optimally coordinated to promote splicing. Specific factors such as H2A.Z appear to ensure the appropriate tuning of this coordination to promote splicing for subsets of introns.

Discussion

An ever-growing body of work has established that transcription and RNA processing are spatially and temporally coordinated. Because the spliceosome acts upon nascent mRNA while the transcript is associated with the elongating polymerase, the process of splicing takes place in the context of the transcription machinery and the chromatin it engages. Here we demonstrate that the histone variant H2A.Z plays a novel role in the process of cotranscriptional splicing. Consistent with published studies from the Pleiss and Stevens laboratories (Albulescu et al. 2012; Sorenson and Stevens 2014), we found many genetic interactions between *HTZ1* and genes encoding splicing factors. In particular, mutations to U2 snRNP components render cells reliant on H2A.Z for viability. Additionally, H2A.Z is necessary for optimal splicing of many endogenous ICGs, particularly when introns contain weak splice sites. Furthermore H2A.Z facilitates polymerase elongation and ensures appropriate cotranscriptional spliceosome rearrangements. Finally, decreased expression of an elongation factor or a spliceosome disassembly factor modulates the cells sensitivity to the presence of H2A.Z. Our studies support a role for H2A.Z in coordinating the processes of transcription and splicing: H2A.Z regulates transcription elongation, thereby affecting downstream spliceosome dynamics on ICGs.

H2A.Z affects kinetics of polymerase elongation

Our experiments reveal that loss of H2A.Z results in decreased polymerase occupancy across our candidate genes, suggesting that H2A.Z normally promotes RNAPII elongation (Fig. 6; Supplemental Figs. S7, S8). Although our experiments do not directly measure elongation rate, there are several lines of evidence to support a role for H2A.Z in facilitating efficient elongation. The presence of nucleosomes provides a substantial barrier to transcribing polymerase complexes, and RNAPII must overcome this barrier to access the DNA and efficiently transcribe mRNA (for review, see Petesch and Lis 2012). Because H2A.Z is less stably associated with DNA, exchange of canonical histone H2A with variant H2A.Z facilitates nucleosome eviction and helps lower this transcriptional barrier (Zhang et al. 2005; Weber et al. 2014). In fact, using an in vivo run-off assay, Santisteban et al. (2011) show that H2A.Z loss decreases the rate of elongation across the ORF of a representative gene. Similar decreases in elongation rate have been observed in mammalian systems (Rudnizky et al. 2016). Additionally, we found that CTD Ser2-P accumulates closer to the TSS and remains high throughout the body of candidate genes in *htz1*Δ cells (Fig. 6D; Supplemental Fig. S7B). These findings are similar to past studies that have shown transcription elongation defects correlate with increased Ser2-P. In yeast, deletion of transcription coactivator Sub1 decreases elongation rate and increases total Ser2-P (Garcia et al. 2010, 2012), while, in human cells, increased polymerase pausing leads to Ser2-P accumulation (Davidson et al. 2014), suggesting that Ser2-P levels correlate with the time RNAPII is engaged with the DNA. Therefore, increased and premature Ser2-P in *htz1*Δ cells may reflect polymerase elongation defects. While our results are consistent with past findings that H2A.Z loss results in slowed elongation, we cannot rule out the possibility that H2A.Z influences polymerase kinetics in additional ways, such as altered pausing, backtracking, and/or processivity. Although we did not observe physical interactions, we also cannot rule out that contact between H2A.Z and components of the splicing machinery may contribute to H2A.Z's effects on splicing. In any case, the evidence described here and elsewhere that deletion of H2A.Z negatively impacts elongation and that further compromising elongation (as in *dst1*Δ *htz1*Δ cells) further impairs splicing suggests that the kinetics of transcription and splicing are intimately coordinated and that H2A.Z is important for this coordination.

How do changes in polymerase elongation affect spliceosome dynamics?

Growing evidence supports a model in which splicing is kinetically coupled to transcription (Merkhofer et al. 2014). Several studies in yeast suggest that the polymerase pausing can be a "checkpoint" for spliceosome assembly, and splicing catalysis coincides with polymerase elongation (Alexander et al. 2010; Carrillo Oesterreich et al. 2011; Chathoth et al. 2014; Oesterreich et al. 2016). It has also been proposed that changes in polymerase elongation affect the "window of opportunity" available for nascent transcripts to be spliced, and slower elongation increases this available window (Braberg et al. 2013; Dujardin et al. 2014; Oesterreich et al. 2016). Nonetheless, the rates of spliceosome rearrangements are also finely tuned, and slow rearrangements provide the opportunity for spliceosome disassembly and release of unspliced RNAs (Koodathingal et al. 2010; Koodathingal and Staley 2013). Recent mammalian studies demonstrate that an optimal elongation rate is required for proper pre-mRNA splicing. Both increased and decreased elongation rates

can alter alternative splicing and intron retention, indicating that transcription and splicing are coupled in a "Goldilocks-like phenomenon" (Fong et al. 2014). In yeast, results from splicing analyses in polymerase trigger-loop mutants show that, while splicing of some genes benefit from slowed elongation, numerous genes are more poorly spliced when the polymerase is slow (Braberg et al. 2013). Intriguingly, the combination of "slow polymerase" RNAPII mutations with deletion of H2A.Z or Swr1 renders cells very sick (Braberg et al. 2013). Additionally, we found that deletion of the general elongation factor Dst1, which can negatively impact splicing outcomes (Lacadie et al. 2006; Carey 2015), results in increased U2 association with nascent pre-mRNA, indicating that elongation defects may lead to aberrant spliceosomal rearrangements (Supplemental Fig. S8D). These observations suggest that the timing of polymerase elongation and pausing can have important implications for the fate of the RNA. H2A.Z-mediated splice defects do not entirely mimic those observed in slow polymerase mutants, suggesting that H2A.Z likely influences transcription elongation in more nuanced ways than altering rate alone. Our data suggest a model in which deletion of H2A.Z alters elongation such that the combined effects of poor splice site recognition and RNAPII elongation defects have a deleterious impact on splicing. As a result, spliceosomes are disassembled, leading to release of unspliced products and, ultimately, RNA degradation by nuclear and cytoplasmic machineries. H2A.Z helps coordinate the kinetics of transcription and splicing to ensure proper splicing outcomes.

A subset of DEAD-box and DEAH-box helicases hydrolyzes ATP to drive spliceosomal rearrangements and disassembly and has been proposed to act as "molecular clocks" (Koodathingal and Staley 2013). In particular, DEAH-box helicases Prp16, a factor that ensures splicing fidelity, and Prp43, a disassembly factor, help determine the fate of weak intron substrates when splicing is stalled. Prp16 can recognize and reversibly reject suboptimal slowly spliced substrates to either facilitate proofreading of splice sites or trigger spliceosome disassembly and subsequent degradation of unspliced transcripts (Koodathingal et al. 2010; Koodathingal and Staley 2013). Interestingly, the presence of Prp16 prevents binding of the NTR complex (Chen et al. 2013), which recruits the disassembly factor Prp43 to help mediate spliceosome disassembly. The balance of Prp16 and Prp43 therefore helps determine the fate of the nascent mRNA. Unexpectedly, despite the strong growth defect, splicing of the majority of ICGs in cells containing a hypomorphic Prp43 allele is unaffected, suggesting that decreased Prp43 expression disproportionately affects nonspliceosomal functions of Prp43 (Fig. 7B; Supplemental Fig. S9C). Indeed, Prp43 largely localizes to the nucleolus, where it has functions in ribosome biogenesis (Combs et al. 2006). However, decreased Prp43 expression partially suppresses splicing defects and preferentially improves splicing of introns containing nonconsensus BP sequences in *htz1*Δ cells, suggesting that decreased spliceosome disassembly allows more time for spliceosome rearrangements to occur before RNA is released (Fig. 7B,C). Consistent with these results, the Guthrie laboratory (Nissen et al. 2017) recently found that Prp43 overexpression in *htz1*Δ cells leads to a synthetic growth defect in *S. pombe*. Additionally, they show that Prp16 overexpression suppresses defective splicing caused by H2A.Z deletion (Nissen et al. 2017). It has been shown that Prp16 enables alternative branch site selection; thus, although Prp16 normally antagonizes stalled spliceosomes, excess Prp16 may protect the nascent mRNA by outcompeting disassembly factors and promoting resampling of weak splice sites (Chen et al. 2013; Semlow et al. 2016). Therefore, Prp16 overexpression is expected to have an outcome similar to that of decreased Prp43 expression, favoring splice site resampling over the discard pathway.

We propose that H2A.Z functions to coordinate the kinetics of transcription elongation and spliceosome rearrangements to promote efficient splicing. In the absence of H2A.Z, polymerase elongation is defective and therefore alters the availability of the nascent mRNA to the spliceosome, ultimately altering splicing kinetics. Prp16 and Prp43 may act as intrinsic timing mechanisms that recognize slowed or stalled spliceosomes and target them for splice site resampling or disassembly and the subsequent release of unspliced pre-mRNA. Decreased Prp43 or increased Prp16 allows for decreased reliance on H2A.Z to provide precise coordination of splicing with transcription elongation.

Materials and methods

Yeast strains, media, and DNA constructs

All *S. cerevisiae* strains used in this study are listed in Supplemental Table S2. Strains described in Supplemental Table S2 are in the BY4743 strain background with the exception of the Lea1-HA, Msl1-HA, and Snu114-HA strains used for ChIP, which were provided by Karla Neugebauer. All strains were propagated according to standard procedures in either YPD (1% yeast extract, 2% peptone, 2% dextrose) or the appropriate selective medium.

For deletion of *HTZ1* in *rrp6*Δ and LG1 strains, deletion of genes at their endogenous loci was performed using standard PCR-based homologous recombination while preserving the endogenous promoters (Longtine et al. 1998; Goldstein and McCusker 1999). Deletions were confirmed by whole-cell extract and immunoblot with anti-HTZ1 (Abcam, ab4626).

For all other strains, standard methods for mating, sporulation, transformations, and tetrad analysis were used as described in Amberg et al. (2005). The genotype of each viable spore was confirmed via PCR. Plasmids used in this study are listed in Supplemental Table S3.

Generation of HTZ1 *backup plasmid*

The *HTZ1* gene along with 450 base pairs upstream of and downstream from *HTZ1* was PCR-amplified from *S. cerevisiae* genomics using the primers Htz1InFusion-F and Htz1InFusion-R (Supplemental Table S2). Restriction enzyme cleavage sites for HinDIII were introduced into both primers. PCR products were digested with HinDIII and cloned into pRS316 (*URA3*) using the InFusion Cloning HD Plus system (Clontech). Selected clones were verified by sequencing. Plasmids were transformed into

*htz1*Δ cells, and expression of Htz1 was verified by whole-cell extract and immunoblot with anti-HTZ1 (Abcam, ab4626).

Viability assay/dilution series

For growth analysis of *msl1*Δ and *lea1*Δ strains containing a centromeric pRS316 (*URA3*) plasmid, strains were grown overnight in SC−URA liquid medium at 30°C. Cells were diluted to an OD_{600} of 0.1 in 5 mL of SC−URA medium and incubated at 30°C until all strains reached early log phase. A 10-fold serial dilution of each strain was spotted onto SC−URA plates or 5-FOA plates to select for plasmid loss and incubated at 25°C, 30°C, or 37°C. The SC−URA plates were incubated for 2 d. The 5-FOA plates were incubated for 4 d.

For growth analysis of viable double mutants, strains were grown overnight in YPD liquid medium at 30°C. Cells were diluted to an OD_{600} of 0.1 in 5 mL of YPD and incubated at 30°C until all strains reached early log phase. A 10-fold serial dilution of each strain was spotted onto YPD plates and incubated for 2 d at 25°C, 30°C, or 37°C. For $prp43^{DAmP}$ strains, cells were grown in liquid YPD + G418 and plated on YPD + G418 for growth.

RNA-seq library preparation and alignment

RNA-seq libraries were prepared using an Illumina Truseq V3 kit and ribosomal RNA depletion. Sequence reads were aligned to SacCer3 and spliced transcripts from the Ares Lab Yeast Intron Database version 3 (Grate and Ares 2002) in a single step using STAR (Dobin et al. 2013). Only the highest-scoring alignments for each read were kept, allowing for a single tie at most. Gene Expression Omnibus accession numbers are as follows: GSE97416 and GSE94404:GSM2474880 (for wild-type replicate #2).

RNA-seq RPKM and splicing efficiency calculation

RPKMs were computed for each gene by dividing the total number of reads that aligned entirely within the gene's exon boundaries by the gene's total exon length in kilobase pairs per million mapped reads. Reads within ICGs were categorized as exonic, spliced, or unspliced. Exonic reads were those that mapped entirely within a single exon, as defined by the Ares Lab Yeast Intron Database. Spliced reads were those that aligned with a gap that corresponded to an annotated intron, and unspliced reads mapped partially within an exon and partially within an intron with no gap. Spliced and unspliced read counts were normalized by dividing each count value by the number of unique alignment positions that were able to contribute to the total. For spliced reads, this normalization value was the length of the read minus 1 for every intron. For unspliced read counts, this was the length of the intron plus the read length minus 1. Splicing efficiency for each intron was calculated as normalized spliced counts divided by the sum of the normalized spliced and normalized unspliced counts.

RT–PCR analysis and quantification

Cells were grown in YPD medium to an OD_{600} between 0.4 and 0.7. For $prp43^{DAmP}$ strains, cells were grown in YPD + G418. Total RNA was isolated from 10 mL of cells using a hot phenol extraction method and dissolved in 100 µL of diethylpyrocarbonate (DEPC)-treated water. Ten micrograms to 20 µg of RNA was DNase-treated (Roche), and treated RNA concentration was measured by spectrophotometer. Two micrograms to 4 µg of RNA was used to make cDNA using the Maxima first strand cDNA synthesis kit (Fermentas). cDNA was diluted 1:20 and used for PCR. To detect splicing isoforms, primers flanking the intronic sequences were used for 27-cycle PCR using 1 µL of diluted cDNA. PCR products were diluted 1:5 and run on a 6% TBE polyacrylamide gel. *SUS1* products were run on an 8% TBE polyacrylamide gel. Gels were stained with SYBR Green (Sigma), and images were captured using Image Lab (Bio-Rad). Bands were quantified as percent total of band intensity using Image Lab software.

ChIP-seq analysis

ChIP-seq reads were obtained from Gu et al. (2015) and converted to FastQ format using the NCBI Sequence Read Archive (SRA) toolkit. Contaminating adapter sequences were trimmed, and Bowtie2 was used to align the FastQ reads of two replicates to sacCer3 with only one reported alignment (-k 1). Genomic track files from immunoprecipitation and input alignments were created using SAMTools, BEDTools, and the University of California at Santa Cruz bedgraphToBigWig utility. After the input and immunoprecipitation pileup tracks were normalized for differential read count, a ratio track was created by dividing the normalized immunoprecipitation track by the normalized input track.

Metagenes and heat maps were plotted using the R package seqPlots (http://github.com/przemol/seqplots). For metagenes, transcripts were scaled to 1000 nucleotides (nt) between the TSS and transcription termination site (TTS). For metagenes across ORFs, transcripts were scaled to 1000 nt between the TSS and TTS. Metagenes were also plotted for 600 nt upstream of the TSS as well as 600 nt downstream from the TTS and scaled 1:1. Heat maps were plotted of fixed distances upstream of and downstream from TSS, BP, and 3′SS sequences, separately for intron-containing RPGs and non-RPGs.

ChIP and quantitative PCR

Cells were grown in YPD to an OD_{600} between 0.5 and 0.7 and then cross-linked for 15 min at room temperature with formaldehyde to a final concentration of 1%. Cross-linking was quenched for 5 min at room temperature with glycine to a final concentration of 125 mM. Cells were disrupted with 0.5-mm glass beads for 40 min at 4°C. To shear chromatin for Msl1 samples, lysates were sonicated for a total of 3 min and 20 sec at 15% intensity (10 sec on and 15 sec off on ice). For all other samples, lysates were sonicated for a total of 2 min and 30 sec. After sonication, lysates were cleared by centrifugation. For Msl1, Prp42, and Snu114, samples were then used for immunoprecipitation with anti-HA Y11 (Santa Cruz Biotechnology). For Rpb3 and Ser2 samples, samples were used for immunoprecipitation with anti-Rpb3 (BioLegend) and anti-phospho-S2 (Abcam), respectively. After immunoprecipitation, samples were washed and incubated overnight at 65°C to reverse cross-linking.

All samples were incubated with Proteinase K (Sigma) and RNase A (Ambion) followed by purification using a PCR product purification kit (Qiagen).

DNA samples were then analyzed by real-time PCR. Input DNA was diluted 1:10, and 1 µL of this was used in a 20-µL (for Msl1 and Prp42) or 10-µL (for Snu114, Ser-2, and Rpb3) reaction volume. For ChIP DNA, samples were diluted 1:2, and 1 µL of this was used in a 20- or 10-µL reaction volume. Reactions consisted of 1× Perfecta SYBR Green master mix (Quanta Biosciences) and 0.5 µL of primers. Real-time PCR was performed using a CFX96 touch system (Bio-Rad). All samples were run in technical duplicate for each independent experiment.

For quantification, standard curves were generated for each primer set, and DNA concentration for each input and ChIP sample

was calculated. ChIP values were divided by the input, and these values were divided by the nontranscribed control and expressed as fold accumulation over the nontranscribed control. Reported values are averages of three or more independent experiments, and error bars represent the standard error of the mean.

Acknowledgments

This work was supported by grants to T.L.J. from the National Institute of General Medical Sciences (GM-085474 and U01 HG007912), and grants to T.L.K. from the Research Corporation for the Advancement of Science (Cottrell College Science award no. 20186) and the National Institutes of Health (R15GM122026). This work was also supported by the Cellular and Molecular Biology Training Program Ruth L. Kirschstein National Research Service Award (GM007185) (awarded to L.T.N.) and the Whitcome Predoctoral Fellowship in Molecular Biology (awarded to L.T.N. and S.V.). We also acknowledge support from a Quantitative and Computational Biosciences (QCB) Collaboratory Post-doctoral Fellowship (awarded to R.S.) and the OCB Collaborator community, directed by Matteo Pellegrini. We acknowledge Dr. Alexander Hoffmann for providing mentorship to R.S.

References

Albulescu LO, Sabet N, Gudipati M, Stepankiw N, Bergman ZJ, Huffaker TC, Pleiss JA. 2012. A quantitative, high-throughput reverse genetic screen reveals novel connections between Pre-mRNA splicing and 5′ and 3′ end transcript determinants. *PLoS Genet* **8:** e1002530.

Alexander RD, Innocente SA, Barrass JD, Beggs JD. 2010. Splicing-dependent RNA polymerase pausing in yeast. *Mol Cell* **40:** 582–593.

Allepuz-Fuster P, Martinez-Fernandez V, Garrido-Godino AI, Alonso-Aguado S, Hanes SD, Navarro F, Calvo O. 2014. Rpb4/7 facilitates RNA polymerase II CTD dephosphorylation. *Nucleic Acids Res* **42:** 13674–13688.

Amberg DC, Burke D, Strathern J. 2005. *Methods in yeast genetics: a Cold Spring Harbor Laboratory course manual.* Cold Spring Harbor Laboratory Press, Cold Spring Harbor, NY.

Amit M, Donyo M, Hollander D, Goren A, Kim E, Gelfman S, Lev-Maor G, Burstein D, Schwartz S, Postolsky B, et al. 2012. Differential GC content between exons and introns establishes distinct strategies of splice-site recognition. *Cell Rep* **1:** 543–556.

Arenas JE, Abelson JN. 1997. Prp43: an RNA helicase-like factor involved in spliceosome disassembly. *Proc Natl Acad Sci* **94:** 11798–11802.

Bauren G, Wieslander L. 1994. Splicing of Balbiani ring 1 gene pre-mRNA occurs simultaneously with transcription. *Cell* **76:** 183–192.

Bauren G, Jiang WQ, Bernholm K, Gu F, Wieslander L. 1996. Demonstration of a dynamic, transcription-dependent organization of pre-mRNA splicing factors in polytene nuclei. *J Cell Biol* **133:** 929–941.

Beyer AL, Osheim YN. 1988. Splice site selection, rate of splicing, and alternative splicing on nascent transcripts. *Genes Dev* **2:** 754–765.

Beyer AL, Osheim YN. 1991. Visualization of RNA transcription and processing. *Semin Cell Biol* **2:** 131–140.

Bousquet-Antonelli C, Presutti C, Tollervey D. 2000. Identification of a regulated pathway for nuclear pre-mRNA turnover. *Cell* **102:** 765–775.

Braberg H, Jin H, Moehle EA, Chan YA, Wang S, Shales M, Benschop JJ, Morris JH, Qiu C, Hu F, et al. 2013. From structure to systems: high-resolution, quantitative genetic analysis of RNA polymerase II. *Cell* **154:** 775–788.

Brown SJ, Stoilov P, Xing Y. 2012. Chromatin and epigenetic regulation of pre-mRNA processing. *Hum Mol Genet* **21:** R90–R96.

Carey LB. 2015. RNA polymerase errors cause splicing defects and can be regulated by differential expression of RNA polymerase subunits. *Elife* **4:** e09945.

Carrillo Oesterreich F, Preibisch S, Neugebauer KM. 2010. Global analysis of nascent RNA reveals transcriptional pausing in terminal exons. *Mol Cell* **40:** 571–581.

Carrillo Oesterreich F, Bieberstein N, Neugebauer KM. 2011. Pause locally, splice globally. *Trends Cell Biol* **21:** 328–335.

Chathoth KT, Barrass JD, Webb S, Beggs JD. 2014. A splicing-dependent transcriptional checkpoint associated with prespliceosome formation. *Mol Cell* **53:** 779–790.

Chen HC, Cheng SC. 2012. Functional roles of protein splicing factors. *Biosci Rep* **32:** 345–359.

Chen HC, Tseng CK, Tsai RT, Chung CS, Cheng SC. 2013. Link of NTR-mediated spliceosome disassembly with DEAH-box ATPases Prp2, Prp16, and Prp22. *Mol Cell Biol* **33:** 514–525.

Churchman LS, Weissman JS. 2011. Nascent transcript sequencing visualizes transcription at nucleotide resolution. *Nature* **469:** 368–373.

Combs DJ, Nagel RJ, Ares M Jr, Stevens SW. 2006. Prp43p is a DEAH-box spliceosome disassembly factor essential for ribosome biogenesis. *Mol Cell Biol* **26:** 523–534.

Davidson L, Muniz L, West S. 2014. 3′ end formation of pre-mRNA and phosphorylation of Ser2 on the RNA polymerase II CTD are reciprocally coupled in human cells. *Genes Dev* **28:** 342–356.

de la Mata M, Alonso CR, Kadener S, Fededa JP, Blaustein M, Pelisch F, Cramer P, Bentley D, Kornblihtt AR. 2003. A slow RNA polymerase II affects alternative splicing in vivo. *Mol Cell* **12:** 525–532.

Dobin A, Davis CA, Schlesinger F, Drenkow J, Zaleski C, Jha S, Batut P, Chaisson M, Gingeras TR. 2013. STAR: ultrafast universal RNA-seq aligner. *Bioinformatics* **29:** 15–21.

Dujardin G, Kornblihtt AR, Corcos L. 2014. [Kinetic regulation of pre-messenger RNA alternative splicing]. *Med Sci (Paris)* **30:** 940–943.

Fong N, Kim H, Zhou Y, Ji X, Qiu J, Saldi T, Diener K, Jones K, Fu XD, Bentley DL. 2014. Pre-mRNA splicing is facilitated by an optimal RNA polymerase II elongation rate. *Genes Dev* **28:** 2663–2676.

Freedman MS, Kaplan JM, Markovic-Plese S. 2013. Insights into the mechanisms of the therapeutic efficacy of alemtuzumab in multiple sclerosis. *J Clin Cell Immunol* **4:** 1000152.

Garcia A, Rosonina E, Manley JL, Calvo O. 2010. Sub1 globally regulates RNA polymerase II C-terminal domain phosphorylation. *Mol Cell Biol* **30:** 5180–5193.

Garcia A, Collin A, Calvo O. 2012. Sub1 associates with Spt5 and influences RNA polymerase II transcription elongation rate. *Mol Biol Cell* **23:** 4297–4312.

Ghavi-Helm Y, Michaut M, Acker J, Aude JC, Thuriaux P, Werner M, Soutourina J. 2008. Genome-wide location analysis reveals a role of TFIIS in RNA polymerase III transcription. *Genes Dev* **22:** 1934–1947.

Goldstein AL, McCusker JH. 1999. Three new dominant drug resistance cassettes for gene disruption in *Saccharomyces cerevisiae*. *Yeast (Chichester, England)* **15:** 1541–1553.

Gornemann J, Kotovic KM, Hujer K, Neugebauer KM. 2005. Cotranscriptional spliceosome assembly occurs in a stepwise

fashion and requires the cap binding complex. *Mol Cell* **19:** 53–63.
Gottschalk A, Bartels C, Neubauer G, Luhrmann R, Fabrizio P. 2001. A novel yeast U2 snRNP protein, Snu17p, is required for the first catalytic step of splicing and for progression of spliceosome assembly. *Mol Cell Biol* **21:** 3037–3046.
Grate L, Ares M Jr. 2002. Searching yeast intron data at Ares lab Web site. *Methods Enzymol* **350:** 380–392.
Gu M, Naiyachit Y, Wood TJ, Millar CB. 2015. H2A.Z marks antisense promoters and has positive effects on antisense transcript levels in budding yeast. *BMC Genomics* **16:** 99.
Guillemette B, Bataille AR, Gevry N, Adam M, Blanchette M, Robert F, Gaudreau L. 2005. Variant histone H2A.Z is globally localized to the promoters of inactive yeast genes and regulates nucleosome positioning. *PLoS Biol* **3:** e384.
Gunderson FQ, Johnson TL. 2009. Acetylation by the transcriptional coactivator Gcn5 plays a novel role in co-transcriptional spliceosome assembly. *PLoS Genet* **5:** e1000682.
Gunderson FQ, Merkhofer EC, Johnson TL. 2011. Dynamic histone acetylation is critical for cotranscriptional spliceosome assembly and spliceosomal rearrangements. *Proc Natl Acad Sci* **108:** 2004–2009.
Guo R, Zheng L, Park JW, Lv R, Chen H, Jiao F, Xu W, Mu S, Wen H, Qiu J, et al. 2014. BS69/ZMYND11 reads and connects histone H3.3 lysine 36 trimethylation-decorated chromatin to regulated pre-mRNA processing. *Mol Cell* **56:** 298–310.
Hossain MA, Claggett JM, Nguyen T, Johnson TL. 2009. The cap binding complex influences H2B ubiquitination by facilitating splicing of the SUS1 pre-mRNA. *RNA* **15:** 1515–1527.
Hossain MA, Rodriguez CM, Johnson TL. 2011. Key features of the two-intron *Saccharomyces cerevisiae* gene *SUS1* contribute to its alternative splicing. *Nucleic Acids Res* **39:** 8612–8627.
Howe KJ, Kane CM, Ares M Jr. 2003. Perturbation of transcription elongation influences the fidelity of internal exon inclusion in *Saccharomyces cerevisiae*. *RNA* **9:** 993–1006.
Hsin JP, Manley JL. 2012. The RNA polymerase II CTD coordinates transcription and RNA processing. *Genes Dev* **26:** 2119–2137.
Huang S, Spector DL. 1996. Intron-dependent recruitment of pre-mRNA splicing factors to sites of transcription. *J Cell Biol* **133:** 719–732.
Kawashima T, Douglass S, Gabunilas J, Pellegrini M, Chanfreau GF. 2014. Widespread use of non-productive alternative splice sites in *Saccharomyces cerevisiae*. *PLoS Genet* **10:** e1004249.
Kobor MS, Venkatasubrahmanyam S, Meneghini MD, Gin JW, Jennings JL, Link AJ, Madhani HD, Rine J. 2004. A protein complex containing the conserved Swi2/Snf2-related ATPase Swr1p deposits histone variant H2A.Z into euchromatin. *PLoS Biol* **2:** E131.
Komarnitsky P, Cho EJ, Buratowski S. 2000. Different phosphorylated forms of RNA polymerase II and associated mRNA processing factors during transcription. *Gene Dev* **14:** 2452–2460.
Koodathingal P, Staley JP. 2013. Splicing fidelity DEAD/H-box ATPases as molecular clocks. *RNA Biol* **10:** 1073–1079.
Koodathingal P, Novak T, Piccirilli JA, Staley JP. 2010. The DEAH box ATPases Prp16 and Prp43 cooperate to proofread 5′ splice site cleavage during pre-mRNA splicing. *Mol Cell* **39:** 385–395.
Kotovic KM, Lockshon D, Boric L, Neugebauer KM. 2003. Cotranscriptional recruitment of the U1 snRNP to intron-containing genes in yeast. *Mol Cell Biol* **23:** 5768–5779.
Krogan NJ, Keogh MC, Datta N, Sawa C, Ryan OW, Ding H, Haw RA, Pootoolal J, Tong A, Canadien V, et al. 2003. A Snf2 family ATPase complex required for recruitment of the histone H2A variant Htz1. *Mol Cell* **12:** 1565–1576.
Lacadie SA, Rosbash M. 2005. Cotranscriptional spliceosome assembly dynamics and the role of U1 snRNA:5′ss base pairing in yeast. *Mol Cell* **19:** 65–75.
Lacadie SA, Tardiff DF, Kadener S, Rosbash M. 2006. In vivo commitment to yeast cotranscriptional splicing is sensitive to transcription elongation mutants. *Genes Dev* **20:** 2055–2066.
Larimer FW, Stevens A. 1990. Disruption of the gene *XRN1*, coding for a 5′ → 3′ exoribonuclease, restricts yeast cell growth. *Gene* **95:** 85–90.
Leeds NB, Small EC, Hiley SL, Hughes TR, Staley JP. 2006. The splicing factor Prp43p, a DEAH box ATPase, functions in ribosome biogenesis. *Mol Cell Biol* **26:** 513–522.
Li Z, Gadue P, Chen K, Jiao Y, Tuteja G, Schug J, Li W, Kaestner KH. 2012. Foxa2 and H2A.Z mediate nucleosome depletion during embryonic stem cell differentiation. *Cell* **151:** 1608–1616.
Listerman I, Sapra AK, Neugebauer KM. 2006. Cotranscriptional coupling of splicing factor recruitment and precursor messenger RNA splicing in mammalian cells. *Nat Struct Mol Biol* **13:** 815–822.
Longtine MS, McKenzie A III, Demarini DJ, Shah NG, Wach A, Brachat A, Philippsen P, Pringle JR. 1998. Additional modules for versatile and economical PCR-based gene deletion and modification in *Saccharomyces cerevisiae*. *Yeast (Chichester, England)* **14:** 953–961.
Luco RF, Pan Q, Tominaga K, Blencowe BJ, Pereira-Smith OM, Misteli T. 2010. Regulation of alternative splicing by histone modifications. *Science* **327:** 996–1000.
Malagon F, Tong AH, Shafer BK, Strathern JN. 2004. Genetic interactions of DST1 in *Saccharomyces cerevisiae* suggest a role of TFIIS in the initiation-elongation transition. *Genetics* **166:** 1215–1227.
Malik I, Qiu C, Snavely T, Kaplan CD. 2017. Wide-ranging and unexpected consequences of altered Pol II catalytic activity in vivo. *Nucleic Acids Res* doi: 10.1093/nar/gkx037.
Maniatis T, Reed R. 2002. An extensive network of coupling among gene expression machines. *Nature* **416:** 499–506.
Mason PB, Struhl K. 2005. Distinction and relationship between elongation rate and processivity of RNA polymerase II in vivo. *Mol Cell* **17:** 831–840.
Merkhofer EC, Hu P, Johnson TL. 2014. Introduction to cotranscriptional RNA splicing. *Methods Mol Biology* **1126:** 83–96.
Mizuguchi G, Shen X, Landry J, Wu WH, Sen S, Wu C. 2004. ATP-driven exchange of histone H2AZ variant catalyzed by SWR1 chromatin remodeling complex. *Science* **303:** 343–348.
Moehle EA, Ryan CJ, Krogan NJ, Kress TL, Guthrie C. 2012. The yeast SR-like protein Npl3 links chromatin modification to mRNA processing. *PLoS Genet* **8:** e1003101.
Munding EM, Shiue L, Katzman S, Donohue JP, Ares M Jr. 2013. Competition between pre-mRNAs for the splicing machinery drives global regulation of splicing. *Mol Cell* **51:** 338–348.
Naftelberg S, Schor IE, Ast G, Kornblihtt AR. 2015. Regulation of alternative splicing through coupling with transcription and chromatin structure. *Annu Rev Biochem* **84:** 165–198.
Nissen KE, Homer CM, Ryan CJ, Shales M, Krogan NJ, Patrick KL, Guthrie C. 2017. The histone variant H2A.Z promotes splicing of weak introns. *Genes Dev* (this issue). doi: 10.1101/gad.295287.116.
Oesterreich FC, Herzel L, Straube K, Hujer K, Howard J, Neugebauer KM. 2016. Splicing of nascent RNA coincides with intron exit from RNA polymerase II. *Cell* **165:** 372–381.
Ono B, Yoshida R, Kamiya K, Sugimoto T. 2005. Suppression of termination mutations caused by defects of the NMD

machinery in *Saccharomyces cerevisiae*. *Genes Genet Syst* **80:** 311–316.
Petesch SJ, Lis JT. 2012. Overcoming the nucleosome barrier during transcript elongation. *Trends Genet* **28:** 285–294.
Raisner RM, Hartley PD, Meneghini MD, Bao MZ, Liu CL, Schreiber SL, Rando OJ, Madhani HD. 2005. Histone variant H2A.Z marks the 5′ ends of both active and inactive genes in euchromatin. *Cell* **123:** 233–248.
Ranjan A, Mizuguchi G, FitzGerald PC, Wei D, Wang F, Huang Y, Luk E, Woodcock CL, Wu C. 2013. Nucleosome-free region dominates histone acetylation in targeting SWR1 to promoters for H2A.Z replacement. *Cell* **154:** 1232–1245.
Rege M, Subramanian V, Zhu C, Hsieh TH, Weiner A, Friedman N, Clauder-Munster S, Steinmetz LM, Rando OJ, Boyer LA, et al. 2015. Chromatin dynamics and the RNA exosome function in concert to regulate transcriptional homeostasis. *Cell Rep* **13:** 1610–1622.
Rudnizky S, Bavly A, Malik O, Pnueli L, Melamed P, Kaplan A. 2016. H2A.Z controls the stability and mobility of nucleosomes to regulate expression of the LH genes. *Nat Commun* **7:** 12958.
Sadeghi L, Bonilla C, Stralfors A, Ekwall K, Svensson JP. 2011. Podbat: a novel genomic tool reveals Swr1-independent H2A.Z incorporation at gene coding sequences through epigenetic meta-analysis. *PLoS Comput Biol* **7:** e1002163.
Saldi T, Cortazar MA, Sheridan RM, Bentley DL. 2016. Coupling of RNA Polymerase II Transcription Elongation with Pre-mRNA Splicing. *J Mol Biol* **428:** 2623–2635.
Santisteban MS, Kalashnikova T, Smith MM. 2000. Histone H2A.Z regulates transcription and is partially redundant with nucleosome remodeling complexes. *Cell* **103:** 411–422.
Santisteban MS, Hang M, Smith MM. 2011. Histone variant H2A.Z and RNA polymerase II transcription elongation. *Mol Cell Biol* **31:** 1848–1860.
Sayani S, Chanfreau GF. 2012. Sequential RNA degradation pathways provide a fail-safe mechanism to limit the accumulation of unspliced transcripts in *Saccharomyces cerevisiae*. *RNA* **18:** 1563–1572.
Schwartz S, Meshorer E, Ast G. 2009. Chromatin organization marks exon–intron structure. *Nat Struct Mol Biol* **16:** 990–995.
Semlow DR, Blanco MR, Walter NG, Staley JP. 2016. Spliceosomal DEAH-Box ATPases remodel pre-mRNA to activate alternative splice sites. *Cell* **164:** 985–998.
Sims RJ III, Millhouse S, Chen CF, Lewis BA, Erdjument-Bromage H, Tempst P, Manley JL, Reinberg D. 2007. Recognition of trimethylated histone H3 lysine 4 facilitates the recruitment of transcription postinitiation factors and pre-mRNA splicing. *Mol Cell* **28:** 665–676.
Sorenson MR, Stevens SW. 2014. Rapid identification of mRNA processing defects with a novel single-cell yeast reporter. *RNA* **20:** 732–745.
Sorenson MR, Jha DK, Ucles SA, Flood DM, Strahl BD, Stevens SW, Kress TL. 2016. Histone H3K36 methylation regulates pre-mRNA splicing in *Saccharomyces cerevisiae*. *RNA Biol* **13:** 412–426.
Spingola M, Ares M Jr. 2000. A yeast intronic splicing enhancer and Nam8p are required for Mer1p-activated splicing. *Mol Cell* **6:** 329–338.
Subramanian V, Fields PA, Boyer LA. 2015. H2A.Z: a molecular rheostat for transcriptional control. *F1000Prime Rep* **7:** 01.
Tang J, Abovich N, Rosbash M. 1996. Identification and characterization of a yeast gene encoding the U2 small nuclear ribonucleoprotein particle B″ protein. *Mol Cell Biol* **16:** 2787–2795.
Tardiff DF, Rosbash M. 2006. Arrested yeast splicing complexes indicate stepwise snRNP recruitment during in vivo spliceosome assembly. *RNA* **12:** 968–979.
Tolstorukov MY, Goldman JA, Gilbert C, Ogryzko V, Kingston RE, Park PJ. 2012. Histone variant H2A.Bbd is associated with active transcription and mRNA processing in human cells. *Mol Cell* **47:** 596–607.
Tramantano M, Sun L, Au C, Labuz D, Liu Z, Chou M, Shen C, Luk E. 2016. Constitutive turnover of histone H2A.Z at yeast promoters requires the preinitiation complex. *Elife* **5:** e14243.
Wan Y, Saleem RA, Ratushny AV, Roda O, Smith JJ, Lin CH, Chiang JH, Aitchison JD. 2009. Role of the histone variant H2A.Z/Htz1p in TBP recruitment, chromatin dynamics, and regulated expression of oleate-responsive genes. *Mol Cell Biol* **29:** 2346–2358.
Weber CM, Henikoff JG, Henikoff S. 2010. H2A.Z nucleosomes enriched over active genes are homotypic. *Nat Struct Mol Biol* **17:** 1500–1507.
Weber CM, Ramachandran S, Henikoff S. 2014. Nucleosomes are context-specific, H2A.Z-modulated barriers to RNA polymerase. *Mol Cell* **53:** 819–830.
Zhang H, Roberts DN, Cairns BR. 2005. Genome-wide dynamics of Htz1, a histone H2A variant that poises repressed/basal promoters for activation through histone loss. *Cell* **123:** 219–231.
Zlatanova J, Thakar A. 2008. H2A.Z: view from the top. *Structure* **16:** 166–179.

The histone variant H2A.Z promotes efficient co-transcriptional splicing in *S. cerevisiae*

Lauren T. Neves[1,2], Stephen Douglass[1], Roberto Spreafico[4], Srivats Venkataramanan[1], Tracy L. Kress[5] and Tracy L. Johnson, Ph.D.[1,3]*

Supplemental Materials and Methods

RNA-seq minimum-read filters: Raw reads for two biological replicate samples of wild-type, *xrn1*Δ, and *upf1*Δ cells were normalized based on read depth. The geometric mean of both spliced and unspliced reads was calculated for each gene in each pair of biological replicates. The minimum-read threshold was defined as a geometric mean of 10 counts. Any genes with a geometric mean of <10 spliced counts or <10 unspliced counts (Figure S3, in orange) were deemed noise and disregarded in the analysis. Due to the high number of unusual isoforms, YKL186C was omitted for this study. Thresholds for *xrn1*Δ samples were applied to *prp43*^{DAmP} sample analysis (Figures 7 and S9). Number of genes that passed threshold: WT background: RPG n = 90, non-RPG n =129; *xrn1*Δ, *prp43*^{DAmP} background: RPG n=92, non-RPG n=164; *upf1*Δ background: RPG n=92, non-RPG n=141.

qRT-PCR analysis and quantification: For qRT-PCR analysis of *mud1*Δ and *isy1*Δ mutants: RNA isolation, cDNA synthesis and qPCR was performed as previously described (Kress et. al, 2008). Yeast cultures were grow at 30°C n to OD 0.35-0.5 and shifted to 37°C for 30 minutes. RNA was isolated using hot phenol chloroform extraction. Prior to conversion to cDNA, 10 ug RNA was treated with 5 units of RQ1 DNase I (Promega) for 40 min. at 37°C and cDNA was then generated using 1ug dN_9

oligo. The reverse transcription reaction was stopped with 1.0 mL of water. QPCR was performed using a Stratagene MX3500) with 58°C annealing for 35 cycles (20 uL of cDNA and 0.5 uL Taq DNA polymerase (NEB standard Taq). cDNA was analyzed by qPCR with primers that detect the intron levels or the total levels of the mRNA. Percent unspliced RNA (pre-mRNA) was determined by dividing the relative amounts of the intron product (pre-mRNA) by the relative amount of the total product (total mRNA) and multiplying by 100. A standard curve was generated using 100 ng of genomic DNA isolated from WT cells titrated 2-fold down to 1.25 ng.

Whole cell extract and immunoblot: Cells were grown in YPD media to an OD_{600} between 0.5-0.7 and lysed using FA-1 Lysis buffer (50mM HEPES-KOH pH 7.5, 140 mM NaCl, 1 mM EDTA pH 8.0, 1% Triton-X, .1% Deoxycholate, plus protease inhibitors) and .3 mm glass beads with 5 minutes of vortexing at 4°C. The supernated was cleared by centrifugation and protein concentration was determined by spectrophotometer. Total protein was resolved by a 15% SDS-PAGE and transferred to a PVDF membrane for immunoblotting with a 1:4000 dilution of anti-PGK (Molecular Probes) and a 1:10,000 dilution of anti-HA 12CA5 (Roche), 1:5000 dilution of anti-Rpb3 (BioLegend) or a 1:5000 dilution of anti-phospho S2 (Abcam). Signal was detected using Pierce ECL Western Blotting Solution (ThermoScientific).

Supplemental Figure Legends

Figure S1: Splicing of non-consensus splice sites

A. Distribution of changes in splicing in groups of intron-containing genes characterized by RPGs or nonRPGs, and any consensus or non-consensus splice sites.

   c5'ss: consensus 5' splice site. cBP: consensus branch point. c3'SS: consensus 3' splice site. nc5'ss: non-consensus 5' splice site. ncBP: non-consensus branch point. nc3'SS: non-consensus 3' splice

B. Venn diagram representing overlap of intron-containing genes with ≥10% splicing defect in WT, *xrn1*Δ, and *upf1*Δ cells.

Figure S2: Genetic interactions and splicing profile of *swr1*Δ cells resembles those of *htz1*Δ cells.

A. Serial dilution assay of double mutants, *mud1*Δ *swr1*Δ and *isy1*Δ *swr1*Δ. Cells were grown at 30°C in YPD liquid media until desired OD_{600} was obtained. Cells were spotted as a ten-fold dilution onto YPD plates and incubated at 30°C or 37°C for two days.

B. Distribution in splicing efficiencies of all intron-containing genes upon deletion of *SWR1* in either WT (left), *xrn1*Δ (middle) or *upf1*Δ (right) cells, represented as an X-Y plot. RPGs are denoted in orange.

C. Comparison of splicing efficiencies of all intron-containing genes upon deletion of *HTZ1* or *SWR1* in WT(left), *xrn1*Δ (middle) or *upf1*Δ (right) cells, represented as an X-Y plot.

D. Comparison of change in splicing efficiencies of all intron-containing genes in the WT background upon deletion of *HTZ1* or *SWR1*, represented as an X-Y plot. There is strong overlap in the subset of genes whose splicing is negatively affected in *htz1*Δ cells and *swr1*Δ cells (3rd quadrant).

Figure S3: Analysis of RNA-seq samples removed by minimum-read filter.

A. As in Figures 2A and 2B, but including genes removed by filtering process. Distribution in splicing efficiencies of all intron-containing genes upon deletion of *HTZ1*, represented as an X-Y plot, in WT (left), *xrn1*Δ (middle), or *upf1*Δ (right) cells. Genes that did not pass our minimum-read filter are indicated by open circles.

B. As in Figure 2C, but including genes removed by filtering process. Distribution of changes in splicing efficiency upon deletion of *HTZ1* compared to RPKM in WT (top), *xrn1*Δ (middle) and *upf1*Δ (bottom) cells. Vertical dotted line represents RPKM of 150. Horizontal lines represent 10% change in splicing efficiency. Genes that did not pass our minimum-read filter are indicated by open circles. Changes in splicing of removed points are evenly distributed between increased and decreased splicing (Chi-square test, p-values indicated).

Figure S4: H2A.Z affects splicing of ribosomal protein genes when the spliceosome is compromised.

A. RT-qPCR analysis of levels of unspliced (pre-mRNA) products of nonRPGs in WT, *mud1*Δ, and *isy1*Δ cells ± *HTZ1*. cDNA was collected after temperature shift

to 37°C for 30 minutes. Graphs represent average of three to four independent experiments and error bars represent the SEM.

B. Top: Analysis of intron-containing RPGs by RT-PCR in the presence and absence of HTZ1. Products were analyzed on 6% PAGE gels. Pre-mRNA size indicated by genomic DNA size. Bottom: Quantification of intron-containing RPG RT-PCR products. pre-mRNA denoted in grey and spliced mRNA denoted in black. Graphs represent the average of two independent experiments and error bars represent the SD.

C. RT-qPCR analysis of levels of unspliced (pre-mRNA) products of RPGs in WT, *mud1*Δ, and *isy1*Δ cells ± *HTZ1*. cDNA was collected after temperature shift to 37°C for 30 minutes. Graphs represent average of three to four independent experiments and error bars represent the SEM.

Figure S5: H2A.Z-mediated splicing changes are not due to changes in spliceosome availability

A. Log-2 fold change in RPKM for all genes, general splicing factor genes (Table S1), and spliceosomal snRNAs upon deletion of *HTZ1* in WT (left), *xrn1*Δ (middle), or *upf1*Δ (right) cells. Less than 2-fold change was observed for all splicing factors and snRNAs.

B. Log-2 fold change in RPKM for all genes, and intron-containing RPGs upon deletion of *HTZ1* in WT (left), *xrn1*Δ (middle), or *upf1*Δ (right) cells. Less than 2-fold change was observed for all RPGs.

Figure S6: Deletion of *HTZ1* does not affect protein expression of ChIP splice factors or RNAPII core protein

A. Protein immunoblot of Msl1-HA and Lea1-HA strains used for ChIP assays in Figure 5D. WT and htz1Δ cultures were grown in YPD liquid media and whole cell extracts were prepared and probed with anti-HA 12CA5 (Roche) (top), and anti-PGK1 as a loading control (Molecular Probes) (bottom).
B. Protein immunoblot for Prp42-HA used for ChIP assays in Figure 5E. Samples prepared as in figure S5A.
C. Protein immunoblot for Snu114-HA used for ChIP assays in Figure 5F. Samples prepared as in figure S5A.
D. Protein immunoblot for Rpb3 and serine2-P used for ChIP assays in Figure 6B. Samples prepared as in figure S5A. Whole cell extracts were probed with anti-Rpb3 (BioLegend) (top), anti-phospho S2 (Abcam) (middle), and anti-PGK1 as a loading control (Molecular Probes) (bottom).

Figure S7: RNAPII CTD Ser-2 is phosphorylated earlier in gene body.

A. Schematic of intron-containing genes, *YCL002C, ECM33, RPL13A,* and intronless gene *PMA1*. Underlined numbers represent amplicons generated by each primer set used in this experiment.
B. Percent change in Rpb3 occupancy and Ser2-P enrichment (normalized to Rpb3) in *htz1*Δ cells as compared to WT.

Figure S8: Deletion of *DST1* exacerbates polymerase kinetics defect in cells lacking *HTZ1*.

A. Serial dilution assay of double mutant *dst1*Δ *htz1*Δ. Cells were grown at 30°C in YPD liquid media until desired OD_{600} was obtained. Cells were spotted as a ten-fold dilution onto YPD plates and incubated at 25°C, 30°C, or 37°C for two days.

B. Left: Analysis of candidate genes by RT-PCR in WT, and *dst1*Δ cells ± *HTZ1*. Products were analyzed on 6% PAGE gels (8% for *SUS1*). Pre-mRNA size indicated by genomic DNA size. Middle: Quantification of RT-PCR pre-mRNA products. Right: Quantification of *SUS1* RT-PCR pre-mRNA and splicing intermediate containing only the second *SUS1* intron. Quantification graphs represent the average of three independent experiments (four for *YCL002C* in WT) and error bars represent the SD.

C. Schematic of intron-containing genes, *YCL002C, ECM33,* and *RPL13A*. Underlined numbers represent amplicons generated by each primer set used in this experiment.

D. Occupancy of Msl1 at each region of *YCL002C* (left), *ECM33* (middle), or *RPL13A* (right) relative to the non-transcribed region in WT or *dst1*Δ. Graphs represent the average of six (WT) or three (*dst1*Δ) independent experiments and error bars represent the standard error of the means. P-values for each primer set determined by students t-test. Significant values indicated.

gDNA: genomic DNA. s: spliced mRNA product. *: p-value < .01 **: p-value < .001. ***: p-value < .0001.

Figure S9: *prp43*^{DAmP} decreases *PRP43* RNA levels and suppresses H2A.Z-mediated splice defects.

A. RT-qPCR analysis of levels of Prp43 RNA in WT and *prp43*^{DAmP} cells, normalized to *SCR1*, a RNAPIII transcript. Graphs represent average of three independent experiments and error bars represent the SD.

B. Analysis of candidate genes by RT-PCR in WT and *prp43*^{DAmP} cells ± *HTZ1.* Products were analyzed on 6% PAGE gels (8% for *SUS1*). Pre-mRNA size indicated by genomic DNA size.

C. Distribution in splicing efficiencies of all intron-containing genes in *prp43*^{DAmP} cells compared to WT cells.

D. Distribution of changes in splicing in groups of intron-containing genes characterized by RPGs or nonRPGs, and any consensus or non consensus splice sites.

c5'ss: consensus 5' splice site. cBP: consensus branch point. c3'SS: consensus 3' splice site. nc5'ss: non-consensus 5' splice site. ncBP: non-consensus branch point. nc3'SS: non-consensus 3' splice

Supplemental Table Legends

Supplemental Table S1: Splicing factors

List of all genes encoding splicing factors as defined by Chen & Cheng, 2012 [49].

Supplemental Table S2: Splicing factors

List of all strains described in this paper.

Supplemental Table S3: Plasmids

List of all plasmids used in this paper.

Supplemental Table S4: Primers

List of all primers used in this paper.

Supplemental Table S5: RNA-Seq Count Data

Splicing efficiency, unspliced and spliced counts, RPKMs for all genes. Replicate 2 data only pertains to figure S3.

Supplemental Figures

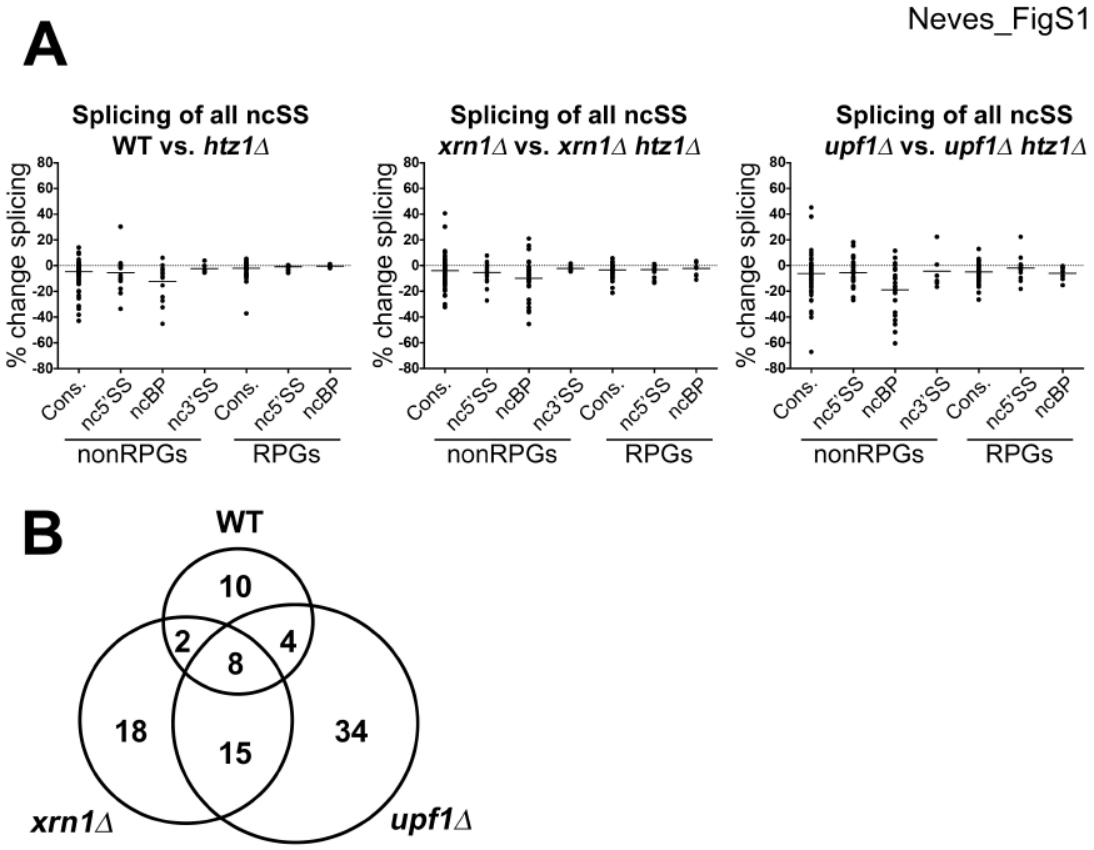

Neves_FigS2

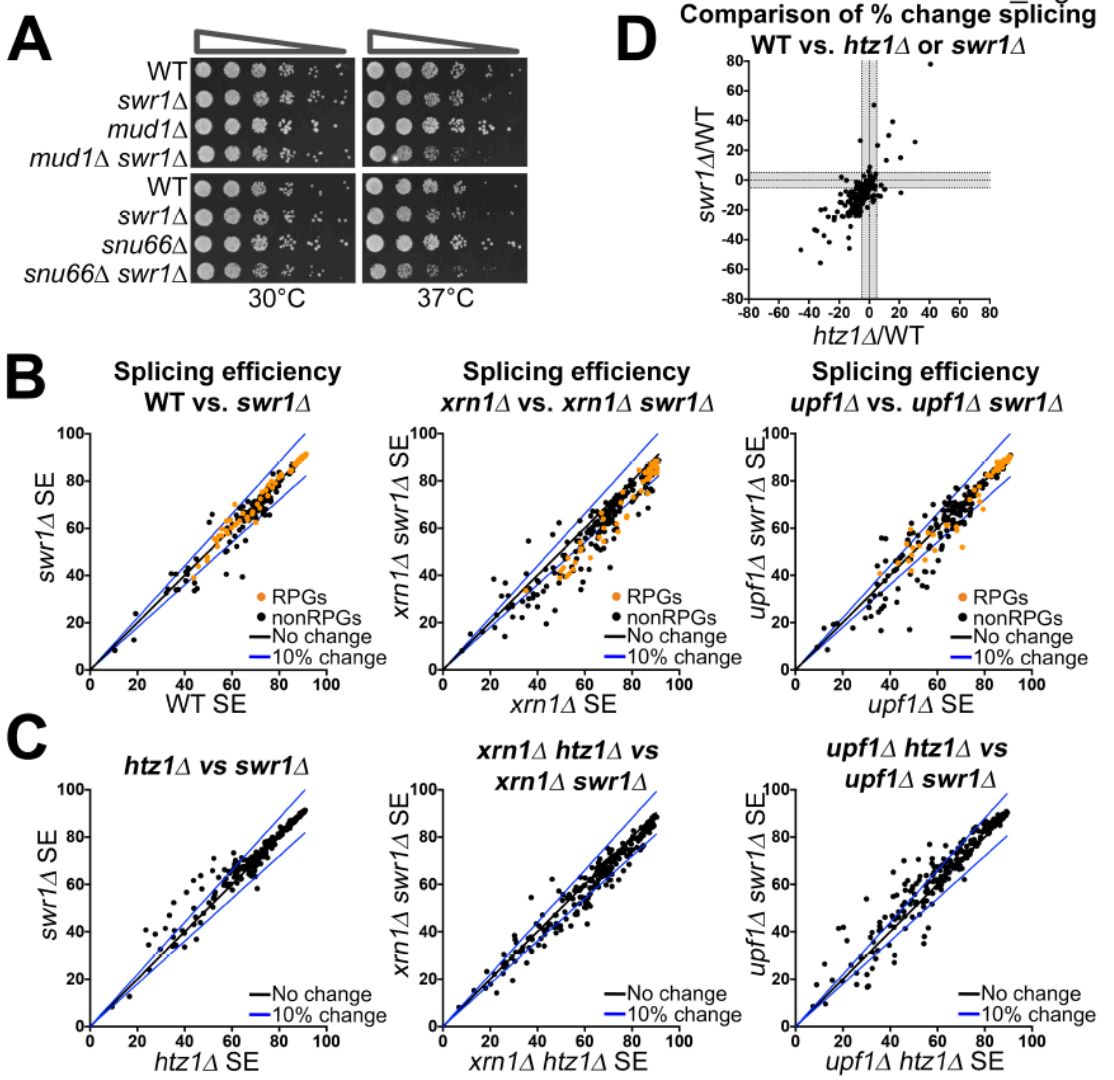
A
WT
swr1Δ
mud1Δ
mud1Δ swr1Δ
WT
swr1Δ
snu66Δ
snu66Δ swr1Δ
30°C
37°C
D
Comparison of % change splicing
WT vs. htz1Δ or swr1Δ
swr1Δ/WT
htz1Δ/WT
B
Splicing efficiency
WT vs. swr1Δ
swr1Δ SE
WT SE
Splicing efficiency
xrn1Δ vs. xrn1Δ swr1Δ
xrn1Δ swr1Δ SE
xrn1Δ SE
Splicing efficiency
upf1Δ vs. upf1Δ swr1Δ
upf1Δ swr1Δ SE
upf1Δ SE
RPGs
nonRPGs
No change
10% change
C
htz1Δ vs swr1Δ
swr1Δ SE
htz1Δ SE
xrn1Δ htz1Δ vs
xrn1Δ swr1Δ
xrn1Δ swr1Δ SE
xrn1Δ htz1Δ SE
upf1Δ htz1Δ vs
upf1Δ swr1Δ
upf1Δ swr1Δ SE
upf1Δ htz1Δ SE

Neves_FigS3

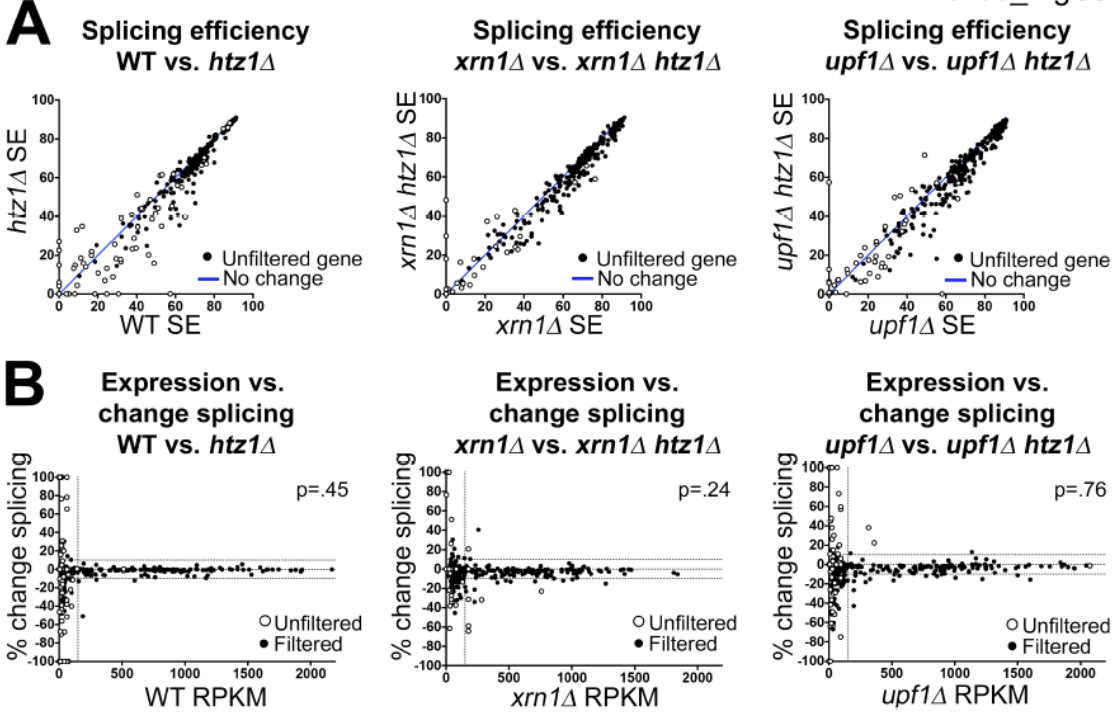
A
Splicing efficiency
WT vs. htz1Δ
htz1Δ SE
WT SE
Unfiltered gene
No change
Splicing efficiency
xrn1Δ vs. xrn1Δ htz1Δ
xrn1Δ htz1Δ SE
xrn1Δ SE
Unfiltered gene
No change
Splicing efficiency
upf1Δ vs. upf1Δ htz1Δ
upf1Δ htz1Δ SE
upf1Δ SE
Unfiltered gene
No change
B
Expression vs.
change splicing
WT vs. htz1Δ
% change splicing
WT RPKM
p=.45
Unfiltered
Filtered
Expression vs.
change splicing
xrn1Δ vs. xrn1Δ htz1Δ
% change splicing
xrn1Δ RPKM
p=.24
Unfiltered
Filtered
Expression vs.
change splicing
upf1Δ vs. upf1Δ htz1Δ
% change splicing
upf1Δ RPKM
p=.76
Unfiltered
Filtered

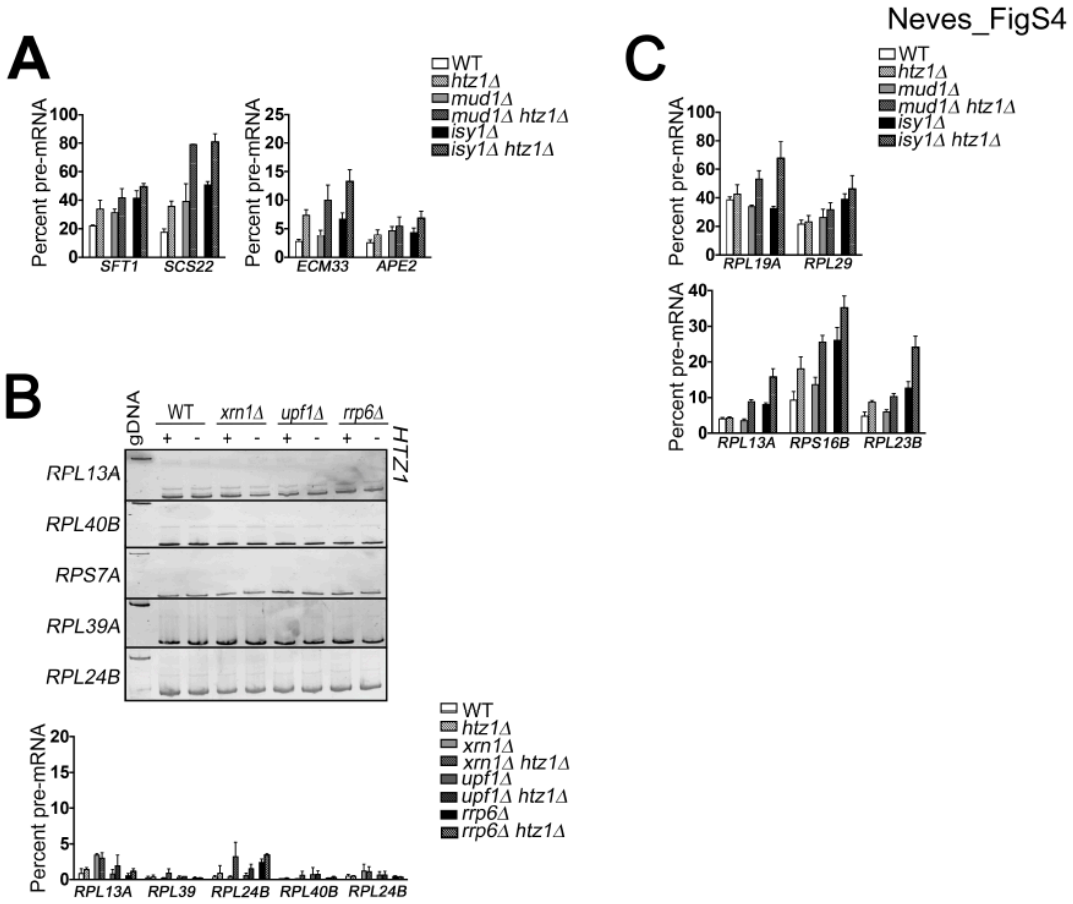
Neves_FigS4
A
Percent pre-mRNA
SFT1
SCS22
ECM33
APE2
WT
htz1Δ
mud1Δ
mud1Δ htz1Δ
isy1Δ
isy1Δ htz1Δ
B
gDNA
WT
xrn1Δ
upf1Δ
rrp6Δ
HTZ1
RPL13A
RPL40B
RPS7A
RPL39A
RPL24B
RPL13A
RPL39
RPL24B
RPL40B
RPL24B
xrn1Δ
xrn1Δ htz1Δ
upf1Δ
upf1Δ htz1Δ
rrp6Δ
rrp6Δ htz1Δ
C
RPL19A
RPL29
RPL13A
RPS16B
RPL23B

Neves_FigS5

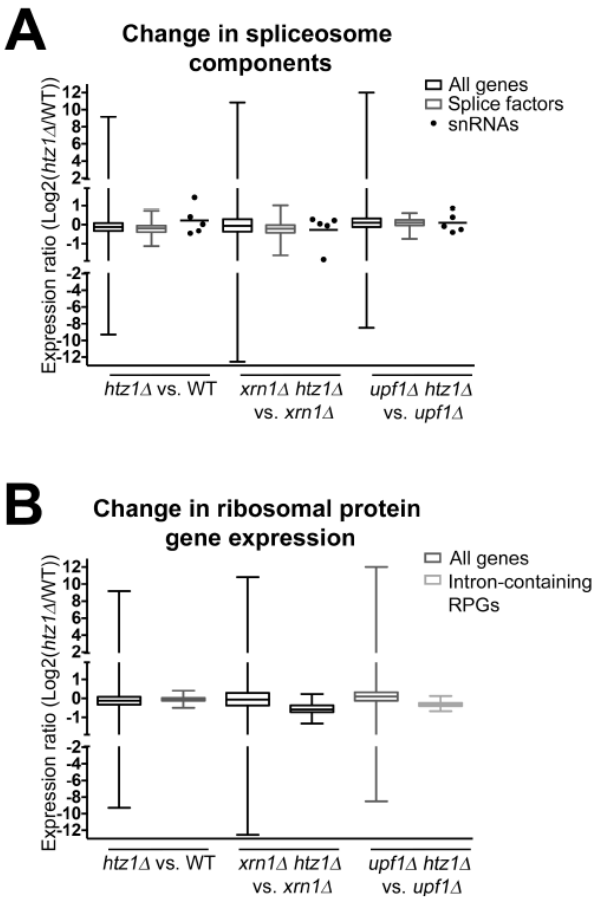
A
Change in spliceosome components
All genes
Splice factors
snRNAs
Expression ratio (Log2(htz1Δ/WT))
12
10
8
6
4
2
1
0
-1
-2
-4
-6
-8
-10
-12
htz1Δ vs. WT
xrn1Δ htz1Δ vs. xrn1Δ
upf1Δ htz1Δ vs. upf1Δ
B
Change in ribosomal protein gene expression
All genes
Intron-containing RPGs
Expression ratio (Log2(htz1Δ/WT))
htz1Δ vs. WT
xrn1Δ htz1Δ vs. xrn1Δ
upf1Δ htz1Δ vs. upf1Δ

Neves_FigS6

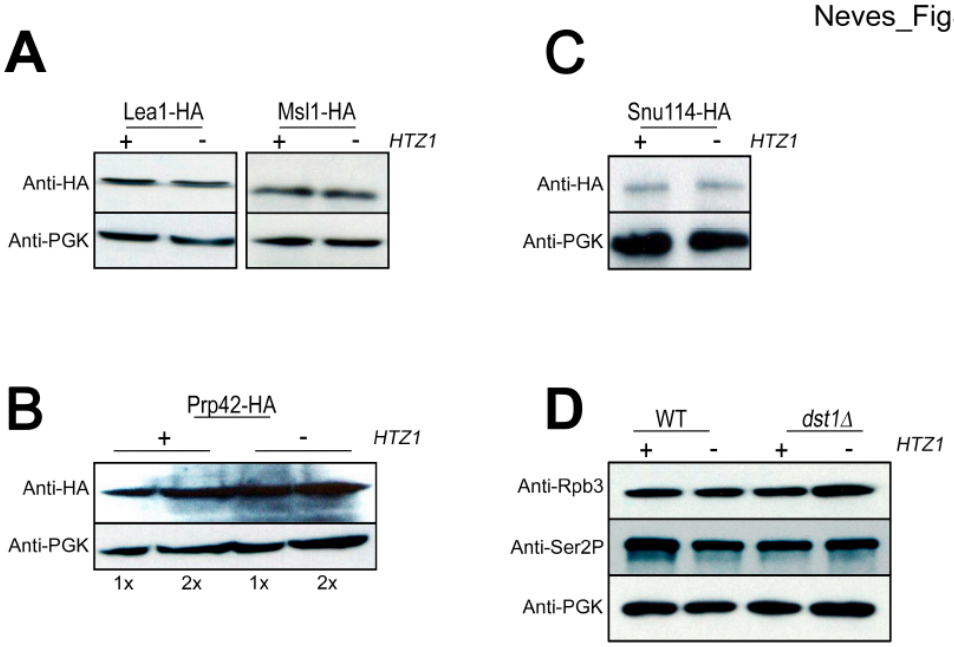
A
Lea1-HA
Msl1-HA
+ - + -
HTZ1
Anti-HA
Anti-PGK
C
Snu114-HA
+ -
HTZ1
Anti-HA
Anti-PGK
B
Prp42-HA
+ -
HTZ1
Anti-HA
Anti-PGK
1x 2x 1x 2x
D
WT
dst1Δ
+ - + -
HTZ1
Anti-Rpb3
Anti-Ser2P
Anti-PGK

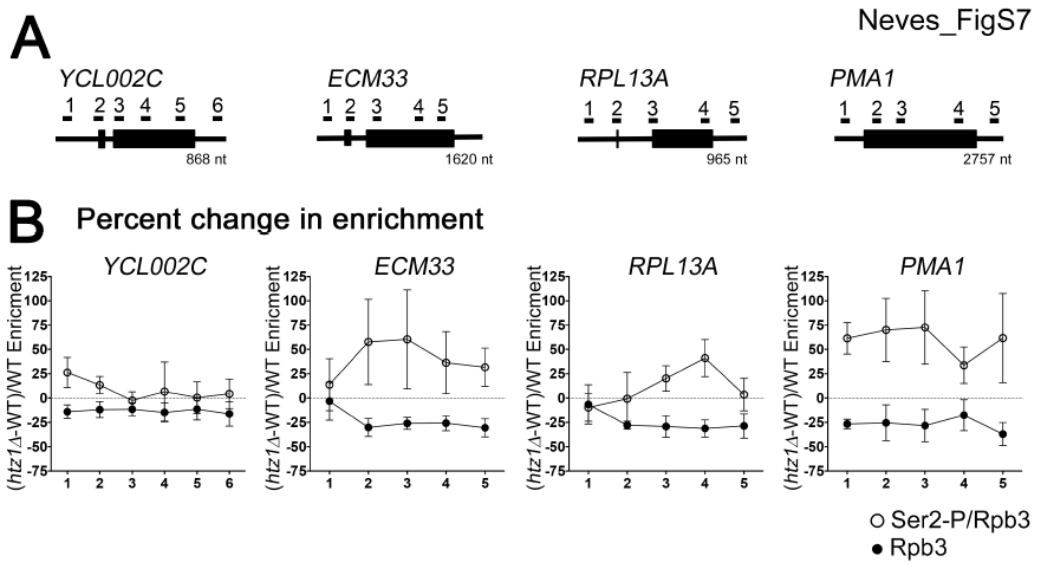
A
Neves_FigS7
YCL002C
1 2 3 4 5 6
868 nt
ECM33
1 2 3 4 5
1620 nt
RPL13A
1 2 3 4 5
965 nt
PMA1
1 2 3 4 5
2757 nt
B
Percent change in enrichment
YCL002C
ECM33
RPL13A
PMA1
(htz1Δ-WT)/WT Enricment
125
100
75
50
25
0
-25
-50
-75
1 2 3 4 5 6
1 2 3 4 5
Ser2-P/Rpb3
Rpb3

Neves_FigS8

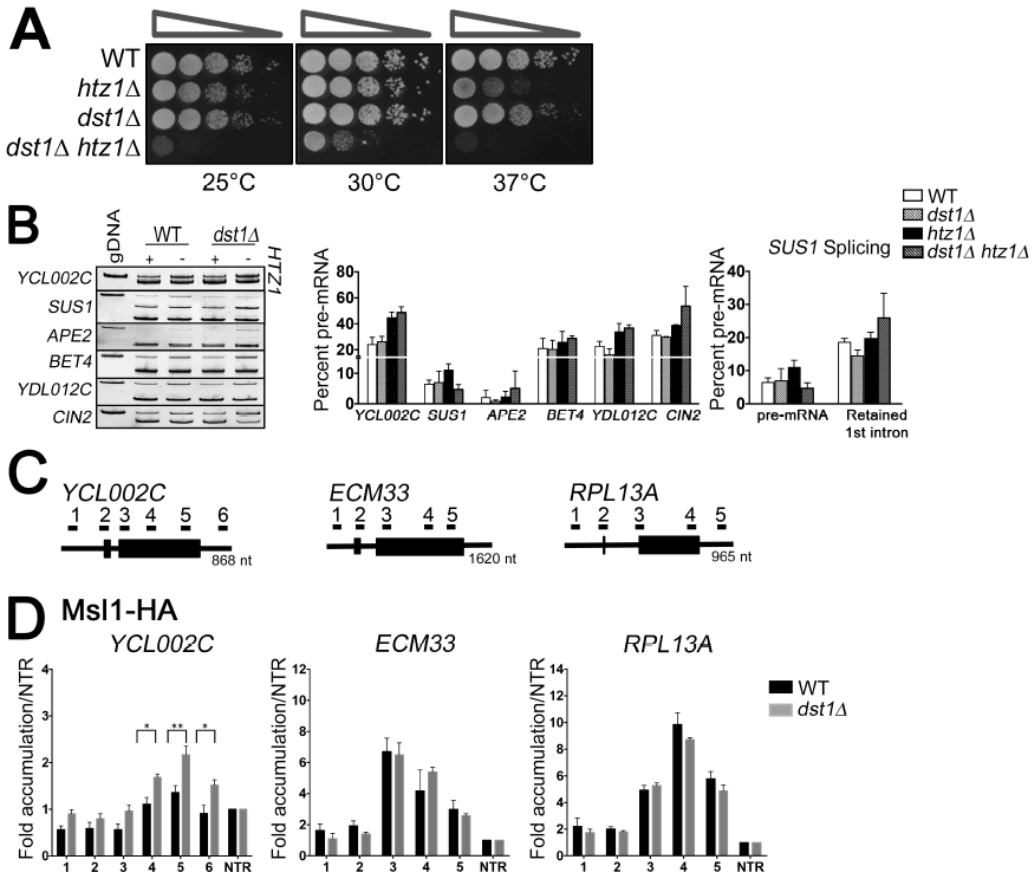
A
WT
htz1Δ
dst1Δ
dst1Δ htz1Δ
25°C
30°C
37°C
B
gDNA
WT
dst1Δ
+
-
+
-
HTZ1
YCL002C
SUS1
APE2
BET4
YDL012C
CIN2
Percent pre-mRNA
YCL002C
SUS1
APE2
BET4
YDL012C
CIN2
WT
dst1Δ
htz1Δ
dst1Δ htz1Δ
SUS1 Splicing
Percent pre-mRNA
pre-mRNA
Retained 1st intron
C
YCL002C
1 2 3 4 5 6
868 nt
ECM33
1 2 3 4 5
1620 nt
RPL13A
1 2 3 4 5
965 nt
D
Msl1-HA
YCL002C
ECM33
RPL13A
Fold accumulation/NTR
1 2 3 4 5 6 NTR
1 2 3 4 5 NTR
1 2 3 4 5 NTR
WT
dst1Δ

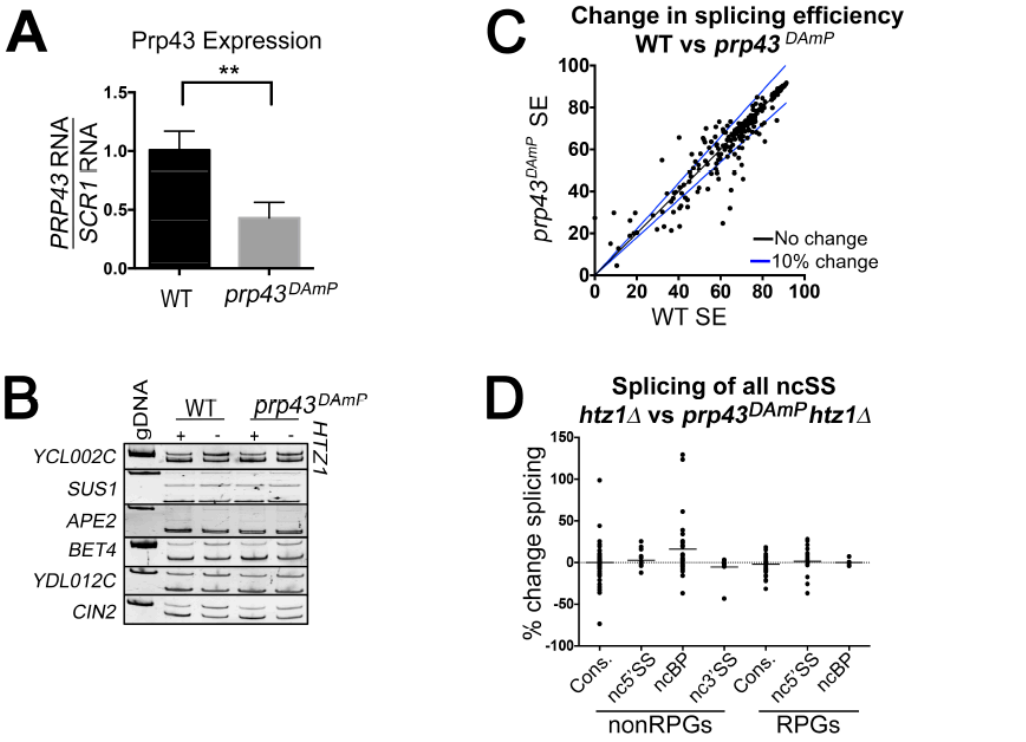
A
Prp43 Expression
**
PRP43 RNA / SCR1 RNA
1.5
1.0
0.5
0.0
WT
prp43DAmP
B
gDNA
WT
prp43DAmP
+
-
+
-
HTZ1
YCL002C
SUS1
APE2
BET4
YDL012C
CIN2
C
Change in splicing efficiency
WT vs prp43 DAmP
prp43DAmP SE
100
80
60
40
20
0
0
20
40
60
80
100
WT SE
No change
10% change
D
Splicing of all ncSS
htz1Δ vs prp43DAmP htz1Δ
% change splicing
150
100
50
0
-50
-100
Cons.
nc5'SS
ncBP
nc3'SS
Cons.
nc5'SS
ncBP
nonRPGs
RPGs

CHAPTER 3

The chromatin remodeling complex SWI/SNF regulates splicing of meiotic transcripts in *Saccharomyces cerevisiae.*

The chromatin remodeling complex Swi/Snf regulates splicing of meiotic transcripts in *Saccharomyces cerevisiae*

Srivats Venkataramanan[1,2], Stephen Douglass[1,2], Anoop R. Galivanche[1,2] and Tracy L. Johnson[1,2,*]

[1]Department of Molecular Cell and Developmental Biology, University of California, Los Angeles, CA 90095, USA and [2]Molecular Biology Institute, University of California, Los Angeles, CA 90095, USA

Received February 1, 2017; Revised March 31, 2017; Editorial Decision April 18, 2017; Accepted May 01, 2017

ABSTRACT

Despite its relatively streamlined genome, there are important examples of regulated RNA splicing in *Saccharomyces cerevisiae*, such as splicing of meiotic transcripts. Like other eukaryotes, *S. cerevisiae* undergoes a dramatic reprogramming of gene expression during meiosis, including regulated splicing of a number of crucial meiosis-specific RNAs. Splicing of a subset of these is dependent upon the splicing activator Mer1. Here we show a crucial role for the chromatin remodeler Swi/Snf in regulation of splicing of meiotic genes and find that the complex affects meiotic splicing in two ways. First, we show that Swi/Snf regulates nutrient-dependent downregulation of ribosomal protein encoding RNAs, leading to the redistribution of spliceosomes from this abundant class of intron-containing RNAs (the ribosomal protein genes) to Mer1-regulated transcripts. We also demonstrate that Mer1 expression is dependent on Snf2, its acetylation state and histone H3 lysine 9 acetylation at the *MER1* locus. Hence, Snf2 exerts systems level control of meiotic gene expression through two temporally distinct mechanisms, demonstrating that it is a key regulator of meiotic splicing in *S. cerevisiae*. We also reveal an evolutionarily conserved mechanism whereby the cell redirects its energy from maintaining its translational capacity to the process of meiosis.

INTRODUCTION

Saccharomyces cerevisiae, like all eukaryotes, contains genes interrupted by non-coding intron sequences. Introns are removed from the pre-messenger RNA by the spliceosome, a large macromolecular assembly of five small nuclear ribonucleoprotein complexes (snRNPs). Pre-messenger RNA splicing is critical for proper expression of eukaryotic genes. Although important insights into the mechanisms of RNA splicing have been gleaned from *in vitro* analysis of the reaction, over the last decade it has become increasingly clear that, in fact, assembly of the spliceosome occurs co-transcriptionally, while the RNA polymerase is actively engaged with a chromatin template. Moreover, changes in the state of the chromatin can affect splicing (1). However, understanding the nature of the causal relationships between chromatin modification and splicing has been difficult to decipher, even in an organism with a relatively streamlined genome such as *S. cerevisiae*.

Unlike metazoans, *S. cerevisiae* contains a relatively small number of introns, suggesting that those RNAs that have retained their introns may be subject to important and/or intron-tuned regulation. The largest single class of intron-containing genes (ICGs) in yeast is comprised of ribosomal protein genes (RPGs), which ensures that a critical step in gene regulation is dependent upon accurate and efficient splicing. Furthermore, splicing of RPGs can be regulated by the cell's environmental conditions (2). For example, a decrease in amino acid availability leads to a dramatic downregulation of RPG splicing (3) and hence downregulation of the energy-intensive process of translation.

In the last several years, there have been a number of other documented examples of splicing regulation in yeast (reviewed in (4)). Perhaps one of the best examples is found in the meiotic regulatory program. One of the largest classes of genes containing introns is made up of those involved in meiosis. Transcription of intron-containing meiotic transcripts and a critical meiotic splicing regulator, Mer1, is dependent upon degradation of the meiotic transcription inhibitor Ume6 (5). Mer1, in turn, regulates the splicing of four of the meiotic pre-mRNAs (*MER2, MER3, AMA1* and *SPO22*) via its interaction with a conserved intronic enhancer sequence (5′-AYACCCYU-3′) (6,7). Ume6-dependent repression of meiotic gene transcription (including *MER1*), in part by recruiting the deacetylase Rpd3 (8),

*To whom correspondence should be addressed. Tel: +1 310 206 2416; Email: tljohnson@ucla.edu

is critical for timing the onset of meiosis. However, while it is clear that cells entering meiosis rapidly adjust their gene expression profiles, neither the molecular basis of this massive reprogramming nor the specific consequences of this shift in the cell's gene expression are fully understood.

Although yeast genes typically have well-conserved splicing signals, particularly when compared to other eukaryotes, meiotic genes, in general, show lower conservation of their branch point (BP) and 5′ splice site (SS) sequences, making these introns weak substrates for the spliceosome. However, the splicing of these introns becomes more likely when there is decreased competition for a limited pool of spliceosomes. In fact, artificially decreasing the pool of intron-containing RPGs (IC-RPGs) by treating cells with rapamycin effectively shifts the pool of spliceosomes to the other intron-containing RNAs and increases splicing of genes with non-canonical SSs, including meiotic genes (9). This is reminiscent of other examples whereby redistribution of gene expression machineries that are typically envisioned to be plentiful, allows regulated expression of the appropriate substrates under specific environmental conditions. For example, in *S. cerevisiae* competition for available ribosomes by different transcripts is overcome by spatial redistribution of ribosomes (10). In human cells, it has recently been shown that the seemingly abundant U1 snRNP becomes transiently limiting during neuronal activation due to transcriptional upregulation, presumably because of the high abundance of U1 substrates. As a consequence, U1-dependent repression of the use of cryptic polyadenylation signals is decreased (11,12). Such examples suggest that RNA competition for limited pools of regulatory machinery such as the ribosome or the spliceosome may be a more general mechanism whereby eukaryotic organisms regulate expression of specific transcripts in response to cellular needs (8).

Here we describe a central role for the chromatin remodeling complex Swi/Snf in meiotic splicing regulation, by controlling the competition of different transcripts for the spliceosome and regulating the expression of the meiotic splicing activator. First, we show that deletion of Snf2 activates increased use of non-canonical BPs and 5′ SS and also causes a dramatic downregulation of RPG expression. Moreover, in the absence of Snf2 the efficiency of splicing of meiotic RNAs in particular, which are enriched in non-consensus (nc) SSs, is increased, while RPG expression is downregulated. In fact, the extent of enhanced splicing mirrors the effect of Snf2-independent RPG downregulation via treatment of cells with rapamycin. To determine if our genetic manipulation of Snf2 recapitulates what occurs under physiological conditions, we examined Snf2 levels under sporulation conditions, in both the strain background that allows for the genetic manipulation of Snf2 as well as in the SK1 background, which undergoes meiosis synchronously and efficiently. Snf2 protein levels decrease in both strain backgrounds. We also observe a corresponding decrease in RPG expression and an increase in splicing of meiotic transcripts. However, the timing of Snf2 downregulation is important. In fact, before Snf2 is downregulated, it persists in a deacetylated form and the *MER1* locus is hyperacetylated creating optimal conditions for Snf2 binding to the *MER1* locus and expression of the splicing activator. These data reveal that fine-tuned regulation of Snf2 activity is important for regulated splicing during meiosis.

MATERIALS AND METHODS

Yeast strains and growth

The yeast strains used in this study are listed in Table 1. All strains except the SK1 strain are derived from BY4743 and individual deletion strains were obtained from Open Biosystems. The Snf2-FLAG and Snf2K1493,1497R-FLAG strains were a kind gift from Dr Jerry Workman (described in (13)). Yeast strains were grown in Yeast extract-Peptone-Dextrose (YPD) (1% yeast extract, 2% peptone and 2% dextrose) media at 30°C. For rapamycin experiments, overnight yeast cultures were diluted in 25 ml media to OD_{600} of 0.1 and then grown to OD_{600} of 0.3. Rapamycin (Sigma) was then added to a final concentration of 200 ng/μl (Stock concentration of 1 mg/ml in Dimethyl Sulfoxide (DMSO)). Cells were precipitated after 90 min of treatment with rapamycin.

RNA-seq analysis

RNA-seq libraries were prepared using Illumina Truseq® V3 kit and ribosomal RNA depletion (Ribo-Zero, Illumina). Single-end, 50 nucleotide sequence reads (HiSeq 2000) were aligned to SacCer3 and spliced transcripts from the Ares Lab Yeast Intron Database Version 3 (14) in a single step using STAR (15) with a maximum of two mismatches and a minimum overhang of four nucleotides for spliced alignments. In the case of reads aligning to multiple loci, we kept only the highest scoring alignments. Reads that aligned with the same score to more than two loci were discarded. Library depth was an average of ∼18 million reads per sample with an average of 13 million successfully aligned to annotated gene models per sample. RPKMs were computed for each gene by dividing the total number of reads that aligned entirely within the gene's exon boundaries by the gene's total exon length in kilobase pairs per million mapped reads. Reads within ICGs were categorized as exonic, spliced or unspliced. Exonic reads are those that map entirely within an exon, as defined by the Ares Lab Yeast Intron Database. Introns with annotated snoRNAs within the defined intron boundaries were disregarded in this analysis. Spliced reads are those that align with a gap that corresponds to an annotated intron and unspliced reads map partially within an exon and partially within an intron with no gap. Spliced and unspliced read counts were normalized by dividing total spliced counts by the number of potential unique alignment positions that contribute to the total. For spliced reads, this is read length minus one for every intron. For unspliced read counts, this is the length of the intron plus the read length minus one. Splicing efficiency (SE) for each intron was calculated as normalized spliced counts divided by the sum of the normalized spliced and normalized unspliced counts. Percent (%) increase in splicing efficiency was calculated as: 100 * (SE in $snf2\Delta$ − SE in WT)/(SE in WT).

To assess global splicing changes, a chi-squared test was used to measure the deviation of our RNA-seq data ('observed' distribution) from a random distribution of splicing

Table 1. List of yeast strains used in this study

Strain Number	Name	Genotype
TJY6724	*WT*	*his3Δ leu2Δ LYS2 met15Δ ura3Δ*
TJY6727	*snf2Δ*	*his3Δ leu2Δ ura3Δ snf2Δ::NatMX*
TJY6729	*ume6Δ*	*his3Δ leu2Δ ura3Δ ume6Δ::KanMX*
TJY6797	*ume6Δ snf2Δ*	*his3Δ leu2Δ ura3Δ ume6Δ::KanMX snf2Δ::NatMX*
TJY6726	*WT*	*Mata/Matα his3Δ/his3Δ leu2Δ/leu2Δ LYS2/lys2Δ met15Δ/MET15 ura3Δ/ura3*
TJY6856	*snf2Δ*	*Mata/Matα his3Δ/his3Δ leu2Δ/leu2Δ LYS2/lys2Δ met15Δ/MET15 ura3Δ/ura3 snf2Δ::NatMX/snf2Δ::NatMX*
TJY6917	SK1 K8409	*SK1 MATa/MAT_ HO URA3::tetO224 LEU2::tetR-GFP REC8-HA3::URA3 lys2 his3 trp1*
TJY7086	Snf2-FLAG	*his3Δ1 leu2Δ0 met15Δ0 ura3Δ0 SNF2-Flag::LEU2*
TJY7087	Snf2 K1493,1497R-FLAG	*his3Δ1 leu2Δ0 met15Δ0 ura3Δ0 Snf2 K1493R, K1497R-Flag::LEU2*

efficiency changes in *snf2Δ* ('expected' distribution). Under our null model that *snf2Δ* does not effect splicing, there would be an equal number of introns showing increased splicing as decreased splicing. To assess enrichment of ncSSs in the genes with the greatest improvement in splicing, the two outcomes were defined as 'all-consensus SSs' or 'ncSSs' (including nc 5′ SS, BP or both). The 'expected' group is populated by the products of the fraction of introns in each category (indicated in Figure 1B, left panel) and number of genes considered ($n = 40$). The 'observed' group was populated based on the RNA-seq analysis. To calculate the distribution functions of ncSSs in an unbiased manner, ICGs were ranked according to magnitude of improvement in splicing upon deletion of *SNF2*. The cumulative occurrence of ncSS at each position was plotted and compared against a uniform distribution function generated by averaging the total number of ncSS in the yeast genome. Significance was assessed using a one-sample non-parametric Kolmogorov–Smirnov test.

RT-PCR and real time PCR analysis

RNA was isolated from cells at indicated time points. After DNase treatment (Roche), 4 μg of total RNA from each time point was used to make cDNA using a cDNA synthesis kit (Fermentas). To detect splicing isoforms, primers flanking the intronic sequences were used for polymerase chain reaction (PCR) using 1 μl of cDNA diluted to 1:20. PCR products were then run on 6% Tris/Borate/EDTA (TBE) polyacrylamide gel. The gel was stained with SYBR green (Sigma) and imaged. qRT-PCR was done in 10 μl reaction with gene specific primers using 1 μl of cDNA diluted 1:20 using Perfecta Sybr Green Fastmix (Quanta Biosciences) and a CFX96 Touch System (BioRad). All samples were run in triplicate for each independent experiment. qRT-PCR was also performed for *scR1* gene from each cDNA sample. Gene expression analysis was done by $2^{-\Delta C}{}_t$ methods using *scR1* as reference gene. Fold expression of mRNA was measured compared to WT by $2^{-\Delta\Delta C}{}_t$ methods (16).

ChIP-Seq analysis

Chromatin immunoprecipitation (ChIP)-seq reads (13) were obtained (GEO accession number GSE61210) and converted to FastQ format using the NCBI SRA Toolkit. Bowtie2 was used to align FastQ reads to SacCer3 with only one reported alignment (−k 1). Genomic track files from immunoprecipitation and input alignments were created using SAMTools, BEDTools and the UCSC bedgraphToBigWig utility. After normalizing input and immunoprecipitation pileup tracks for differential read count, a ratio track was created by dividing the normalized immunoprecipitation track by the normalized input track. Pileup ratios of the region 500+/− of the Translation Start Site (TSS) of genes of interest were retrieved and were added coordinate-wise to generate a 500+/− association array for each list of genes. Association array values were normalized for the number of genes included and vertically scaled between 0 and 100 to generate the meta-association array.

Induction of sporulation

All diploid strains derived from BY4743 were grown in YPD overnight and diluted in pre-sporulation media (5% glucose, 3% Difco Nutrient Broth and 1% Yeast Extract) to a final OD of 0.1. After 4 h, the cells are pelleted, washed with SPO media (1% potassium acetate, 0.005% zinc acetate and amino acid supplements as needed) and resuspended in SPO media and grown at 25°C (17). At the indicated time points, cells were pelleted each for RNA and/or protein analysis. For SK1 strains, SPorulation Media (SPM) media (0.3% potassium acetate, 0.02% raffinose and amino acid supplements as needed) was used in place of SPO (18).

Western blot

Protein was isolated from cells pellets with FA-1 lysis buffer (50 mM HEPES pH 7.5, 150 mM NaCl, 1 mM ethylenediaminetetraacetic acid (EDTA), 1% Triton X-100, 0.1% Sodium Deoxycholate, 1 mM phenylmethylsulfonyl fluoride (PMSF) and protease inhibitors) using bead-beating. The buffer was supplemented with protease inhibitor cocktail tablet (Roche). Total protein was resolved by sodium dodecyl sulphate-polyacrylamide gel electrophoresis. The gel was transferred to Polyvinylidene fluoride (PVDF) membrane, probed with anti-SNF2 antibody (yN-20, Santa Cruz) at a 1:200 dilution in 2% milk or anti-acetylated lysine (ST1027, Millipore) at a 1:2000 dilution in 5% milk. Signal was detected using ECL (Thermo Scientific) as per the manufacturer's instructions. For Pgk1 western blotting, the membrane was probed with anti Pgk1 antibody (Molecular probes) at a 1:3000 dilution in 5% milk.

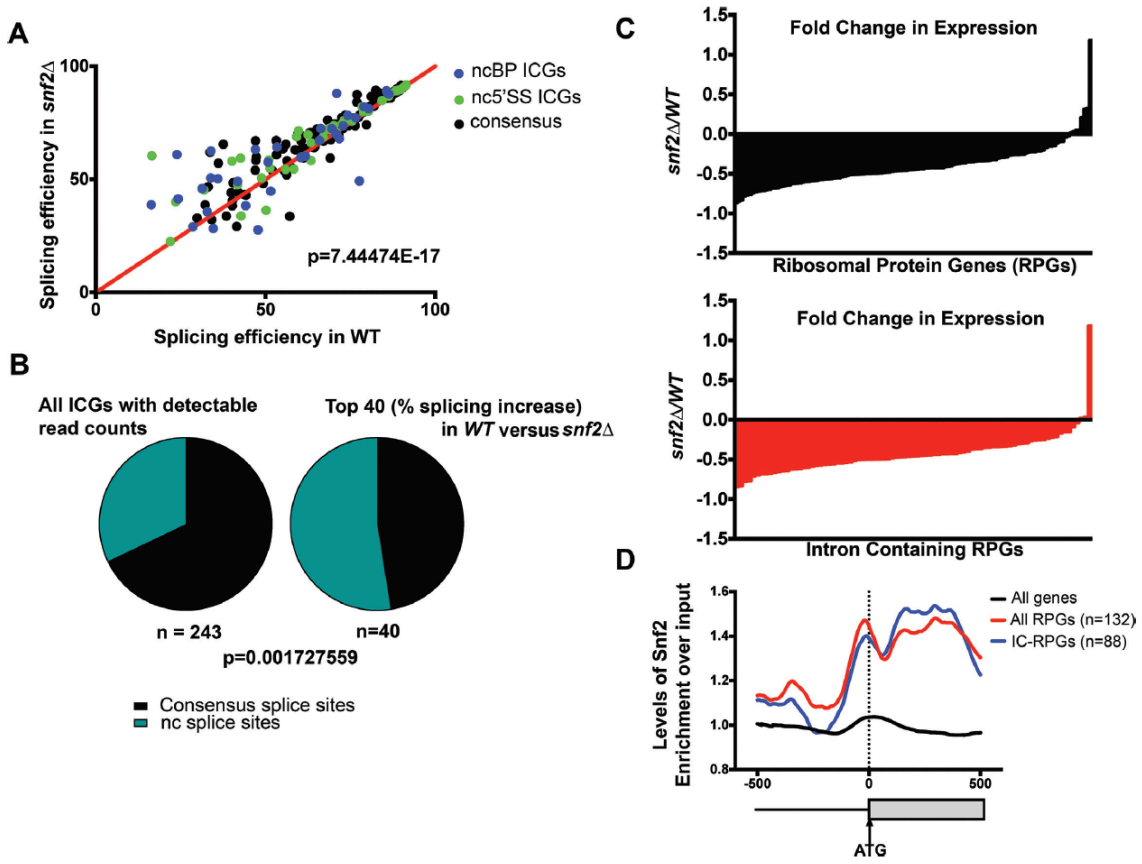

Figure 1. Deletion of Snf2 improves splicing globally. (**A**) Changes in splicing efficiencies of all intron-containing genes (ICGs) upon deletion of Snf2, represented as an X–Y plot. Overall splicing improves in *snf2Δ* yeast over *WT* (Chi-squared test, approximate *P*-value indicated). Largest changes in splicing are observed in genes with nc 5′SS (green dots) or nc branch point (BP) sequences (blue dots). (**B**) Left: distribution of non-consensus (nc) splice sites (SSs) (5′ SS and/or BP) in *Saccharomyces cerevisiae* ICGs, among all ICGs expressed in our samples. Right: distribution of ncSSs among genes showing highest improvements in splicing upon deletion in Snf2. ncSS-containing introns are enriched (Chi-squared test, approximate *P*-value indicated). (**C**) Top: log2-fold change in expression of ribosomal protein genes (RPG) upon deletion of Snf2, relative to *scR1*. Each bar represents an individual RPG ($n = 128$). Bottom: log2-fold change in expression of intron-containing RPGs (IC-RPGs) upon deletion of *SNF2* ($n = 84$). (**D**) Fold enrichment of occupancy of Snf2 over input by chromatin immunoprecipitation (ChIP)-Seq across the 500 nucleotides upstream and downstream of translational starts for all genes, RPGs and IC-RPGs. Dotted line represents the annotated translational start (ATG). Analysis of data from (13).

Random spore analysis

Sporulation was set up as described above. After 7 days of sporulation (BY background), 10^6 cells were pelleted and resuspended in 500 μl of water containing 0.5 mg/ml Zymolyase-100T (Zymo research) and 1% β-mercaptoethanol and incubated overnight at 30°C with gentle rocking to lyse unsporulated diploid cells. A total of 200 μl of 1.5% NP-40 was added to the solution and vortexed to disrupt tetrads (as observed by microscopy). Spores were centrifuged, resuspended in water and plated on YPD plates in serial dilutions to count the number of viable spores (19,20).

Immunoprecipitation

Sporulation was induced as described earlier and 50 ml of cells at various time points were pelleted. Protein was isolated from cells pellets with FA-1 lysis buffer (50 mM HEPES pH 7.5, 150 mM NaCl, 1 mM EDTA, 1% Triton X-100, 0.1% Sodium Deoxycholate, 1 mM PMSF and protease inhibitors) using bead-beating methods. Immunoprecipitation was performed with anti-SNF2 antibody (yN-20, Santa Cruz, 10 μl per IP) and γ-G sepharose beads and washed with the lysis buffer. Western blots were performed as described above.

Chromatin immunoprecipitation (ChIP) and qPCR

Sporulation was induced as described earlier and 50 ml of cells at various time points were crosslinked at room temperature for 15 min with formaldehyde to a final concentration of 1%. Crosslinking was quenched at room temperature for 5 min with glycine to a final concentration of 125 mM. Cells were disrupted with glass beads (0.5 mm) for 40 min at 4°C. To shear chromatin, lysates were sonicated on ice for a total of 3 min 20 sec at 15% intensity (10 s on, 15

s off and on ice). After sonication, lysates were cleared by centrifugation. Samples were then used for immunoprecipitation with anti-H3K9ac (07-352, Millipore) or anti-Snf2 antibody (yN-20, Santa Cruz). After immunoprecipitation, samples were washed with the lysis buffer and incubated overnight at 65°C to reverse crosslinking. Samples were incubated with Proteinase K (Sigma) and RNAse Cocktail (Ambion), followed by purification using a PCR product purification kit (Qiagen). DNA samples were then analyzed by real-time PCR. Input DNA was serially diluted and 1 μl of these dilutions was used in a 20 μl reaction volume to calculate 'percentage input'. One microliter of ChIP DNA samples were used in a 20 μl reaction volume. Real-time PCR was performed using a CFX96 Touch System (Bio-Rad) as described earlier. All samples were run in triplicate for each independent experiment. ChIP samples were quantified as a function of percentage input as indicated by standard curves generated by serial dilutions of the input. Values are reported as enrichment over a beads-only control. Reported values are averages of three independent experiments and error bars represent the standard deviation.

RESULTS

Deletion of Snf2 leads to global enhancement of splicing through RPG depletion and spliceosome redistribution

We previously demonstrated an important relationship between chromatin and splicing. For example, we have shown that chromatin modifiers are important for spliceosome recruitment and rearrangements in *S. cerevisiae* (21,22). These data led us to explore the possibility that other chromatin modifiers can influence splicing. So the splicing of all ICGs in *S. cerevisiae* was assayed in cells deleted of Snf2, the adenosine triphosphatase (ATPase) component of the Swi/Snf chromatin-remodeling complex. To our surprise, upon Snf2 deletion, we found that a majority of introns show enhanced splicing, particularly those introns with ncSSs (Figure 1A). In fact, although yeast introns generally have highly conserved intron sequences, the genes showing the largest improvement in splicing are significantly enriched in nc 5′ SS or BP sequences (Figure 1B; Supplementary Figure S1A and B), which we confirm by RT-PCR of several candidate genes with ncSSs (Supplementary Figure S1C).

Recent studies have revealed a surprising mechanism for increased splicing of poorly recognized introns—namely by decreased expression of competing, highly expressed RPGs (9). So we considered the possibility that the change in splicing efficiency in cells deleted of Snf2 might be due to redistribution of spliceosomes away from RPGs. When we analyzed the RNA sequencing data from cells deleted of Snf2, we observed dramatic Snf2-dependent downregulation of RPGs (Figure 1C). Consistent with this, recent analysis of the promoter architecture of RPGs reveals increased MNase sensitivity at their promoters (23). Our own analysis of ChIP-Seq datasets for Snf2 occupancy (13) revealed Snf2 enrichment at the promoters and gene bodies of RPGs, and this enrichment remained consistent when the analysis was restricted to IC-RPGs (Figure 1D). Finally, the Snf2 enrichment profile persisted and was unique to RPGs, even when compared to other highly expressed genes (Supplementary Figure S1D). These data suggest that the nucleosome remodeling activity of the Swi/Snf complex at the promoters and gene bodies of RPGs leads to decreased nucleosome occupancy at these regions, and is crucial for the efficient transcription of these genes. Deletion of Snf2, on the other hand, leads to downregulation of RPGs, including the genes containing the majority of yeast introns.

Snf2-dependent RPG downregulation causes an improvement in the splicing of Mer1-regulated introns

The process of yeast meiosis or sporulation in response to nitrogen starvation, relies on numerous ICGs significantly enriched in ncSS sequences. Since introns with ncSSs appear to receive a significant benefit from cellular conditions lacking Snf2, we next evaluated whether the meiotic splicing program might be under the control of Snf2. However, the transcriptional repressor Ume6 negatively regulates expression of these transcripts until it is degraded during meiosis (24). In order to assay whether the absence of Snf2 results in an improvement in the splicing of the meiotic ICGs, the RNA-seq analysis was repeated in a *ume6Δ* background. While a substantial fraction of ICGs show no increase in splicing, we observe a significant improvement in the splicing of most of the meiotic ICGs upon deletion of Snf2 (Figure 2A and Table 2). Once again, genes showing the greatest improvements in splicing are significantly enriched in intron-containing nc 5′SS or BP sequences. Interestingly, *SPO22, MER2* and *MER3*, three of the four genes whose splicing have previously been demonstrated to be regulated by the meiosis-specific splice enhancer Mer1 (6) are the most significantly affected by the deletion of Snf2 (Figure 2B and C, Supplementary Figure S2A and Table 2). It is worth noting that although *AMA1* did not make our read cutoff filters for the RNA-seq analysis, its splicing is significantly improved in the absence of Snf2 (Figure 2C). One explanation for these results could be that in the *ume6Δ snf2Δ* cells grown under vegetative conditions, Mer1 or other factors required for Mer1-dependent splicing such as Nam8 (6), are transcribed at higher levels. However, we observe virtually no effect on the levels of these RNAs, indicating that deletion of Snf2 under vegetative conditions affects the splicing of the Mer1 regulon via a mechanism not involving the levels of Mer1 or Nam8 (Supplementary Figure S2B).

Not surprisingly, IC-RPGs are downregulated upon deletion of Snf2 in the *ume6Δ* strain background as well (Supplementary Figure S2C). To determine if downregulation of RPGs by another Snf2-independent method could lead to a comparable degree of splicing enhancement, *ume6Δ* yeast cells were treated with rapamycin to inhibit TOR (Target of Rapamycin)-dependent RPG transcription (25) (Supplementary Figure S2D and E) and observed that the splicing of the four genes of the Mer1 regulon increases significantly (Figure 2D and Supplementary Figure S2F). Intriguingly, maximum splicing efficiency achieved by Snf2 deletion is comparable to rapamycin-dependent RPG downregulation (Compare quantitation in Figures S2A and Figure S2F). This supports the model that Snf2-dependent RPG downregulation and subsequent spliceosome redistribution is a mechanism for the improved splicing of the genes of the Mer1 regulon.

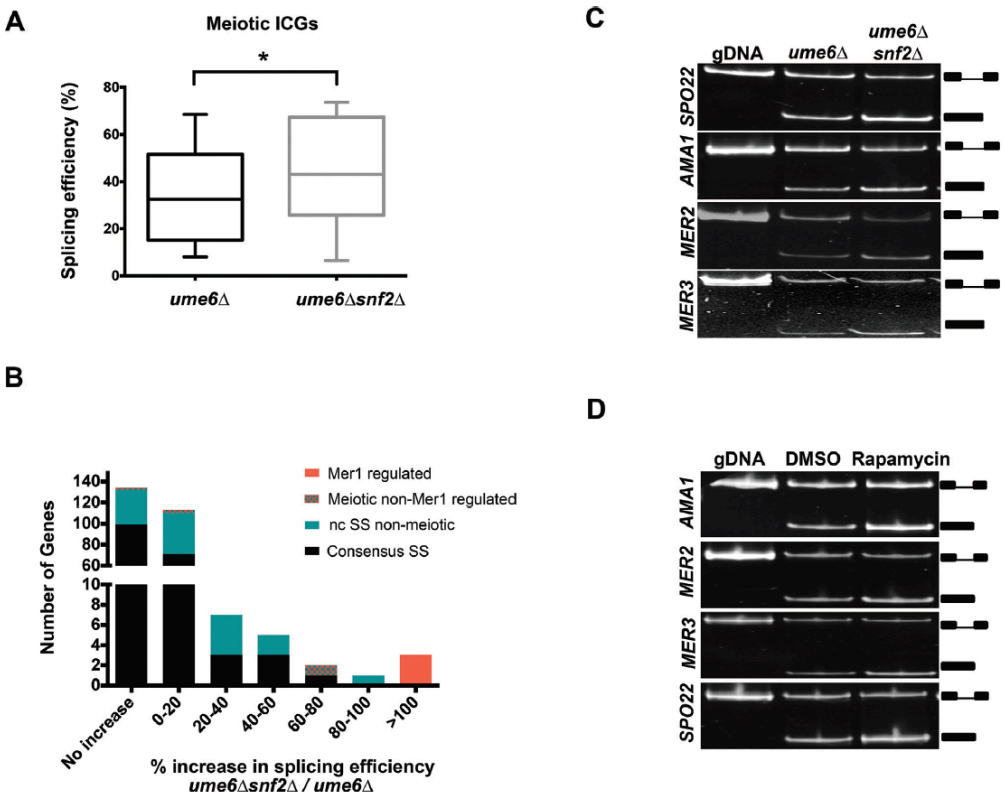

Figure 2. Snf2-dependent RPG downregulation activates meiotic splicing. (**A**) Changes in splicing efficiencies of meiotic ICGs upon deletion of *SNF2* in an Ume6 null background, represented as a box-and-whisker plot (Paired two-tailed students *t*-test, $P < 0.05$). (**B**) Distribution of changes in splicing efficiencies upon deletion of *SNF2* in a Ume6-null background. Mer1-regulated genes are represented by red bars. Meiotic ICGs whose splicing is not regulated by Mer1 are represented by teal and red-checkered bars. ncSS-containing genes that are not involved in meiosis are represented by teal bars. Black bars represent genes containing introns with all consensus sites. (**C**) Expression and splicing of Mer1-regulated meiotic transcripts *SPO22, AMA1, MER2* and *MER3* in *ume6Δ* and *ume6Δsnf2Δ* vegetative cells. Genomic DNA (gDNA) PCR products indicate the mobility of the unspliced form. PCR products representing the spliced and unspliced forms are indicated. (**D**) Expression and splicing of Mer1 regulated meiotic transcripts *SPO22, AMA1, MER2* and *MER3* in *ume6Δ* vegetative cells treated with rapamycin and control vehicle (DMSO). gDNA PCR products indicate the mobility of the unspliced form. PCR products representing the spliced and unspliced forms are indicated.

Table 2. Deletion of Snf2 improves splicing of meiotic ICGs

Gene name	Function	% increase in splicing efficiency between *ume6Δ snf2Δ* and *ume6Δ*
MER3	Meiotic recombination	508.2
SPO22	Meiotic nuclear division	143.7
MER2	Meiotic recombination	118.2
REC102	Chromosome synapsis	60.5
SAE3	Meiotic recombination	16.5
SPO1	Transcriptional regulator	8.0
DMC1	Meiotic recombination	7.5
MEI4	Meiotic recombination	−1.6
HOP2	Homologous chromosome pairing	−6.6

Percentage improvements in splicing of intron-containing meiotic genes in *ume6Δsnf2Δ* versus *ume6Δ* yeast, determined by RNA-seq. This is not an exhaustive list of meiotic ICGs, as *AMA1, MND1, PCH2* and *REC114* did not pass RNA-seq read count filters.

Levels of Snf2 decrease under sporulation conditions

In light of the effect Snf2 has on the splicing of meiotic transcripts we predicted that Snf2 might itself be subject to regulation under sporulation conditions. To test this prediction, wild-type S288C-derived diploid yeast (in the BY strain background) were shifted to sporulation media and allowed to sporulate over 7 days, a typical time course for this strain. Snf2 protein levels are undetectable at the end of the time course and, in fact, fall below the limits of detection within 24 h of transferring cells to sporulation media (Figure 3A). This downregulation of Snf2 occurs at the level of the protein, as *SNF2* mRNA levels do not drop significantly under these conditions (data not shown). These data indicate that Snf2 protein is downregulated under the conditions that support meiosis.

To determine the correlation between Snf2 downregulation and RPG expression, we measured the levels of representative IC-RPGs and the splicing of the genes of the Mer1 regulon through the 7-day sporulation time course and observed a dramatic decrease in RPG levels (Figure 3B) and a concomitant rise in splicing of the transcripts in the Mer1 regulon (Figure 3C and D).

If the only role of Snf2 in meiosis is to downregulate RPG expression, we predicted that deletion of Snf2 would allow cells to sporulate, perhaps even more efficiently. So Snf2 deficient diploid BY cells were transferred to sporulation media and sporulation was measured using random spore analysis (19,20). Diploid cells lacking Snf2 produce no viable spores (Supplementary Figure S3). Moreover, when expression and splicing of Mer1-dependent transcripts was analyzed in these diploid cells under meiotic conditions, the Mer1-dependent transcripts are expressed but are not spliced (Figure 3E). Analysis of *MER1* expression in these cells revealed that in diploid cells entering meiosis, unlike haploid cells lacking Ume6, *MER1* expression requires Snf2 (Figure 3F). These data suggest that Snf2 has another role in the meiotic program in *S. cerevisiae* in addition to regulating the levels of free spliceosomes, which appears to occur prior to its downregulation. While the S288C-derived strain (BY4743, which we refer to as 'BY') provides a useful tool for genetic analysis (e.g. *SNF2* deletion is tolerated in these diploid cells), it was clear from these studies that a strain that was more amenable to finer temporal dissection of molecular changes under sporulation conditions was necessary. So we analyzed the meiotically synchronous, sporulation efficient SK1 strain.

Snf2 downregulation occurs in the meiotically efficient SK1 strain

In order to maintain consistency in the way SK1 and BY strains were sporulated, SK1 K8409 diploid cells were moved directly from rich media to sporulation media (0.3% KOAc, 0.02% Raffinose and amino acids as needed). The SK1 diploid yeast achieve near complete sporulation (∼100%) within 36 h of shifting to sporulation media, compared to about 30% for the BY strain under our experimental conditions.

To determine how Snf2 levels change in the SK1 strain under sporulation conditions, SK1 diploid yeast were shifted to sporulation media and allowed to sporulate over 48 h. As we previously observed in the BY strain background, Snf2 protein levels are undetectable at the end of the sporulation time course. In fact, Snf2 falls below the limits of detection within 5 h of the shift into sporulation media (Figure 4A). Similar to the BY strain, this downregulation of Snf2 occurs at the level of the protein (data not shown). Over this time course, levels of RPG RNAs were also measured and they also decrease between 4- and 6-fold **(**Figure 4**B,** three representative RPGs are shown**).** Interestingly, there does appear to be a slight increase in RPG expression at ∼12 h which may be indicative of a requirement for mid-meiotic translation (26). Nonetheless, RPGs remain at around 10% of their pre-sporulation levels even with this slight increase.

With these finer time points, we noted a discrepancy between the levels of Snf2 at early time points and the downregulation of RPGs. The decrease in Snf2 is most dramatic after 3 h (Figure 4A), while RPG downregulation is initiated almost immediately after the shift to sporulation media. Furthermore, in light of the results from the BY diploid strain deleted of *SNF2*, which demonstrate that Snf2 is required for *MER1* expression and Mer1-dependent splicing, presumably before its downregulation (Figure 3E and F), it became clear that it was important to examine more closely the activity of Snf2 in *MER1* expression and RPG downregulation during this 0–3 h time period. As is often the case, different yeast strains show differential tolerance to deletion of specific genes, and deletion of *SNF2* is lethal in the SK1 strain. So, Mer1-dependent splicing in *snf2Δ* SK1 cells could not be examined (data not shown). Nonetheless, deletion of Snf2 in the BY strain reveals a previously unexplored role for Snf2 in the expression of *MER1*. This led us to examine more closely how Snf2 affects RPG expression at early time points before its absence leads to decreased RPG expression (Figure 2) and to assess the mechanism by which Snf2 affects *MER1* expression.

First, we assessed the meiotic state of the SK1 cells by measuring the expression of the key meiotic transcription factor *Initiator of Meiotic Entry 1 (IME1)* **(**Figure 4C**)** (27). Moreover, to monitor Mer1-dependent splicing, we measured the levels of *MER1* by qRT-PCR (Figure 4D) as well as the splicing of *MER2,* one of the genes of the Mer1 regulon (Figure 4E) over 48 h. Consistent with literature that has established that Ime1 is required for *MER1* transcription (28), *MER1* expression and Mer1-dependent splicing follow *IME1* expression. It is also evident from that timing that even after Snf2 decreases to undetectable levels, other molecular events (such as Ime1-dependent *MER1* expression), support meiotic splicing. The results with both strains also show that Snf2 is not dispensable for meiosis, but may affect both the levels of the Mer1 splicing activator and the spliceosomes that the activator helps to recruit to the meiotic transcripts. Next we explored how Snf2 can perform both functions.

Snf2 levels and acetylation are temporally coordinated to direct meiosis specific splicing regulation

In light of our observation that Snf2 is required for *MER1* expression in diploid cells, we next examined how Snf2 activity at the *MER1* locus might be regulated. Snf2 contains

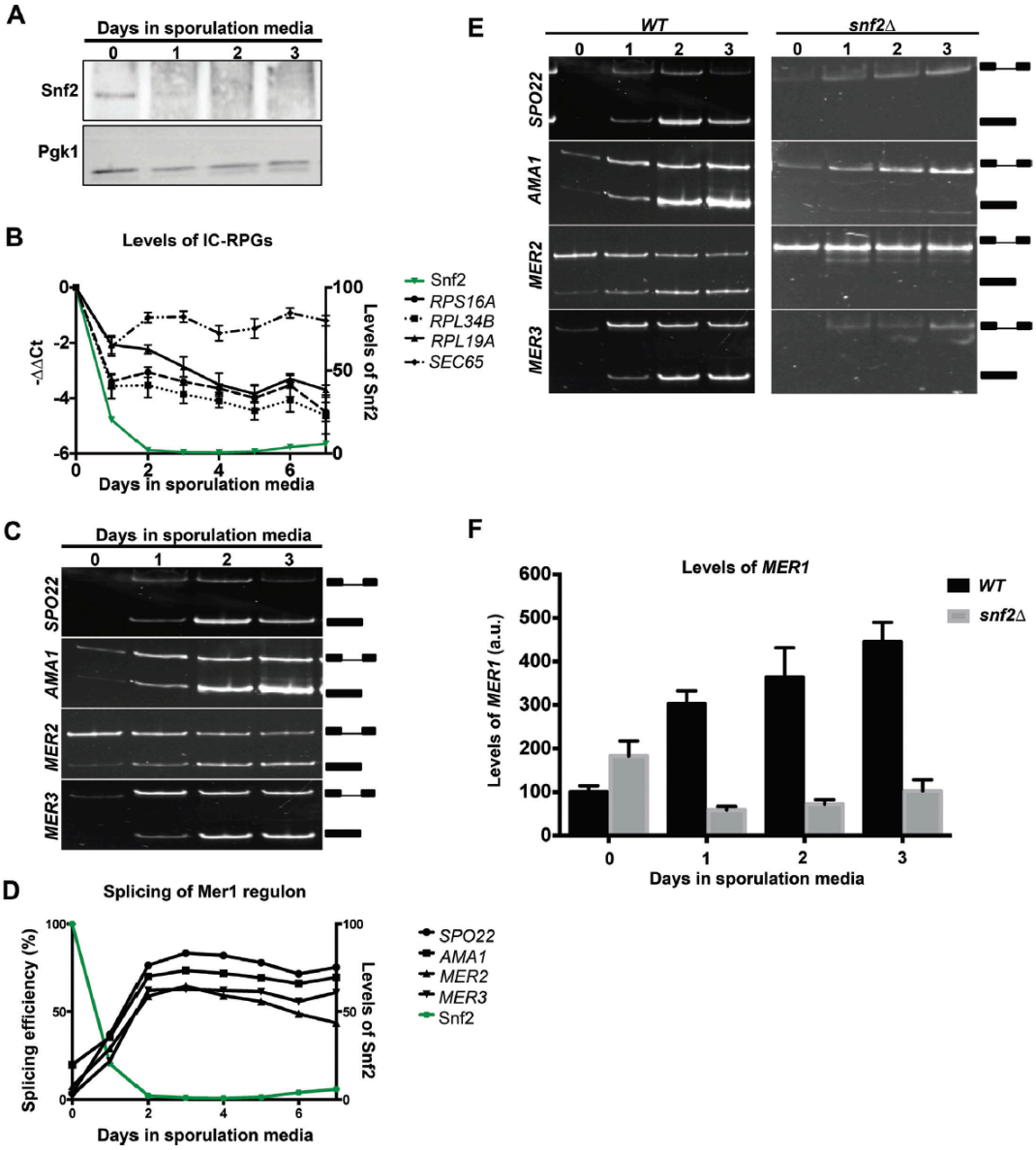

Figure 3. Levels of Snf2 decrease when cells are shifted to sporulation media, corresponding with RPG downregulation and increase in meiotic splicing. (**A**) Western blot for levels of Snf2 protein through a time course of meiosis. Pgk1 is an internal control. (**B**) Quantification of total (exon 2) transcript levels for *RPS16A, RPL34B* and *RPL19A* by RT-qPCR relative to *scR1* and normalized to $t = 0$ in *WT* yeast at indicated times after shifting to sporulation media. *SEC65* encodes a component of the signal recognition complex and is a control. Error bars represent ± 1 Standard Deviation (SD). Levels of Snf2 protein as detected by western blot and normalized to $t = 0$ are indicated by the green line. (**C**) Expression and splicing of Mer1 regulated meiotic transcripts *SPO22, AMA1, MER2* and *MER3* at indicated times under sporulation conditions. PCR products representing the spliced and unspliced forms are indicated. (**D**) Quantification of splicing efficiencies from (C). Levels of Snf2 protein as detected by western blot and normalized to $t = 0$ are indicated by the green line. (**E**) Left panel: identical to Figure 3C, provided for side-by-side comparison. Expression and splicing of Mer1 regulated meiotic transcripts *SPO22, AMA1, MER2* and *MER3* at indicated times under sporulation conditions. PCR products representing the spliced and unspliced forms are indicated. Right Panel: expression and splicing of Mer1 regulated meiotic transcripts *SPO22, AMA1, MER2* and *MER3* in *snf2Δ* yeast at indicated times after the transfer into sporulation media. PCR products representing the spliced and unspliced forms are indicated. (**F**) Fold-change RT-qPCR measurement of *MER1* transcripts between *WT* and *snf2Δ* diploid strains at indicated times after the transfer to sporulation media. Error bars represent ± 1 SD.

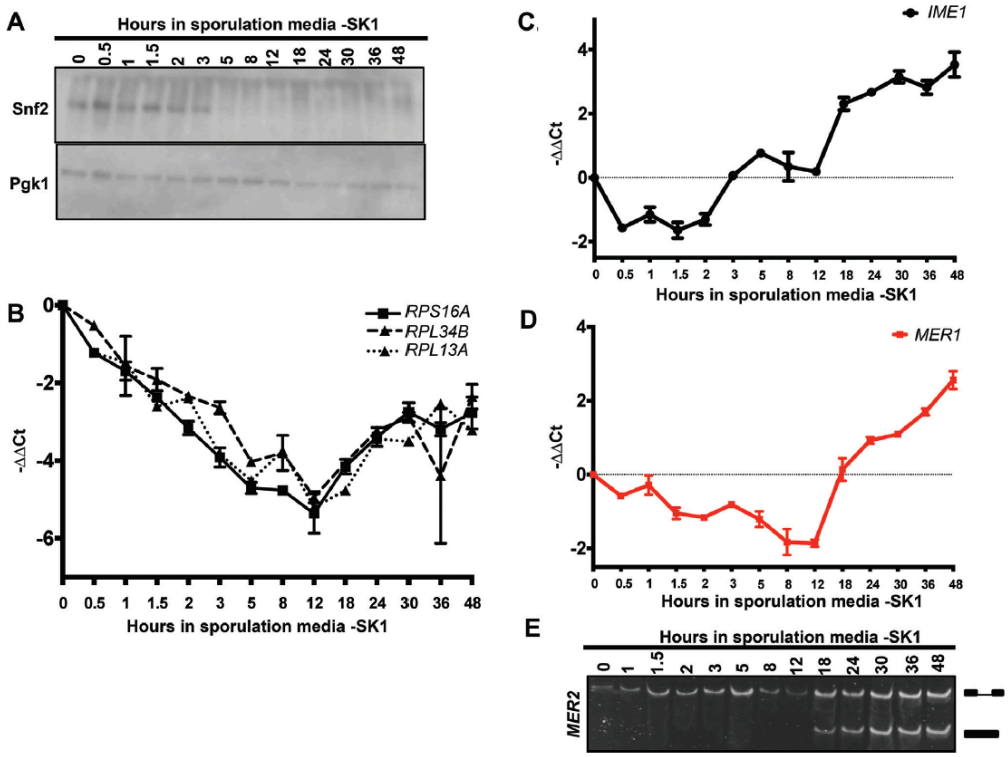

Figure 4. Snf2 is downregulated in the meiotically efficient SK1 yeast strain. (**A**) Western blot for levels of Snf2 protein through a time course of sporulation in the SK1 strain. Pgk1 is an internal control. (**B**) Quantification of total (exon 2) transcript levels for *RPS16A, RPL34B* and *RPL13A* by RT-qPCR relative to *scR1* and normalized to $t = 0$ in *WT* yeast (SK1 strain) at indicated times after shift to sporulation media. Error bars represent ± 1 SD. (**C**) Quantification of total transcript levels for *Initiator of Meiotic Entry 1 (IME1)* by RT-qPCR relative to *scR1* and normalized to $t = 0$ in *WT* yeast (SK1 strain) at indicated times after shift to sporulation media. Error bars represent ± 1 SD. (**D**) Quantification of total transcript levels for *MER1* by RT-qPCR relative to *scR1* and normalized to $t = 0$ in *WT* yeast (SK1 strain) at indicated times after shift to sporulation media. Error bars represent ± 1 SD. (**E**). Expression and splicing of Mer1-regulated meiotic transcript *MER2* at indicated times after shift to sporulation media. PCR products representing the spliced and unspliced forms are indicated.

a bromodomain that directs its interactions with acetylated histones (29). It has recently been shown that the Snf2 protein itself can also be acetylated. Moreover, Snf2 acetylation competes with acetylated histones for recognition by the Snf2 bromodomain. In other words, the bromodomain on acetylated Snf2 can recognize itself over acetylated histones and this effect is counteracted by Snf2 deacetylation (13). With this in mind, we hypothesized that Snf2 acetylation might change early in meiosis. Snf2 was immunoprecipitated from sporulating SK1 diploid cells and probed for acetylated lysines. Importantly, the assay was performed within the first few hours of sporulation during the period in which Snf2 levels remain high. We observed that acetylated Snf2 decreased to undetectable levels within the first 3 h of transfer to sporulation media although Snf2 levels remain high, even when Snf2 is overloaded (Figure 5A, 3-h time point). These data show that the Snf2 present in these cells is largely unacetylated.

We hypothesized that the early role for Snf2 in *MER1* expression suggested by Figure 3 and 4 may involve this deacetylated form of Snf2. Hence we analyzed Snf2 occupancy and histone acetylation at the *MER1* locus under sporulation conditions between 0 and 3 h. We find that both Snf2 (Figure 5B) and importantly, H3K9ac (Figure 5C) increase at the *MER1* locus over this time course. Over this same time course, we previously found that RPG transcript levels decrease (Figure 4B). Consistent with this, Snf2 is redistributed away from RPGs (Figure 5D) in a manner concomitant with the downregulation of RPG transcript levels (Figures 5E and 4B) and the ratio of Snf2 at RPGs versus *MER1* shifts over the 3-h time course, toward *MER1* (Figure 5F). This redistribution of Snf2 also follows a shift in the relative H3K9ac levels from the RPGs to the *MER1* locus (Supplementary Figure S4).

We also analyzed these molecular events in the BY diploid strain. Again we observed that the levels of acetylated Snf2 decrease before the levels of total Snf2, indicating that the Snf2 present in the cells is deacetylated rapidly when shifted to sporulation conditions (Supplementary Figure S5A). As is the case with the SK1 cells, we observe an increase in Snf2 occupancy at the *MER1* locus (Supplementary Figure S5B and D) in a manner coincident with a change in H3K9 acetylation (Supplementary Figure S5C and E). This redistribution is due to the change in Snf2 acetylation, as demonstrated by the increased occupancy of a mutant form of Snf2 that cannot be acetylated

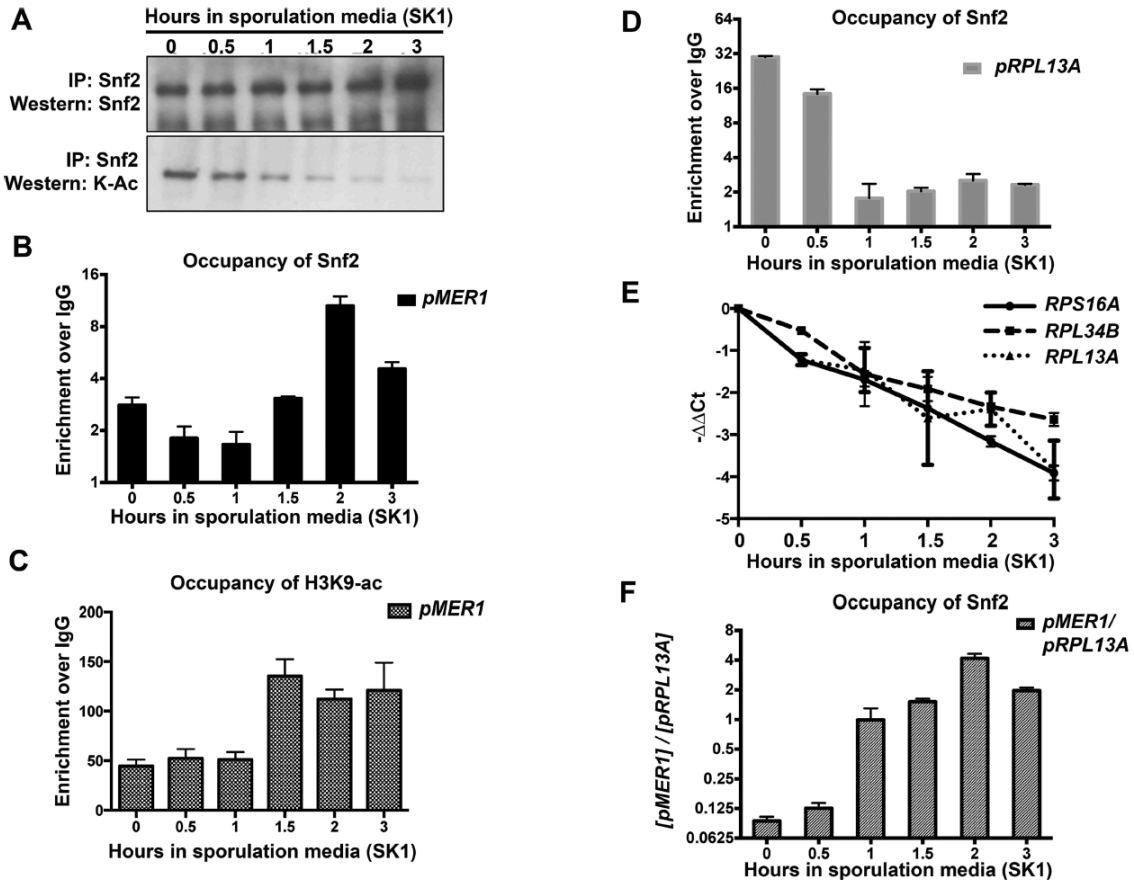

Figure 5. The timing of Snf2 activity is coordinated by its acetylation and acetylation of histones. (**A**) Immunoprecipitation of Snf2 during a time course of meiosis in *WT* SK1 yeast. Snf2 acetylation decreases steadily between 0 and 3 h after transfer into sporulation media, but Snf2 levels remain constant. The immunoprecipitate at the 3-h time point is slightly overloaded (compare with Figure 4A) and acetylation is still barely detectable. (**B**) Bar graph showing Snf2 occupancy at the *MER1* promoter in the SK1 strain over time. Error bars represent ± 1 SD. Quantification from three biological replicates. (**C**) Bar graph showing H3K9ac occupancy at the *MER1* promoter in the SK1 strain over time in sporulation media. Error bars represent ± 1 SD. Quantification from three biological replicates. (**D**) Bar graph showing Snf2 occupancy at the *RPL13A* promoter in the SK1 strain over time. Error bars represent ± 1 SD. Quantification from three biological replicates. (**E**) Quantification of total (exon 2) transcript levels for *RPS16A, RPL34B* and *RPL13A* by RT-qPCR relative to *scR1* and normalized to $t = 0$ in SK1 strain at indicated times after shift to sporulation media (part of Figure 4B). (**F**) Relative Snf2 occupancy at the *MER1* promoter to an RPG locus, upon ChIP using an anti-Snf2 antibody, in a SK1 strain. Error bars represent ± 1 SD. Quantification from three biological replicates. Relative and absolute levels of Snf2 increases at the *MER1* locus after transfer to sporulation media.

(K1493,1497R, referred to as '2R' (13) at the *MER1* promoter (Supplementary Figure S6).

As described above, an intriguing difference between *snf2Δ* in haploid cells in which *UME6* is deleted and WT diploid cells (Compare Supplementary Figure S2 to Figure 4) is that Snf2 is required for *MER1* expression in the diploid cells. Previous studies have shown that Ume6 recruits the histone deacetylase Rpd3 to target promoters and represses expression of early meiotic genes; Ume6 degradation is required to relieve this inhibition (8,30). Our results suggest that the repressive conditions inhibiting *MER1* expression in Ume6-expressing cells require Snf2 for them to be overcome. It is also interesting that both BY, a poorly sporulating strain and SK1, a strain that sporulates efficiently, show similar downregulation by Snf2. Although it remains unclear why BY undergoes meiosis poorly, it does not appear to be due to a defect in Snf2-mediated regulation of meiotic splicing.

These data reveal that there is a temporally regulated role for Snf2 in meiotic splicing, which is illustrated in the model in Figure 6. Under vegetative conditions, with relatively high levels of Snf2, Snf2-dependent transcription of RPGs sequesters spliceosomes away from transcripts with weak SSs, such as the meiotic transcripts. At the same time, *MER1* transcription is repressed by Ume6, in part, via the activity of histone deacetylase Rpd3. Upon shift to sporulation media, Snf2 deacetylation/histone acetylation is associated with de-repression at the *MER1* locus. This, combined with subsequent molecular events (e.g. Ime1 activity), allows Mer1 levels to rise. Our data suggests that the well-correlated events: meiosis-specific expression of Mer1, downregulation of Snf2, and downregulation of RPG ex-

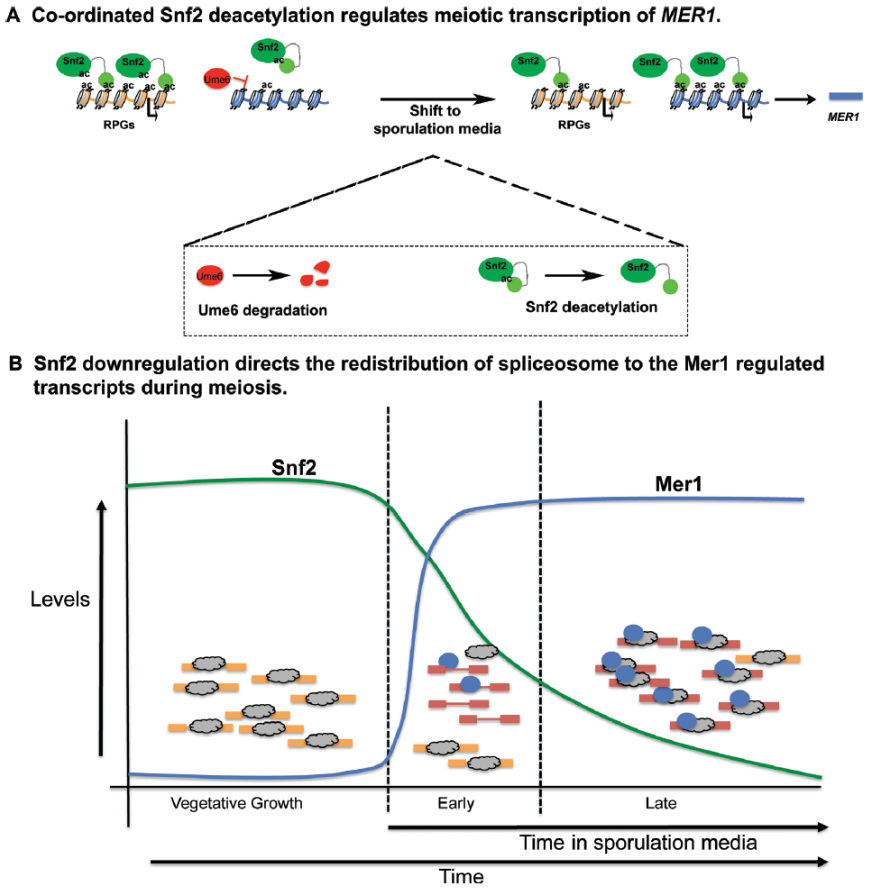

Figure 6. Temporal control of meiotic splicing by Snf2. (**A**) Upon shift into sporulation media, Ume6 is degraded and Snf2 is deacetylated. This contributes to its relocalization to the *MER1* promoter from the RPGs in a manner correlated with H3K9ac. Snf2 reverses Ume6-dependent repression at the *MER1* promoter and *MER1* mRNA levels rise. (**B**) Snf2 regulates RPG transcription, such that under vegetative growth conditions, high levels of RPGs titrates away the free pool of active spliceosomes. Ume6 represses expression of meiotic transcripts. Upon shift to sporulation media and the establishment of favorable conditions for *MER1* transcription (see panel A), Snf2 is downregulated, which is correlated with repressed RPG expression and the freeing up of active spliceosomes to increase splicing and expression of the meiotic RNAs.

pression create conditions whereby active spliceosomes are free to fine tune expression of the meiotic RNAs; in some cases increasing splicing efficiency by as much as 500%.

The shift between splicing that supports ribosome biogenesis/translation to splicing that allows spore formation and meiosis seems likely to be an evolutionarily conserved 'choice' that the cell makes and in fact, the mechanisms described here appear to be evolutionarily conserved among related *Saccharomyces* species separated by between 5 and 20 million years of evolution. The genome of the *Saccharomyces* sensu stricto group possess relatively few introns and there is a significant enrichment of the highly expressed RPGs among ICGs (Table 3). This enrichment persists in even more distant hemiascomycetous yeast as evolutionarily distant as *Candida albicans* (31). Additionally, all the members of the sensu stricto group possess a homolog of the Mer1 protein, as well as of the four genes of the Mer1 regulon. Importantly, all of these genes in the Mer1 regulon contain a putative Mer1 binding site and nonconsensus SSs, which can tune these introns to the activity of Mer1 and to the level of free spliceosomes. Finally, as we describe below, the Swi/Snf complex is conserved all the way to metazoans. These studies suggest an evolutionarily conserved mechanism whereby the cell redirects its energy from maintaining its translational capacity to the process of meiosis.

DISCUSSION

One of the outstanding challenges has been to identify specific mechanisms by which changes in chromatin can influence splicing, distinguish between direct (i.e. co-transcriptional) versus transcription-dependent effects of chromatin on splicing and identify biologically important conditions under which these mechanisms are utilized by the cell. Here we show that the chromatin remodeling complex Swi/Snf plays a previously unexplored but fundamental role in regulating meiotic splicing. We propose a model whereby the Swi/Snf complex controls meiotic splicing on multiple levels. We demonstrate that Snf2 is nec-

Table 3. The Mer1 regulon is conserved across closely related *Saccharomyces* species

Species	# introns	#RPG introns	Mer1	*MER2*		*MER3*		*SPO22*		*AMA1*	
				5'SS	BP	5'SS	BP	5'SS	BP	5'SS	BP
S. cerevisiae	290	88	+	GT**TC**GT	TACTAAC	GTA**GTA**	**G**ACTAAC	GTAT**A**T	**A**ACTAAC	GTA**C**GT	TACTAAC
S. paradoxus	ND	ND	+	GT**TC**GT	TACTAAC	GTA**GTA**	**G**ACTAAC	GTAT**A**T	**A**ACTAAC	GTA**C**GT	TACTAAC
S. mikatae	288	85	+	GT**TC**GT	TACTAAC	GTA**GTA**	TACTAAC	GTAT**A**T	**A**ACTAAC	GTA**C**GT	TACTAAC
S. kudriavzevii	288	86	+	GTTTGT	TACTAAC	GTA**GTA**	**G**ACTAAC	GTAT**A**T	TACTAAC	GTA**C**GT	TACTAAC
S. bayanus	288	86	+	GTTTGT	TACTAAC	GTA**GTA**	**G**ACTAAC	GTAT**A**T	**A**ACTAAC	GTA**C**GT	TACTAAC

Genes of the Mer1 regulon are conserved across the Saccharomyces sensu stricto group, and retain non-consensus splice sites. The consensus 5'SS sequence is GTATGT, and the consensus BP sequence is TACTAAC. Deviations from the consensus splice site sequences are in bold. Ribosomal protein gene enrichment among intron containing genes also persists. Data are from (31) and the Fungal BLAST project on the Saccharomyces Genome Database.

essary (albeit not sufficient) for expression of *MER1* in diploid Ume6-containing cells. As it was previously demonstrated that other factors contribute to *MER1* expression (28), it will be important to decipher how the Swi/Snf complex may prime the chromatin environment of the *MER1* promoter to facilitate *MER1* mRNA expression (Figures 4 and 5, Supplementary Figure S6). Interestingly, this is not the only example of chromatin remodeling contributing to finely timed transcription factor binding and transcriptional activation in the meiotic program. For example, Inai *et al.* demonstrated that expression of *IME2* involves chromatin remodeling to overcome HDAC-dependent nucleosome placement over the *IME2* TATA element (32). Moreover, temporally regulated binding of Ime1p to the *IME2* gene ensures a biologically important lag in *IME2* expression (32).

We also show a crucial role for competitive acetyl marks on histone H3 and Snf2 to achieve temporal and spatial specificity of Snf2 targeting. While it is possible that there is active deacetylation of Snf2 (33), another possibility is that continued translation of *SNF2* leads to a rapid replacement of the acetylated population of Snf2 with an unacetylated one, allowing the protein to be targeted to the *MER1* locus. The retargeting of deacetylated Snf2 away from the RPG promoters and subsequent rapid downregulation of Snf2 corresponds to downregulation of ribosomal protein gene expression and a complete reprogramming of the cell's splicing landscape. Sustained translation and rapid turnover could also explain Snf2 downregulation a few hours after transfer to sporulation media. Once translation of *SNF2* is downregulated, potentially due to decrease in ribosomal activity, the existing degradation pathway turns over the remaining protein, leading to a loss Snf2. The relationship between Snf2 translation, deacetylation and degradation is likely to be important for fine-tuned control of the protein, which we are actively exploring. Remarkably, Snf2 expression is so tightly controlled during meiosis that its overexpression (an experiment we attempted to establish causation between Snf2 levels and meiotic events) is buffered in meiotic cells (data not shown). Nonetheless, our results illustrate the principle that competition (competition amongst acetylated residues for the Snf2 bromodomain and competition amongst different introns for the spliceosome) is an essential part of cellular adaptation to various environmental and/or developmental stresses. While core gene expression machineries, such as the transcription apparatus, the spliceosome and the ribosome appear to be abundant, new models must take into account that not only are these machineries limiting, but they can be more so under specific cellular conditions and substrate induced competition for gene expression machineries plays an important role in the determining regulatory outcomes (9,10).

Although Snf2 is the core catalytic component of the Swi/Snf complex and it has not been shown to function as an independent subunit, an outstanding question is whether Snf2 is the only component of Swi/Snf that contributes to meiotic regulation. Recent studies that measured changes in gene expression upon deletion of components of the Swi/Snf complex showed that deletion of Snf2 had broader and more significant changes in cellular expression profiles than other non-essential components of the complex (34,35). Importantly, expression of genes involved in translation and ribosomal assembly is downregulated in cells deleted of *SNF2*, but not when genes encoding other components of the Swi/Snf complex such as *SNF5* and *SNF12* are deleted. It has been suggested that the peripheral components of Swi/Snf perform regulatory and/or targeting roles within the complex and are dispensable for certain functions of Snf2. It has also been suggested that Snf2 can be targeted to genes with high H3K9-ac occupancy (such as the RPGs) even when the structural integrity of the Swi/Snf complex is compromised (34). Further studies are required to assess the degree to which the other subunits of the complex contribute to Snf2 regulation and activity during meiosis.

Interestingly, there is significant evidence that the process of translation is under heavy regulatory control during meiosis, across eukaryotes even as far as humans (36), perhaps for energetic reasons. We provide evidence here that the principle effector of this coordination between translational regulation and meiosis in hemiascomycetous yeast is the chromatin remodeling complex Swi/Snf.

One striking result is that the benefits of RPG downregulation and subsequent spliceosome redistribution are preferentially reaped by the genes of the Mer1 regulon (Supplementary Figure 2B). Snf2′s role in Mer1 expression is an important contributor to this effect since, as others have shown, Mer1 helps recruit spliceosomes to these pre-mRNAs (6). It may be unexpected, then, that the four Mer1-dependent introns all still have a range of splicing efficiency well below 100% (from about 50–75%). Other reports in the literature suggest that introns may possess intrinsic splicing properties. For example, different introns respond differently to perturbations in the splicing environment and

demonstrate variable dependencies on components of the spliceosome (2). Hence, each intron may also have an intrinsic 'maximum possible splicing efficiency,' a parameter determined by factors specific to the intron itself, such as the nature of its SSs, its length, its genetic context and the specific environmental conditions. Consistent with this, even though rapamycin treatment downregulates RPGs to an even greater extent than the deletion of Snf2 (Supplementary Figure S2D and E), the end point in terms of splicing efficiency remains the same. Hence, even with Mer1 present to 'attract' spliceosomes to RNAs, splicing efficiency appears to be an intrinsic property of these ICGs.

Although it does not appear to significantly impact Snf2's RPG/Mer1-dependent mechanism of meiotic splicing regulation, we cannot exclude the possibility that Snf2 may affect spliceosome assembly co-transcriptionally. Recent observations from studies in *Schizosaccharomyces pombe* also describe a role for Swi/Snf in splicing. However, these studies suggest that Swi/Snf stimulates spliceosome *activation* via its role in nucleosome deposition and maintenance (37). There exist significant functional differences between the complexes of the two yeast species. For example, reports suggest that many of the roles that the Swi/Snf complex performs in *S. cerevisiae* are, in *S. pombe*, divided between the RSC and Snf2 complexes (38), which might serve to explain differences in the specific roles of the complexes in splicing regulation. The studies in *S. pombe* nevertheless implicate the Swi/Snf chromatin remodeling activity in splicing regulation, a feature that appears to be conserved among metazoans as well (39,40).

Intriguingly, Swi/Snf has been shown to have roles in metazoan meiosis, although the molecular mechanisms underlying these roles are not known. Brg1, the ATPase subunit of the mammalian Swi/Snf complex, peaks in expression during the early stages of meiosis and is turned off in maturing round spermatids. Moreover, knocking down Brg1 results in prophase arrest during meiosis I, due to a failure to complete synapsis (41,42). Another protein involved in meiosis, mammalian HFM1/Mer3, is an integral part of the ZMM group of proteins. HFM1/Mer3 has been shown to be required for the completion of synapsis during meiosis, and deletion of Hfm1 closely resembles the phenotype of a Brg1 knockdown (43). While the details of meiotic regulation are unlikely to be exactly the same, it is interesting to note that the Swi/Snf complex has retained a role in regulating meiosis through evolution. Finally, global changes in splicing have been reported during male meiosis in mammals (44), so understanding the mechanism underlying this regulation and determining if Snf2 contributes to it are of particular interest.

This work reveals multiple mechanisms by which Swi/Snf acts as a nexus point in the regulation of meiosis in *S. cerevisiae*. All or a subset of these mechanisms may also be crucial in the gene regulation response to other physiological conditions that yeast might experience, which we are currently exploring.

ACCESSION NUMBERS

Data generated in this study is available under GEO accession number GSE94404.

SUPPLEMENTARY DATA

Supplementary Data are available at NAR Online.

ACKNOWLEDGEMENTS

We would also like to thank Dr Jerry Workman for the kind gift of the Snf2 K1493,1497R strain and the isogenic WT. We would also like to thank Lauren Neves and other members of the lab for critical reading of the manuscript.

FUNDING

National Institute of General Medical Sciences [GM-085474]; Whitcome Molecular Biology Pre-doctoral Fellowship (to S.V.); Whitcome Summer Research Fellowship (to A.R.G.). Funding for open access charge: National Institute of General Medical Sciences [GM-085474].
Conflict of interest statement. None declared.

REFERENCES

1. Naftelberg,S., Schor,I.E., Ast,G. and Kornblihtt,A.R. (2015) Regulation of alternative splicing through coupling with transcription and chromatin structure. *Annu. Rev. Biochem.*, **84**, 165–198.
2. Pleiss,J.A., Whitworth,G.B., Bergkessel,M. and Guthrie,C. (2007) Rapid, transcript-specific changes in splicing in response to environmental stress. *Mol. Cell*, **27**, 928–937.
3. Bergkessel,M., Whitworth,G.B. and Guthrie,C. (2011) Diverse environmental stresses elicit distinct responses at the level of pre-mRNA processing in yeast. *RNA*, **17**, 1461–1478.
4. Johnson,T.L. and Vilardell,J. (2012) Regulated pre-mRNA splicing: the ghostwriter of the eukaryotic genome. *Biochim. Biophys. Acta*, **1819**, 538–545.
5. Munding,E.M., Igel,A.H., Shiue,L., Dorighi,K.M., Trevino,L.R. and Ares,M. Jr (2010) Integration of a splicing regulatory network within the meiotic gene expression program of Saccharomyces cerevisiae. *Genes Dev.*, **24**, 2693–2704.
6. Spingola,M. and Ares,M. Jr (2000) A yeast intronic splicing enhancer and Nam8p are required for Mer1p-activated splicing. *Mol. Cell*, **6**, 329–338.
7. Qiu,Z.R., Schwer,B. and Shuman,S. (2011) Determinants of Nam8-dependent splicing of meiotic pre-mRNAs. *Nucleic Acids Res.*, **39**, 3427–3445.
8. Kadosh,D. and Struhl,K. (1997) Repression by Ume6 involves recruitment of a complex containing Sin3 corepressor and Rpd3 histone deacetylase to target promoters. *Cell*, **89**, 365–371.
9. Munding,E.M., Shiue,L., Katzman,S., Donohue,J.P. and Ares,M. Jr (2013) Competition between pre-mRNAs for the splicing machinery drives global regulation of splicing. *Mol. Cell*, **51**, 338–348.
10. Baumgartner,B.L., Bennett,M.R., Ferry,M., Johnson,T.L., Tsimring,L.S. and Hasty,J. (2011) Antagonistic gene transcripts regulate adaptation to new growth environments. *Proc. Natl. Acad. Sci. U.S.A.*, **108**, 21087–21092.
11. Berg,M.G., Singh,L.N., Younis,I., Liu,Q., Pinto,A.M., Kaida,D., Zhang,Z., Cho,S., Sherrill-Mix,S., Wan,L. *et al.* (2012) U1 snRNP determines mRNA length and regulates isoform expression. *Cell*, **150**, 53–64.
12. Merkhofer,E.C. and Johnson,T.L. (2012) U1 snRNA rewrites the "script". *Cell*, **150**, 9–11.
13. Dutta,A., Gogol,M., Kim,J.H., Smolle,M., Venkatesh,S., Gilmore,J., Florens,L., Washburn,M.P. and Workman,J.L. (2014) Swi/Snf dynamics on stress-responsive genes is governed by competitive bromodomain interactions. *Genes Dev.*, **28**, 2314–2330.
14. Grate,L. and Ares,M. Jr (2002) Searching yeast intron data at Ares lab web site. *Methods Enzymol.*, **350**, 380–392.
15. Dobin,A., Davis,C.A., Schlesinger,F., Drenkow,J., Zaleski,C., Jha,S., Batut,P., Chaisson,M. and Gingeras,T.R. (2013) STAR: ultrafast universal RNA-seq aligner. *Bioinformatics*, **29**, 15–21.

16. Livak,K.J. and Schmittgen,T.D. (2001) Analysis of relative gene expression data using real-time quantitative PCR and the 2(-Delta Delta C(T)) Method. *Methods*, **25**, 402–408.
17. Deutschbauer,A.M., Williams,R.M., Chu,A.M. and Davis,R.W. (2002) Parallel phenotypic analysis of sporulation and postgermination growth in Saccharomyces cerevisiae. *Proc. Natl. Acad. Sci. U.S.A.*, **99**, 15530–15535.
18. Padmore,R., Cao,L. and Kleckner,N. (1991) Temporal comparison of recombination and synaptonemal complex formation during meiosis in S. cerevisiae. *Cell*, **66**, 1239–1256.
19. Rockmill,B., Lambie,E.J. and Roeder,G.S. (1991) Spore enrichment. *Methods Enzymol.*, **194**, 146–149.
20. Khare,A.K., Singh,B. and Singh,J. (2011) A fast and inexpensive method for random spore analysis in Schizosaccharomyces pombe. *Yeast*, **28**, 527–533.
21. Gunderson,F.Q. and Johnson,T.L. (2009) Acetylation by the transcriptional coactivator Gcn5 plays a novel role in co-transcriptional spliceosome assembly. *PLoS Genet.*, **5**, e1000682.
22. Gunderson,F.Q., Merkhofer,E.C. and Johnson,T.L. (2011) Dynamic histone acetylation is critical for cotranscriptional spliceosome assembly and spliceosomal rearrangements. *Proc. Natl. Acad. Sci. U.S.A.*, **108**, 2004–2009.
23. Knight,B., Kubik,S., Ghosh,B., Bruzzone,M.J., Geertz,M., Martin,V., Denervaud,N., Jacquet,P., Ozkan,B., Rougemont,J. *et al.* (2014) Two distinct promoter architectures centered on dynamic nucleosomes control ribosomal protein gene transcription. *Genes Dev.*, **28**, 1695–1709.
24. Mallory,M.J., Cooper,K.F. and Strich,R. (2007) Meiosis-specific destruction of the Ume6p repressor by the Cdc20-directed APC/C. *Mol. Cell*, **27**, 951–961.
25. Martin,D.E., Soulard,A. and Hall,M.N. (2004) TOR regulates ribosomal protein gene expression via PKA and the Forkhead transcription factor FHL1. *Cell*, **119**, 969–979.
26. Brar,G.A., Yassour,M., Friedman,N., Regev,A., Ingolia,N.T. and Weissman,J.S. (2012) High-resolution view of the yeast meiotic program revealed by ribosome profiling. *Science*, **335**, 552–557.
27. Nachman,I., Regev,A. and Ramanathan,S. (2007) Dissecting timing variability in yeast meiosis. *Cell*, **131**, 544–556.
28. Engebrecht,J. and Roeder,G.S. (1990) MER1, a yeast gene required for chromosome pairing and genetic recombination, is induced in meiosis. *Mol. Cell. Biol.*, **10**, 2379–2389.
29. Awad,S. and Hassan,A.H. (2008) The Swi2/Snf2 bromodomain is important for the full binding and remodeling activity of the Swi/Snf complex on H3- and H4-acetylated nucleosomes. *Ann. N.Y. Acad. Sci.*, **1138**, 366–375.
30. Pnueli,L., Edry,I., Cohen,M. and Kassir,Y. (2004) Glucose and nitrogen regulate the switch from histone deacetylation to acetylation for expression of early meiosis-specific genes in budding yeast. *Mol. Cell. Biol.*, **24**, 5197–5208.
31. Hooks,K.B., Delneri,D. and Griffiths-Jones,S. (2014) Intron evolution in Saccharomycetaceae. *Genome Biol. Evol.*, **6**, 2543–2556.
32. Inai,T., Yukawa,M. and Tsuchiya,E. (2007) Interplay between chromatin and trans-acting factors on the IME2 promoter upon induction of the gene at the onset of meiosis. *Mol. Cell. Biol.*, **27**, 1254–1263.
33. Kim,J.H., Saraf,A., Florens,L., Washburn,M. and Workman,J.L. (2010) Gcn5 regulates the dissociation of Swi/Snf from chromatin by acetylation of Swi2/Snf2. *Genes Dev.*, **24**, 2766–2771.
34. Dutta,A., Sardiu,M., Gogol,M., Gilmore,J., Zhang,D., Florens,L., Abmayr,S.M., Washburn,M.P. and Workman,J.L. (2017) Composition and function of mutant Swi/Snf complexes. *Cell Rep.*, **18**, 2124–2134.
35. Sen,P., Luo,J., Hada,A., Hailu,S.G., Dechassa,M.L., Persinger,J., Brahma,S., Paul,S., Ranish,J. and Bartholomew,B. (2017) Loss of Snf5 induces formation of an aberrant Swi/Snf complex. *Cell Rep.*, **18**, 2135–2147.
36. Kleene,K.C. (2003) Patterns, mechanisms, and functions of translation regulation in mammalian spermatogenic cells. *Cytogenet. Genome Res.*, **103**, 217–224.
37. Patrick,K.L., Ryan,C.J., Xu,J., Lipp,J.J., Nissen,K.E., Roguev,A., Shales,M., Krogan,N.J. and Guthrie,C. (2015) Genetic interaction mapping reveals a role for the Swi/Snf nucleosome remodeler in spliceosome activation in fission yeast. *PLoS Genet.*, **11**, e1005074.
38. Monahan,B.J., Villen,J., Marguerat,S., Bahler,J., Gygi,S.P. and Winston,F. (2008) Fission yeast Swi/Snf and RSC complexes show compositional and functional differences from budding yeast. *Nat. Struct. Mol. Biol.*, **15**, 873–880.
39. Batsche,E., Yaniv,M. and Muchardt,C. (2006) The human Swi/Snf subunit Brm is a regulator of alternative splicing. *Nat. Struct. Mol. Biol.*, **13**, 22–29.
40. Tyagi,A., Ryme,J., Brodin,D., Ostlund Farrants,A.K. and Visa,N. (2009) Swi/Snf associates with nascent pre-mRNPs and regulates alternative pre-mRNA processing. *PLoS Genet.*, **5**, e1000470.
41. Kim,Y., Fedoriw,A.M. and Magnuson,T. (2012) An essential role for a mammalian Swi/Snf chromatin-remodeling complex during male meiosis. *Development*, **139**, 1133–1140.
42. Wang,J., Gu,H., Lin,H. and Chi,T. (2012) Essential roles of the chromatin remodeling factor BRG1 in spermatogenesis in mice. *Biol. Reprod.*, **86**, 186.
43. Guiraldelli,M.F., Eyster,C., Wilkerson,J.L., Dresser,M.E. and Pezza,R.J. (2013) Mouse HFM1/Mer3 is required for crossover formation and complete synapsis of homologous chromosomes during meiosis. *PLoS Genet.*, **9**, e1003383.
44. Schmid,R., Grellscheid,S.N., Ehrmann,I., Dalgliesh,C., Danilenko,M., Paronetto,M.P., Pedrotti,S., Grellscheid,D., Dixon,R.J., Sette,C. *et al.* (2013) The splicing landscape is globally reprogrammed during male meiosis. *Nucleic Acids Res.*, **41**, 10170–10184.

The chromatin remodeling complex SWI/SNF regulates splicing of meiotic transcripts in *S. cerevisiae*

Supplemental Materials

Srivats Venkataramanan[1,2], Stephen Douglass[1,2], Anoop Raj Galivanche[1,2], and Tracy L. Johnson[1,2*]
[1]Department of Molecular Cell and Developmental Biology
University of California, Los Angeles
[2]Molecular Biology Institute
University of California, Los Angeles

***To whom correspondence should be addressed**

Running title: Swi/Snf regulates meiotic splicing in *S. cerevisiae.*

Supplemental Figures

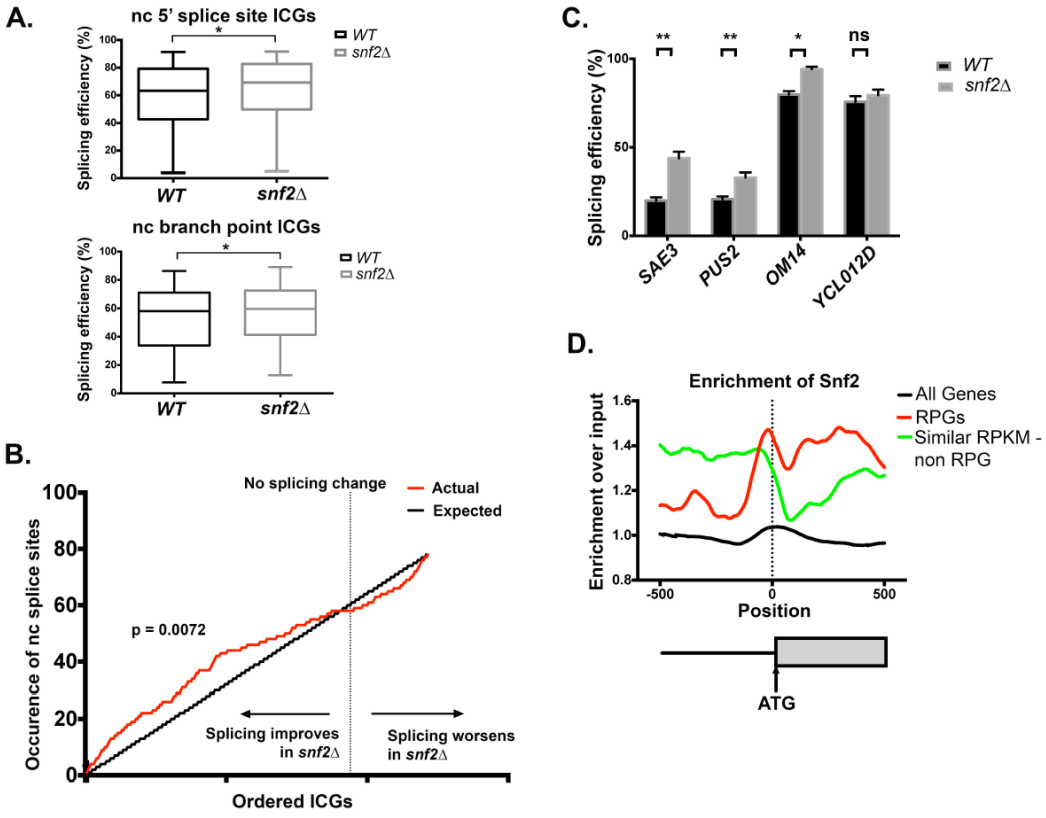

Figure S1

Figure S1: Deletion of Snf2 improves splicing of non-consensus splice site-containing introns.

A. Top: Changes in splicing efficiencies of ICGs with non-consensus 5' splice sites upon deletion of Snf2 (Paired two-tailed students t-test, n=46, $p<0.05$). Bottom: Changes in splicing efficiencies of ICGs with non-consensus branch points upon deletion of Snf2 (Paired two-tailed students t-test, n=39, $p<0.05$).

B. Cumulative frequency distribution plots indicating the cumulative number of introns containing nc splice sites (Y-axis) in an ordered list of ICGs ranked based on magnitude of splicing change in *snf2*Δ compared to *WT* (X-axis; most increase in splicing in *snf2*Δ on the left). Red line indicates the actual distribution, black line the average expected distribution based on total number of ncSS containing introns and total number of ICGs. Dotted line indicates position of

gene with no change in splicing in the ordered list of ICGs (Kolmogorov-Smirnov test, p=0.0072).

C. RT-PCR determining changes in splicing efficiencies of selected intron-containing genes with non consensus splice sites, upon deletion of *SNF2*. *YCL012C* has consensus splice sites. Quantification of splicing from three biological replicates. Black bars indicate splicing efficiency in *WT* vegetative cells. Grey bars indicate splicing efficiencies in *snf2*Δ vegetative cells. Error bars represent ± 1 SD (unpaired two-tailed Student's t-test; single asterisk represents $p<0.05$, two asterisks represents $p<0.005$).

D. Fold enrichment over input of Snf2 across the 500 nucleotides upstream and downstream of translational starts for all genes, RPGs and genes with RPKMs closest to the RPGs. Dotted line represents the annotated translational start (ATG). Analysis of data from [1].

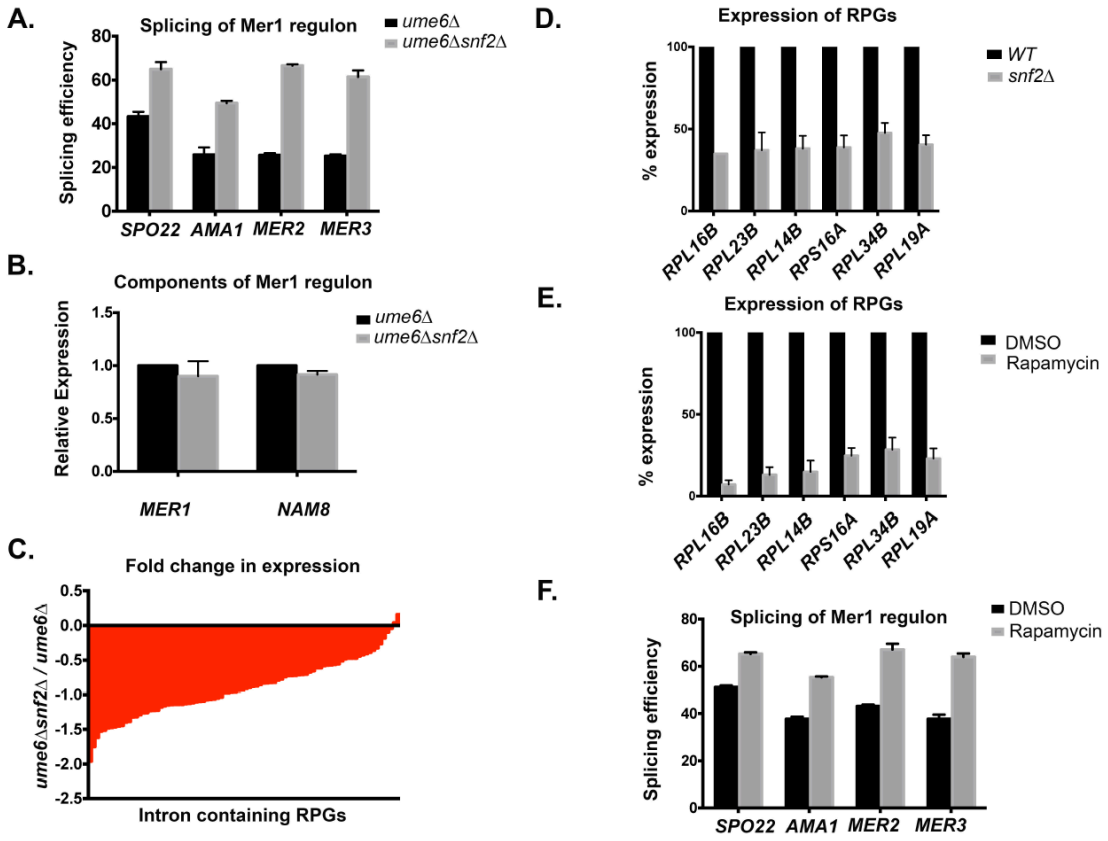

Figure S2

Figure S2: Deletion of Snf2 as well as rapamycin treatment decreases RPG expression.

A. Quantification of splicing from at least three biological replicates, corresponding to Figure 2C. Black bars indicate splicing efficiencies in *ume6Δ* vegetative cells. Grey bars indicate splicing efficiencies in *ume6*Δ*snf2*Δ vegetative cells. Note that *ume6Δ* also de-represses *MER1* [2]. Error bars represent ± 1 SD.

B. RT-qPCR measurement of *MER1* and *NAM8* transcripts between *ume6*Δ and *ume6*Δ*snf2*Δ strains. Mean of 3 biological replicates. Error bars represent ± 1 SD.

C. Log2-fold change in expression of intron-containing ribosomal protein genes upon deletion of *SNF2* in an *ume6*Δ background (n=88).

D. RT-qPCR measurement of selected intron-containing RPG transcripts between *WT* and *snf2*Δ strains. Mean of 3 biological replicates. Error bars represent ± 1 SD.

E. RT-qPCR measurement of selected intron-containing RPG transcripts between *ume6*Δ strain treated with rapamycin and control vehicle (DMSO). Mean of 3 biological replicates. Error bars represent ± 1 SD.

F. Quantification of splicing from at least two biological replicates, corresponding to Figure 2D. Black bars indicate splicing efficiencies in *ume6* Δ vegetative cells treated with DMSO. Grey bars indicate splicing efficiencies in *ume6*Δ vegetative cells treated with rapamycin. Error bars represent ± 1 SD.

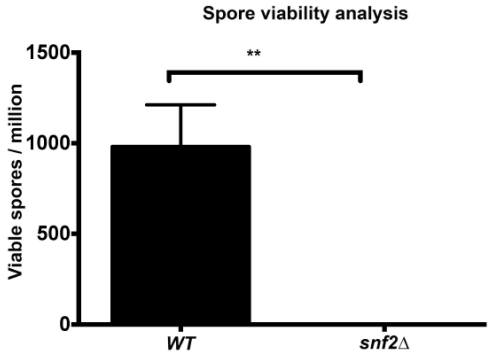

Figure S3

Figure S3: Absence of Snf2 abolishes spore formation.

*snf2*Δ diploid cells do not form viable spores. Spores counted from at least three biological replicates. Error bars represent ± 1 SD (Two tailed unpaired Student's t-test, $p<0.005$).

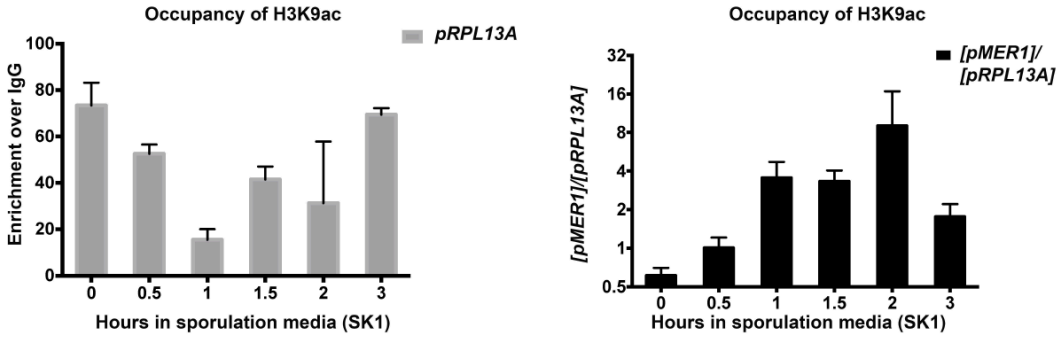

Figure S4

Figure S4: H3K9 acetylation at the RPG promoter and relative H3K9ac occupancy at the *MER1* and RPG promoters.

Left panel: Bar graph showing H3K9ac occupancy at the RPG promoter over time in sporulation media in the SK1 strain. Error bars represent ± 1 SD. Quantification from 3 biological replicates. Right panel: Relative H3K9ac at the *MER1* promoter to an RPG locus, upon chromatin immunoprecipitation using an anti-H3K9ac antibody, in a SK1 strain. Error bars represent ± 1 SD. Quantification from 3 biological replicates. Relative and absolute levels of Snf2 increases at the *MER1* locus after transfer to sporulation media.

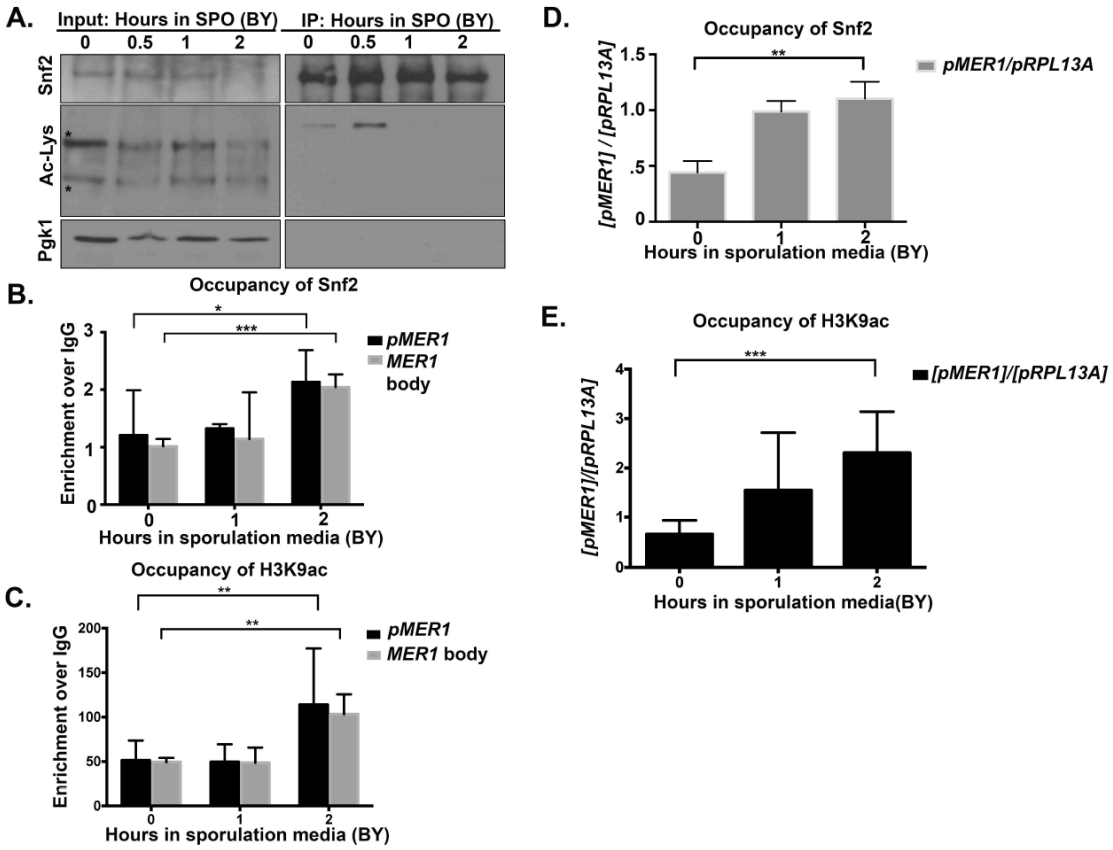

Figure S5

Figure S5: The timing of Snf2 activity is coordinated by its acetylation and acetylation of histones in the BY diploid yeast.

A. Immunoprecipitation of Snf2 during a time course of meiosis in *WT* BY diploid yeast. Snf2 acetylation decreases steadily between 0-2 hours after transfer into sporulation media, but Snf2 levels remain constant.

B. Bar graph showing Snf2 occupancy at the *MER1* promoter and gene body in the BY strain over time. Error bars represent ± 1 SD. Quantification from 3 biological replicates (unpaired two-tailed Student's t-test; one asterisk:$p<0.05$, three asterisks: $p<0.0005$).

C. Bar graph showing H3K9ac occupancy at the *MER1* promoter and body in the BY strain over time. Error bars represent ± 1 SD. Quantification from 3 biological replicates (unpaired two-tailed Student's t-test; $p<0.005$).

D. Relative Snf2 occupancy at the *MER1* promoter to an RPG locus, upon chromatin immunoprecipitation using an anti-Snf2 antibody, in a BY diploid strain. Error bars represent ± 1 SD. Quantification from 3 biological replicates (unpaired two-tailed Student's t-test; $p<0.005$). Relative and absolute levels of Snf2 increases at the *MER1* locus after transfer to sporulation media. Relative H3K9ac occupancy at the *MER1* promoter and gene body to an RPG locus, upon chromatin immunoprecipitation using an anti-H3K9ac antibody, in a BY diploid strain. Error bars represent ± 1 SD. Quantification from 3 biological replicates (unpaired two-tailed Student's t-test; $p<0.0005$). Relative and absolute levels of H3K9ac increases at the *MER1* locus after transfer to sporulation media.

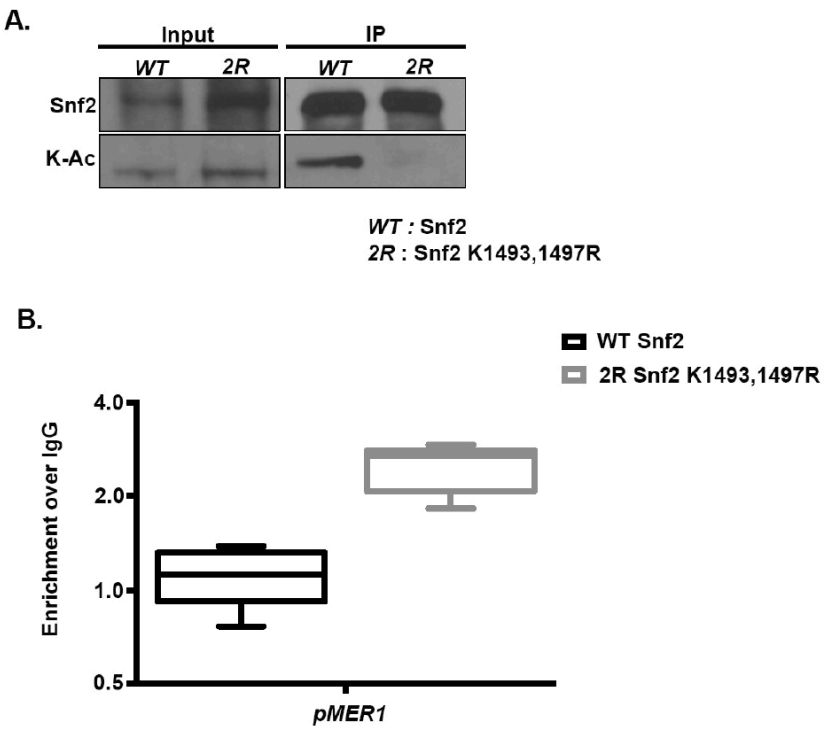

Figure S6

Figure S6: Occupancy of unacetylatable Snf2 at the *MER1* promoter.

A. Immunoprecipitation of a *WT* and unacetylable (*K1493,1497R*) mutant of Snf2. The mutant does not display any acetylation of Snf2.

B. Box-whisker graph showing occupancy at the *MER1* promoter of an unacetylatable mutant of Snf2 (*K1493,1497R*) compared to *WT*.

Supplemental Tables

Table S1

List of primers used in this study.

Table S2

List of splicing efficiencies of introns meeting read count filters in *WT* and *snf2*Δ, sorted by nature of splice site. Corresponds to Figure 1A. Note that certain introns have both non-consensus 5'SS and BP. These introns have only been considered once in the statistical analysis.

Table S3

Change in splicing efficiencies of introns meeting read count filters in *ume6*Δ and *ume6*Δ*snf2*Δ. Corresponds to Figure 2B.

Supplemental References

1. Dutta, A., Gogol, M., Kim, J.H., Smolle, M., Venkatesh, S., Gilmore, J., Florens, L., Washburn, M.P. and Workman, J.L. (2014) Swi/Snf dynamics on stress-responsive genes is governed by competitive bromodomain interactions. *Genes & development*, **28**, 2314-2330.

2. Munding, E.M., et al., *Integration of a splicing regulatory network within the meiotic gene expression program of Saccharomyces cerevisiae.* Genes Dev, 2010. **24**(23): p. 2693-704.

CHAPTER 4

Regulation of Snf2 during meiosis in *Saccharomyces cerevisiae.*

Introduction

Although they are both types of cell division, mitosis and meiosis are vastly different processes with profoundly distinct outcomes. Mitosis is a process in which a diploid parent cell gives rise to two identical daughter cells, retaining the amount of genetic material per cell. Meiosis, on the other hand, results in the formation of four haploid gametes from a single diploid parent cell, thereby halving the amount of genetic material per cell and permitting mating and sexual reproduction in a manner that still retains the genetic stability of the species. In higher eukaryotes, meiosis is a process restricted to progenitor germ cells. However, in unicellular eukaryotes such as yeast, the same diploid cell is capable of both mitotic and meiotic divisions in response to environmental cues (Honigberg, 2016). Switching from a mitotic to a meiotic mode of cell division requires extensive changes in gene expression and the cellular proteome (Kassir et al., 2003, Kumar et al., 2014).

In the budding yeast *Saccharomyces cerevisiae*, meiosis is induced in the absence of fermentable carbon sources and nitrogen starvation. The presence of either of these components has been proposed to inhibit the induction of meiosis via activation of the protein kinase A (PKA) pathway (Bolte et al., 2003). In addition, Ume6, a C6 zinc cluster DNA binding protein, also represses the transcription of numerous meiotic genes under non-meiotic conditions (Strich et al., 1994, Bowdish and Mitchell, 1993). Ume6 recruits the histone deacetylase Rpd3 to the loci where it is found, preventing initiation of transcription (Lardenois et al., 2015, Lamb and Mitchell, 2001, Kadosh and Struhl, 1997). However, Ume6 is converted to an activator early in meiosis, likely upon association with Ime1, the master regulator of meiotic induction (Washburn and Esposito, 2001, Rubin-Bejerano et al., 1996, Bowdish et al., 1995). The degradation of Ume6 is a key event in the induction of meiosis, and is performed by the anaphase-promoting

complex/cyclosome (APC/C) ubiquitin ligase, when it is activated by Cdc20 (Mallory et al., 2007). In addition to Cdc20, the APC/C has two other known stage-specific activators, Ama1 and Hct1/Cdh1 (Cooper et al., 2000, Schwab et al., 1997). Along with Cdc20, these activators also serve as specificity factors, targeting the activity of the APC/C to specific substrates in a cell-cycle dependent manner (Tan et al., 2011, Schwab et al., 1997, Visintin et al., 1997). The importance of the APC/C in meiosis is underscored by the requirement not only of Cdc20 for the initiation of meiosis, but also Ama1 for cellular exit from meiosis II, via targeted degradation of the Clb1 cyclin (Cooper et al., 2000). Interestingly, Ama1 is encoded by the *AMA1* intron-containing transcript, whose transcription is repressed by Ume6, and whose splicing is dependent on Mer1, a meiosis specific splicing enhancer also repressed by Ume6 (Munding et al., 2013, Spingola and Ares, 2000). Thus, APC/C association with Ama1 during meiosis absolutely requires the previous association with Cdc20. Ama1 association with the APC/C eventually degrades Cdc20 (Tan et al., 2011).

In addition to Ume6, numerous other proteins are degraded upon the induction of sporulation (or meiosis) in yeast (Kumar et al., 2014). The degradation of a number of these are dependent on the Cdc20 mediated activity of the APC/C. For example, Cdc20-activated APC/C is also required for the degradation of Pds1, an event that promotes chromosome segregation (Salah and Nasmyth, 2000, Visintin et al., 1997). However, it is also likely that numerous other contributing factors are required to degrade one or more specific proteins. In fact, since Cdc20 is also mitotically active, other proteins/factors are likely required for targeting specifically to meiotic targets (Harper et al., 2002). For instance, the degradation of Ume6 itself is induced by its acetylation by Gcn5, and repressed by deacetylation by Rpd3 (Mallory et al., 2012). Numerous proteins are absent in various stages during meiosis, despite the fact that their cognate

mRNAs have been observed at the same times, indicating the prevalence and importance of protein degradation mechanisms in shaping and maintaining the meiotic proteome (Kumar et al., 2014).

The meiotic proteome is also heavily regulated at the level of translation. Meiosis in *S. cerevisiae* is fundamentally a response to stress, and as such translation is globally repressed during meiosis. This is evidenced by downregulation of the translational machinery during meiosis, as well as proteomic analyses of yeast cells undergoing meiosis (Venkataramanan et al., 2017, Munding et al., 2013, Kumar et al., 2014). While this global downregulation of translation helps restrict the cells overall energy consumption, several transcripts whose products are essential for survival and/or recovery have to be translated. In order to achieve this, yeast cells have adopted numerous meiotic translational regulatory mechanisms, involving both cis-elements within the mRNAs as well as trans- regulatory factors that recognize specific features within transcripts. Specialized regulation of translation during meiosis is not unique to yeast. In fact, mammalian spermatogenic cells have diverse mechanisms of specialized translation, including but not limited to the expression of specific translational regulators, modifying the canonical machinery of translation, and modulating transcript architecture (UTRs) to regulate translational output (reviewed in (Kleene, 2013, Kleene, 2003)).

Since the translation of most eukaryotic mRNAs occurs via the scanning mechanism, the 5’ untranslated regions (5’ UTRs) of transcripts are rich in regulatory potential. The 5’ UTR and cap are critical for the recruitment of the ribosome to the transcript as well as the choice of the start codon. The canonical mechanism of translation initiation is reviewed elsewhere (Hinnebusch, 2017, Aylett and Ban, 2017). Briefly, the assembled translation pre-initiation complex (PIC) loads onto a capped mRNA transcript in an eIF4F dependent manner. The PIC

scans the 5' UTR for an AUG start codon using complementarity with the anticodon of Met-$tRNA_i$. Once a start codon is identified, the rest of the ribosome is assembled, and translation elongation proceeds. The choice of start codon is influenced by numerous factors, including but not limited to 5' UTR structure, near-cognate start codons, RNA modifications; and is critical for the regulation of translation.

One of the most common ways by which 5' UTRs influence the translation of the downstream coding sequence (CDS) is via the utilization of upstream open reading frames (uORFs). Often, the first cognate or near-cognate start codon the ribosome encounters as it scans the transcript from the 5' end is not the correct start for the major protein encoded by that transcript. This start codon can however recruit scanning ribosomes to itself, reducing the fraction that reaches the downstream, 'correct' start codon. Such start codons are most often associated with a stop codon in the same frame, giving rise to a short upstream open reading frame (uORF) (Hinnebusch et al., 2016). In most cases, uORFs are inhibitory or neutral to the translation efficiency of the downstream CDS, since they prevent the initiating ribosome from reaching the CDS (Johnstone et al., 2016). The canonical example of such regulation was described for the *GCN4* transcript in yeast (Mueller and Hinnebusch, 1986). In addition, uORFs appear to have negative effects on mRNA abundance, likely due to the presence of stalled ribosomes within the uORF targeting the transcript towards quality control pathways (Johnstone et al., 2016).

In *S. cerevisiae*, the 5' ends of transcripts vary drastically under a variety of stress conditions, including DNA damage, salt stress, and nitrogen starvation (Waern and Snyder, 2013). This widespread use of alternative 5' ends exposes numerous uORFs with regulatory potential in response to stress, indicating that regulation of 5' UTRs and uORFs might be a

general stress-response mechanism in budding yeast (Waern and Snyder, 2013). Previous studies have indicated that the meiotic transcriptome in yeast is extraordinarily plastic and numerous individual transcript undergo profound changes in their architecture during the process of meiosis (Guisbert et al., 2012). A number of these transcripts experience either 5' UTR elongation or regression at specific stages during meiosis, in some cases exposing uORFs with potential regulatory function (Guisbert et al., 2012). Ribosome occupancy studies have recently shown that this change in transcript architecture is in fact coupled to uORF 'functionality', as it relates to the ability of the uORF to recruit ribosomes (Brar et al., 2012). Transcripts with uORFs containing a cognate start codon (AUG) broadly showed decreased translation efficiency of the downstream ORF. Surprisingly, transcripts with ORFs containing only near-cognate start codons (UUG and CUG being the most prevalent), show a positive correlation with the translation of their downstream ORF (Brar et al., 2012). It is as yet unclear how these near cognate uORFs increase the translation of their downstream coding sequences. One potential model is that the uORF increases ribosomal buildup upstream of the start codon of the CDS, and under conditions that favor leaky scanning or reinitiation over disassembly of the ribosome, increase the functional rate of initiation at the CDS.

The regulatory potential of uORFs is not limited to their post-termination based regulation of ribosome occupancy on their associated downstream CDS. Occasionally, the small peptides encoded by the uORFs possess regulatory function. The first described example of this was the arginine attenuator peptide (AAP) encoded by a uORF within the *CPA1* transcript. AAP inhibits the translation of the downstream *CPA1* ORF in response to a surplus of arginine within the media (Gaba et al., 2001). In at least one case, transient elongation of a transcript during meiosis (*SPO24*) exposes a uORF that encodes for a conserved, small (67 amino acid) factor that

is required for efficient sporulation (Hurtado et al., 2014). In addition, the meiotic transcriptome includes many transcripts from regions of the genome with little to no protein-coding capacity (Smith et al., 2014). However, these transcripts associate with ribosomes, and in at least two cases, small peptides of unknown function arising from them have been detected (Smith et al., 2014).

In addition to changing transcript architecture, epitranscriptomic modifications on mRNAs have also been shown to have profound effects on gene regulation. Perhaps the best studied of these modifications is the addition of a methyl group at the N^6 position of an adenosine base to form N^6-methyladenosine, or m^6A. m^6A is an ubiquitous modification amongst eukaryotes, and has been shown to have profound roles in development, differentiation and disease (Roignant and Soller, 2017). The m^6A modification is likely 'written' co-transcriptionally (Ke et al., 2017), and is involved in every aspect of gene regulation, including splicing, export, translation and decay (reviewed in (Yue et al., 2015, Roignant and Soller, 2017)). m^6A is a dynamic modification, and is found predominantly in the 3'UTRs and near the stop codons of transcripts (Meyer et al., 2012, Ke et al., 2015). m^6A has been shown to regulate translation via different mechanisms. Binding of YTHDF1 'reader' proteins to m^6A containing transcripts recruits translation machinery to said trasncripts (Wang et al., 2015). m^6A is also found in the 5' UTR of transcripts, where it serves as a regulator of translation (Meyer et al., 2015a). m^6A found within the 5' UTR has been shown to directly recruit eIF3 and the 43S complex in a cap-independent manner, promoting the translation of specific transcripts in response to stress, such as *HSP70* (Meyer et al., 2015b, Zhou et al., 2015). Interestingly, eIF3 has also been shown to be required for the reinitiation of translation by ribosomes that terminate on

short uORFs within a transcript, suggesting potential co-regulation of translation by uORFs and m^6A methylation (Mohammad et al., 2017).

m^6A is involved in various aspects of sexual reproduction across eukaryotes. It has been shown to be crucial for the determination of sex in *Drosophila* (Kan et al., 2017, Lence et al., 2016, Haussmann et al., 2016). In zebrafish, clearance of maternal mRNA transcripts and the maternal to zygotic transition (MZT) is dependent on m^6A modification of maternal transcripts (Zhao et al., 2017). In *Schizosacchoromyces pombe*, a YTH domain m^6A 'reader' protein has adopted a novel role to clear meiotic transcripts during vegetative growth (Wang et al., 2016, Harigaya et al., 2006). *S. cerevisiae* have only a single identified m^6A methyltransferase complex, the catalytic subunit of which is Ime4 (Bodi et al., 2010, Agarwala et al., 2012). Ime4 was originally thought to be only active during meiosis; however, a recent study has demonstrated low level Ime4 activity under vegetative growth and a role in vacuolar morphology (Clancy et al., 2002, Yadav and Rajasekharan, 2017). Nonfunctional Ime4 abolishes meiosis in *S. cerevisiae*, and a recent study provided a comprehensive map of m^6A methylation sites within the yeast transcriptome through meiosis, revealing that m^6A methylation through meiosis is dynamic, and that the methylation sites are conserved (Schwartz et al., 2013). Interestingly, a previous study had also shown induction of Ime4 and m^6A methylation upon prolonged rapamycin treatment (Bodi et al., 2015). Both meiosis and rapamycin treatment cause enrichment of m^6A methylated transcripts on translating ribosomes, indicating that in sporulating yeast, m^6A might promote translation (Bodi et al., 2015).

We have previously shown that the levels of Snf2, the ATPase subunit of the chromatin-remodeling SWI/SNF complex, decreases dramatically and rapidly upon the induction of sporulation (Venkataramanan et al., 2017). Here we show that regulated degradation, changes in

transcript architecture, and N^6-methyladenosine (m^6A) modification of the *SNF2* mRNA potentially contribute to multi-level control of Snf2 protein during sporulation.

Results

Degradation of Snf2 during sporulation requires *de novo* translation: The degradation of Snf2 is specific to the transition to sporulation conditions, i.e. Snf2 is not degraded upon continuing growth in a high nutrient environment **(Figure 4.1A)** In order to better understand the mechanism of Snf2 downregulation during sporulation, we treated BY diploid cells with cycloheximide (CHX), a potent inhibitor of translation elongation, to block *de novo* protein synthesis and measured Snf2 protein levels by western blot (Schneider-Poetsch et al., 2010, Siegel and Sisler, 1963). To our surprise, treatment with CHX stabilized Snf2 levels during sporulation dramatically. While cells treated with control vehicle (DMSO) exhibited downregulation of Snf2 protein within 2 hours post-shift to sporulation media, cells treated with CHX showed no appreciable decline in Snf2 levels up to 4 hours post-shift to sporulation media **(Figure 4.1B)**.

To rationalize the effect of CHX on Snf2 protein levels, we propose that Snf2 is targeted for degradation by an as yet unknown sporulation-specific factor 'X'. The degradation of Snf2 requires prior translation of X from the transcript that encodes for it. The addition of CHX blocks not only the translation of Snf2 from its pre-mRNA (which in isolation would be predicted to increase the rate of degradation of Snf2), but also the translation of protein X. Since Snf2 is also an intrinsically stable protein, with a half-life of 4.6 hours (Christiano et al., 2014), CHX effectively stabilizes the Snf2 protein under sporulation conditions **(Figure 4.1C)**. It is important

to mention that neither protein X nor a mechanism for its action has as yet been identified. Experiments to answer these outstanding questions are ongoing.

Relative abundance of *SNF2* transcript isoforms changes during sporulation: We have previously shown that Snf2 downregulation during sporulation is preceded by its deacetylation, and that this pool of deacetylated Snf2 is crucial for the induction of meiosis (Venkataramanan et al., 2017). However, an outstanding question is whether the existing cellular pool of Snf2 is actively deacetylated early in sporulation; or if the acetylated Snf2 is degraded and a new, non-acetylated pool of Snf2 protein is translated *de novo*. Although putative enzymes that partially deacetylate Snf2 have been identified, their meiotic activity remains unknown (Kim et al., 2010).

To determine whether the *SNF2* transcript contained features that could potentially contribute to its regulated translation during sporulation, we examined the genomic locus of *SNF2*. We observed the presence of a putative 39-base long uORF with a cognate (AUG) start codon approximately 500 bases upstream of the *SNF2* coding sequence **(Figure 4.2)**. However, this uORF was located roughly 350 bases upstream of the annotated transcription start site for the *SNF2* transcript (Malabat et al., 2015) **(Figure 4.2)**. Regulated 5' leader extension and usage of uORFs has been previously shown to be a pervasive phenomenon during meiosis in S. cerevisiae, although the significance of such events is as yet unknown (Brar et al., 2012, Hurtado et al., 2014). Therefore, we assayed whether the *SNF2* transcript shows 5' leader extension in a manner that would be predicted to include the uORF during sporulation. We found that a form of the *SNF2* transcript with a longer 5' leader region ($SNF2_{5'long}$ - potentially from an upstream promoter) is expressed in a transient burst during early sporulation in both BY and SK1 strain backgrounds, albeit with different expression patterns **(Figure 4.3A, 4.3D).** We further

confirmed that this was not spurious meiotic transcription, and was in fact a *bona fide* 5' leader for the *SNF2* CDS using a forward primer within the uORF unique to the elongated transcript, and a reverse within the *SNF2* CDS, with the amplicon demonstrating the contiguous nature of this transcript **(Figure 4.3B, 4.3E)**. uORFs have previously been demonstrated to exert both positive and negative translational control on the downstream coding sequences within the same transcript via a variety of mechanisms (Wethmar, 2014). The uORF within the elongated *SNF2* transcript also demonstrates ribosome occupancy under conditions of nutrient starvation (Pieter Spealman and Dr. Joel McManus, private communication), suggesting that production of Snf2 protein during sporulation could be partially regulated by its uORF. However, we observe no changes in bulk Snf2 levels over the first two hours of sporulation, corresponding to the wave of $SNF2_{5'long}$ expression **(Figure 4.3C, 4.3F).** This does not preclude the possibility that translation $SNF2_{5'long}$ is utilized to maintain bulk Snf2 levels, compensating for turnover of the existing, acetylated cellular pool of Snf2.

Absence of *SNF2* uORF leads to a modest decrease in Snf2 acetylation and bulk protein levels early in sporulation: uORFs with cognate start codons have previously been reported to repress the translation of the downstream coding sequence (Brar et al., 2012). To determine the role of the *SNF2* uORF on Snf2 during meiosis, we performed a clean deletion of the uORF using the *delitto-perfetto* method in the BY strain background (Storici and Resnick, 2006). Surprisingly, we observed that upon deletion of the uORF, the rate of downregulation of Snf2 is increased slightly **(Figure 4.4A).** We further examined the acetylation state of Snf2 post transition to sporulation media. We observed that the absence of the uORF results in more rapid deacetylation of Snf2 during sporulation **(Figure 4.4B).** These results indicate that the uORF has

an overall positive, albeit modest, effect on the translation of Snf2 early upon transfer to sporulation media.

A possibly confounding observation is that although the fraction of total *SNF2* transcript made up by $SNF2_{5'long}$ increases during sporulation **(Figure 4.4C)**, the total *SNF2* transcript levels pre-sporulation decreases upon the deletion of the uORF region **(Figure 4.4D)**. This is likely because the uORF forms part of the promoter utilized to generate the *SNF2* transcript during vegetative growth. However, after 1 hour of growth in sporulation media, no difference in the total *SNF2* mRNA levels is observed **(Figure 4.4D)**, indicating possible usage of a different promoter, consistent with the shift in the TSS observed previously during sporulation. The possibility that the changes in Snf2 protein are a consequence of this difference in pre-sporulation *SNF2* transcript levels cannot be eliminated.

Proportion of $SNF2_{5'long}$ increases dramatically late in sporulation: While a modest increase in the fraction of total *SNF2* transcript made up of $SNF2_{5'long}$ is observed early in sporulation in the BY strain **(Figure 4.4C, 4.5A),** we observe a far greater increase later in sporulation (~18 hours post transfer to sporulation media) **(Figure 4.5A).** This change is not precipitated by major changes in total *SNF2* transcript levels, which remain steady through sporulation (data not shown), but is likely rather due to preferential transcription of $SNF2_{5'long}$ during sporulation. It is important to note that at these time points, Snf2 protein is completely undetectable (Venkataramanan et al., 2017). The *SNF2* transcripts are therefore likely being retained in a translation-repressed state. Interestingly, while the SK1 strain does not show the same small increase in $SNF2_{5'long}$ early in sporulation, the pre-sporulation proportion of $SNF2_{5'long}$ is substantially larger than in the BY strain **(Figure 4.5A)**. However, the SK1 strain

also demonstrates a similar increase in the proportion of $SNF2_{5'long}$ later in sporulation **(Figure 4.5A).**

***SNF2* uORF confers no fitness advantage post-sporulation:** We hypothesized that the uORF contributed to the translation-repression of the *SNF2* transcript late in sporulation and allowed the yeast cell to retain levels of the transcript comparable to that during vegetative growth without expending the energy to translate it. Further, we speculated that this retention of the *SNF2* transcript during sporulation is a form of 'bet-hedging', and helps the yeast recover faster when it subsequently encounters a nutrient rich environment after an extended time in a nutrient-deprived environment, such as sporulation conditions (Arribere et al., 2011).

In order to test this hypothesis, we co-inoculated equal numbers of post-sporulation *WT* and $uORF^{\Delta/\Delta}$ spores (SK1 background) into YPD, and monitored their growth over 24 hours. We measured the relative levels of each strain at the indicated time points by isolating total genomic DNA from the culture and measuring the ratio of the uORF:SNF2 CDS as a readout of the fraction of *WT* cells. We observed that the uORF confers no observable fitness advantage to the yeast cells for growth in glucose containing media post-sporulation **(Figure 4.5B).** However, this does not exclude the possibility of fitness advantages during growth in other, perhaps sub-optimal media conditions.

Yeast undergoing sporulation experience two waves of m^6A RNA methylation: It is well documented that yeast experience m^6A RNA methylation during sporulation (Clancy et al., 2002, Bodi et al., 2010, Schwartz et al., 2013). However, the differences in sporulation protocols used in these prior studies and ours means that these prior observations miss out on a number of early sporulation events (Venkataramanan et al., 2017). Directly transferring logarithmically growing yeast (BY or SK1 strains) to sporulation media results in two distinct waves of m^6A

RNA methylation. The first wave of total m^6A methylation peaks within 1 hour after the shift to sporulation media and drops down to pre-sporulation levels within 2 hours **(Figure 4.6A)**. Intriguingly, this tracks well with the first peak of the *SNF2*$_{5'long}$ transcript **(Figure 4.3A, 4.5A)**. The second wave of m^6A RNA methylation during sporulation kicks off between 4-6 hours and is sustained at least until about 18 hours after the shift to sporulation media **(Figure 4.6A)**. Satisfyingly, this also tracks with the second, sustained peak of *SNF2*$_{5'long}$ transcript, suggesting that the methylation of the transcript and the 5' leader extension might play complementary roles in the regulation of Snf2 translation.

In order to further examine the dynamics of m^6A RNA methylation during early sporulation, we performed a finer time course of methylation. In the BY strain, total m^6A RNA methylation peaks rapidly (within 30 minutes of transfer to sporulation media), and falls equally rapidly **(Figure 4.6B)**. The differences between the precise timing of the short and long time courses can be attributed to experimental variability. However, while methylation in the SK1 strain follows the same overall pattern, we observe that it demonstrates far higher pre-sporulation m^6A RNA methylation than the BY strain **(Figure 4.6B)**.

The remarkable similarity between the observed patterns of m^6A RNA methylation and abundance of *SNF2*$_{5'long}$ transcript during sporulation in yeast led us to query whether the *SNF2* transcript is methylated during sporulation. A previous study mapped the yeast RNA methylome during sporulation (Schwartz et al., 2013) and demonstrated that the *SNF2* transcript has two annotated sites of m^6A methylation, one within the 5' UTR of the transcript, and the other near the 3' end of the coding sequence **(Figure 4.6C)**. This pattern was not surprising, since m^6A methylation is known to cluster in the 5' and 3' UTRs of mRNA transcripts (Meyer et al., 2015a, Ke et al., 2015). Intriguingly, the 5' UTR methylation site for the *SNF2* transcript is

upstream of the canonical transcription start site, implying that is unique to the *SNF2*$_{5'long}$ transcript isoform **(Figure 4.6C)**. This further supports the model of co-regulation of Snf2 translation by methylation and 5' leader extension during early sporulation.

The data presented in this chapter argue that Snf2 deacetylation, degradation, and translation are highly regulated during sporulation. Changes in transcript leader length, dynamic m^{6}A methylation of the Snf2 transcript as well as meiosis specific factors involved in degradation of Snf2 coordinate to orchestrate the molecular events that leading to the dual role of the SWI/SNF complex in yeast sporulation described previously (Venkataramanan et al., 2017). We propose a model wherein the pre-sporulation pool of acetylated Snf2 is degraded rapidly upon transition to sporulation media. Translation from the pulse of the *SNF2*$_{5'long}$ transcript during early sporulation results in the synthesis of *de novo,* unacetylated Snf2, which subsequently localizes to the *MER1* promoter (and other targets) as previously demonstrated (Venkataramanan et al., 2017). This translation is aided, via as yet undetermined mechanisms, by the presence of the uORF and m^{6}A methylation site within *SNF2*$_{5'long}$. Later in sporulation, *SNF2*$_{5'long}$ is translationally repressed and sequestered, possibly in stress granules, as part of a 'bet-hedging' strategy by the yeast cells. Further experimentation is required to reveal the exact nature of the regulatory elements involved in this process.

Discussion

The meiotic proteome in *Saccharomyces cerevisiae* is complex, temporally dynamic and highly regulated (Becker et al., 2017). Early studies demonstrated that turnover of a substantial fraction of the pre-sporulation proteome was essential for the progression of meiosis in yeast (Klar and Halvorson, 1975, Zubenko and Jones, 1981). Subsequent work has demonstrated

extensive temporal regulation of translation during meiosis in yeast, serving to shape and reshape the meiotic proteome in a stage-specific manner (Brar et al., 2012). This precise regulation of protein products has been shown to be significant in numerous cases, such as the regulated degradation of Ume6 for meiotic entry, or delayed translation of Ssp2 for spore wall assembly, amongst others (Mallory et al., 2007, Tio et al., 2015, Whinston et al., 2013, Brar et al., 2012). We have previously shown that the temporally coordinated deacetylation and degradation of Snf2 is required for the proper progression of meiosis in *S. cerevisiae* (Venkataramanan et al., 2017). In this chapter we show that Snf2 protein is subject to regulation at the levels of translation, deacetylation, and degradation during sporulation in yeast, and begin to explore the mechanisms of this multi-level control.

The stabilization of Snf2 during sporulation upon inhibition of *de novo* translation by CHX treatment suggests that the synthesis of sporulation-specific factors is required for its degradation **(Figure 4.1)**. While the identity of these potential factors is unknown, there exist numerous potential candidates. Degradation of Ume6 is absolutely critical for meiotic induction, and is mediated by Cdc20-dependent activation of the APC/C E3 ubiquitin ligase complex (Mallory et al., 2007). Cdc20 is also required during G2 and M phases of the mitotic cell cycle. The exact mechanism of the specificity of APC/C^{Cdc20} during meiosis remains unknown, although it has been suggested that specificity is conferred via its association with Ime1 (Prinz et al., 1998, Mallory et al., 2007). Since we have previously shown that the degradation of Snf2 during sporulation precedes the induction of *IME1* transcription, it seems unlikely that Ime1 could bestow APC/C^{Cdc20} with its specificity (Venkataramanan et al., 2017). However, that does not preclude the possible existence of other activators of the APC/C playing a role in the degradation of Snf2 during sporulation.

Apart from the APC/C, other E3 ubiquitin ligase complexes in yeast have been shown to respond to the availability of nutrients. For example, the transition from logarithmic growth to quiescence upon the depletion of nutrients induces the degradation of proteins like Aah1, an adenine deaminase, by Saf1 mediated activation of the SCF ubiquitin ligase complex (Escusa et al., 2006). The activity of the Rsp5 ubiquitin ligase complex has been shown to be required for the remodeling of gene expression upon nutrient depletion in yeast, and reversing the effects of the TOR complex (Crespo et al., 2004, Cardona et al., 2009). Interestingly, Rsp5 has roles not only in inducing stress-response genes, but also in downregulating RPG mRNA levels in response to nutrient deprivation, via an as-yet-unknown mechanism (Cardona et al., 2009). Snf2 is downregulated in response to nutrient depletion during sporulation as well as during diauxic shift, which in turn leads to RPG downregulation (Venkataramanan et al., 2017, Awad et al., 2017). We postulate that the role of Rsp5 in downregulating RPG transcripts could be achieved via its targeted degradation of Snf2 in response to nutrient deprivation. Although a high-throughput screen of Rsp5 targets failed to identify Snf2 as a candidate under nutrient dense conditions, the possibility of a specific activator of Rsp5 being synthesized under nutrient deplete conditions and targeting Snf2 for degradation remains (Kus et al., 2005).

Although there is active degradation of *SNF2* in early sporulation, deletion of the uORF specific to the $SNF2_{5'long}$ transcript leads to a more rapid decrease in Snf2 levels during sporulation, indicating that the $SNF2_{5'long}$ transcript might be experiencing active translation and contributing to the cellular pool of Snf2 **(Figure 4.4A)**. We hypothesize that the existing pre-sporulation pool of Snf2 is degraded, replaced by *de novo* translated Snf2, partially from the canonical 5' UTR containing transcript, and partially from $SNF2_{5'long}$. The reduced acetylation of Snf2 in the $uORF^{\Delta/\Delta}$ strain could be due to preferential degradation of acetylated Snf2, via the

mechanisms postulated previously **(Figure 4.4B)**. Results from previously published reports would predict the uORF within the *SNF2*$_{5'long}$ transcript to have a repressive effect on the translation of the downstream ORF (since the uORF has a cognate start codon- AUG), however, our results demonstrate the opposite (Brar et al., 2012). Production of Snf2 from *SNF2*$_{5'long}$ could be due to leaky scanning of the ribosome through the start codon of the uORF, a feature whose frequency increases under the conditions of nutrient stress under which *SNF2*$_{5'long}$'s abundance increases **(Figure 4.2)** (Lee et al., 2009, Palam et al., 2011, Sundaram and Grant, 2014). Alternatively, the small subunit of the ribosome could be retained on the mRNA post termination at the stop codon of the uORF followed by reformation of a ternary complex and subsequent reinitiation at the start site of the Snf2 coding sequence. In the example of the *GCN4* mRNA, reinitiation has been shown to be dependent on numerous *cis*- and *trans*- factors, including the sequences flanking the uORFs, eIF3 retention on the mRNA post termination and the uORF, and the abundance of ribosomal components (reviewed in (Valasek, 2012)). Similar to the reinitiation-competent uORF1 within the *GCN4* transcript, the stop codon the uORF within *SNF2*$_{5'long}$ is flanked by AU-rich sequences (data not shown), which have been suggested to favor reinitiation (Grant and Hinnebusch, 1994). However, more recently, it has been demonstrated that specific sequences (Reinitiation Promoting Elements – RPEs) flanking uORF1 interact with eIF3 post termination at that uORF, and that this contact is crucial for retaining the small subunit of the ribosome and the resumption of scanning (Szamecz et al., 2008). While the nature of flanking sequences within the uORF in *SNF2*$_{5'long}$ has not been experimentally tested for the presence of functional RPEs, the transcript does possess another interesting feature that could contribute to the retention of eIF3. The *SNF2*$_{5'long}$ transcript has a specific, annotated m^6A methylation site between the uORF and the CDS **(Figure 4.6C)** (Schwartz et al., 2013).

Interestingly, the methylation at the 5' UTR site of the *SNF2*$_{5'long}$ transcript shows a pulsed pattern that appears similar to the early peak of total m^{6}A methylation that we observe during sporulation **(Figure 4.6)** (Schwartz et al., 2013). Crucially, m^{6}A within the 5' UTR has been shown to be able to directly bind eIF3 and promote cap-independent translation initiation (Meyer et al., 2015a). Therefore, we propose a model whereby a combination of transcript elongation to expose the uORF and the m^{6}A modification within the 5'UTR promotes reinitiation of translation within the *SNF2*$_{5'long}$ transcript, synthesizing *de novo,* unacetylated Snf2 to replace acetylated Snf2 that has previously been degraded. This new, unacetylated Snf2 is then localized to a new set of sporulation specific genomic loci, such as *MER1*, which promotes the progression of meiosis (Venkataramanan et al., 2017).

However, later in sporulation, a far larger fraction of the total *SNF2* transcript comprises of the *SNF2*$_{5'long}$ transcript isoform **(Figure 4.5A)**. If the model above were applicable throughout the process of sporulation, this, combined with the observed second wave of global m^{6}A modification would predict increased translation of Snf2 late in sporulation; and yet, there is no detectable Snf2 protein in the yeast cells at these time points **(Figure 4.6A)** (Venkataramanan et al., 2017). We propose that while the *SNF2*$_{5'long}$ transcript isoform and m^{6}A methylation of the transcript promote the translation of Snf2 during early sporulation, they in fact repress the production of new Snf2 protein late in sporulation. While the mechanisms by which this translational repression of the *SNF2* transcript occurs are as yet unknown, both uORFs as well as m^{6}A methylation have been shown to have context-specific repressive effects on translation. Of course, the canonical example of repression of translation by uORFs in yeast is *GCN4,* which has been discussed extensively in a previous section (Sundaram and Grant, 2014, Mueller and Hinnebusch, 1986). m^{6}A modification has also been shown to target transcripts for

rapid degradation, thus downregulating their translation (Shi et al., 2017a, Wang et al., 2014a, Wang et al., 2014b, Schwartz et al., 2014). In the case of *Xenopus* oocyte maturation, m^6A modified transcripts have also been shown to have decreased translation, but in a stability independent manner, indicating multiple context dependent mechanisms by which m^6A modification within the *SNF2* transcript could cause translational repression (Qi et al., 2016).

Since the overall levels of the *SNF2* transcript do not suffer any sharp decline that might be indicative of degradation (data not shown), it is instructive to consider other mechanisms by which its translation could be repressed. The translation of numerous transcripts during meiosis is temporally regulated (Brar et al., 2012) and a number of meiotic transcripts are 'protected' from either translation or degradation through almost the entirety of meiosis (Jin et al., 2015). For at least a subset of these transcripts, this protection is achieved by the binding of Rim4 to the 5' UTRs of the RNAs (Berchowitz et al., 2013). Rim4 is a protein that forms amyloid-like aggregates during sporulation in yeast, and in conjunction with the predicted RNA binding proteins Pes4 and Mip6, targets the localization of a number of transcripts to discrete foci within the yeast cytoplasm (Berchowitz et al., 2015, Jin et al., 2015, Jin et al., 2017). The foci serve as protective 'storage' for these transcripts until they are required to be translated, at which point they are dissolved by the action of the Ime2 kinase (Berchowitz et al., 2013). While the precise nature of these foci (whether they are out of phase with respect to the cytoplasm, akin to stress granules etc.) is unknown, it is feasible that the *SNF2* transcript is sequestered within them through the meiotic process.

In addition to sequestration of transcripts, there exist other mechanisms for selectivity of translation. Recently, specialized ribosomes have been shown to translate specific subsets of transcripts in mammalian cells (Simsek et al., 2017, Shi et al., 2017b). In yeast, the translation of

IME1, the primary factor that induces the meiotic transcription program, is dependent on Rpl22, a non-essential protein of the large subunit of the ribosome (Kim and Strich, 2016). The requirement for Rpl22 for translation of *IME1* is relieved by the truncation of the unusually long 5' UTR within the *IME1* transcript (Kim and Strich, 2016). Interestingly, two genes, *RPL22A* and *RPL22B*, whose protein products differ very slightly, encode for Rpl22. The Rpl22 protein product specifically inhibits the splicing of the *RPL22B* pre-mRNA. The downregulation of the ribosome during sporulation or stationary phase greatly increases the efficiency of splicing of *RPL22B,* potentially altering the composition of the ribosome (Gabunilas and Chanfreau, 2016, Venkataramanan et al., 2017, Awad et al., 2017). This or other changes within the ribosome could be involved in the selective translational repression of transcripts such as *SNF2* late in sporulation.

Interestingly, in addition to the 5' m^6A modification specific to $SNF2_{5'long}$ isoform, *SNF2* has been annotated to have an additional site of meiotically sustained m^6A modification within the CDS. Prior observations have noted that transcripts that are translationally repressed under conditions of nutrient starvation are localized to stress granules (Zid and O'Shea, 2014). Remarkably, the information specifying the localization of these transcripts is encoded within the promoters of the genes (Zid and O'Shea, 2014). Although there have been no direct connections demonstrated between RNA methylation and localization to stress granules, the previously described observations combined with recent reports that m^6A modifications are 'written' onto RNA in a co-transcriptional manner (Ke et al., 2017), as well as the observation that Ime4 is active in haploid, non-meiotic cells under conditions of nutrient stress (Yadav and Rajasekharan, 2017), lead us to hypothesize that co-transcriptional m^6A modifications of the *SNF2* transcript specify transcript fates. We postulate that while the 'pulsed' 5' modification increases translation

efficiency of the *SNF2*$_{5'long}$ isoform early in sporulation, the sustained CDS modification (perhaps in combination with the uORFs) targets the *SNF2* transcript towards stress granules during meiosis, where they are protected from both translation as well as degradation.

Why would the yeast cell store *SNF2* transcript in a translationally null state? A previous study has indicated that translational repression without degradation in response to nutrient starvation is not a particularly widespread phenomenon in *S. cerevisiae* (Arribere et al., 2011). Interestingly, that study identified two different classes of repressed transcripts. The first was a class of pre-shift 'privileged ' transcripts that included the RPG encoding RNAs. The second was a set of transcripts transcribed post-shift to starvation conditions (Arribere et al., 2011). The authors postulated that the preservation of the RPG transcripts is a form of 'bet-hedging' by the yeast cells, conferring upon the cells a selective advantage by quickly and efficiently return to logarithmic growth upon re-encountering nutrient-replete conditions (Arribere et al., 2011). A different study showed that a set of transcripts encoding genes involved in alternate carbon source metabolism were transcriptionally upregulated but translationally repressed by localization to stress granules upon glucose starvation (Zid and O'Shea, 2014). We postulate that translational repression of the *SNF2* transcript may be a form of the same bet-hedging phenomenon. Since Snf2 is a key transcriptional effector of the nutrient sensing Ras/PKA pathway, the low energetic requirements of its de-repression ensures rapid resumption of the glucose-dependent transcriptional program when the yeast spores reencounter nutrients after a period of sporulation. However, specifically under conditions of reintroduction of glucose and nitrogen rich media, we do not see any growth advantage conferred to the yeast cells by the uORF within the *SNF2* transcript **(Figure 4.5B)**. This could imply perhaps that the uORF is not the key feature in stably repressing the translation of the *SNF2* transcript. Another possible

explanation for this observation is that the benefit conferred by the uORF may be experienced under conditions different from the ones tested. Further experiments to understand the translational regulation of *SNF2*, as well as how it relates to the degradation and deacetylation of the Snf2 protein, are required.

Future directions: Several aspects of the model proposed in previous sections remain to be tested. The outstanding question remains whether the elongated UTR of the $SNF2_{5'long}$ transcript is in fact functional in regulating Snf2 translation after transition to sporulation media. Polysome profiling experiments to measure ribosome occupancy within the *SNF2* transcript CDS and 5' UTR during sporulation are in progress. Further, the specific roles of various features of the elongated 5' UTR (such as the uORF) in modulating the translation of the downstream ORF remain to be assayed. Construction of a series of reporters with various segments of the $SNF2_{5'long}$ 5' UTR is currently underway, and these constructs will hopefully provide greater insight into the mechanisms and context-dependence of uORF regulation of Snf2 translation.

The precise consequences of the regulated translation of Snf2 early in sporulation are also incompletely understood. As previously mentioned, we postulate that a 'burst' of translation early in sporulation serves to replace the pre-existing acetylated cellular pool of Snf2 with *de novo* synthesized unacetylated protein. A significant challenge to testing this hypothesis is the two-fold downregulation of *SNF2* transcript observed upon deletion of the uORF region **(Figure 4.4D)**, perhaps indicating that the genetic locus forms part of the vegetative *SNF2* promoter. A workaround for this could be ablating only the start codon of the uORF, thereby retaining most, if not all of its promoter activity while removing its capacity to engage the ribosome, and measuring the impact on the levels and acetylation of Snf2 during early sporulation, and strain construction for this experiment is currently underway.

The broad question of adaptive benefits conferred by the uORF remains an intriguing one. While we observed no discernible growth advantage upon transition back into nutrient-replete media post sporulation **(Figure 4.5B)**, it is entirely conceivable that the maintenance of the $SNF2_{5'long}$ transcript could prove useful for cellular growth under other sub-par conditions the yeast cells are more likely to experience in nature and are therefore more likely to be adapted to. Subjecting sporulated yeast cells to a wide variety of conditions and stresses would yield a more comprehensive picture of any potential role of the *SNF2* uORF in conferring an adaptive fitness advantage to *Saccharomyces cerevisiae.*

Materials and Methods

Yeast strains and culture: The yeast strains used in this study are listed in Table 4.1. All strains are derived from the BY or SK1 background. Yeast strains were grown in YPD (1% yeast extract, 2% peptone, 2% dextrose) medium at 30 °C.

TABLE 4.1: Genotype and Source of Yeast Strains

Strain Number	Name	Genotype	Source or reference
TJY6726	*WT (BY)*	*Mata/Matα his3Δ/his3Δ leu2Δ/leu2Δ LYS2/lys2Δ met15Δ/MET15 ura3Δ/ura3*	(Venkataramanan et al., 2017)
TJY6917	*SK1 K8409*	*SK1 MATa/MAT_ HO URA3::tetO224 LEU2::tetR-GFP REC8-HA3::URA3 lys2 his3 trp1*	(Venkataramanan et al., 2017)
TJY7168	*SNF2 uORF$^{\Delta/\Delta}$(BY)*	*Mata/Matα his3Δ/his3Δ leu2Δ/leu2Δ LYS2/lys2Δ met15Δ/MET15 ura3Δ/ura3 SNF2uORFΔ/ SNF2uORFΔ*	This study.

TJY7146	*SK1 K8409 uORF*$^{\Delta/\Delta}$	*SK1 MATa/MAT_ HO URA3::tetO224 LEU2::tetR-GFP REC8-HA3::URA3 lys2 his3 trp1 SNF2uORFΔ:KanMX6/ SNF2uORFΔ:KanMX6*	This study.

The *SNF2 uORF*$^{\Delta/\Delta}$*(BY)* 'clean' deletion of the uORF was generated using the delitto-perfetto method (Storici and Resnick, 2006). Briefly, in step 1, the uORF was deleted by homologous recombination and replaced with the pCORE cassette containing selectable markers KanMX6 and URA3. Subsequently, in step 2, oligonucleotides were designed to recombine with and replace the cassette introduced in step 1, generating a 'clean' deletion of the uORF. Deletion was confirmed by PCR amplification of the region of interest and Sanger sequencing. The *SK1 K8409 uORF*$^{\Delta/\Delta}$ was generated using recombination based disruption of the uORF (Longtine et al., 1998). Primers used are listed in Table 4.2.

TABLE 4.2: Primers used for strain construction

Primer Name	5' to 3' Sequence
FP_DelPerfetto_ Step1	TTATTGAAACTCCTTCACTTCCAAAAAGACACGATTCTTAgagctc gttttcgacactgg
RP_DelPerfetto _Step1	CTTCTTCATCATGTCTTCTTCTTTTTTTTTCAATTACTTGtccttaccat taagttgatc
FP_DelPerfetto_ Step2	TTATTGAAACTCCTTCACTTCCAAAAAGACACGATTCTTACAA GTAATTGAAAAAAAAAG
RP_DelPerfetto _Step2	CTTCTTCATCATGTCTTCTTCTTTTTTTTTCAATTACTTGTAAGA ATCGTGTCTTTTTGG
FP_Longtine	TTATTGAAACTCCTTCACTTCCAAAAAGACACGATTCTTACGG

	ATCCCCGGGTTAATTAA
RP_Longtine	CTTCTTCATCATGTCTTCTTCTTTTTTTTTCAATTACTTGGAATT CGAGCTCGTTTAAAC

Induction of sporulation: Strains were grown in YPD overnight and diluted in GNA pre-sporulation media (5% glucose, 3% Difco Nutrient Broth and 1% Yeast Extract) to a final OD of 0.2. After 4 h, the cells are pelleted, washed with SPO media in the case of BY strains (1% potassium acetate, 0.005% zinc acetate and amino acid supplements as needed) and resuspended in SPO media and grown at 25°C (Deutschbauer et al., 2002). At the indicated time points, cells were pelleted each for RNA and/or protein analysis. For SK1 strains, SPorulation Media (SPM) media (0.3% potassium acetate, 0.02% raffinose and amino acid supplements as needed) was used in place of SPO (Padmore et al., 1991). For cycloheximide experiments, cycloheximide (Sigma) was added to sporulation cultures at a final concentration of 200 µg/ml (Stock concentration of 100 mg/ml in Dimethyl Sulfoxide (DMSO)). Cells were precipitated at the indicated times after treatment.

RT-PCR and Real-Time PCR analysis: RNA was isolated from cells at indicated time points using hot-phenol method. After DNase treatment (Williams et al.), 4 µg of total RNA from each time point was used to make cDNA using a cDNA synthesis kit (Fermentas). qRT-PCR was done in 10 µl reaction with gene specific primers using 1 µl of cDNA diluted 1:20 using Perfecta Sybr Green Fastmix (Quanta Biosciences) and a CFX96 Touch System (BioRad). All samples were run in triplicate for each independent experiment. qPCR primers specific to the *SNF2* coding sequence (CDS) (FP: TCTGGGCTTACCAGAAATGC, RP: TATCGAGGGTGCCATTCTTC), the 5' UTR common to both long and short *SNF2* transcript

isoforms (FP: TGACGTACGTGGACCTTTTG, RP: AGCAGAAAGTCGCGATTAGAG), and *SNF2* uORF (specific to $SNF2_{5'long}$ isoform, FP: GGCTATTCTGAGTGAACATAAGGACAC, RP: AGCGTTAGGAACTTCAACTGTATTTTGC) were used to measure relative expression of each isoform (each normalized to t=0). Fraction of $SNF2_{5'long}$ in total *SNF2* transcript was determined by mapping C_t values to a genomic DNA standard curve to calculate 'gDNA equivalents' (since gDNA has intrinsic 1:1:1 abundance ratio of each amplified segment). Contiguity of $SNF2_{5'long}$ transcript was determined using a forward primer within the uORF and a reverse primer within the *SNF2* CDS for polymerase chain reaction (PCR) with 1 µl of cDNA diluted to 1:20. PCR products were then run on 1.5% agarose gel with ethidium bromide. RT-PCR was also performed for *scR1* gene from each cDNA sample.

Western Blot: Protein was isolated from cells pellets with FA-1 lysis buffer (50 mM HEPES pH 7.5, 150 mM NaCl, 1 mM ethylenediaminetetraacetic acid (EDTA), 1% Triton X-100, 0.1% Sodium Deoxycholate, 1 mM phenylmethylsulfonyl fluoride (PMSF) and protease inhibitors) using bead-beating. The buffer was supplemented with protease inhibitor cocktail tablet (Williams et al.). Total protein was resolved by sodium dodecyl sulphate-polyacrylamide gel electrophoresis. The gel was transferred to Polyvinylidene fluoride (PVDF) membrane, probed with anti-SNF2 antibody (yN-20, Santa Cruz) at a 1:200 dilution in 2% milk or anti-acetylated lysine (ST1027, Millipore) at a 1:2000 dilution in 5% milk. Signal was detected using ECL (Thermo Scientific) as per the manufacturer's instructions. For Pgk1 western blotting, the membrane was probed with anti Pgk1 antibody (Molecular probes) at a 1:3000 dilution in 5% milk.

Immunoprecipitation: Sporulation was induced as described earlier and 50 ml of cells at various time points were pelleted. Protein was isolated from cell pellets with FA-1 lysis buffer

(50 mM HEPES pH 7.5, 150 mM NaCl, 1 mM EDTA, 1% Triton X-100, 0.1% Sodium Deoxycholate, 1 mM PMSF and protease inhibitors) using bead-beating methods. Immunoprecipitation was performed with anti-SNF2 antibody (yN-20, Santa Cruz, 10 µl per IP) and γ-G sepharose beads and washed with the lysis buffer. Western blots were performed as described above.

Competitive fitness assay: SK1 yeast were sporulated to completion (~4 days in SPM) and equal number of sporulated tetrads WT and $uORF^{\Delta/\Delta}$ were inoculated into YPD. Cell pellets were collected and the indicated time points and genomic DNA isolation was performed using bead-beating methods. The fractions of WT and $uORF^{\Delta/\Delta}$ strains were measured by calculating the relative amounts of *SNF2 uORF* to CDS using the qRT-PCR method described in a previous section.

m^{6}A Dot Blot: RNA was isolated from cells at indicated time points using hot-phenol method. After DNase treatment (Williams et al.), equal amounts of RNA (minimum of 5 ug) from each time point were denatured for 10 minutes at 65 degrees Celsius, and spotted onto ZetaProbe nylon membrane (BioRad) and allowed to dry. The membrane was then UV crosslinked, blocked with 5% non-fat dry milk in 1X TBST and probed with anti-m^{6}A antibody (202-003, Synaptic Systems) at a 1:1000 dilution in 5% milk.

Acknowledgements

Data in igures 4.6A-B were generated by Lauren Thurlow during her rotation in Dr. Tracy Johnson's laboratory. I am grateful for her intellectual and technical contributions to this chapter.

Figures

Figure 4.1

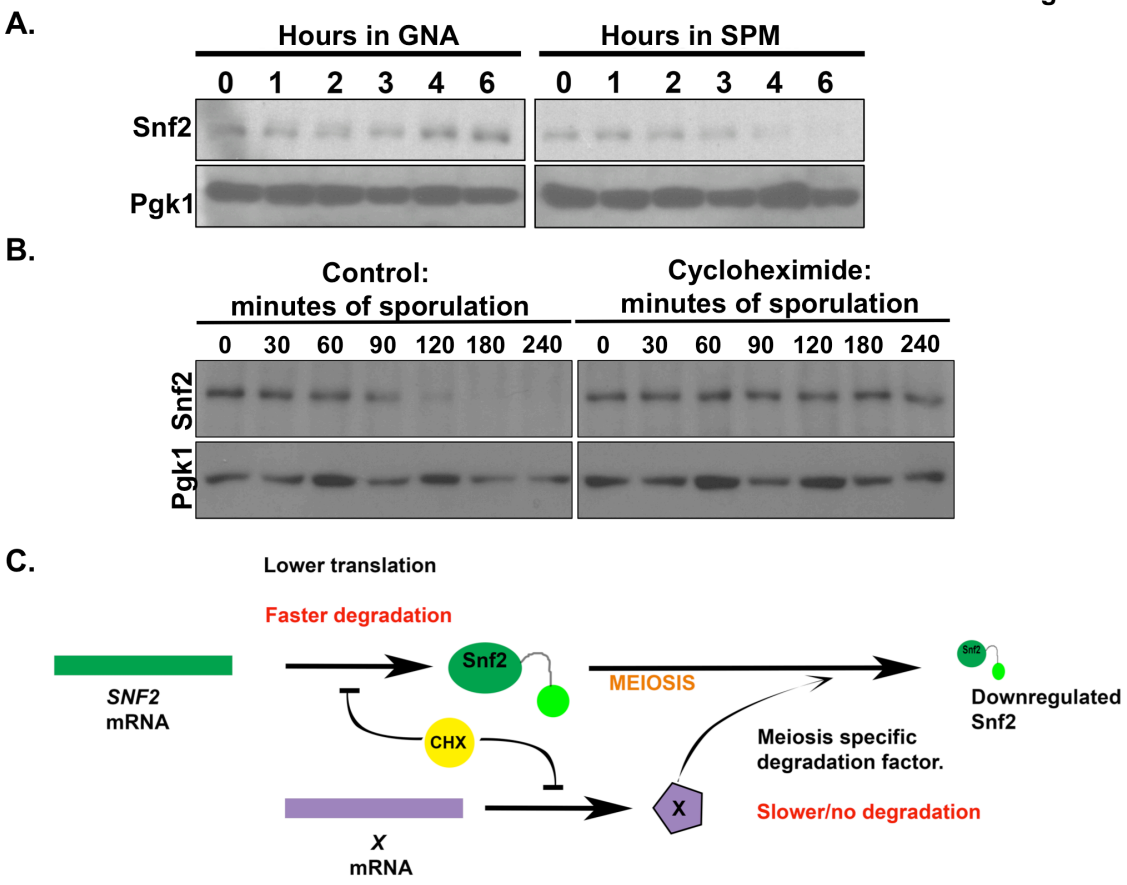

Figure 4.1: Degradation of Snf2 during sporulation requires *de novo* translation of one or more unknown meiotic factor(s).

A. Western blot for levels of Snf2 protein through a time course in the BY strain, after transfer to either fresh nutrient replete media (GNA) or sporulation media (SPM). The instability of Snf2 is specific to the nutrient deficient sporulation media. Pgk1 is an internal control.

B. Western blot for levels of Snf2 protein through a time course of sporulation in the BY strain, with and without the addition of cycloheximide (CHX). The presence of CHX in

the sporulation media stabilizes Snf2 through at least 4 hours of sporulation. Pgk1 is an internal control.

C. Proposed model for the role of *de novo* translation in the degradation of Snf2. Treatment with CHX inhibits both production of Snf2 itself, as well as an as-yet-unknown sporulation-specific factor (X) targeting Snf2 for degradation. The net effect of CHX mediated translation inhibition is therefore to stabilize the existing pool of Snf2 protein.

Figure 4.2

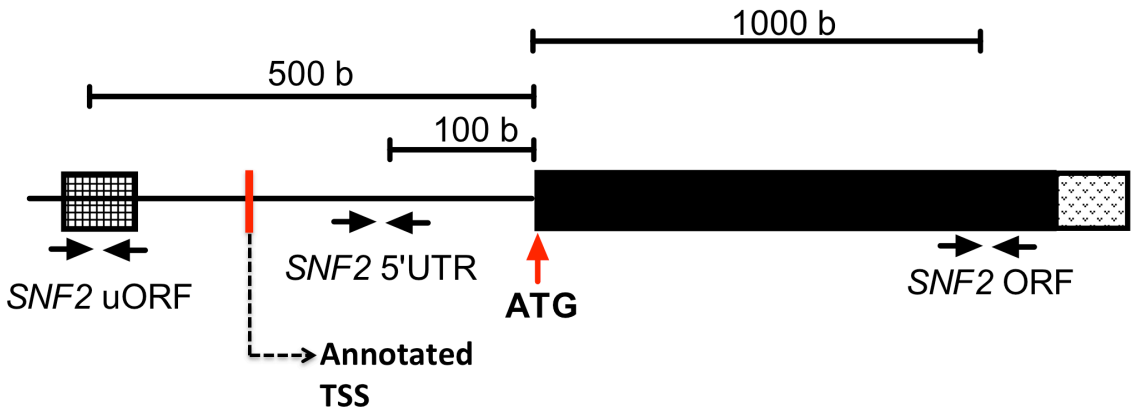

Figure 4.2 Architecture of the *SNF2* transcript. The transcriptional start site of the *SNF2* coding sequence is indicated with a red arrow. The annotated transcription start site is indicated with a red bar within the 5' UTR (Malabat et al., 2015). The 39 base long uORF is indicated with the checked box. qPCR primers for detecting the various regions of the *SNF2* transcript are indicated. Schematic is not to scale.

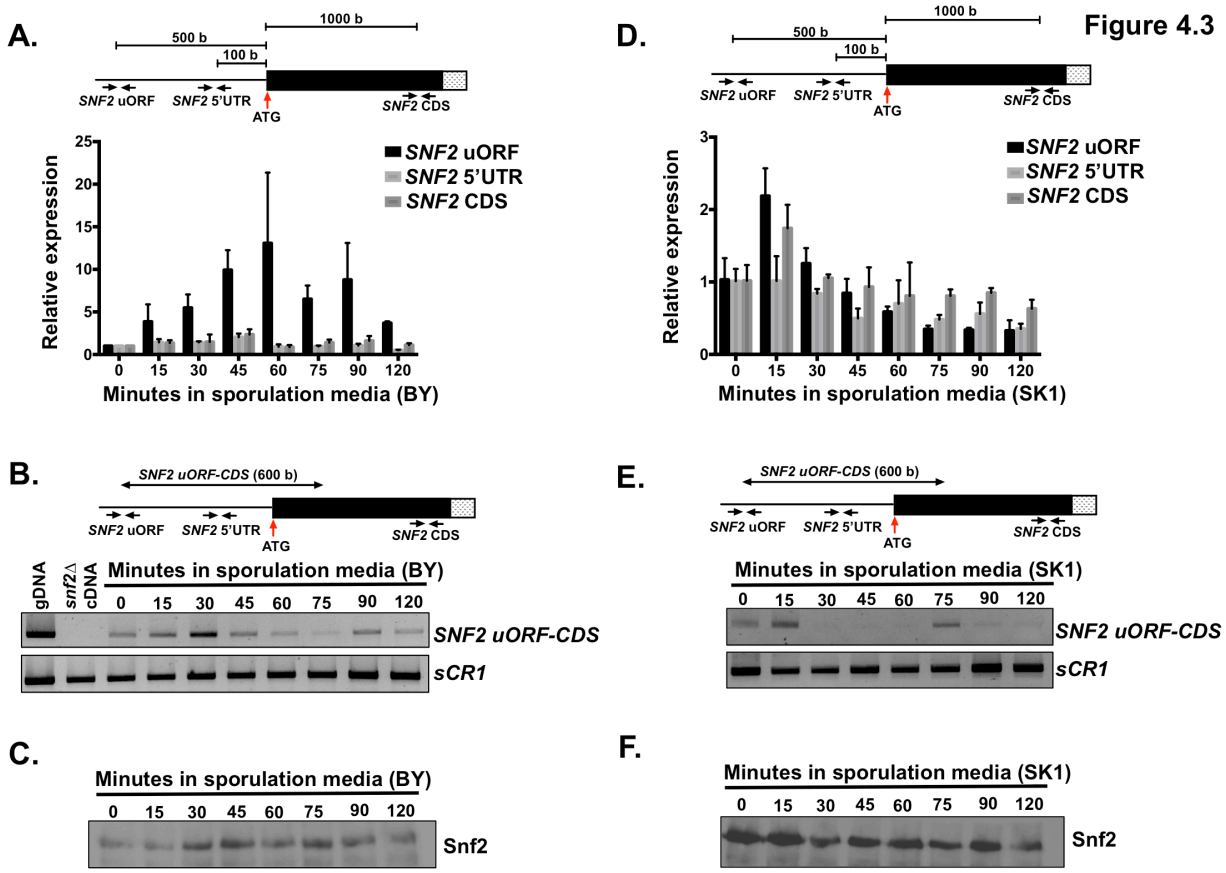

Figure 4.3 Abundance of a *SNF2* transcript with an extended 5' leader transiently increases early in sporulation.

A. Quantification of transcript levels for various regions of the *SNF2* transcript (uORF in $SNF2_{5'long}$, *SNF2* 5' UTR common to all transcript isoforms, and *SNF2* CDS) by RT-qPCR normalized to $t = 0$ in *WT* yeast (BY strain) at indicated times after shift to sporulation media. Error bars represent ± 1 SD. Expression of *SNF2* uORF (and consequently $SNF2_{5'long}$) increases dramatically within 1 hour of sporulation and decreases by 2 hours. Expression of total *SNF2*, as measured by *SNF2* CDS levels, remains mostly unchanged.

B. PCR product indicating $SNF2_{5'long}$, with forward primer within *SNF2* uORF and reverse primer within *SNF2* CDS in *WT* yeast (BY strain) at indicated times after shift to sporulation media.

C. Western blot for levels of Snf2 protein in *WT* yeast (BY strain) at indicated times after shift to sporulation media.

D. Quantification of transcript levels for various regions of the *SNF2* transcript (uORF in $SNF2_{5'long}$, *SNF2* 5' UTR common to all transcript isoforms, and *SNF2* CDS) by RT-qPCR normalized to $t = 0$ in *WT* yeast (SK1 strain) at indicated times after shift to sporulation media. Error bars represent ± 1 SD. Expression of *SNF2* uORF (and consequently $SNF2_{5'long}$) increases dramatically within 15 minutes of sporulation and decreases by 2 hours. Expression of total *SNF2*, as measured by *SNF2* CDS levels, remains mostly unchanged.

E. PCR product indicating $SNF2_{5'long}$, with forward primer within *SNF2* uORF and reverse primer within *SNF2* CDS in *WT* yeast (SK1 strain) at indicated times after shift to sporulation media.

F. Western blot for levels of Snf2 protein in *WT* yeast (SK1 strain) at indicated times after shift to sporulation media.

Figure 4.4

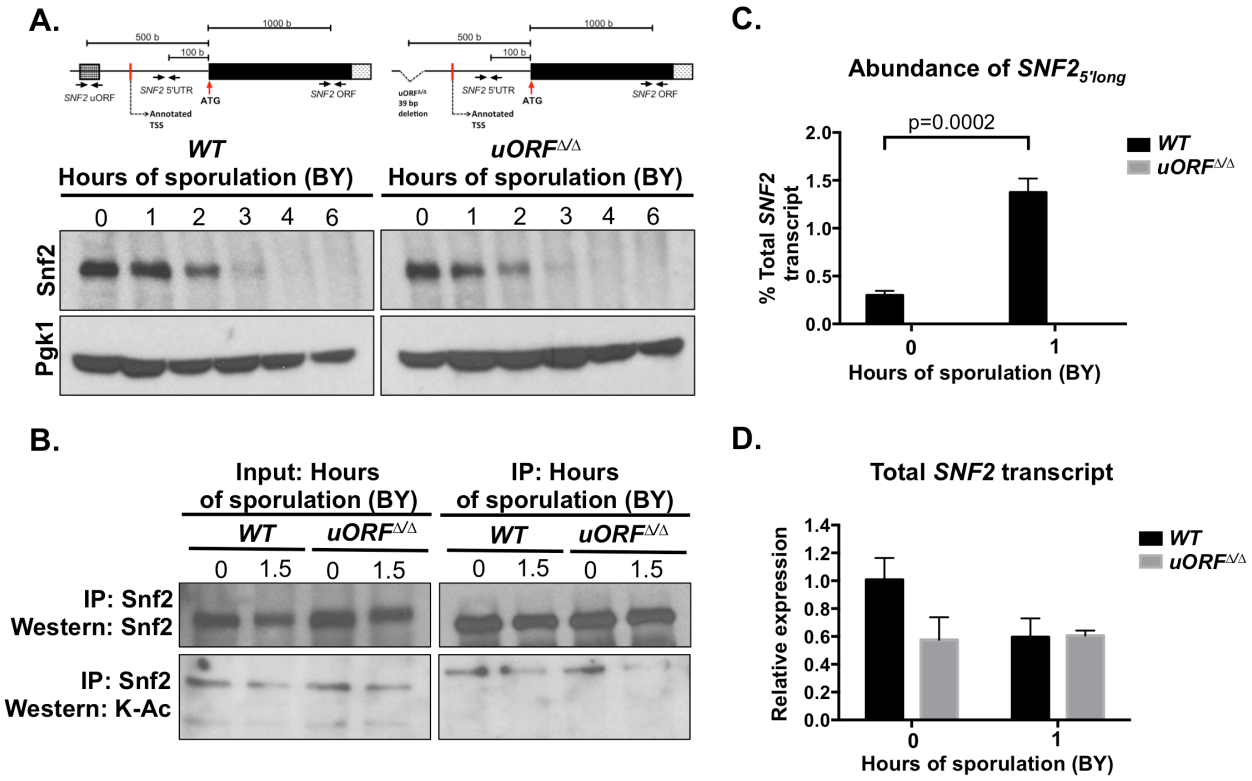

Figure 4.4 Absence of the *SNF2* uORF region leads to decreased total *SNF2* RNA as well as slightly faster degradation and deacetylation of Snf2 protein early in sporulation.

A. Western blot for levels of Snf2 protein in *WT* and *uORF*$^{\Delta/\Delta}$ yeast (BY strain) at indicated times after shift to sporulation media. The *uORF*$^{\Delta/\Delta}$ strain shows slightly faster degradation of Snf2 that *WT* (compare 1 and 2 hour time points between the two strains). Schematic of the deletion is show above the blots.

B. Immunoprecipitation of Snf2 at the indicated times after shift to sporulation media in *WT* and *uORF*$^{\Delta/\Delta}$ yeast (BY strain). Snf2 acetylation decreases more rapidly in *uORF*$^{\Delta/\Delta}$ strain (compare IP lanes 2 and 4).

C. Percent total *SNF2* transcript that has an elongated 5' UTR ($SNF2_{5'long}$) at the indicated time points after shift to sporulation media in *WT* and $uORF^{\Delta/\Delta}$ yeast (BY strain). The fraction of the total transcript that has the elongated 5' UTR increases 3-fold in *WT,* and is undetectable in the $uORF^{\Delta/\Delta}$ strain.

D. Total *SNF2* transcript at the indicated time points after shift to sporulation media in *WT* and $uORF^{\Delta/\Delta}$ yeast (BY strain), normalized to t=0 for the *WT*. The $uORF^{\Delta/\Delta}$ strain shows a 50% decrease in transcript levels pre-sporulation. Transcript level after 1 hour in sporulation media shows no variation between the two strains.

Figure 4.5

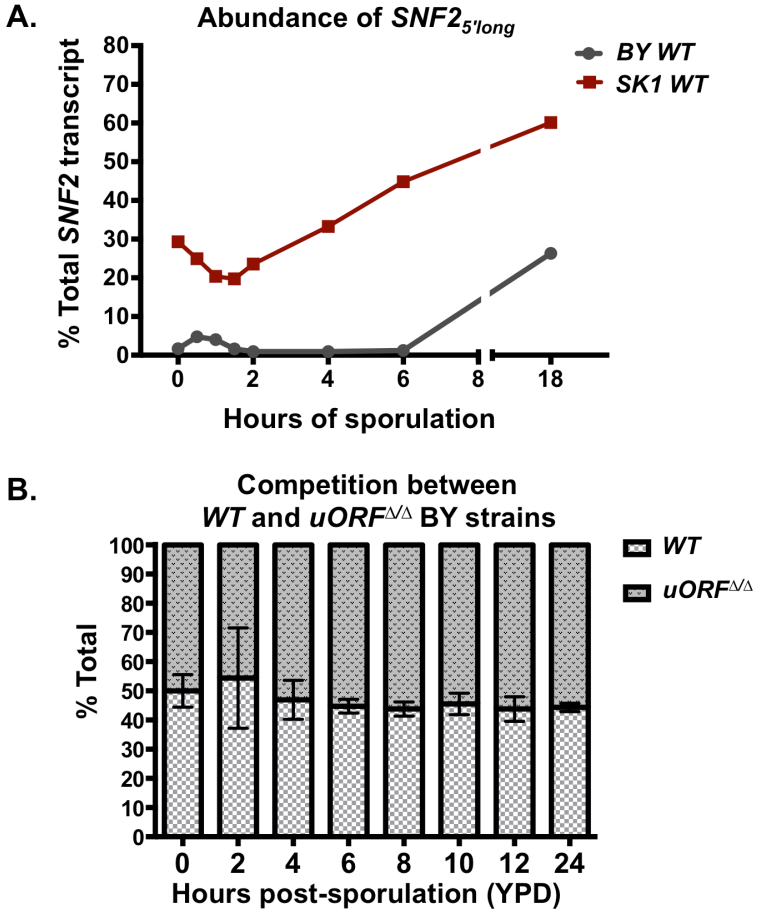

Figure 4.5 Proportion of *SNF2*$_{5'long}$ transcript increases dramatically late in sporulation, but confers no detectable fitness advantage post-sporulation in glucose-containing media.

A. Percent total *SNF2* transcript that has an elongated 5' UTR (*SNF2*$_{5'long}$) at the indicated time points after shift to sporulation media in BY and SK1 strain backgrounds. Approximately a quarter to a third of total *SNF2* transcripts have the elongated 5' UTR within 18 hours in sporulation media in the BY strain. Note that there is no detectable Snf2 protein at this late time point (Venkataramanan et al., 2017). SK1 strain has significantly higher pre-sporulation fraction of the *SNF2*$_{5'long}$ transcript, but also shows increase within 18 hours of sporulation.

B. Competitive fitness assay between *WT* and *uORF*$^{\Delta:KanMx/\Delta:KanMX}$ yeast (SK1 strain) in

YPD post-sporulation. Relative levels of each strain were assayed at the indicated time points using qPCR on gDNA isolated from the culture. Strains grew at comparable rates through a 24-hour time course. The *SNF2* uORF confers no observable post-sporulation advantage to the yeast.

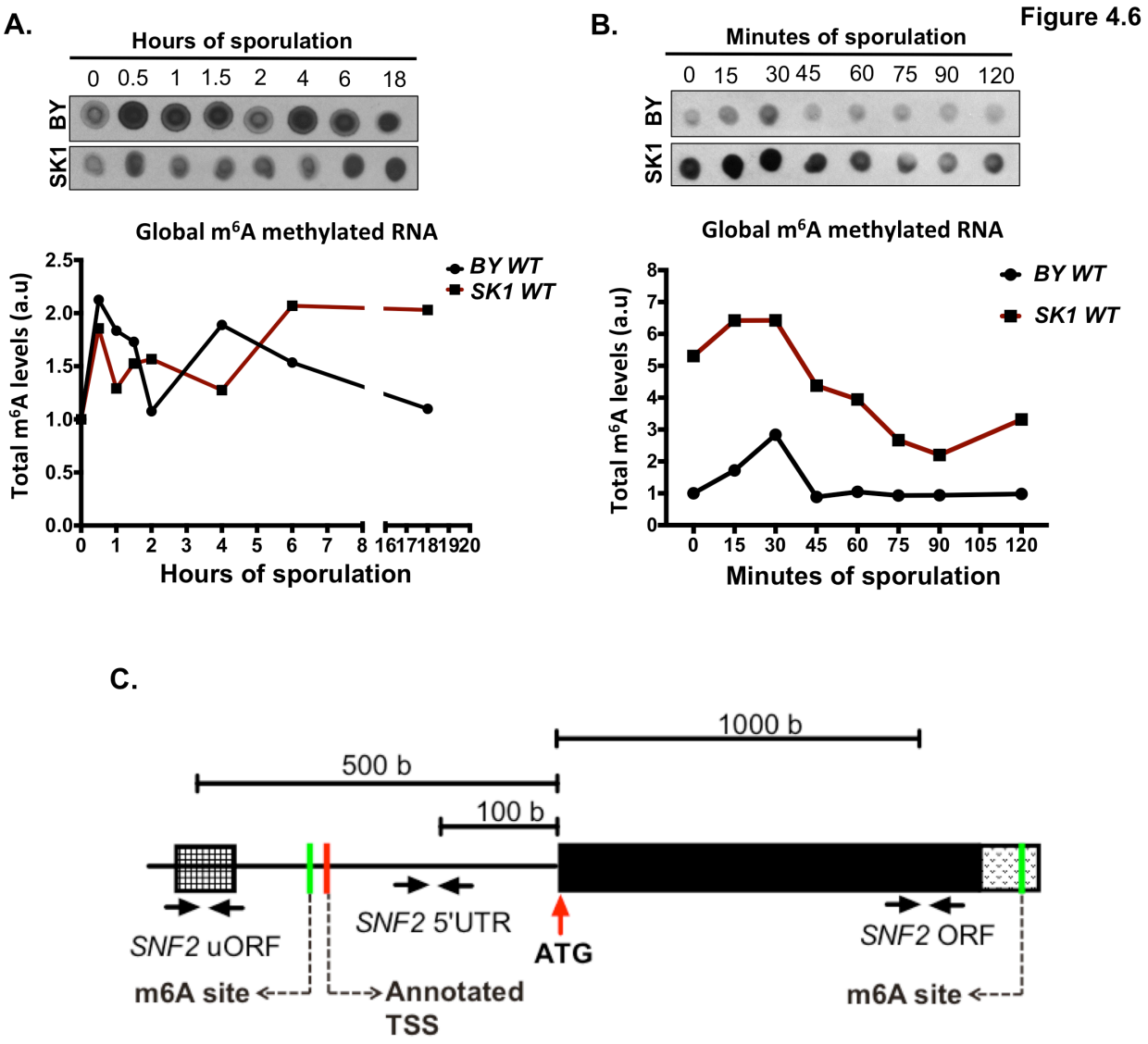

Figure 4.6 Two waves of global m^{6}A methylation during sporulation; and methylation sites on the *SNF2* transcript.

A. Top panel: Dot blot for levels of total m^{6}A methylated RNA in diploid BY and SK1 yeast strains undergoing sporulation. Bottom panel: Quantification of top, normalized to t=0 of the respective strain. Two temporally distinct waves of m^{6}A methylation are observed;

the first wave cresting and ebbing within 2 hours of transfer to sporulation media, and a second, sustained wave between 6-18 hours post transfer.

B. Top panel: Dot blot for levels of total m^6A methylated RNA in diploid BY and SK1 yeast strains transferred to sporulation media. Bottom panel: Quantification of top, normalized to t=0 of BY yeast. The first wave of m^6A methylation (0-2 hours) mimics the wave of $SNF2_{5'long}$ observed in early sporulation **(Figure 4.3)**. SK1 strains display far higher methylation levels than BY.

C. Potential m^6A methylation sites within the *SNF2* transcript, as identified previously (Schwartz et al., 2013). Note that the methylation site within the 5' UTR is upstream of the annotated TSS and is therefore unique to the $SNF2_{5'long}$ transcript isoform. The methylation site within the coding sequence is 4973 nucleotides from the start (AUG), and 140 nucleotides from the end of the coding sequence. Schematic is not to scale.

References

Agarwala, S. D., Blitzblau, H. G., Hochwagen, A. & Fink, G. R. 2012. RNA methylation by the MIS complex regulates a cell fate decision in yeast. *PLoS Genet,* 8**,** e1002732.

Arribere, J. A., Doudna, J. A. & Gilbert, W. V. 2011. Reconsidering movement of eukaryotic mRNAs between polysomes and P bodies. *Mol Cell,* 44**,** 745-58.

Awad, A. M., Venkataramanan, S., Nag, A., Galivanche, A. R., Bradley, M. C., Neves, L., Douglass, S., Clarke, C. F. & Johnson, T. L. 2017. Chromatin-remodeling SWI/SNF complex regulates coenzyme Q6 synthesis and a metabolic shift to respiration in yeast. *Journal of Biological Chemistry*.

Aylett, C. H. & Ban, N. 2017. Eukaryotic aspects of translation initiation brought into focus. *Philos Trans R Soc Lond B Biol Sci,* 372.

Becker, E., Com, E., Lavigne, R., Guilleux, M. H., Evrard, B., Pineau, C. & Primig, M. 2017. The protein expression landscape of mitosis and meiosis in diploid budding yeast. *J Proteomics,* 156**,** 5-19.

Berchowitz, L. E., Gajadhar, A. S., van Werven, F. J., De Rosa, A. A., Samoylova, M. L., Brar, G. A., Xu, Y., Xiao, C., Futcher, B., Weissman, J. S., White, F. M. & Amon, A. 2013. A developmentally regulated translational control pathway establishes the meiotic chromosome segregation pattern. *Genes Dev,* 27**,** 2147-63.

Berchowitz, L. E., Kabachinski, G., Walker, M. R., Carlile, T. M., Gilbert, W. V., Schwartz, T. U. & Amon, A. 2015. Regulated Formation of an Amyloid-like Translational Repressor Governs Gametogenesis. *Cell,* 163**,** 406-18.

Bodi, Z., Bottley, A., Archer, N., May, S. T. & Fray, R. G. 2015. Yeast m6A Methylated mRNAs Are Enriched on Translating Ribosomes during Meiosis, and under Rapamycin Treatment. *PLoS One,* 10**,** e0132090.

Bodi, Z., Button, J. D., Grierson, D. & Fray, R. G. 2010. Yeast targets for mRNA methylation. *Nucleic Acids Res,* 38**,** 5327-35.

Bolte, M., Dieckhoff, P., Krause, C., Braus, G. H. & Irniger, S. 2003. Synergistic inhibition of APC/C by glucose and activated Ras proteins can be mediated by each of the Tpk1-3 proteins in Saccharomyces cerevisiae. *Microbiology,* 149**,** 1205-16.

Bowdish, K. S. & Mitchell, A. P. 1993. Bipartite structure of an early meiotic upstream activation sequence from Saccharomyces cerevisiae. *Mol Cell Biol,* 13**,** 2172-81.

Bowdish, K. S., Yuan, H. E. & Mitchell, A. P. 1995. Positive control of yeast meiotic genes by the negative regulator UME6. *Mol Cell Biol,* 15**,** 2955-61.

Brar, G. A., Yassour, M., Friedman, N., Regev, A., Ingolia, N. T. & Weissman, J. S. 2012. High-resolution view of the yeast meiotic program revealed by ribosome profiling. *Science,* 335**,** 552-7.

Cardona, F., Aranda, A. & del Olmo, M. 2009. Ubiquitin ligase Rsp5p is involved in the gene expression changes during nutrient limitation in Saccharomyces cerevisiae. *Yeast,* 26**,** 1-15.

Christiano, R., Nagaraj, N., Frohlich, F. & Walther, T. C. 2014. Global proteome turnover analyses of the Yeasts S. cerevisiae and S. pombe. *Cell Rep,* 9**,** 1959-65.

Clancy, M. J., Shambaugh, M. E., Timpte, C. S. & Bokar, J. A. 2002. Induction of sporulation in Saccharomyces cerevisiae leads to the formation of N6-methyladenosine in mRNA: a potential mechanism for the activity of the IME4 gene. *Nucleic Acids Res.,* 30**,** 4509-4518.

Cooper, K. F., Mallory, M. J., Egeland, D. B., Jarnik, M. & Strich, R. 2000. Ama1p is a meiosis-specific regulator of the anaphase promoting complex/cyclosome in yeast. *Proc Natl Acad Sci U S A,* 97**,** 14548-53.

Crespo, J. L., Helliwell, S. B., Wiederkehr, C., Demougin, P., Fowler, B., Primig, M. & Hall, M. N. 2004. NPR1 kinase and RSP5-BUL1/2 ubiquitin ligase control GLN3-dependent transcription in Saccharomyces cerevisiae. *J Biol Chem,* 279**,** 37512-7.

Deutschbauer, A. M., Williams, R. M., Chu, A. M. & Davis, R. W. 2002. Parallel phenotypic analysis of sporulation and postgermination growth in Saccharomyces cerevisiae. *Proc Natl Acad Sci U S A,* 99**,** 15530-5.

Escusa, S., Camblong, J., Galan, J. M., Pinson, B. & Daignan-Fornier, B. 2006. Proteasome- and SCF-dependent degradation of yeast adenine deaminase upon transition from proliferation to quiescence requires a new F-box protein named Saf1p. *Mol Microbiol,* 60**,** 1014-25.

Gaba, A., Wang, Z., Krishnamoorthy, T., Hinnebusch, A. G. & Sachs, M. S. 2001. Physical evidence for distinct mechanisms of translational control by upstream open reading frames. *EMBO J,* 20**,** 6453-63.

Gabunilas, J. & Chanfreau, G. 2016. Splicing-Mediated Autoregulation Modulates Rpl22p Expression in Saccharomyces cerevisiae. *PLoS Genet,* 12**,** e1005999.

Grant, C. M. & Hinnebusch, A. G. 1994. Effect of sequence context at stop codons on efficiency of reinitiation in GCN4 translational control. *Mol Cell Biol,* 14**,** 606-18.

Guisbert, K. S., Zhang, Y., Flatow, J., Hurtado, S., Staley, J. P., Lin, S. & Sontheimer, E. J. 2012. Meiosis-induced alterations in transcript architecture and noncoding RNA expression in S. cerevisiae. *Rna,* 18**,** 1142-53.

Harigaya, Y., Tanaka, H., Yamanaka, S., Tanaka, K., Watanabe, Y., Tsutsumi, C., Chikashige, Y., Hiraoka, Y., Yamashita, A. & Yamamoto, M. 2006. Selective elimination of messenger RNA prevents an incidence of untimely meiosis. *Nature,* 442**,** 45-50.

Harper, J. W., Burton, J. L. & Solomon, M. J. 2002. The anaphase-promoting complex: it's not just for mitosis any more. *Genes Dev,* 16**,** 2179-206.

Haussmann, I. U., Bodi, Z., Sanchez-Moran, E., Mongan, N. P., Archer, N., Fray, R. G. & Soller, M. 2016. m6A potentiates Sxl alternative pre-mRNA splicing for robust Drosophila sex determination. *Nature,* 540**,** 301-304.

Hinnebusch, A. G. 2017. Structural Insights into the Mechanism of Scanning and Start Codon Recognition in Eukaryotic Translation Initiation. *Trends Biochem Sci,* 42**,** 589-611.

Hinnebusch, A. G., Ivanov, I. P. & Sonenberg, N. 2016. Translational control by 5'-untranslated regions of eukaryotic mRNAs. *Science,* 352**,** 1413-6.

Honigberg, S. M. 2016. Similar environments but diverse fates: Responses of budding yeast to nutrient deprivation. *Microb Cell,* 3**,** 302-328.

Hurtado, S., Kim Guisbert, K. S. & Sontheimer, E. J. 2014. SPO24 is a transcriptionally dynamic, small ORF-encoding locus required for efficient sporulation in Saccharomyces cerevisiae. *PLoS One,* 9**,** e105058.

Jin, L., Zhang, K., Sternglanz, R. & Neiman, A. M. 2017. Predicted RNA Binding Proteins Pes4 and Mip6 Regulate mRNA Levels, Translation, and Localization during Sporulation in Budding Yeast. *Mol Cell Biol,* 37.

Jin, L., Zhang, K., Xu, Y., Sternglanz, R. & Neiman, A. M. 2015. Sequestration of mRNAs Modulates the Timing of Translation during Meiosis in Budding Yeast. *Mol Cell Biol,* 35**,** 3448-58.

Johnstone, T. G., Bazzini, A. A. & Giraldez, A. J. 2016. Upstream ORFs are prevalent translational repressors in vertebrates. *EMBO J,* 35**,** 706-23.

Kadosh, D. & Struhl, K. 1997. Repression by Ume6 involves recruitment of a complex containing Sin3 corepressor and Rpd3 histone deacetylase to target promoters. *Cell,* 89**,** 365-71.

Kan, L., Grozhik, A. V., Vedanayagam, J., Patil, D. P., Pang, N., Lim, K. S., Huang, Y. C., Joseph, B., Lin, C. J., Despic, V., Guo, J., Yan, D., Kondo, S., Deng, W. M., Dedon, P. C., Jaffrey, S. R. & Lai, E. C. 2017. The m6A pathway facilitates sex determination in Drosophila. *Nat Commun,* 8**,** 15737.

Kassir, Y., Adir, N., Boger-Nadjar, E., Raviv, N. G., Rubin-Bejerano, I., Sagee, S. & Shenhar, G. 2003. Transcriptional regulation of meiosis in budding yeast. *Int Rev Cytol,* 224**,** 111-71.

Ke, S., Alemu, E. A., Mertens, C., Gantman, E. C., Fak, J. J., Mele, A., Haripal, B., Zucker-Scharff, I., Moore, M. J., Park, C. Y., Vagbo, C. B., Kussnierczyk, A., Klungland, A., Darnell, J. E., Jr. & Darnell, R. B. 2015. A majority of m6A residues are in the last exons, allowing the potential for 3' UTR regulation. *Genes Dev,* 29**,** 2037-53.

Ke, S., Pandya-Jones, A., Saito, Y., Fak, J. J., Vagbo, C. B., Geula, S., Hanna, J. H., Black, D. L., Darnell, J. E., Jr. & Darnell, R. B. 2017. m6A mRNA modifications are deposited in nascent pre-mRNA and are not required for splicing but do specify cytoplasmic turnover. *Genes Dev,* 31**,** 990-1006.

Kim, J. H., Saraf, A., Florens, L., Washburn, M. & Workman, J. L. 2010. Gcn5 regulates the dissociation of SWI/SNF from chromatin by acetylation of Swi2/Snf2. *Genes Dev,* 24**,** 2766-71.

Kim, S. J. & Strich, R. 2016. Rpl22 is required for IME1 mRNA translation and meiotic induction in S. cerevisiae. *Cell Div,* 11**,** 10.

Klar, A. J. & Halvorson, H. O. 1975. Proteinase activities of Saccharomyces cerevisiae during sporulation. *J Bacteriol,* 124**,** 863-9.

Kleene, K. C. 2003. Patterns, mechanisms, and functions of translation regulation in mammalian spermatogenic cells. *Cytogenet Genome Res,* 103**,** 217-24.

Kleene, K. C. 2013. Connecting cis-elements and trans-factors with mechanisms of developmental regulation of mRNA translation in meiotic and haploid mammalian spermatogenic cells. *Reproduction,* 146**,** R1-19.

Kumar, R., Dhali, S., Srikanth, R., Ghosh, S. K. & Srivastava, S. 2014. Comparative proteomics of mitosis and meiosis in Saccharomyces cerevisiae. *J Proteomics,* 109**,** 1-15.

Kus, B., Gajadhar, A., Stanger, K., Cho, R., Sun, W., Rouleau, N., Lee, T., Chan, D., Wolting, C., Edwards, A., Bosse, R. & Rotin, D. 2005. A high throughput screen to identify substrates for the ubiquitin ligase Rsp5. *J Biol Chem,* 280**,** 29470-8.

Lamb, T. M. & Mitchell, A. P. 2001. Coupling of Saccharomyces cerevisiae early meiotic gene expression to DNA replication depends upon RPD3 and SIN3. *Genetics,* 157**,** 545-556.

Lardenois, A., Stuparevic, I., Liu, Y., Law, M. J., Becker, E., Smagulova, F., Waern, K., Guilleux, M.-H., Horecka, J., Chu, A., Kervarrec, C., Strich, R., Snyder, M., Davis, R. W., Steinmetz, L. M. & Primig, M. 2015. The conserved histone deacetylase Rpd3 and its DNA binding subunit Ume6 control dynamic transcript architecture during mitotic growth and meiotic development. *Nucleic Acids Res.,* 43**,** 115-128.

Lee, Y. Y., Cevallos, R. C. & Jan, E. 2009. An upstream open reading frame regulates translation of GADD34 during cellular stresses that induce eIF2alpha phosphorylation. *J Biol Chem,* 284**,** 6661-73.

Lence, T., Akhtar, J., Bayer, M., Schmid, K., Spindler, L., Ho, C. H., Kreim, N., Andrade-Navarro, M. A., Poeck, B., Helm, M. & Roignant, J. Y. 2016. m6A modulates neuronal functions and sex determination in Drosophila. *Nature,* 540**,** 242-247.

Longtine, M. S., McKenzie, A., 3rd, Demarini, D. J., Shah, N. G., Wach, A., Brachat, A., Philippsen, P. & Pringle, J. R. 1998. Additional modules for versatile and economical PCR-based gene deletion and modification in Saccharomyces cerevisiae. *Yeast,* 14**,** 953-61.

Malabat, C., Feuerbach, F., Ma, L., Saveanu, C. & Jacquier, A. 2015. Quality control of transcription start site selection by nonsense-mediated-mRNA decay. *Elife,* 4.

Mallory, M. J., Cooper, K. F. & Strich, R. 2007. Meiosis-specific destruction of the Ume6p repressor by the Cdc20-directed APC/C. *Mol. Cell,* 27**,** 951-961.

Mallory, M. J., Law, M. J., Sterner, D. E., Berger, S. L. & Strich, R. 2012. Gcn5p-dependent acetylation induces degradation of the meiotic transcriptional repressor Ume6p. *Mol Biol Cell,* 23**,** 1609-17.

Meyer, K. D., Patil, D. P., Zhou, J., Zinoviev, A., Skabkin, M. A., Elemento, O., Pestova, T. V., Qian, S.-B. & Jaffrey, S. R. 2015a. 5′ UTR m6A Promotes Cap-Independent Translation. *Cell,* 163**,** 999-1010.

Meyer, K. D., Patil, D. P., Zhou, J., Zinoviev, A., Skabkin, M. A., Elemento, O., Pestova, T. V., Qian, S. B. & Jaffrey, S. R. 2015b. 5' UTR m(6)A Promotes Cap-Independent Translation. *Cell,* 163**,** 999-1010.

Meyer, K. D., Saletore, Y., Zumbo, P., Elemento, O., Mason, C. E. & Jaffrey, S. R. 2012. Comprehensive analysis of mRNA methylation reveals enrichment in 3' UTRs and near stop codons. *Cell,* 149**,** 1635-46.

Mohammad, M. P., Munzarova Pondelickova, V., Zeman, J., Gunisova, S. & Valasek, L. S. 2017. In vivo evidence that eIF3 stays bound to ribosomes elongating and terminating on short upstream ORFs to promote reinitiation. *Nucleic Acids Res,* 45**,** 2658-2674.

Mueller, P. P. & Hinnebusch, A. G. 1986. Multiple upstream AUG codons mediate translational control of GCN4. *Cell,* 45**,** 201-7.

Munding, E. M., Shiue, L., Katzman, S., Donohue, J. P. & Ares, M. 2013. Competition between Pre-mRNAs for the Splicing Machinery Drives Global Regulation of Splicing. *Mol. Cell,* 51**,** 338-348.

Padmore, R., Cao, L. & Kleckner, N. 1991. Temporal comparison of recombination and synaptonemal complex formation during meiosis in S. cerevisiae. *Cell,* 66**,** 1239-56.

Palam, L. R., Baird, T. D. & Wek, R. C. 2011. Phosphorylation of eIF2 facilitates ribosomal bypass of an inhibitory upstream ORF to enhance CHOP translation. *J Biol Chem,* 286**,** 10939-49.

Prinz, S., Hwang, E. S., Visintin, R. & Amon, A. 1998. The regulation of Cdc20 proteolysis reveals a role for APC components Cdc23 and Cdc27 during S phase and early mitosis. *Curr Biol,* 8**,** 750-60.

Qi, S. T., Ma, J. Y., Wang, Z. B., Guo, L., Hou, Y. & Sun, Q. Y. 2016. N6-Methyladenosine Sequencing Highlights the Involvement of mRNA Methylation in Oocyte Meiotic Maturation and Embryo Development by Regulating Translation in Xenopus laevis. *J Biol Chem,* 291**,** 23020-23026.

Roignant, J. Y. & Soller, M. 2017. m6A in mRNA: An Ancient Mechanism for Fine-Tuning Gene Expression. *Trends Genet,* 33**,** 380-390.

Rubin-Bejerano, I., Mandel, S., Robzyk, K. & Kassir, Y. 1996. Induction of meiosis in Saccharomyces cerevisiae depends on conversion of the transcriptional represssor Ume6 to a positive regulator by its regulated association with the transcriptional activator Ime1. *Mol Cell Biol,* 16**,** 2518-26.

Salah, S. M. & Nasmyth, K. 2000. Destruction of the securin Pds1p occurs at the onset of anaphase during both meiotic divisions in yeast. *Chromosoma,* 109**,** 27-34.

Schneider-Poetsch, T., Ju, J., Eyler, D. E., Dang, Y., Bhat, S., Merrick, W. C., Green, R., Shen, B. & Liu, J. O. 2010. Inhibition of eukaryotic translation elongation by cycloheximide and lactimidomycin. *Nat Chem Biol,* 6**,** 209-217.

Schwab, M., Lutum, A. S. & Seufert, W. 1997. Yeast Hct1 is a regulator of Clb2 cyclin proteolysis. *Cell,* 90**,** 683-93.

Schwartz, S., Agarwala, S. D., Mumbach, M. R., Jovanovic, M., Mertins, P., Shishkin, A., Tabach, Y., Mikkelsen, T. S., Satija, R., Ruvkun, G., Carr, S. A., Lander, E. S., Fink, G. R. &

Regev, A. 2013. High-resolution mapping reveals a conserved, widespread, dynamic mRNA methylation program in yeast meiosis. *Cell,* 155**,** 1409-1421.

Schwartz, S., Mumbach, M. R., Jovanovic, M., Wang, T., Maciag, K., Bushkin, G. G., Mertins, P., Ter-Ovanesyan, D., Habib, N., Cacchiarelli, D., Sanjana, N. E., Freinkman, E., Pacold, M. E., Satija, R., Mikkelsen, T. S., Hacohen, N., Zhang, F., Carr, S. A., Lander, E. S. & Regev, A. 2014. Perturbation of m6A writers reveals two distinct classes of mRNA methylation at internal and 5' sites. *Cell Rep,* 8**,** 284-96.

Shi, H., Wang, X., Lu, Z., Zhao, B. S., Ma, H., Hsu, P. J., Liu, C. & He, C. 2017a. YTHDF3 facilitates translation and decay of N6-methyladenosine-modified RNA. *Cell Res,* 27**,** 315-328.

Shi, Z., Fujii, K., Kovary, K. M., Genuth, N. R., Rost, H. L., Teruel, M. N. & Barna, M. 2017b. Heterogeneous Ribosomes Preferentially Translate Distinct Subpools of mRNAs Genome-wide. *Mol Cell,* 67**,** 71-83 e7.

Siegel, M. R. & Sisler, H. D. 1963. Inhibition of Protein Synthesis in Vitro by Cycloheximide. *Nature,* 200**,** 675-6.

Simsek, D., Tiu, G. C., Flynn, R. A., Byeon, G. W., Leppek, K., Xu, A. F., Chang, H. Y. & Barna, M. 2017. The Mammalian Ribo-interactome Reveals Ribosome Functional Diversity and Heterogeneity. *Cell,* 169**,** 1051-1065 e18.

Smith, J. E., Alvarez-Dominguez, J. R., Kline, N., Huynh, N. J., Geisler, S., Hu, W., Coller, J. & Baker, K. E. 2014. Translation of small open reading frames within unannotated RNA transcripts in Saccharomyces cerevisiae. *Cell Rep,* 7**,** 1858-66.

Spingola, M. & Ares, M., Jr. 2000. A yeast intronic splicing enhancer and Nam8p are required for Mer1p-activated splicing. *Mol Cell,* 6**,** 329-38.

Storici, F. & Resnick, M. A. 2006. The delitto perfetto approach to in vivo site-directed mutagenesis and chromosome rearrangements with synthetic oligonucleotides in yeast. *Methods Enzymol.,* 409**,** 329-345.

Strich, R., Surosky, R. T., Steber, C., Dubois, E., Messenguy, F. & Esposito, R. E. 1994. UME6 is a key regulator of nitrogen repression and meiotic development. *Genes Dev,* 8**,** 796-810.

Sundaram, A. & Grant, C. M. 2014. A single inhibitory upstream open reading frame (uORF) is sufficient to regulate Candida albicans GCN4 translation in response to amino acid starvation conditions. *RNA,* 20**,** 559-67.

Szamecz, B., Rutkai, E., Cuchalova, L., Munzarova, V., Herrmannova, A., Nielsen, K. H., Burela, L., Hinnebusch, A. G. & Valasek, L. 2008. eIF3a cooperates with sequences 5' of uORF1

to promote resumption of scanning by post-termination ribosomes for reinitiation on GCN4 mRNA. *Genes Dev,* 22**,** 2414-25.

Tan, G. S., Magurno, J. & Cooper, K. F. 2011. Ama1p-activated anaphase-promoting complex regulates the destruction of Cdc20p during meiosis II. *Mol. Biol. Cell,* 22**,** 315-326.

Tio, C. W., Omerza, G., Sunder, S. & Winter, E. 2015. Autophosphorylation of the Smk1 MAPK is spatially and temporally regulated by Ssp2 during meiotic development in yeast. *Mol Biol Cell,* 26**,** 3546-55.

Valasek, L. S. 2012. 'Ribozoomin'--translation initiation from the perspective of the ribosome-bound eukaryotic initiation factors (eIFs). *Curr Protein Pept Sci,* 13**,** 305-30.

Venkataramanan, S., Douglass, S., Galivanche, A. R. & Johnson, T. L. 2017. The chromatin remodeling complex Swi/Snf regulates splicing of meiotic transcripts in Saccharomyces cerevisiae. *Nucleic Acids Research*.

Visintin, R., Prinz, S. & Amon, A. 1997. CDC20 and CDH1: a family of substrate-specific activators of APC-dependent proteolysis. *Science,* 278**,** 460-3.

Waern, K. & Snyder, M. 2013. Extensive transcript diversity and novel upstream open reading frame regulation in yeast. *G3 (Bethesda),* 3**,** 343-52.

Wang, C., Zhu, Y., Bao, H., Jiang, Y., Xu, C., Wu, J. & Shi, Y. 2016. A novel RNA-binding mode of the YTH domain reveals the mechanism for recognition of determinant of selective removal by Mmi1. *Nucleic Acids Res,* 44**,** 969-82.

Wang, X., Lu, Z., Gomez, A., Hon, G. C., Yue, Y., Han, D., Fu, Y., Parisien, M., Dai, Q., Jia, G., Ren, B., Pan, T. & He, C. 2014a. N6-methyladenosine-dependent regulation of messenger RNA stability. *Nature,* 505**,** 117-120.

Wang, X., Zhao, B. S., Roundtree, I. A., Lu, Z., Han, D., Ma, H., Weng, X., Chen, K., Shi, H. & He, C. 2015. N(6)-methyladenosine Modulates Messenger RNA Translation Efficiency. *Cell,* 161**,** 1388-1399.

Wang, Y., Li, Y., Toth, J. I., Petroski, M. D., Zhang, Z. & Zhao, J. C. 2014b. N6-methyladenosine modification destabilizes developmental regulators in embryonic stem cells. *Nat Cell Biol,* 16**,** 191-8.

Washburn, B. K. & Esposito, R. E. 2001. Identification of the Sin3-binding site in Ume6 defines a two-step process for conversion of Ume6 from a transcriptional repressor to an activator in yeast. *Mol Cell Biol,* 21**,** 2057-69.

Wethmar, K. 2014. The regulatory potential of upstream open reading frames in eukaryotic gene expression. *Wiley Interdiscip. Rev. RNA,* 5**,** 765-778.

Whinston, E., Omerza, G., Singh, A., Tio, C. W. & Winter, E. 2013. Activation of the Smk1 mitogen-activated protein kinase by developmentally regulated autophosphorylation. *Mol Cell Biol,* 33**,** 688-700.

Williams, R. M., Primig, M., Washburn, B. K., Winzeler, E. A., Bellis, M., Sarrauste de Menthiere, C., Davis, R. W. & Esposito, R. E. 2002. The Ume6 regulon coordinates metabolic and meiotic gene expression in yeast. *Proc. Natl. Acad. Sci. U. S. A.,* 99**,** 13431-13436.

Yadav, P. K. & Rajasekharan, R. 2017. The m6A methyltransferase Ime4 epitranscriptionally regulates triacylglycerol metabolism and vacuolar morphology in haploid yeast cells. *J. Biol. Chem.*

Yue, Y., Liu, J. & He, C. 2015. RNA N6-methyladenosine methylation in post-transcriptional gene expression regulation. *Genes Dev,* 29**,** 1343-55.

Zhao, B. S., Wang, X., Beadell, A. V., Lu, Z., Shi, H., Kuuspalu, A., Ho, R. K. & He, C. 2017. m6A-dependent maternal mRNA clearance facilitates zebrafish maternal-to-zygotic transition. *Nature,* 542**,** 475-478.

Zhou, J., Wan, J., Gao, X., Zhang, X., Jaffrey, S. R. & Qian, S. B. 2015. Dynamic m(6)A mRNA methylation directs translational control of heat shock response. *Nature,* 526**,** 591-4.

Zid, B. M. & O'Shea, E. K. 2014. Promoter sequences direct cytoplasmic localization and translation of mRNAs during starvation in yeast. *Nature,* 514**,** 117-21.

Zubenko, G. S. & Jones, E. W. 1981. Protein degradation, meiosis and sporulation in proteinase-deficient mutants of Saccharomyces cerevisiae. *Genetics,* 97**,** 45-64.

CHAPTER 5

Chromatin-remodeling SWI/SNF complex regulates Coenzyme Q_6 synthesis and a metabolic shift to respiration in yeast.

Chromatin-remodeling SWI/SNF complex regulates coenzyme Q_6 synthesis and a metabolic shift to respiration in yeast

Received for publication, May 23, 2017, and in revised form, July 17, 2017 Published, Papers in Press, July 24, 2017, DOI 10.1074/jbc.M117.798397

Agape M. Awad[‡§1], Srivats Venkataramanan[§¶1], Anish Nag[‡§], Anoop Raj Galivanche[¶], Michelle C. Bradley[‡§], Lauren T. Neves[§¶], Stephen Douglass[¶], Catherine F. Clarke[‡§2], and Tracy L. Johnson[§¶3]

From the [‡]Department of Chemistry and Biochemistry, the [§]Molecular Biology Institute, and the [¶]Department of Molecular Cell and Developmental Biology, UCLA, Los Angeles, California 90095

Edited by Dennis R. Voelker

Despite its relatively streamlined genome, there are many important examples of regulated RNA splicing in *Saccharomyces cerevisiae*. Here, we report a role for the chromatin remodeler SWI/SNF in respiration, partially via the regulation of splicing. We find that a nutrient-dependent decrease in Snf2 leads to an increase in splicing of the *PTC7* transcript. The spliced *PTC7* transcript encodes a mitochondrial phosphatase regulator of biosynthesis of coenzyme Q_6 (ubiquinone or CoQ_6) and a mitochondrial redox-active lipid essential for electron and proton transport in respiration. Increased splicing of *PTC7* increases CoQ_6 levels. The increase in *PTC7* splicing occurs at least in part due to down-regulation of ribosomal protein gene expression, leading to the redistribution of spliceosomes from this abundant class of intron-containing RNAs to otherwise poorly spliced transcripts. In contrast, a protein encoded by the nonspliced isoform of *PTC7* represses CoQ_6 biosynthesis. Taken together, these findings uncover a link between Snf2 expression and the splicing of *PTC7* and establish a previously unknown role for the SWI/SNF complex in the transition of yeast cells from fermentative to respiratory modes of metabolism.

Similar to other eukaryotic genomes, genes in *Saccharomyces cerevisiae* may be interrupted by non-coding sequences, called introns. Introns are removed from the pre-mRNA through the action of the spliceosome, a macromolecular machine composed of five small nuclear ribonucleoproteins. The spliceosome recognizes consensus sequence signals on the pre-mRNA, termed splice sites, by which it subsequently binds to the intron and catalyzes its removal via two transesterification reactions (1). Pre-mRNA splicing is critical for accurate gene expression in all eukaryotes, and there is significant evidence that alterations in microenvironments, such as changes in the chromatin state or chromatin-modifying factors, can affect splicing outcomes (1). However, the mechanisms for how chromatin and chromatin factors influence splicing are not completely understood.

Although the genome of *S. cerevisiae* contains a smaller number of introns than metazoan genomes, there are, nonetheless, numerous examples of intron-dependent gene regulation (2). The largest functional class of intron-containing genes (ICGs)[4] in budding yeast is ribosomal protein genes (RPGs) that encode the protein components of the ribosome. Therefore, the energy-intensive process of translation is under the heavy regulatory control of the spliceosome, such that splicing of RPGs can be finely tuned to the cells' environmental conditions and to nutrient availability (3).

Interestingly, this enrichment of introns within RPGs impacts the splicing of, as well as provides an opportunity for the regulation of, other ICGs within the yeast genome. About a third of yeast introns occur in RPGs, and the high transcription levels of these genes means that about 90% of the intron load encountered by the spliceosome is from this one functional class of genes (4). Indeed, the prevalence of RPG introns functions to titrate spliceosomes away from other introns, especially those containing suboptimal splice sites. Conversely, down-regulating RPG expression promotes the splicing of transcripts harboring suboptimal splice sites. This effect is perhaps best described during the process of yeast meiosis. Under conditions of vegetative growth, a number of meiosis-specific ICGs are expressed, but they possess suboptimal splice sites and are therefore poorly recognized by the spliceosome and suboptimally spliced. However, upon the down-regulation of RPGs during meiosis, increased availability of the previously limiting pool of spliceosomes leads to improved splicing efficiency of introns in meiosis-specific transcripts (5, 6).

This work was supported by National Science Foundation Grants MCB-1330803 and 1518316, and by NIGMS, National Institutes of Health, Grant GM-085474; the Whitcome Pre-doctoral Fellowship in Molecular Biology (to S. V.); and Ruth L. Kirschstein National Service Award GM-007185 (to M. B). The authors declare that they have no conflicts of interest with the contents of this article. The content is solely the responsibility of the authors and does not necessarily represent the official views of the National Institutes of Health.

RNA-seq data are available in the Gene Expression Omnibus (GEO) under accession number GSE94404.

[1] Both authors contributed equally to this work.

[2] To whom correspondence may be addressed: UCLA Dept. of Chemistry and Biochemistry, 607 Charles E. Young Dr. E., Box 156905, Los Angeles, CA 90095. Tel. 310-825-0771; Fax: 310-206-5213; E-mail: cathy@chem.ucla.edu.

[3] To whom correspondence may be addressed: UCLA Dept. of Molecular Cell and Developmental Biology, 610 Charles E. Young Dr. S., Los Angeles, CA 90095. Tel.: 310-206-2416; E-mail: tljohnson@ucla.edu.

[4] The abbreviations used are: ICG, intron-containing gene; RPG, ribosomal protein gene; ns, non-spliced; s, spliced; CoQ, coenzyme Q; DMQ_6, 5-demethoxy-Q_6; 4HB, 4-hydroxybenzoic acid; HHB, 3-hexaprenyl-4-hydroxybenzoic acid; qPCR, quantitative PCR; TOR, target of rapamycin.

There are other important examples of intron-based regulation in *S. cerevisiae*, especially among ICGs with non-consensus splice sites (7, 8). One such gene is *PTC7*, which encodes a Mg^{2+}/Mn^{2+}-dependent, type 2C serine/threonine protein phosphatase (9). The intron within *PTC7* is particularly intriguing because it contains a non-consensus branch-point sequence, rendering its splicing relatively inefficient under logarithmic growth conditions. The *PTC7* intron lacks a premature termination codon and is translated in-frame. The longer, non-spliced (ns) form of the *PTC7* RNA encodes a longer protein ($Ptc7_{ns}$) that contains a single trans-membrane helix located near the N terminus but is otherwise identical to the protein isoform derived from the spliced *PTC7* RNA ($Ptc7_s$). The read-through nature of the *PTC7* intron is conserved across yeast species, indicating potential functionality for both $Ptc7_s$ and $Ptc7_{ns}$ protein isoforms (10). $Ptc7_{ns}$ has been localized to the nuclear membrane, whereas $Ptc7_s$ is located within mitochondria (10). $Ptc7_s$ has been implicated in regulation of coenzyme Q (also termed ubiquinone or CoQ) biosynthesis via its phosphatase activity (11, 12). However, mechanisms of regulation of Ptc7 itself and the role of the evolutionarily conserved $Ptc7_{ns}$ isoform remain outstanding questions.

CoQ is a redox-active lipid composed of a fully substituted benzoquinone ring and a polyisoprenoid tail and is required for mitochondrial electron transport. The length of the polyisoprenoid group is species-specific; humans produce CoQ_{10}, and *S. cerevisiae* produce CoQ_6, with 10 and 6 isoprene units, respectively. The primary role of CoQ in the inner mitochondrial membrane is to accept the electrons from complex I and complex II and pass those electrons to complex III. Several other metabolic pathways, such as pyrimidine synthesis, sulfide oxidation, and fatty acid β-oxidation, rely on CoQ as an electron carrier (13). CoQ is present in all intracellular membranes, where it may function as a lipid-soluble antioxidant. Several human syndromes, including encephalomyopathy, ataxia, cerebellar atrophy, myopathy, and steroid-resistant nephrotic syndrome, are linked to primary deficiencies in CoQ biosynthesis (14–17).

Mitochondrial proteins are responsible for facilitating the biosynthesis of CoQ_6 in *S. cerevisiae* and include Coq1–Coq11 (18). Many of the Coq proteins necessary for the biosynthesis of CoQ_6 associate in a high-molecular weight complex (termed the "CoQ-synthome"), a multisubunit complex that is peripherally associated with the inner mitochondrial membrane on the matrix side (18). $Ptc7_s$ has been shown to localize to the mitochondria, where it is thought to regulate the phosphorylation state of Coq7 (11) and/or influence mitochondrial respiratory metabolism (12). In the former case, Ptc7s is believed to control, at least in part, the phosphorylation state of the Coq7 polypeptide, which modulates its hydroxylase activity. Coq7 catalyzes the hydroxylation of 5-demethoxy-Q_6 (DMQ_6), the penultimate step in the biosynthesis of CoQ_6 in yeast (19, 20).

The conserved SWI/SNF complex utilizes ATP hydrolysis by Snf2, the catalytic subunit, to disrupt specific histone–DNA contacts, resulting in the sliding or eviction of nucleosomes from the locus. As a result, Snf2 activity contributes to transcriptional regulation (21, 22). The genome-wide distribution of SWI/SNF is responsive to conditions of stress, and the complex is required for transcription of a number of stress response genes (23, 24). We have previously reported that levels of Snf2 change in response to nutrient conditions. We have also reported that the change in Snf2 leads to changes in levels of RPG transcripts, thereby regulating splicing outcomes (6). Here, we show that changes in levels of Snf2 modulate the CoQ_6 biosynthetic pathway in *S. cerevisiae*. First, we show that deletion of Snf2 alters the relative levels of $Ptc7_s$ and $Ptc7_{ns}$ isoforms in yeast and increases both the rate of synthesis and steady-state levels of CoQ_6. This is due to down-regulation of RPG transcripts and an increase in the available pool of spliceosomes. Moreover, we find that the Snf2 protein is down-regulated over time under batch growth conditions and nutrient depletion, and together with a concomitant increase in the splicing of *PTC7*, this leads to higher CoQ_6 levels in preparation for the transition from a fermentative mode of metabolism to a respiratory mode. Furthermore, we show that the two Ptc7 isoforms have opposing effects on the CoQ_6 biosynthetic pathway, which may explain contradictory reports in the literature about the effects of Ptc7 on CoQ_6 levels (11, 12). Importantly, although Snf2 is down-regulated in response to nutrient-depleted conditions, it is nonetheless required for growth on nonfermentable carbon sources, suggesting that dynamic control of Snf2 levels is crucial for the transition from fermentation to respiration.

Results

Deletion of Snf2 leads to enhanced splicing of PTC7 and a shift in the ratios of Ptc7 protein isoforms

Previously published RNA sequencing data for yeast lacking Snf2, the core ATPase component of the SWI/SNF complex (GEO accession number GSE94404), revealed an increase in splicing of a number of introns (6). Satisfyingly, the greatest improvement in splicing upon deletion of Snf2 is experienced by *RPL22B*, via a previously described mechanism consistent with down-regulation of RPG expression (25). The next two largest improvements in splicing efficiency are experienced by *YBR062C* (an ORF of unknown function) and *PTC7*, a previously described type 2C serine-threonine mitochondrial phosphatase that contains all 11 canonical motifs of the PPM family (type 2C) protein phosphatases, previously reported to play a role in CoQ_6 biosynthesis in yeast (11) (Fig. 1*A*). This increase in splicing of *PTC7* RNA was verified by RT-PCR (Fig. 1*B*). In addition, the results from the RNA-seq and RT-PCR were also independently verified by qPCR (data not shown). It has previously been demonstrated that increased splicing of poorly recognized introns can be achieved by decreased expression of competing, highly expressed RPGs (5). Furthermore, we have shown that deletion of Snf2 causes *en masse* down-regulation of RPGs and consequent improvement in splicing of a large number of introns (6). RPG down-regulation in the absence of Snf2 was validated by RT-PCR analysis. For example, expression of RPS16A and RPL34B, two intron-containing RPGs, is down-regulated in *snf2*Δ yeast compared with WT (Fig. 1*C*).

The *PTC7* transcript makes two distinct protein isoforms, one from the nonspliced and one from the spliced RNA. The spliced isoform ($Ptc7_s$) localizes to the mitochondria, whereas

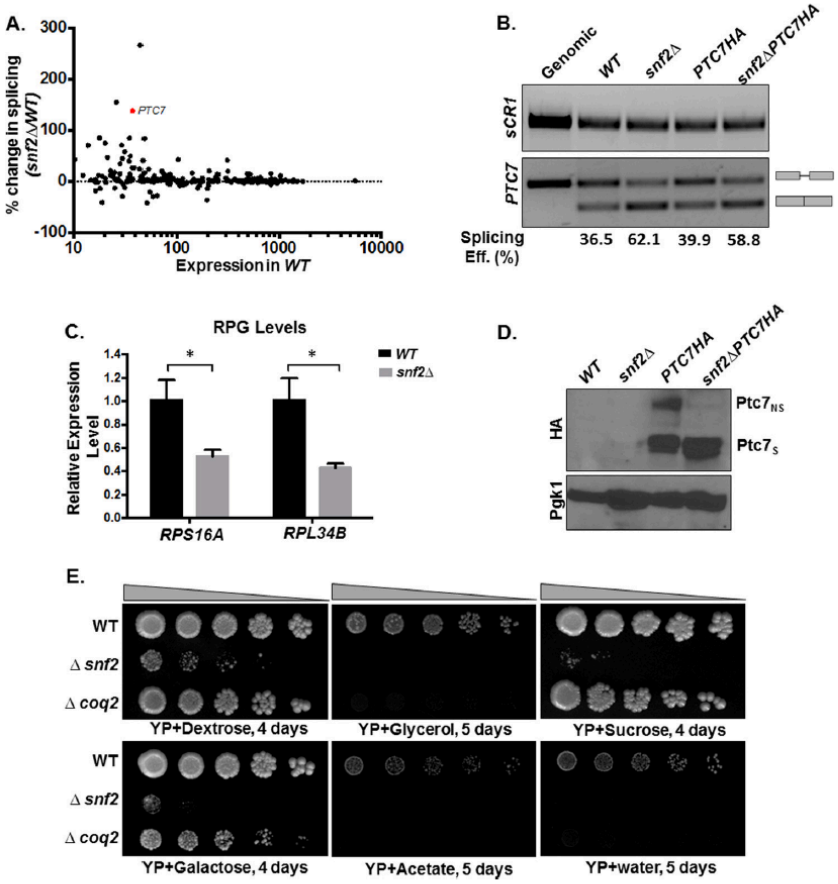

Figure 1. Deletion of *SNF2* enhances splicing of *PTC7* and the steady-state levels of the short Ptc7 protein isoform. *A*, deletion of *SNF2* enhances splicing of a subset of yeast RNAs, including *PTC7*. The scatter plot shows changes in splicing of individual introns in *snf2*Δ yeast over WT plotted against expression in WT. Percentage change in splicing is calculated as 100 × (S.E. in *snf2*Δ − S.E. in WT)/(S.E. in WT). *PTC7* is represented by the *red dot*. *B*, expression and splicing of *PTC7* in *WT* and *snf2*Δ yeast with HA-tagged and untagged Ptc7. Semiquantitative analysis of splicing efficiency of *PTC7* mRNA is indicated *below* each *lane*. *sCR1* served as an internal control. *Gray bars*, exons of the RNA; *thin gray line*, intron. *C*, RT-qPCR measurement of selected intron-containing RPG transcripts between WT and *snf2*Δ yeast strains. Shown is the mean of three biological replicates (unpaired Student's *t* test; *, $p < 0.05$). *Error bars*, S.D. *D*, deletion of *SNF2* affects steady-state levels of HA-tagged Ptc7 proteins. Proteins derived from the nonspliced and spliced forms of the *PTC7*-HA RNA are denoted as $Ptc7_{ns}HA$ and $Ptc7_sHA$, respectively. Pgk1 (phosphoglycerate kinase 1) served as a loading control. *E*, serial dilutions (5-fold) of WT BY4741, *snf2*Δ, and *coq2*Δ (negative respiratory-deficient control; W303 background, because the deletion is unstable in the BY background) on YP agar plates with the indicated carbon sources.

the nonspliced isoform ($Ptc7_{ns}$) has been reported to localize to the nuclear envelope (10). The *PTC7* gene was endogenously HA-tagged, and Western blot analysis demonstrated that deletion of Snf2 leads to an increase in the levels of $Ptc7_s$ compared with $Ptc7_{ns}$ (Fig. 1*D*). It is noteworthy that the increase in the ratio of $Ptc7_s/Ptc7_{ns}$ polypeptides in the WT and *snf2*Δ cells appears to be greater than the increased ratio of spliced/unspliced RNA.

It has previously been demonstrated that yeast strains lacking Snf2 fail to grow on non-fermentable carbon sources, such as glycerol or acetate (26). However, *snf2*Δ mutants frequently incur secondary mutations, and the growth of such strains can resemble WT. Therefore, growth on fermentable and non-fermentable carbon sources was used as a quality control for the assessment of the *bona fide* phenotype (24) of *snf2*Δ prior to each experiment (Fig. 1*E*).

Deletion of Snf2 leads to increased CoQ_6 synthesis in yeast and improves the flux from DMQ_6 to CoQ_6

$Ptc7_s$ has previously been described as playing a role in regulating CoQ_6 synthesis in *S. cerevisiae* (11). A schematic of the entire CoQ_6 biosynthetic pathway with 4-hydroxybenzoic acid as the ring precursor and the role of Ptc7 is detailed in Fig. 2*A*. $Ptc7_s$ is thought to enhance CoQ_6 biosynthesis via its activation of Coq7 and subsequent catalysis of the hydroxylation of DMQ_6, the penultimate step of CoQ_6 biosynthesis (Fig. 2*B*) (11, 27).

$^{13}C_6$-Labeled 4-hydroxybenzoic acid ($^{13}C_6$-4HB), a ring precursor for Q biosynthesis, was used to determine the levels of $^{13}C_6$-CoQ_6 biosynthesis in WT *versus* *snf2*Δ yeast grown to similar culture densities. The absence of Snf2 causes increased steady-state levels of CoQ_6 and increased *de novo* biogenesis of $^{13}C_6$-CoQ_6 (Fig. 3*A*). Additionally, there are significant changes in the levels of *de novo* synthesized DMQ_6, as well as 3-hexa-

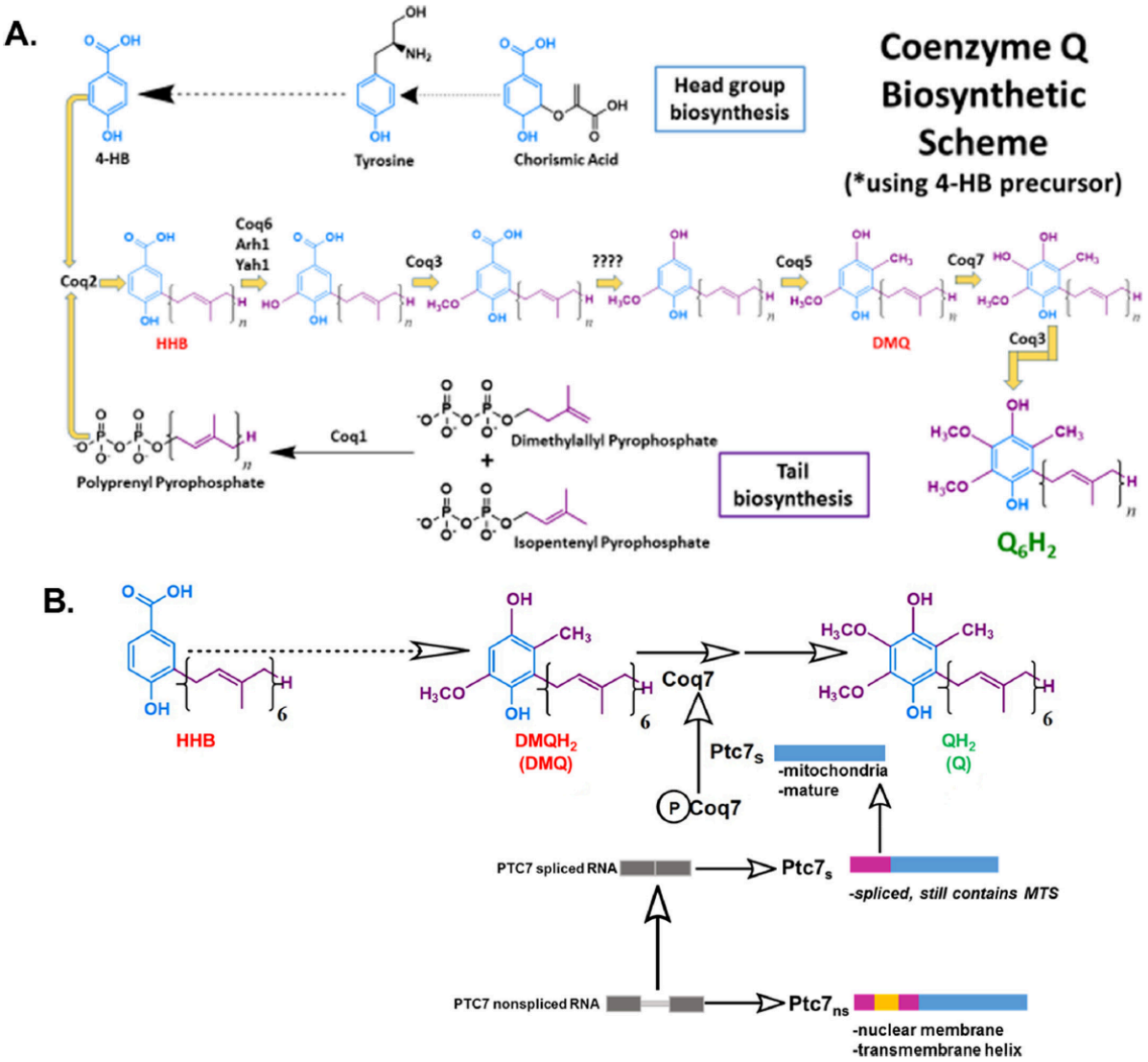

Figure 2. CoQ_6 biosynthetic pathway in *S. cerevisiae* and role of $Ptc7_s$ isoform on Coq7 phosphorylation and function. *A*, schematic of CoQ_6 biosynthetic pathway in yeast using 4HB as a ring precursor, ultimately forming the reduced CoQ_6H_2 product *in vivo*. The *question marks above* the decarboxylation and second hydroxylation steps denote that the enzyme(s) responsible is still unknown. *B*, schematic of the CoQ_6 biosynthetic pathway in yeast. The proposed function of $Ptc7_s$ as a mitochondrial phosphatase modulating Coq7 activity is indicated. $Ptc7_{ns}$ has been localized to nuclear membrane. The *gray bars* represent the exon regions of the RNA, and the *thin gray line* represents the intron region of the RNA. The *pink-colored regions* represent the predicted 38-amino acid mitochondrial targeting sequence (*MTS*) of the protein, the *yellow region* represents the 31-amino acid intron of the protein (which interrupts the MTS after amino acid 19, hence spanning from amino acid 20 to 50), and the *blue region* depicts the mature and spliced polypeptide, which spans from amino acid 51 to 374 (47).

prenyl-4-hydroxybenzoic acid (HHB), an early CoQ_6 biosynthetic intermediate (Fig. 3, *B* and *D*). Consistent with the increased synthesis of CoQ_6 being a consequence of Ptc7 action, the *snf2*Δ yeast show significantly lower ratios of $^{13}C_6$-DMQ_6 level to $^{13}C_6$-CoQ_6 content, indicating a significant increase in the efficiency of conversion of DMQ_6 to CoQ_6, namely the step catalyzed by Coq7, a target of $Ptc7_s$ (Fig. 3*C*) (11). Strikingly, we also observe that the levels of both steady-state and *de novo* synthesized HHB are significantly lower in *snf2*Δ than in the WT yeast (Fig. 3*D*). This suggests that the deletion of Snf2 not only causes higher CoQ_6 production by regulating catalysis from DMQ_6 but that it also funnels the early precursors more efficiently than WT, thus allowing a more streamlined conversion of intermediates of the pathway to the overall product of CoQ_6. This is reinforced by the observation that *snf2*Δ yeast show significantly lower ratios of $^{13}C_6$-HHB to $^{13}C_6$-CoQ_6 content (Fig. 3*E*).

Depletion of Snf2 during batch growth is associated with increased PTC7 splicing and increased CoQ_6 production

Because *snf2*Δ yeast have a significantly slower growth rate than WT, we considered the possibility that the increased CoQ_6

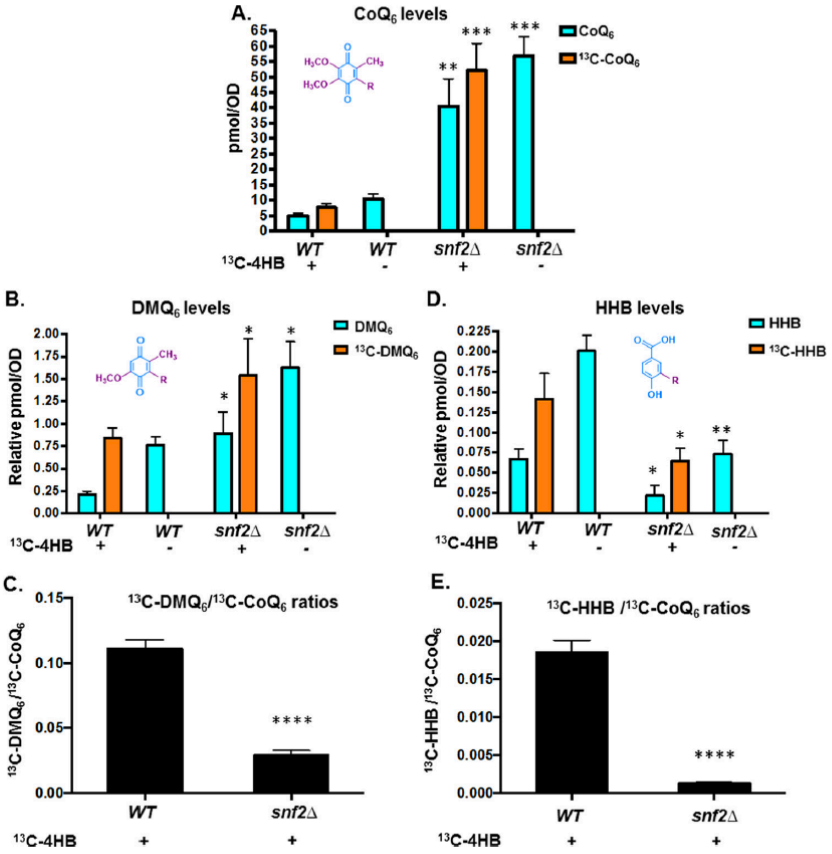

Figure 3. Deletion of *SNF2* leads to increased steady state levels and *de novo* CoQ_6 biosynthesis in yeast and improves the flux from DMQ_6 to CoQ_6. *A*, levels of steady-state CoQ_6 (^{12}C-CoQ_6, *blue bars*) and *de novo* synthesized CoQ_6 ($^{13}C_6$-CoQ_6, *orange bars*) were determined in WT and *snf2*Δ yeast. $^{13}C_6$-4HB was added during midlog phase (A_{600} = 0.5), and labeling was allowed to proceed until a cell density of A_{600} ~1.75 was reached by both strains. ^{12}C-CoQ_6 and $^{13}C_6$-CoQ_6 present in yeast cell pellets were quantified by HPLC-MS/MS, as described under "Experimental procedures." *Error bars*, S.D. of $n = 3$ biological replicates (unpaired Student's *t* test between *corresponding bars* for *snf2*Δ and WT; **, $p < 0.005$; ***, $p < 0.0005$). *B*, levels of steady-state (^{12}C-DMQ_6, *blue bars*) and *de novo* synthesized DMQ_6 ($^{13}C_6$-DMQ_6, *orange bars*) were determined in WT and *snf2*Δ yeast. DMQ_6 was determined from the same cultures as in *A*. *Error bars*, S.D. of $n = 3$ biological replicates (unpaired Student's *t* test between corresponding bars for *snf2*Δ and *WT*; *, $p < 0.05$). *C*, ratios of $^{13}C_6$-DMQ_6/$^{13}C_6$-CoQ_6 in WT and *snf2*Δ yeast, depicting flux of conversion of $^{13}C_6$-DMQ_6 to $^{13}C_6$-CoQ_6. *Error bars*, S.D. of $n = 3$ biological replicates (unpaired Student's *t* test between corresponding bars for *snf2*Δ and WT; ****, $p < 0.00005$). *D*, levels of steady-state HHB (^{12}C-HHB, *blue bars*) and *de novo* synthesized HHB ($^{13}C_6$-HHB, *orange bars*) were determined in WT and *snf2*Δ yeast. HHB was determined from the same cultures as in *A*. *Error bars*, S.D. of $n = 3$ biological replicates (unpaired Student's *t* test between *corresponding bars* for *snf2*Δ and WT; *, $p < 0.05$; **, $p < 0.005$). *E*, ratios of ^{13}C-HHB/^{13}C-CoQ_6 in WT and *snf2*Δ yeast, depicting flux of conversion of $^{13}C_6$-HHBto $^{13}C_6$-CoQ_6. *Error bars*, S.D. of $n = 3$ biological replicates (unpaired Student's *t* test between *corresponding bars* for *snf2*Δ and WT; ****, $p <$ 0.00005).

synthesis was a consequence of the increased time in culture required to achieve equal cell density. To address this, rates of CoQ_6 biosynthesis in WT and *snf2*Δ yeast were determined at timed intervals of culture. First, measurements of steady-state and *de novo* synthesis rates of CoQ_6 between 2 and 12 h of batch growth in YPD revealed that whereas there is indeed an increased rate of synthesis in the *snf2*Δ yeast strain, the steady-state levels of CoQ_6 plateau within 4–6 h of labeling (Fig. 4*A*). We also observe decreasing levels of Snf2 as the time course progresses and nutrients are depleted (Fig. 4*B*). Consistent with the role of Snf2 in RPG transcription, RPG levels decrease with time in batch cultures of yeast, in a manner that tracks well with decreasing levels of Snf2 (Fig. 4*C*). This decrease also coincides with a concomitant increase in the splicing of *PTC7* (Fig. 4, *D* and *E*). Notably, splicing of the *PTC7* transcript in *snf2*Δ yeast starts off higher than in WT yeast, but as Snf2 is depleted from the WT strain, splicing of the *PTC7* transcript approaches the levels of splicing in the *snf2*Δ strain (Fig. 4*F*).

To better understand the kinetics of CoQ_6 synthesis, a shorter time course was performed to capture points preceding the plateau, between 0 and 5 h of labeling. Within 4 h after labeling with ^{13}C-4HB precursor, significant down-regulation in the levels of Snf2 protein is evident (Fig. 5*A*). The decrease in the level of Snf2 protein is mirrored in the increase in splicing efficiency of *PTC7* transcript in the WT strain (Fig. 5, *B–E*). It is interesting to note that the *PTC7* transcript is initially better spliced in the *snf2*Δ strain than in WT, but as the levels of Snf2 in the WT yeast decrease, splicing improves to a degree comparable with the *snf2*Δ strain (Fig. 5, *D* and compare *C* and *F*).

Additionally, there is a striking increase in the overall CoQ_6 product and its *de novo* biosynthesis in the *snf2*Δ yeast within 0–5 h of labeling, as compared with CoQ_6 levels of the WT

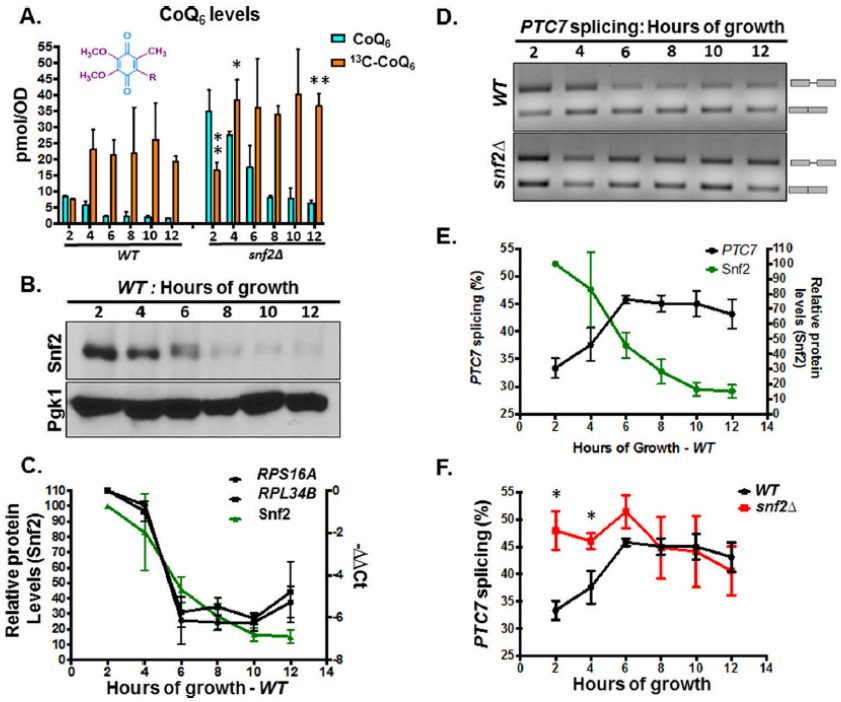

Figure 4. Snf2 levels decrease during batch growth, coinciding with increased *PTC7* splicing and increased CoQ_6 synthesis. *A*, levels of steady-state CoQ_6 (^{12}C-CoQ_6, *blue bars*) and *de novo* synthesized CoQ_6 ($^{13}C_6$-CoQ_6, *orange bars*) in WT and *snf2*Δ yeast were determined at the designated hours after labeling with $^{13}C_6$-4HB. *Error bars*, S.D. of $n = 3$ biological replicates (unpaired Student's *t* test between *corresponding bars* for *snf2*Δ and WT; *, $p < 0.05$; **, $p < 0.005$). *B*, steady-state levels of Snf2 protein in WT cells corresponding to samples from *A* were determined by immunoblot. Pgk1 served as a loading control. *C*, RT-qPCR measurement of selected intron-containing RPG transcripts (*black lines*) and Snf2 protein levels (*green line*) in WT yeast cells were determined at the designated hours after labeling with $^{13}C_6$-4HB as indicated in *A*. Shown is the mean of three biological replicates. *Error bars*, S.D. *D*, expression and splicing of *PTC7* in WT and *snf2*Δ yeast cells corresponding to samples from *A*. PCR products representing the spliced and nonspliced forms are indicated. *E*, quantification of splicing of *PTC7* transcript (*black line*) and Snf2 protein levels (*green line*) in WT yeast cells corresponding to samples from *D*. Snf2 protein levels were previously depicted in *C* and are shown here again for purposes of comparison. Shown is the mean of three biological replicates. *Error bars*, S.D. *F*, quantification of splicing of *PTC7* transcripts in WT and *snf2*Δ yeast cells corresponding to samples from *D*. The splicing of WT *PTC7* shown in *D* is depicted again here for purposes of comparison. Shown is the mean of three biological replicates. *Error bars*, S.D. (unpaired Student's *t* test; *, $p < 0.05$.

during the same time course (Fig. 6, compare *A* and *F*). Furthermore, the gradual increase in CoQ_6 biosynthesis observed in the WT strain plateaus at 3–4 h after labeling (Fig. 6*A*), by which point the significant down-regulation in the levels of Snf2 protein is also evident (Fig. 5*A*). The steady-state and *de novo* synthesized levels of DMQ_6 and HHB were also measured in the 5-h time course of WT and *snf2*Δ yeast (Fig. 6, *B*, *C*, *G*, and *H*). Strikingly, the conversion of *de novo* DMQ_6 to CoQ_6 increases (as shown by the decreased ratio of $^{13}C_6$-DMQ_6 to $^{13}C_6$-CoQ_6) in a manner concurrent with the decrease in Snf2 levels and increase in *PTC7* splicing in WT (compare Fig. 6*D* with Fig. 5 (*A* and *B*)). In fact, as the levels of Snf2 in WT yeast decrease, the conversion efficiency of DMQ_6 to CoQ_6 approaches the low ratio of DMQ_6 to CoQ_6 in *snf2*Δ yeast (Fig. 6, compare *D* and *I*). The role of $Ptc7_s$ in the increased synthesis of CoQ_6 in the absence of Snf2 can be inferred from the observation that whereas the conversion efficiency from DMQ_6 to CoQ_6 is higher in the absence of Snf2, the level of DMQ_6 itself does not change appreciably between WT and *snf2*Δ yeast over the 5-h time course (Fig. 6, compare *B* and *G*). However, the *snf2*Δ cells also show significantly lower rates of HHB synthesis (Fig. 6, compare *C* and *H*), as well as lower ratios of $^{13}C_6$-HHB to $^{13}C_6$-CoQ_6 content (Fig. 6, compare *E* and *J*), consistent with the observation that deletion of Snf2 markedly accelerates the synthesis of CoQ_6, presumably by expediting the conversion of these intermediates to the final product.

RPG down-regulation in general leads to increased PTC7 splicing

Our previous work showed that Snf2-dependent down-regulation of ribosomal protein genes enhances splicing, particularly of genes with nonconsensus splice sites. To determine whether the observed increase in *PTC7* splicing is a consequence of RPG down-regulation *per se*, rapamycin was used to inhibit target of rapamycin (TOR)-dependent RPG transcription in a Snf2-independent manner (28) (Fig. 7*A*). It has also been previously published that rapamycin mitigates certain mitochondrial disorders in *Drosophila* and improves lifespan in response to TOR inhibition, purportedly by modulating carbon metabolism (29). In our work, rapamycin treatment led to a significant increase in the splicing of the *PTC7* transcript (Fig. 7, *B* and *C*). As previously observed, the change in the ratio of $Ptc7_s$/$Ptc7_{ns}$ protein (Fig. 1*D*) is greater than the change in the ratio of spliced to nonspliced transcript upon the deletion of Snf2 (Fig. 1*B*). This suggests that whereas Snf2-dependent RPG down-regulation changes the splicing of the *PTC7* transcript,

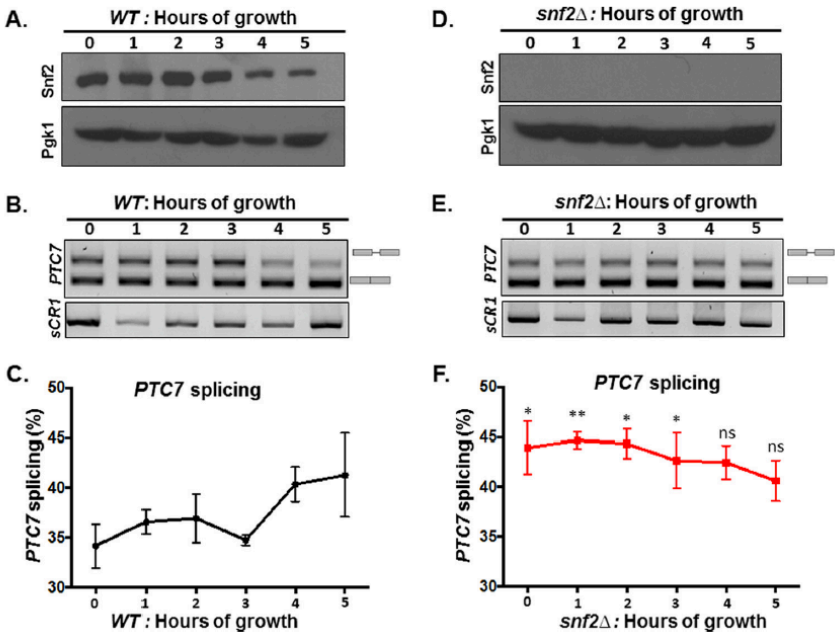

Figure 5. The decrease in Snf2 levels over time in batch cultures of WT yeast correlates with enhanced splicing of *PTC7* RNA. *A*, steady-state levels of Snf2 protein in WT cells corresponding to samples from indicated time points were determined by immunoblot. Pgk1 (phosphoglycerate kinase 1) served as a loading control. *B*, expression and splicing of *PTC7* in WT yeast cells corresponding to samples from *A*; PCR products represent the spliced and nonspliced forms, as indicated. *C*, quantification of splicing of *PTC7* transcript (*black line*) in WT yeast cells corresponding to samples from *B*. Shown is the mean of three biological replicates. *Error bars*, S.D. *D*, the Snf2 protein is absent in *snf2*Δ cells corresponding to samples from the indicated time points as determined by immunoblot. Pgk1 served as a loading control. *E*, expression and splicing of *PTC7* in *snf2*Δ yeast cells corresponding to samples from *D*; PCR products representing the spliced and nonspliced forms are indicated. *F*, quantification of splicing of *PTC7* transcript (*red line*) in *snf2*Δ yeast cells corresponding to samples from *E*. Shown is the mean of three biological replicates. *Error bars*, S.D. (unpaired Student's *t* test between *corresponding bars* for *snf2*Δ and WT in *C*; *, $p < 0.05$; **, $p < 0.005$).

there are probably additional layers of gene regulation that control the relative levels of the $Ptc7_s$ and $Ptc7_{ns}$ protein isoforms. Experiments probing these mechanisms are currently ongoing. Nonetheless, these results are consistent with a model whereby down-regulation of RPG expression redirects spliceosomes from these abundant transcripts to otherwise poorly spliced transcripts, such as *PTC7* (5, 6). In light of the role of Snf2 in RPG expression, changes in Snf2 levels allow fine-tuning of splicing in response to the cell's metabolic needs.

Ptc7 isoforms have differing and opposing effects on CoQ_6 synthesis

The predicted structures of the two isoforms of Ptc7, $Ptc7_s$ and $Ptc7_{ns}$, have been modeled (Fig. 8, *A* and *B*). In fact, the $Ptc7_{ns}$ contains a transmembrane helix, encoded for by the *PTC7* intron, which is capable of spanning the nuclear membrane. Overall, the presence of this transmembrane helix is not predicted to influence the folding of the rest of the protein, thus potentially retaining its phosphatase activity (Fig. 8).

To determine the effect of each Ptc7 isoform on CoQ_6 synthesis, we assayed CoQ_6 levels in cells expressing both forms of Ptc7, $Ptc7_s$ only, $Ptc7_{ns}$ only, or neither (*ptc7*Δ). As reported previously, there is no significant change in CoQ_6 synthesis levels in the *ptc7*Δ mutant (12, 30). However, exclusive expression of $Ptc7_s$ leads to an increase in CoQ_6 synthesis, whereas exclusive expression of $Ptc7_{ns}$ leads to a decrease in CoQ_6 synthesis (Fig. 9*A*). The relative RNA levels from each strain are shown (Fig. 9*B*). Moreover, there are no significant changes observed in the protein levels of Snf2 or Coq7, the target of Ptc7 activity (Fig. 9*C*), in these strains. Whereas each of these isoforms was expressed within the endogenous context and from the endogenous *PTC7* promoter, protein levels of the $Ptc7_{ns}$ appeared to be increased relative to the other isoforms (Fig. 9, *B* and *C*), perhaps due to a cellular feedback mechanism that increases expression or enhances stability of $Ptc7_{ns}$.

The steady-state and *de novo* synthesized levels of CoQ_6 were also measured in a 5-h time course with the yeast strains expressing either $Ptc7_{ns}$ or $Ptc7_s$. Both steady-state and *de novo* CoQ_6 biosynthesis are significantly lower in $Ptc7_{ns}$ strain than in the $Ptc7_s$ and in fact appear to be actively repressed, suggesting that the two isoforms of Ptc7 have differing and opposing effects on CoQ_6 biosynthesis (Fig. 9*D*). In addition, the exclusive presence of $Ptc7_s$ causes increased *de novo* biogenesis of ^{13}C-CoQ_6 as compared with the exclusive presence $Ptc7_{ns}$ (Fig. 9*D*). Whereas the positive effect of $Ptc7_s$ on CoQ_6 biosynthesis is consistent with the mechanisms of Ptc7 action described previously, it is clear that $Ptc7_{ns}$ has a repressive effect on CoQ_6 biosynthesis (compare $Ptc7_{ns}$ and *ptc7*Δ in Fig. 9*A*). To begin to elucidate the mechanism of this repression, we assayed the mRNA transcript levels of genes encoding components of the CoQ_6 biosynthetic complex (*viz. COQ1–11* and *PTC7*). On average, there is little change in the expression of the complex upon deletion of Snf2 (Fig. 9, *G* and *H*) or with the exclusive expression of $Ptc7_s$ or *ptc7*Δ. However, exclusive expression of $Ptc7_{ns}$ is associated with pronounced down-regulation of every

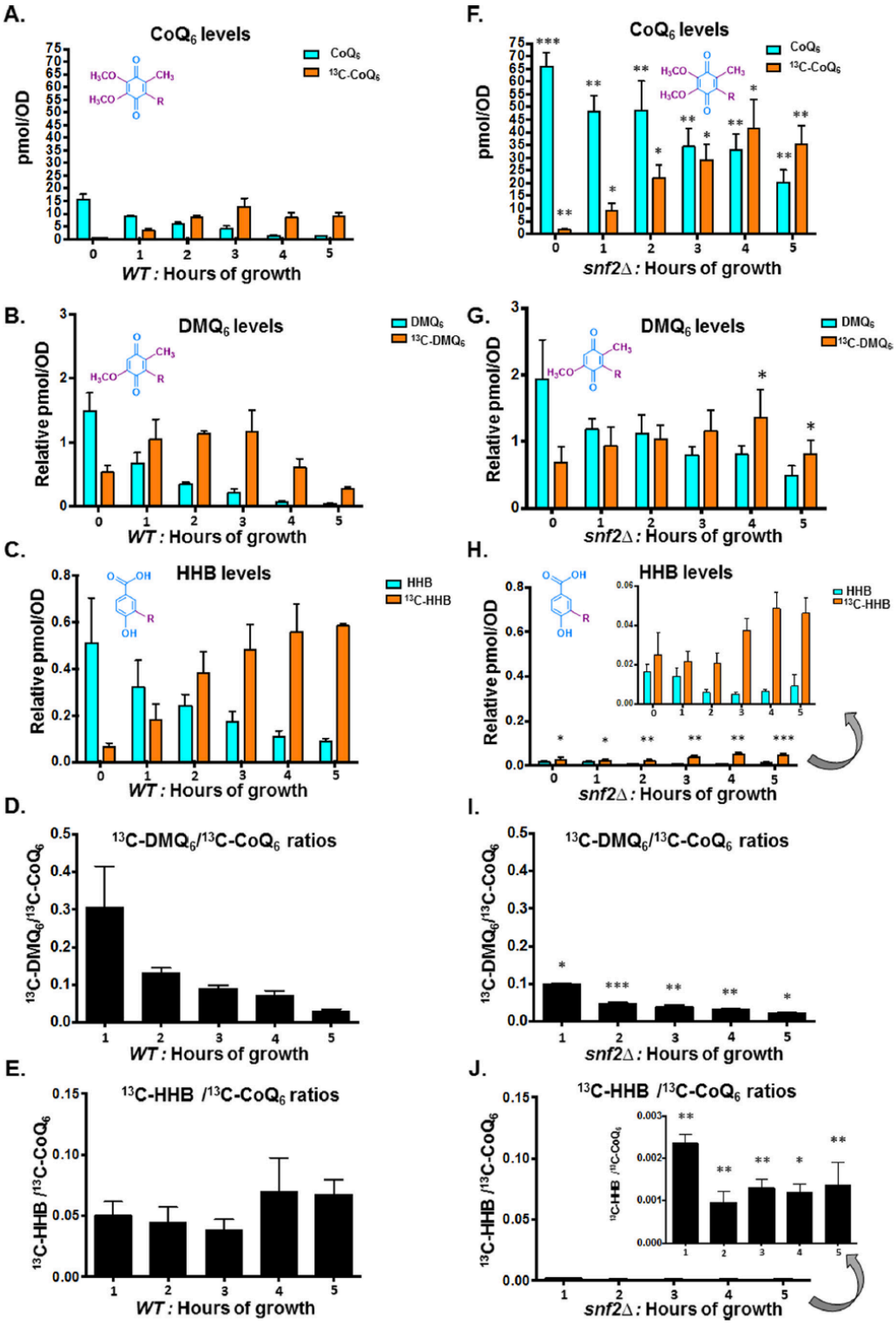
A.
CoQ6 levels
CoQ6
13C-CoQ6
pmol/OD
WT : Hours of growth
F.
CoQ6 levels
snf2Δ : Hours of growth
B.
DMQ6 levels
Relative pmol/OD
G.
C.
HHB levels
HHB
13C-HHB
H.
D.
13C-DMQ6/13C-CoQ6 ratios
I.
E.
13C-HHB /13C-CoQ6 ratios
J.

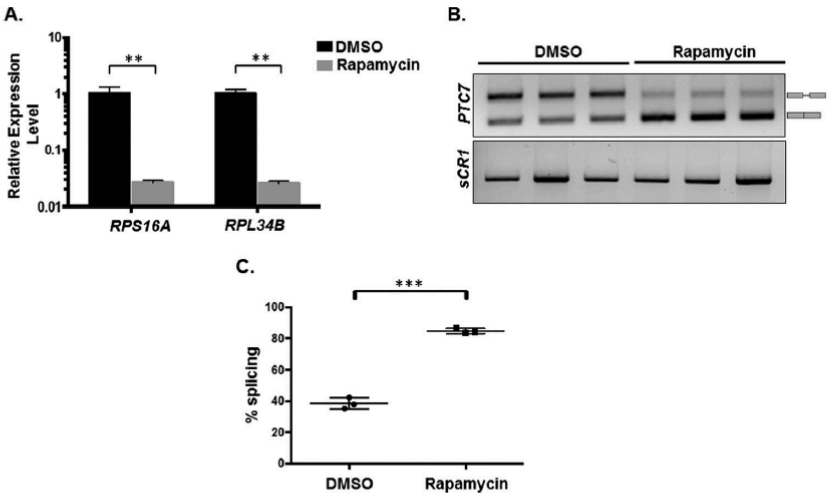

Figure 7. RPG down-regulation and redistribution of spliceosomes result in increased *PTC7* splicing. *A*, RT-qPCR measurement of selected intron-containing RPG transcripts between WT yeast treated with rapamycin and a vehicle control. Mean of three biological replicates (unpaired Student's *t* test, $^{**}p < 0.005$). *Error bars*, S.D. *B*, expression and splicing of *PTC7* in WT yeast treated with rapamycin and a vehicle control (DMSO). PCR products representing the spliced and nonspliced forms are indicated. *C*, quantification of three independent biological replicates of *B* (unpaired Student's *t* test; ***, $p < 0.0005$). *Error bars*, S.D.

member of the CoQ-synthome (Fig. 9, *E* and *F*). Although the mechanism by which these components are down-regulated is unclear, it is interesting that $Ptc7_{ns}$ has previously been localized to the nuclear membrane (10), hinting at a novel role for this isoform in expression of the RNAs encoding the CoQ-synthome. Two possible mechanisms by which nucleus-localized $Ptc7_{ns}$ may affect synthesis of the CoQ-synthome are via direct action on nucleus-localized Coq7 or via indirect effects on gene expression. It is important to mention here that to the best of our knowledge, no reports have demonstrated nuclear localization of, or a nuclear role for, Coq7 in *S. cerevisiae*.

Interestingly, yeast strains engineered to express either $Ptc7_s$ or $Ptc7_{ns}$ still retain the ability to grow on medium containing a non-fermentable carbon source, as do *ptc7*Δ null mutants (data not shown). This is consistent with our prior observations that ~1–10% of CoQ_6 levels are sufficient for comparable growth on medium containing a nonfermentable carbon source. It has been postulated that residual CoQ_6 levels are observed due to the overlapping activities of Ptc5 and/or Ptc6, and in fact the *ptc5*Δ*ptc7*Δ double null mutant has impaired growth under conditions of temperature stress (11, 31). It is also worth noting that unlike the deletion of *SNF2*, the conversion efficiencies or ratios between the early components of the pathway (DMQ_6 or HHB) and CoQ_6 do not vary between strains exclusively expressing either Ptc7 isoform (Fig. 10, *C* and *D*). This is because although there are significant changes in the levels of *de novo* synthesized DMQ_6 as well as HHB when comparing $Ptc7_s$ to $Ptc7_{ns}$ (Fig. 10, *A* and *B*), $Ptc7_s$ is synthesizing higher levels of *de novo* CoQ_6, DMQ_6, and HHB, compared with overall lower levels of these same lipids in $Ptc7_{ns}$ (Fig. 10, *C* and *D*). Thus, the overall conversion efficiencies (ratios) between both isoforms are comparable (Fig. 10, *C* and *D*). This is consistent with our interpretation that the absence of Snf2 contributes to the metabolic state of the cell in other ways in addition to its role in regulation of the Ptc7 isoforms.

Figure 6. Overall conversion efficiency of the CoQ_6 biosynthetic pathway increases upon depletion of Snf2, with increased conversions of both DMQ_6 to Q_6 and HHB to Q_6. *A*, levels of steady-state CoQ_6 (^{12}C-CoQ_6, *blue bars*) and *de novo* synthesized CoQ_6 ($^{13}C_6$-CoQ_6, *orange bars*) in WT yeast cells were determined at the designated hours after labeling with $^{13}C_6$-4HB. *Error bars*, S.D. of $n = 3$ biological replicates. *B*, levels of steady-state DMQ_6 (^{12}C-DMQ_6, *blue bars*) and *de novo* synthesized DMQ_6 ($^{13}C_6$-DMQ_6, *orange bars*) in WT yeast were determined at the designated hours after labeling with $^{13}C_6$-4HB. *Error bars*, S.D. of $n = 3$ biological replicates. *C*, levels of steady-state HHB (^{12}C-HHB, *blue bars*) and *de novo* synthesized ($^{13}C_6$-HHB, *orange bars*) in WT and *snf2*Δ yeast were determined at the designated hours after labeling with $^{13}C_6$-4HB. *Error bars*, S.D. of $n = 3$ biological replicates. *D*, the ratio of $^{13}C_6$-DMQ_6/$^{13}C_6$-CoQ_6 in WT yeast was determined at the designated hours after labeling with $^{13}C_6$-4HB. *Error bars*, S.D. of $n = 3$ biological replicates. The 0-h time point is excluded, because the ratio is not indicative of pathway conversion. *E*, the ratio of $^{13}C_6$-HHB/$^{13}C_6$-CoQ_6 in WT yeast was determined at the designated hours after labeling with $^{13}C_6$-4HB. *Error bars*, S.D. of $n = 3$ biological replicates. The 0-h time point is excluded, because the ratio is not indicative of pathway conversion. *F*, levels of steady-state CoQ_6 (^{12}C-CoQ_6, *blue bars*) and *de novo* synthesized ($^{13}C_6$-CoQ_6, *orange bars*) in *snf2*Δ yeast cells were determined at the designated hours after labeling with $^{13}C_6$-4HB. *Error bars*, S.D. of $n = 3$ biological replicates (unpaired Student's *t* test between *corresponding bars* for *snf2*Δ and WT in *A*; *, $p < 0.05$; **, $p < 0.005$; ***, $p < 0.0005$). *G*, levels of steady-state DMQ_6 (^{12}C-DMQ_6, *blue bars*) and *de novo* synthesized DMQ_6 ($^{13}C_6$-DMQ_6, *orange bars*) in *snf2*Δ yeast were determined at the designated hours after labeling with $^{13}C_6$-4HB. *Error bars*, S.D. of $n = 3$ biological replicates. (unpaired Student's *t* test between *corresponding bars* for *snf2*Δ and WT in *B*; *, $p < 0.05$). *H*, levels of steady-state HHB (^{12}C-HHB, *blue bars*) and *de novo* synthesized HHB ($^{13}C_6$-HHB, *orange bars*) in *snf2*Δ yeast were determined at the designated hours after labeling with ^{13}C-4HB. *Error bars*, S.D. of $n = 3$ biological replicates (unpaired Student's *t* test between corresponding bars for *snf2*Δ and WT in *C*; *, $p < 0.05$; **, $p < 0.005$; ***, $p < 0.0005$). *I*, the ratio of $^{13}C_6$-DMQ_6/$^{13}C_6$-CoQ_6 in *snf2*Δ yeast cells was determined at the designated hours after labeling with $^{13}C_6$-4HB. *Error bars*, S.D. of $n = 3$ biological replicates (unpaired Student's *t* test between corresponding bars for *snf2*Δ and WT in *D*; *, $p < 0.05$; **, $p < 0.005$; ***, $p < 0.0005$). The 0-h time point is excluded, because the ratio is not indicative of pathway conversion. *J*, the ratio of $^{13}C_6$-HHB/$^{13}C_6$-CoQ_6 in *snf2*Δ yeast cells was determined at the designated hours after labeling with $^{13}C_6$-4HB. *Error bars*, S.D. of $n = 3$ biological replicates (unpaired Student's *t* test between *corresponding bars* for *snf2*Δ and WT in *E*; *, $p < 0.05$; **, $p < 0.005$). The 0-h time point is excluded, because the ratio is not indicative of pathway conversion.

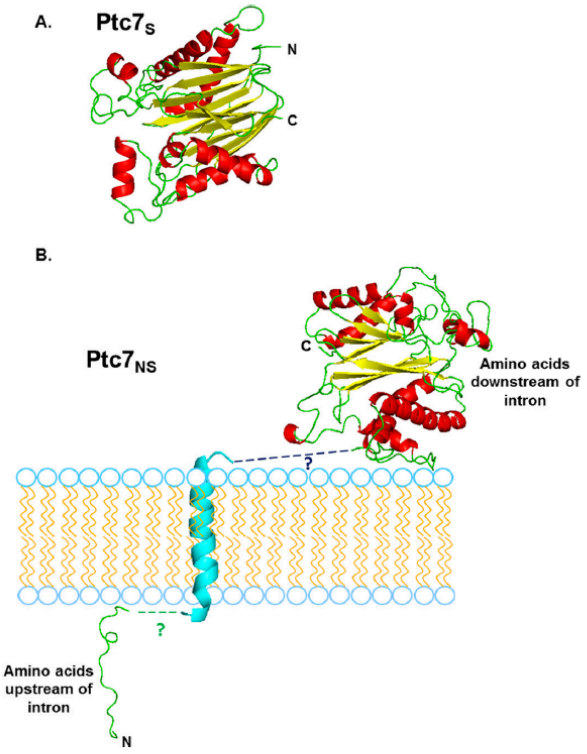

Figure 8. Structural predictions of mitochondrial $Ptc7_s$ and nuclear membrane traversing $Ptc7_{ns}$. *A*, PHYRE2 homology modeling of mature mitochondrial $Ptc7_s$, which is experimentally determined to start at amino acid Gly^{39} (46). 85% of residues modeled at >90% confidence (15% of residues modeled *ab initio*). The N terminus and C terminus of the protein are shown. *B*, PHYRE2 homology modeling of nuclear membrane $Ptc7_{ns}$. The predicted trans-membrane helix encoded by the intron is shown in *cyan*. 86% of residues modeled at >90% confidence (14% of residues modeled *ab initio*. To show the interaction with the nuclear membrane, the N-terminal loop residing on the one side of the nuclear membrane is proposed to be linked to the modeled transmembrane helix, which is then proposed to be linked to the rest of the Ptc7 protein that is predicted to reside on the alternate side of the nuclear membrane. The *nine black dashes* connecting the helix to the larger portion of the protein represent nine amino acids in the intron that were in an unmodeled region.

These data reveal a novel role for Snf2 in respiration and specifically in the transition from a largely fermentative mode of metabolism to a largely respiratory one in *S. cerevisiae*, as shown by the model in Fig. 11. Under conditions of high nutrient availability, Snf2-dependent transcription of intron-rich RPGs sequesters spliceosomes away from transcripts with weak splice sites, such as *PTC7*. As a consequence, both isoforms of the Ptc7 protein are expressed at appreciable levels, and their opposing effects on CoQ_6 synthesis ensure that CoQ_6 is maintained at a relatively low level. As the nutrients in the medium are depleted, the levels of Snf2 and, consequently, RPG transcripts, decrease concurrently, freeing up spliceosomes to act on *PTC7*. This leads to better splicing of *PTC7* and a shift in the relative abundances of the two protein isoforms, which eventually leads to an increase in CoQ_6 synthesis.

Discussion

Whereas it has been broadly acknowledged that chromatin states and chromatin factors influence splicing outcomes in various organisms, identifying the functional importance of such regulation under biologically relevant conditions remains a challenge. We have shown previously that down-regulation of Snf2, the core ATPase component of the SWI/SNF chromatin-remodeling complex, in response to nutrient depletion leads to a change in cellular splicing outcomes due to down-regulation of RPGs and subsequent redistribution of spliceosomes (5, 6). We show here that Snf2-dependent changes in splicing of *PTC7* during yeast growth, combined with the general conditions in the cell in the absence of Snf2, causes a shift in the ratio of two distinct isoforms of the Ptc7 protein that have distinct and opposing effects on CoQ_6 biosynthesis. This change in the ratio of the isoforms is concomitant with an increase in CoQ_6 levels in the cell, preparing for the transition from a largely fermentative to a respiratory mode of metabolism.

Previous studies have presented contradictory evidence regarding the involvement of *PTC7* in CoQ_6 biosynthesis. Ptc7 is required for the dephosphorylation of Coq7, thus transitioning Coq7 to its "active" form, which is able to catalyze the penultimate step of the CoQ_6 pathway. This led to the prediction that the *ptc7*Δ strain would demonstrate decreased CoQ_6 synthesis, as assayed by quantification of lipids from purified mitochondria (11). Surprisingly, although Ptc7 supports general respiratory function, the absence of *PTC7* does not lead to a deficiency in CoQ_6 levels, as assayed in lipid extracts of whole cells (12) (Fig. 9*A*). The studies here help to resolve this apparent contradiction. Studies with the *ptc7*Δ cells fail to address the opposing roles that the two Ptc7 isoforms have in the cell under WT conditions. Only cells with the capacity to express both $Ptc7_s$ and $Ptc7_{ns}$ can accurately reflect the full extent of Ptc7 function. We demonstrate that exclusive expression of $Ptc7_{ns}$ has a significant repressive effect on CoQ_6 biosynthesis (Fig. 9, *A* and *D*). Notably, the rates of conversions from precursors in the pathway to the final product remained unchanged, indicating down-regulation of the entire pathway (Fig. 10, *C* and *D*). Consistent with this, we observe down-regulation of almost all of the components of the CoQ_6 biosynthetic complex upon exclusive expression of $Ptc7_{ns}$ (Fig. 9*F*). The mechanism by which $Ptc7_{ns}$ affects RNA expression is as yet unknown, and investigations to understand the same are ongoing.

PTC7 is not the only known example of a gene in *S. cerevisiae* encoding functional proteins from both the nonspliced pre-mRNA as well as the "mature" spliced mRNA (10). We recently reported translation of unspliced *GCR1* pre-mRNA leading to a functional Gcr1 protein, although in this case, translation starts from within the retained intron (7). Whereas the read-through nature of the intron is conserved across most *Saccharomycetaceae* species, the intron is excised in the same species (analysis of publicly available RNA-seq data sets; data not shown), rendering it likely that both forms of the protein are necessary and functional. This is illustrated in the case of *Tetrapisispora blattae*, which, like *S. cerevisiae*, underwent a whole genome duplication event; but unlike *S. cerevisiae*, which lost the duplications of most of its genes, *T. blattae* retains two copies of the *PTC7* gene. Interestingly, the two *PTC7* genes in *T. blattae* subfunctionalized into a gene that encodes a mitochondrial PP2C ($Ptc7_b$, from a spliced transcript of *PTC7b* con-

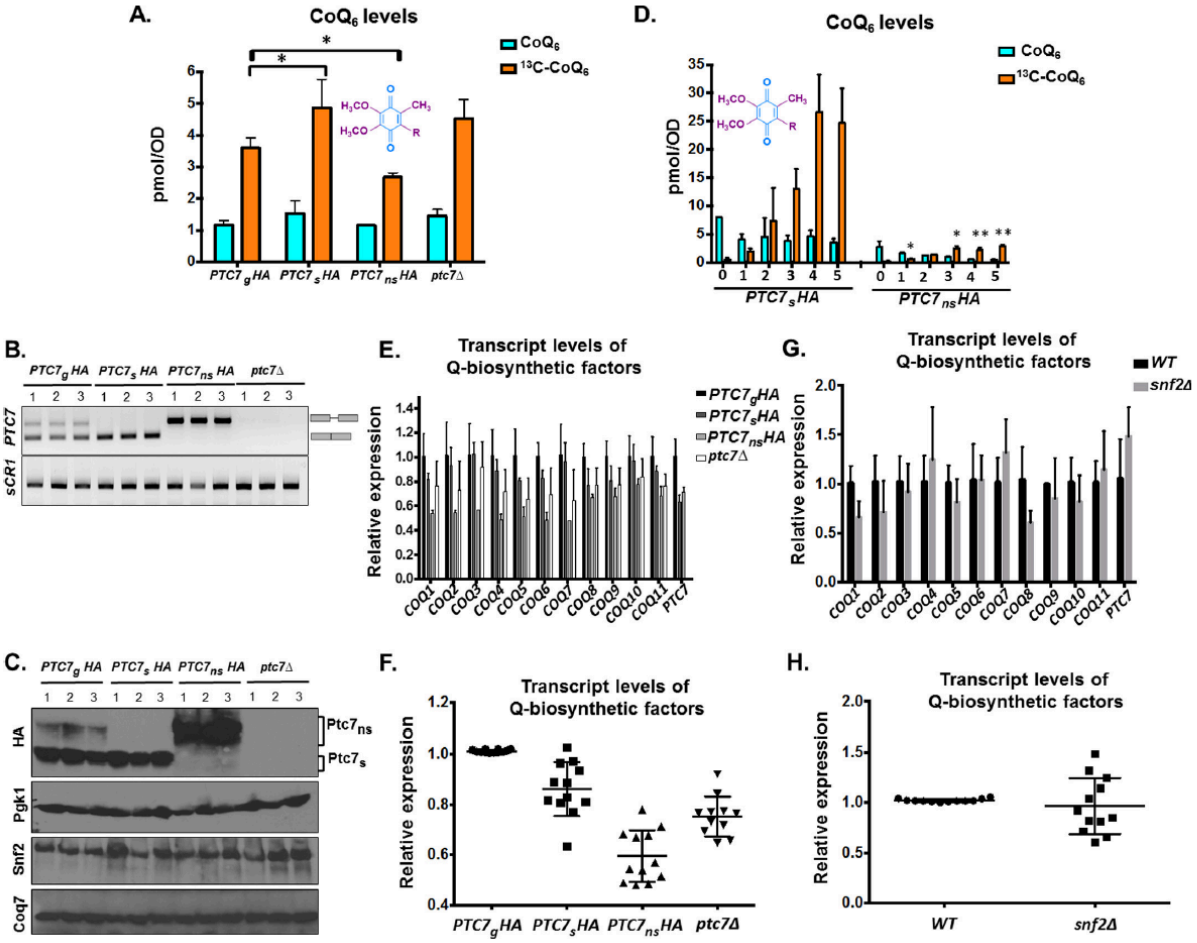

Figure 9. Ptc7 isoforms have differing and opposing effects on CoQ_6 synthesis. *A*, levels of steady-state CoQ_6 (^{12}C-CoQ_6, *blue bars*) and *de novo* synthesized CoQ_6 ($^{13}C_6$-CoQ_6, *orange bars*) in strains expressing distinct Ptc7 isoforms (*$PTC7_gHA$*, genomic, both isoforms expressed; *$PTC7_sHA$*, exclusively expresses the isoform from spliced mRNA; *$PTC7_{ns}HA$*, exclusively expresses the isoform from nonspliced pre-mRNA) and *ptc7*Δ. Labeling with $^{13}C_6$-4HB was allowed to proceed for 3 h. *Error bars*, S.D. of $n = 3$ biological replicates (unpaired Student's *t* test; *, $p < 0.05$). *B*, expression and splicing of *PTC7* for samples corresponding to *A*. PCR products representing the spliced and nonspliced forms are indicated. *C*, steady-state levels of HA-tagged Ptc7 proteins were determined by immunoblotting for samples corresponding to *A*. Proteins derived from the nonspliced and spliced forms of the *PTC7* RNA are denoted as $Ptc7_{ns}$ and $Ptc7_s$, respectively. Pgk1 (phosphoglycerate kinase 1) served as a loading control. Immunoblots for Snf2 and Coq7 are also included. *D*, levels of steady-state (^{12}C-CoQ_6, *blue bars*) and *de novo* synthesized ($^{13}C_6$-CoQ_6, *orange bars*) CoQ_6 in *$PTC7_sHA$* and *$PTC7_{ns}HA$* yeast cells were determined at the designated hours after labeling with $^{13}C_6$-4HB. *Error bars*, S.D. of $n = 3$ biological replicates (unpaired Student's *t* test between corresponding bars for *$PTC7_sHA$* and *$PTC7_{ns}HA$*; *, $p < 0.05$; **, $p < 0.005$). *E*, RT-qPCR measurement of *COQ1–COQ11* and *PTC7* transcript levels between strains expressing different Ptc7 isoforms (*$PTC7_gHA$*, genomic, both isoforms expressed; *$PTC7_sHA$*, exclusively expresses the isoform from spliced mRNA; *$PTC7_{ns}HA$*, exclusively expresses the isoform from non-spliced pre-mRNA) and *ptc7*Δ. Shown is the mean of three biological replicates. *Error bars*, S.D. *F*, summary analysis of transcript levels of Q-biosynthetic factors from *E*. *G*, RT-qPCR measurement of *COQ1-COQ11* and *PTC7* transcript levels between WT and *snf2*Δ yeast. Shown is the mean of three biological replicates. *Error bars*, S.D. *H*, summary analysis of transcript levels of Q-biosynthetic factors from *G*.

taining a stop codon within its intron) and a second gene encoding a PP2C predicted to localize to the nuclear envelope ($Ptc7_a$, from an nonspliced transcript of *PTC7a* (32). This conservation further suggests that both protein isoforms derived from the *PTC7* transcript in *S. cerevisiae* are functional. Cells lacking $Ptc7_{ns}$ show increased sensitivity to latrunculin A treatment, compared with strains expressing both isoforms of Ptc7 or lacking $Ptc7_s$ (10). Such sensitivity might suggest a distinct role for $Ptc7_{ns}$ in actin filament formation.

It is noteworthy that nuclear roles for numerous metabolic enzymes have been described previously. The ability of metabolic enzymes to "moonlight" in the nucleus, affecting gene regulation at various steps, appears to be crucial for the ability of cells to sense and adapt to their potentially distinct nutrient environments (33). Numerous mitochondrial enzymes, such as succinate dehydrogenase, fumarase, aconitase, and malate dehydrogenase (all components of the Krebs cycle), have been shown to have significant nuclear roles in the regulation of gene expression (34–38). In some of these cases, enzymatic activity of these enzymes has been shown to be crucial to their nuclear roles (39). This precedence, combined with the evolutionarily conserved presence of an isoform of Ptc7 in the nuclear membrane, raises the possibility that a nucleus-localized phosphatase is crucial to regulation of components of the CoQ_6 biosyn-

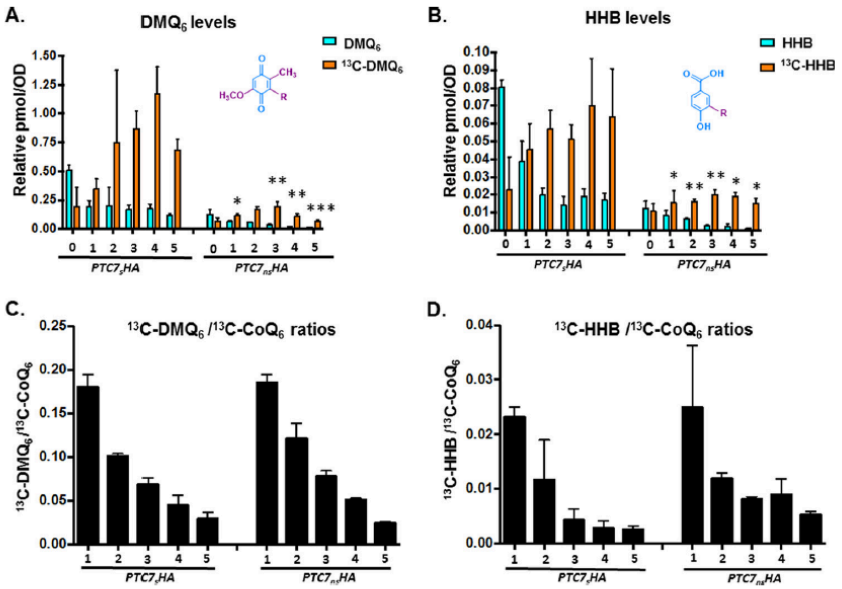

Figure 10. Exclusive expression of Ptc7 isoforms dramatically alters levels of CoQ_6 biosynthetic pathway intermediates DMQ_6 and HHB, yet overall conversion efficiency between both isoforms is comparable. *A*, levels of steady-state DMQ_6 (^{12}C-DMQ_6, *blue bars*) and *de novo* synthesized DMQ_6 ($^{13}C_6$-DMQ_6, *orange bars*) in *PTC7$_s$HA* and *PTC7$_{ns}$HA* yeast cells were determined at the designated hours after labeling with $^{13}C_6$-4HB. *Error bars*, S.D. of $n = 3$ biological replicates (unpaired Student's *t* test between *corresponding bars* for *PTC7$_s$HA* and *PTC7$_{ns}$HA*; *, $p < 0.05$; **, $p < 0.005$; ***, $p < 0.0005$). *B*, levels of steady-state HHB (^{12}C-HHB, *blue bars*) and *de novo* synthesized HHB ($^{13}C_6$-HHB, *orange bars*) in *PTC7$_s$HA* and *PTC7$_{ns}$HA* yeast cells were determined at the designated hours after labeling with $^{13}C_6$-4HB. *Error bars*, S.D. of $n = 3$ biological replicates (unpaired Student's *t* test between *corresponding bars* for *PTC7$_s$HA* and *PTC7$_{ns}$HA*; *, $p < 0.05$; **, $p < 0.005$). *C*, ratio of $^{13}C_6$-DMQ_6/$^{13}C_6$-CoQ_6 in *PTC7$_s$HA* and *PTC7$_{ns}$HA* yeast cells were determined at the designated hours after labeling with $^{13}C_6$-4HB. Ratios were derived from levels of $^{13}C_6$-CoQ_6, as shown in Fig. 7*D*. *Error bars*, S.D. of $n = 3$ biological replicates. The 0-h time point is excluded, because the ratio is not indicative of pathway conversion. *D*, ratio of $^{13}C_6$-HHB/$^{13}C_6$-CoQ_6 in *PTC7$_s$HA* and *PTC7$_{ns}$HA* yeast cells were determined at the designated hours after labeling with $^{13}C_6$-4HB. Ratios were derived from levels of $^{13}C_6$-CoQ_6, as shown in Fig. 7*D*. *Error bars*, S.D. of $n = 3$ biological replicates. The 0-h time point is excluded, because the ratio is not indicative of pathway conversion.

thetic pathway. Intriguingly, CLK-1 and COQ7, the *C. elegans* and human homologs of Coq7, which is a target for Ptc7 in *S. cerevisiae* (11), have been demonstrated to localize to the nucleus and are postulated to have roles independent of CoQ biosynthesis (40). COQ7 has also been shown to associate with chromatin in HeLa cells (40), although recently this has been attributed to a transformed cell phenomenon (41). Whereas nuclear localization of Coq7 in *S. cerevisiae* has not been demonstrated, we suggest a potential role in nuclear gene regulation for Ptc7 via phosphatase activity on Coq7 or other unidentified targets, including conventionally nuclear and other "moonlighting" mitochondrial enzymes.

It is also possible that Ptc7 has a substrate other than Coq7 that affects expression of the CoQ_6-synthome. In fact, a recent study identified with high confidence numerous differentially phosphorylated proteins in a *ptc7*Δ strain (12). Notably, this proteomic analysis does not distinguish between the potential effects of the two Ptc7 isoforms globally. In fact, rescue using plasmid-based expression of *PTC7* (full-length) does not restore dephosphorylation levels for a number of nuclear proteins, although the increased phosphorylation of mitochondrial proteins upon deletion of *PTC7* is almost completely reversed by exogenous expression of Ptc7 (12). Furthermore, it is possible that the mitochondrial role for $Ptc7_s$ is in fact covered by multiple redundancies. Ptc5 and Ptc6, two other PP2C protein phosphatases, also localize to the mitochondrial membrane, and *PTC5* demonstrates a negative genetic interaction with *PTC7*, indicating the possibility of overlapping functions (11, 31).

Interestingly, the effect of Snf2 deletion on CoQ_6 biosynthesis does not perfectly mirror the exclusive expression of $Ptc7_s$. We postulate that this is partially due to the Snf2 affecting the flux of the entire CoQ_6 biosynthetic pathway, as demonstrated by the increased conversion of early precursors. Whereas deletion of Snf2 does not, on average, change the expression of the components of the CoQ_6-synthome (Fig. 9, *G* and *H*), it is possible the Snf2 may have other effects of CoQ_6 flux. We are exploring these possibilities.

Intriguingly, although the absence of Snf2 enhances levels of CoQ_6, yeast strains lacking Snf2 have a severe growth defect on non-fermentable carbon sources, such as glycerol or acetate (26) (Fig. 1*E*). However, Snf2 protein is undetectable by immunoblotting during growth in medium containing glycerol or acetate as the only carbon source (data not shown). This leads us to hypothesize that before Snf2 protein is down-regulated in response to glucose depletion, it is required for the transition from a fermentative metabolic state to one that is predominantly respiratory in nature. The molecular details of the requirement for Snf2 in this transition are the subject of ongoing investigation. However, it is probably at least in part due to its reported role in the activation (de-repression) of genes whose transcription had previously been subject to glucose-mediated catabolite repression. This activation occurs once the glucose has been depleted or the yeast have been shifted to a

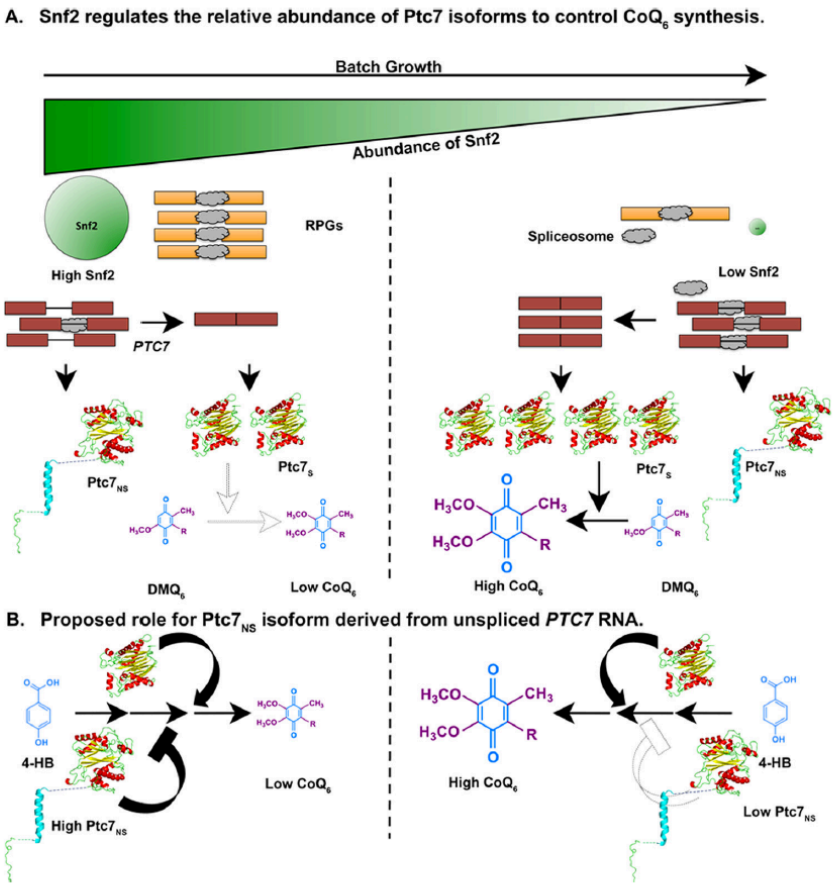

Figure 11. Model for a novel role for Snf2 in respiration, and in the transition from a primarily fermentative mode of metabolism to a primarily respiratory mode of metabolism. *A*, during *S. cerevisiae* batch growth, the abundance of Snf2 decreases in conjunction with depletion of nutrients in the medium. RPGs under the control of Snf2 are down-regulated, allowing redistribution of spliceosomes to other poorly spliced transcripts. Splicing of the *PTC7* transcript increases, enhancing the ratio of $Ptc7_s/Ptc7_{ns}$ and overall levels of $Ptc7_s$. These changes in Ptc7 isoform levels lead to increased conversion of DMQ_6 and increased synthesis of CoQ_6. The *darker arrow* represents a greater effect or reaction conversion, whereas a *lighter arrow* represents a smaller effect or reaction conversion. *B*, $Ptc7_{ns}$ has a repressive effect on CoQ_6 biosynthesis. CoQ_6 levels are low or high, depending on the levels of the $Ptc7_{ns}$ isoform relative to $Ptc7_s$. Similar to *A*, *darker arrows* and *bars* denote a larger effect, whereas *lighter arrows* and *bars* denote a smaller effect.

different, non-fermentable carbon source (26). We postulate that once the gene expression profile required for adaptation to the new nutrient environment has been initiated and/or established, the requirement for Snf2 is relieved, and in fact, the down-regulation of Snf2 enhances splicing of *PTC7*. This transient requirement for Snf2 bears striking similarities to a previous report detailing the role of Snf2 in reversing Ume6-mediated repression at certain meiotic genes early in meiosis, before it is itself down-regulated to enable splicing of meiotic transcripts (6).

This work reveals a mechanism by which SWI/SNF acts as a nexus point in the fermentation–respiratory transition in *S. cerevisiae*. We also demonstrate opposing effects of isoforms of a single gene, *PTC7*, on the process of CoQ_6 biosynthesis, via distinct mechanisms. Numerous aspects of these mechanisms remain to be studied, as well as their potential roles in the gene regulation response to other physiological conditions that yeast might experience.

Experimental procedures

Yeast strains and culture conditions

The yeast strains used in this study are listed in Table 1. All strains except W303Δcoq2 are derived from the BY background. Yeast strains were grown in YPD (1% yeast extract, 2% peptone, 2% dextrose) medium at 30 °C. Snf2 and Ptc7 null strains were maintained with a backup expression plasmid (pRS316 backbone harboring either *SNF2* or *PTC7*). The plasmid was shuffled out by growth on 5-fluoroorotic acid before using the strains in experiments. Strains with tagged isoforms of Ptc7 were a kind gift from Dr. Ron Davis (10). These strains were back-crossed against WT or *snf2*Δ strains, and daughter strains used for this study are listed in Table 1. The *snf2*Δ strain was observed to spontaneously mutate if grown on YPD for longer than 7–8 days, acquiring suppressor mutations that made it difficult to distinguish from WT. Hence, for all experiments with *snf2*Δ, the plasmid contain-

Table 1
Genotype and source of yeast strains

Strain number	Name	Genotype	Source/reference
TJY6724	WT	*MATa his3Δ leu2Δ LYS2 met15Δ ura3Δ*	Ref. 6
TJY6727	*snf2Δ*	*MATα his3Δ leu2Δ ura3Δ snf2Δ::NatMX*	Ref. 6
TJY7114	*$PTC7_g$HA*	*MATa his3Δ leu2Δ ura3Δ $PTC7_g$HA:KanMX*	This study
TJY7115	*snf2Δ$PTC7_g$HA*	*MATa his3Δ leu2Δ ura3Δ snf2Δ::NatMX $PTC7_g$HA:KanMX*	This study
W303Δ*coq2*	*coq2Δ*	*MATa ade2-1 his3-1,15 leu2-3,112 trp1-1 ura3-1 coq2::HIS3*	Ref. 47
TJY7116	*$PTC7_s$HA*	*MATa his3Δ leu2Δ ura3Δ $PTC7_s$HA:KanMX*	This study
TJY7118	*$PTC7_{ns}$HA*	*MATa his3Δ leu2Δ ura3Δ $PTC7_{ns}$HA:KanMX*	This study
TJY7142	*ptc7Δ*	*MATa his3Δ leu2Δ ura3Δ ptc7Δ:KanMX*	This study
BY4741Δ*coq9*	*coq9Δ*	*MATα his3Δ0 leu2Δ0 met15Δ0 ura3Δ0 coq9::KANMX4*	Ref. 48

ing *SNF2* was shuffled out prior to each experiment, allowing a fresh *snf2Δ* strain with each experiment, to avoid these suppressor mutants. We found that this was absolutely instrumental to observe the proper phenotype and behavior of the *snf2Δ* strain.

RNA-sequencing analyses

The RNA-sequencing data reported in this study were generated previously (6). Briefly, RNA sequencing libraries were prepared using the Illumina Truseq® V3 kit and ribosomal RNA depletion (Ribo-Zero, Illumina). Single-end, 50-nucleotide sequence reads (HiSeq 2000) were aligned to SacCer3 and spliced transcripts from the Ares Lab Yeast Intron Database version 3 (42) in a single step using STAR (43). Only the highest scoring alignments for each read were kept, allowing for at most a single tie. Reads/kb/million were computed for each gene by dividing the total number of reads that aligned entirely within the gene's exon boundaries by the gene's total exon length in kilobase pairs per million mapped reads. Reads within ICGs were categorized as exonic, spliced, or unspliced. Exonic reads map entirely within an exon, as defined by the Ares Lab Yeast Intron Database. Introns with annotated small nucleolar RNAs within the defined intron boundaries were disregarded in this analysis. Spliced reads are those that align with a gap that corresponds to an annotated intron, and unspliced reads map partially within an exon and partially within an intron with no gap. Spliced and unspliced read counts were normalized by dividing total spliced counts by the number of potential unique alignment positions that contribute to the total. For spliced reads, this is read length minus one for every intron. For unspliced read counts, this is the length of the intron plus the read length minus one. Splicing efficiency for each intron was calculated as normalized spliced counts divided by the sum of the normalized spliced and normalized unspliced counts. Changes in splicing efficiency were calculated as percentage difference over WT efficiency and plotted against expression levels (reads/kb/million) in WT. Data are available under GEO accession number GSE94404, and detailed methods were described previously (6).

RT-PCR and real-time PCR analysis

RNA was isolated from a 5-ml aliquot of cell culture corresponding to time points described in each experiment. After DNase treatment (Roche Applied Science), equal quantities of total RNA from each sample were used to make cDNA using a cDNA synthesis kit (Fermentas). To detect *PTC7* splicing isoforms, primers flanking the intronic sequences were used for PCR using 1 μl of cDNA diluted 1:20. PCR products were then separated on a 2% agarose gel and imaged. RT-qPCR was done in a 10-μl reaction volume with gene-specific primers using 1 μl of cDNA diluted 1:20 using Perfecta SYBR Green Fastmix (Quanta Biosciences) and a CFX96 Touch System (Bio-Rad). All samples were analyzed in triplicate for each independent experiment. RT-qPCR was also performed for the *scR1* (cytoplasmic signal recognition particle RNA subunit) RNA from each cDNA sample. Gene expression analysis was done by $2^{-\Delta Ct}$ methods using *scR1* as a reference. -Fold expression of mRNA was measured compared with WT by $2^{-\Delta\Delta Ct}$ methods (44).

Immunoblots

Protein was isolated from cell pellets with FA-1 lysis buffer (50 mM HEPES, pH 7.5, 150 mM NaCl, 1 mM EDTA, 1% Triton X-100, 0.1% sodium deoxycholate, 1 mM PMSF, and protease inhibitors) with bead beating. The buffer was supplemented with protease inhibitor mixture tablet (Roche Applied Science). Total protein was resolved by SDS-PAGE. The gel was transferred to PVDF membrane, and proteins were detected with the following antibodies at the stated dilutions: anti-SNF2 antibody (yN-20, Santa Cruz Biotechnology) at a 1:200 dilution in 2% milk, anti-HA antibody (901514, BioLegend) at a 1:2000 dilution in 5% milk, anti-Pgk1 antibody (459250, Invitrogen) at a 1:3000 dilution in 5% milk, or anti-Coq7 antibody (described previously (16) at a 1:2000 dilution in 3% milk. Signal was detected with enhanced chemiluminescence (Thermo Scientific) as described by the manufacturer.

Metabolic labeling of CoQ_6 with $^{13}C_6$-labeled precursors

Yeast strains were grown overnight in 25 ml of YPD in a shaking incubator (30 °C, 250 rpm) and diluted to an A_{600} of 0.1 in 60 ml of fresh YPD the next morning. The cultures were incubated as before to an A_{600} of 0.5 (midlog phase) and subsequently treated with $^{13}C_6$-4HB at 10 μg/ml (600 μg total) or ethanol vehicle control (0.015%, v/v). At designated time periods, cells were harvested by centrifugation at 3000 × *g* for 5 min, from 50-ml aliquots (used for lipid extraction) or 10-ml aliquots (used for RNA and protein analysis). Cell pellets were stored at −20 °C.

Analysis of CoQ_6 and CoQ_6 intermediates

Lipid extraction of cell pellets was conducted as described (18) with methanol and petroleum ether and CoQ_4 as the internal standard. Lipid measurements were performed by HPLC-

MS/MS and normalized to total OD. Prior to mass spectrometry analysis, all samples were treated with 1.0 mg/ml benzoquinone to oxidize hydroquinones to quinones. Mass spectrometry analyses utilized a 4000 QTRAP linear MS/MS spectrometer (Applied Biosystems), and data were acquired and analyzed using Analyst version 1.4.2 and 1.5.2 software (Applied Biosystems). Separation of lipid quinones was performed with a binary HPLC delivery system and a Luna 5μ phenyl-hexyl column (100 × 4.6 mm, 5 μm; Phenomenex). The mobile phase consisted of a 95:5 methanol/isopropyl alcohol solution with 2.5 mM ammonium formate as solution A and a 100% isopropyl alcohol solution with 2.5 mM ammonium formate as solution B. The percentage of solution B was increased linearly from 0 to 5% over 6 min, whereby the flow rate was increased from 600 to 800 μl. Initial flow rate and mobile phase conditions were changed back to initial phase conditions linearly over 3.5 min. Each sample was analyzed using multiple-reaction monitoring mode. The following precursor-to-product ion transitions were detected as well as the +17 *m/z* ammoniated adducts for each of the metabolic products: $^{13}C_6$-HHB *m/z* 553.4/157.0 (ammoniated: 570.4/157.0), ^{12}C-HHB *m/z* 547.4/151.0 (ammoniated: 564.4/151.0), $^{13}C_6$-DMQ_6 *m/z* 567.6/173.0 (ammoniated: 584.6/173.0), ^{12}C-DMQ_6 *m/z* 561.6/167.0 (ammoniated: 578.6/167.0), $^{13}C_6$-CoQ_6 *m/z* 597.4/203.1 (ammoniated: 614.4/203.1), ^{12}C-CoQ_6 *m/z* 591.4/197.1 (ammoniated: 608.4/197.1), and ^{12}C-CoQ_4 *m/z* 455.4/197.0 (ammoniated: 472.4/197.0).

Plate dilution assays

Strains were grown overnight in 5 ml of YPD and diluted to an A_{600} of 0.2 in sterile PBS. A 5-fold serial dilution in PBS was performed, after which 2 μl of each dilution (1×, 5×, 25×, 125×, and 625×) were spotted onto the designated carbon sources. The final A_{600} of the aforementioned dilution series are 0.2, 0.04, 0.008, 0.0016, and 0.00032, respectively.

PHYRE homology modeling

Phyre2 is a modeling program designed to analyze protein structure, function, and mutations (45). It is used to analyze the primary sequence of a protein and, with homology detection methods, constructs a structure that compares the protein of interest with other proteins (or motifs of proteins) with known structure. In regard to Ptc7, the full nonspliced version of the protein ($Ptc7_{ns}$), which is composed of 374 amino acids and retains its 31-amino acid intron (amino acids 19–50), was analyzed. The resulting structure and alignment coverage contained 86% of residues modeled at >90% confidence, with 14% of residues modeled *ab initio*. Additionally, the spliced isoform of Ptc7 ($Ptc7_s$), which is localized and processed in the mitochondria, comprised of 305 amino acids, resulting from the removal of the 31-amino acid intron and the excision of the predicted mitochondrial targeting sequence (the 38 N-terminal amino acids of $Ptc7_s$) (46), was also modeled using the PHYRE2 intensive modeling mode. The resulting structure and alignment coverage contains 85% of residues modeled at >90% confidence, with 15% of residues modeled *ab initio*.

Author contributions—A. M. A. and S. V. contributed equally to this work (both conducted the majority of the experiments, analyzed the results, and wrote the paper together). A. N. and M. C. B. assisted A. M. A. in conducting experiments; A. N. assisted A. M. A. in analyzing mass spectrometry results. A. R. G. and L. N. assisted S. V. in experiments, with A. R. G. also having assisted in the background research relating to PTC7 differential splicing in the snf2Δ strain shown in Fig. 1*A*. S. D. aligned the RNA-sequencing data and calculated splicing efficiencies. M. C. B. and L. N. thoroughly read and edited the working draft of the paper. C. F. C. and T. L. J. oversaw all details related to the project and provided guidance on experiments, data analysis, and the writing of this paper.

Acknowledgments—We thank Dr. James Bowie (UCLA) for advice and guidance in generating the PHYRE models and in the depiction of the spliced and nonspliced versions of Ptc7. We acknowledge the UCLA Molecular Instrumentation Core proteomics facility for the use of the QTRAP4000. We thank the laboratory of Dr. Ronald W. Davis (Stanford) for generously providing the Ptc7 spliced and nonspliced isoforms.

References

1. Naftelberg, S., Schor, I. E., Ast, G., and Kornblihtt, A. R. (2015) Regulation of alternative splicing through coupling with transcription and chromatin structure. *Annu. Rev. Biochem.* **84,** 165–198
2. Johnson, T. L., and Vilardell, J. (2012) Regulated pre-mRNA splicing: the ghostwriter of the eukaryotic genome. *Biochim. Biophys. Acta* **1819,** 538–545
3. Pleiss, J. A., Whitworth, G. B., Bergkessel, M., and Guthrie, C. (2007) Rapid, transcript-specific changes in splicing in response to environmental stress. *Mol. Cell* **27,** 928–937
4. Ares, M., Jr., Grate, L., and Pauling, M. H. (1999) An handful of intron-containing genes produces the lion's share of yeast mRNA. *RNA* **5,** 1138–1139
5. Munding, E. M., Shiue, L., Katzman, S., Donohue, J. P., and Ares, M., Jr. (2013) Competition between pre-mRNAs for the splicing machinery drives global regulation of splicing. *Mol. Cell* **51,** 338–348
6. Venkataramanan, S., Douglass, S., Galivanche, A. R., and Johnson, T. L. (2017) The chromatin remodeling complex Swi/Snf regulates splicing of meiotic transcripts in *Saccharomyces cerevisiae*. *Nucleic Acids Res.* 10.1093/nar/gkx373
7. Hossain, M. A., Claggett, J. M., Edwards, S. R., Shi, A., Pennebaker, S. L., Cheng, M. Y., Hasty, J., and Johnson, T. L. (2016) Posttranscriptional regulation of Gcr1 expression and activity is crucial for metabolic adjustment in response to glucose availability. *Mol. Cell* **62,** 346–358
8. Hossain, M. A., Rodriguez, C. M., and Johnson, T. L. (2011) Key features of the two-intron *Saccharomyces cerevisiae* gene *SUS1* contribute to its alternative splicing. *Nucleic Acids Res.* **39,** 8612–8627
9. Jiang, L., Whiteway, M., Ramos, C. W., Rodriguez-Medina, J. R., and Shen, S.-H. (2002) The YHR076W gene encodes a type 2C protein phosphatase and represents the seventh PP2C gene in budding yeast. *FEBS Lett.* **527,** 323–325
10. Juneau, K., Nislow, C., and Davis, R. W. (2009) Alternative splicing of *PTC7* in *Saccharomyces cerevisiae* determines protein localization. *Genetics* **183,** 185–194
11. Martín-Montalvo, A., González-Mariscal, I., Pomares-Viciana, T., Padilla-López, S., Ballesteros, M., Vazquez-Fonseca, L., Gandolfo, P., Brautigan, D. L., Navas, P., and Santos-Ocaña, C. (2013) The phosphatase Ptc7 induces coenzyme Q biosynthesis by activating the hydroxylase Coq7 in yeast. *J. Biol. Chem.* **288,** 28126–28137
12. Guo, X., Niemi, N. M., Hutchins, P. D., Condon, S. G., Jochem, A., Ulbrich, A., Higbee, A. J., Russell, J. D., Senes, A., Coon, J. J., and Pagliarini, D. J. (2017) Ptc7p dephosphorylates select mitochondrial proteins to enhance metabolic function. *Cell Rep.* **18,** 307–313

13. Turunen, M., Olsson, J., and Dallner, G. (2004) Metabolism and function of coenzyme Q. *Biochim. Biophys. Acta* **1660,** 171–199
14. Doimo, M., Desbats, M. A., Cerqua, C., Cassina, M., Trevisson, E., and Salviati, L. (2014) Genetics of coenzyme Q10 deficiency. *Mol. Syndromol.* **5,** 156–162
15. Quinzii, C. M., Emmanuele, V., and Hirano, M. (2014) Clinical presentations of coenzyme Q10 deficiency syndrome. *Mol. Syndromol.* **5,** 141–146
16. Tran, U. C., and Clarke, C. F. (2007) Endogenous synthesis of coenzyme Q in eukaryotes. *Mitochondrion* **7,** S62–S71
17. González-Mariscal, I., García-Testón, E., Padilla, S., Martín-Montalvo, A., Pomares Viciana, T., Vazquez-Fonseca, L., Gandolfo Domínguez, P., and Santos-Ocaña, C. (2014) The regulation of coenzyme Q biosynthesis in eukaryotic cells: all that yeast can tell us. *Mol. Syndromol.* **5,** 107–118
18. Allan, C. M., Awad, A. M., Johnson, J. S., Shirasaki, D. I., Wang, C., Blaby-Haas, C. E., Merchant, S. S., Loo, J. A., and Clarke, C. F. (2015) Identification of Coq11, a new coenzyme Q biosynthetic protein in the CoQ-synthome in *Saccharomyces cerevisiae*. *J. Biol. Chem.* **290,** 7517–7534
19. Padilla, S., Jonassen, T., Jiménez-Hidalgo, M. A., Fernández-Ayala, D. J., López-Lluch, G., Marbois, B., Navas, P., Clarke, C. F., and Santos-Ocaña, C. (2004) Demethoxy-Q, an intermediate of coenzyme Q biosynthesis, fails to support respiration in Saccharomyces cerevisiae and lacks antioxidant activity. *J. Biol. Chem.* **279,** 25995–26004
20. Padilla, S., Tran, U. C., Jiménez-Hidalgo, M., López-Martín, J. M., Martín-Montalvo, A., Clarke, C. F., Navas, P., and Santos-Ocaña, C. (2009) Hydroxylation of demethoxy-Q6 constitutes a control point in yeast coenzyme Q6 biosynthesis. *Cell Mol. Life Sci.* **66,** 173–186
21. Whitehouse, I., Flaus, A., Cairns, B. R., White, M. F., Workman, J. L., and Owen-Hughes, T. (1999) Nucleosome mobilization catalysed by the yeast SWI/SNF complex. *Nature* **400,** 784–787
22. Liu, X., Li, M., Xia, X., Li, X., and Chen, Z. (2017) Mechanism of chromatin remodelling revealed by the Snf2-nucleosome structure. *Nature* **544,** 440–445
23. Dutta, A., Gogol, M., Kim, J. H., Smolle, M., Venkatesh, S., Gilmore, J., Florens, L., Washburn, M. P., and Workman, J. L. (2014) Swi/Snf dynamics on stress-responsive genes is governed by competitive bromodomain interactions. *Genes Dev.* **28,** 2314–2330
24. Dutta, A., Sardiu, M., Gogol, M., Gilmore, J., Zhang, D., Florens, L., Abmayr, S. M., Washburn, M. P., and Workman, J. L. (2017) Composition and function of mutant Swi/Snf complexes. *Cell Rep.* **18,** 2124–2134
25. Gabunilas, J., and Chanfreau, G. (2016) Splicing-mediated autoregulation modulates Rpl22p expression in *Saccharomyces cerevisiae*. *PLoS Genet.* **12,** e1005999
26. Neigeborn, L., and Carlson, M. (1984) Genes affecting the regulation of SUC2 gene expression by glucose repression in *Saccharomyces cerevisiae*. *Genetics* **108,** 845–858
27. Martín-Montalvo, A., González-Mariscal, I., Padilla, S., Ballesteros, M., Brautigan, D. L., Navas, P., and Santos-Ocaña, C. (2011) Respiratory-induced coenzyme Q biosynthesis is regulated by a phosphorylation cycle of Cat5p/Coq7p. *Biochem. J.* **440,** 107–114
28. Martin, D. E., Soulard, A., and Hall, M. N. (2004) TOR regulates ribosomal protein gene expression via PKA and the Forkhead transcription factor FHL1. *Cell* **119,** 969–979
29. Wang, A., Mouser, J., Pitt, J., Promislow, D., and Kaeberlein, M. (2016) Rapamycin enhances survival in a *Drosophila* model of mitochondrial disease. *Oncotarget* **7,** 80131–80139
30. González-Mariscal, I., Martín-Montalvo, A., Ojeda-González, C., Rodríguez-Eguren, A., Gutiérrez-Rios, P., Navas, P., and Santos-Ocaña, C. (2017) Balanced CoQ6 biosynthesis is required for lifespan and mitophagy in yeast. *Microb. Cell* **4,** 38–51
31. Sharmin, D., Sasano, Y., Sugiyama, M., and Harashima, S. (2014) Effects of deletion of different PP2C protein phosphatase genes on stress responses in *Saccharomyces cerevisiae*. *Yeast* **31,** 393–409
32. Marshall, A. N., Montealegre, M. C., Jiménez-Lopez, C., Lorenz, M. C., and van Hoof, A. (2013) Alternative splicing and subfunctionalization generates functional diversity in fungal proteomes. *PLoS Genet.* **9,** e1003376
33. Boukouris, A. E., Zervopoulos, S. D., and Michelakis, E. D. (2016) Metabolic enzymes moonlighting in the nucleus: metabolic regulation of gene transcription. *Trends Biochem. Sci.* **41,** 712–730
34. De, P., and Chatterjee, R. (1962) Evidence of nucleolar succinic dehydrogenase activity. *Exp. Cell Res.* **27,** 172–173
35. De, P., and Chatterjee, R. (1962) Nucleolar localization of succinic dehydrogenase in human malignant cells with MTT. *Experientia* **18,** 562
36. Yogev, O., Yogev, O., Singer, E., Shaulian, E., Goldberg, M., Fox, T. D., and Pines, O. (2010) Fumarase: a mitochondrial metabolic enzyme and a cytosolic/nuclear component of the DNA damage response. *PLoS Biol.* **8,** e1000328
37. Jung, S. J., Seo, Y., Lee, K. C., Lee, D., and Roe, J. H. (2015) Essential function of Aco2, a fusion protein of aconitase and mitochondrial ribosomal protein bL21, in mitochondrial translation in fission yeast. *FEBS Lett.* **589,** 822–828
38. Lee, S. M., Kim, J. H., Cho, E. J., and Youn, H. D. (2009) A nucleocytoplasmic malate dehydrogenase regulates p53 transcriptional activity in response to metabolic stress. *Cell Death Differ.* **16,** 738–748
39. McEwen, B. S., Allfrey, V. G., and Mirsky, A. E. (1963) Studies on energy-yielding reactions in thymus nuclei. *J. Biol. Chem.* **238,** 2571–2578
40. Monaghan, R. M., Barnes, R. G., Fisher, K., Andreou, T., Rooney, N., Poulin, G. B., and Whitmarsh, A. J. (2015) A nuclear role for the respiratory enzyme CLK-1 in regulating mitochondrial stress responses and longevity. *Nat Cell Biol.* **17,** 782–792
41. Liu, J. L., Yee, C., Wang, Y., and Hekimi, S. (2017) A single biochemical activity underlies the pleiotropy of the aging-related protein CLK-1. *Sci. Rep.* **7,** 859
42. Grate, L., and Ares, M., Jr. (2002) Searching yeast intron data at Ares lab Web site. *Methods Enzymol.* **350,** 380–392
43. Dobin, A., Davis, C. A., Schlesinger, F., Drenkow, J., Zaleski, C., Jha, S., Batut, P., Chaisson, M., and Gingeras, T. R. (2013) STAR: ultrafast universal RNA-seq aligner. *Bioinformatics* **29,** 15–21
44. Livak, K. J., and Schmittgen, T. D. (2001) Analysis of relative gene expression data using real-time quantitative PCR and the $2(-\Delta\Delta C(T))$ method. *Methods* **25,** 402–408
45. Kelley, L. A., Mezulis, S., Yates, C. M., Wass, M. N., and Sternberg, M. J. (2015) The Phyre2 web portal for protein modeling, prediction and analysis. *Nat. Protoc.* **10,** 845–858
46. Vögtle, F. N., Wortelkamp, S., Zahedi, R. P., Becker, D., Leidhold, C., Gevaert, K., Kellermann, J., Voos, W., Sickmann, A., Pfanner, N., and Meisinger, C. (2009) Global analysis of the mitochondrial N-proteome identifies a processing peptidase critical for protein stability. *Cell* **139,** 428–439
47. Ashby, M. N., Kutsunai, S. Y., Ackerman, S., Tzagoloff, A., and Edwards, P. A. (1992) COQ2 is a candidate for the structural gene encoding para-hydroxybenzoate:polyprenyltransferase. *J. Biol. Chem.* **267,** 4128–4136
48. Winzeler, E. A., Shoemaker, D. D., Astromoff, A., Liang, H., Anderson, K., Andre, B., Bangham, R., Benito, R., Boeke, J. D., Bussey, H., Chu, A. M., Connelly, C., Davis, K., Dietrich, F., Dow, S. W., *et al.* (1999) Functional characterization of the *S. cerevisiae* genome by gene deletion and parallel analysis. *Science* **285,** 901–906

CHAPTER 6

Potential roles/functions of $Ptc7_{NS}$ in *Saccharomyces cerevisiae.*

Introduction

Despite the relative paucity of introns within the *Saccharomyces cerevisiae* genome, there are important examples of alternative splicing (described in Chapter 1). Such alternative splicing serves to expand the repertoire of the yeast proteome. One example of alternative splicing in yeast is *PTC7*, which encodes for an intron-containing transcript with non-consensus branch point sequence (GACUAAC) (Awad et al., 2017).

The spliced form of the *PTC7* transcript encodes a PP2C type phosphatase ($Ptc7_S$) that localizes to the mitochondria and has been demonstrated to dephosphorylate Coq7, in addition to other potential roles in mitochondrial metabolism Ptc7 (Guo et al., 2017, Martin-Montalvo et al., 2013, Juneau et al., 2009). Coq7 is a hydroxylase that catalyzes the conversion of 5-demethoxy Q_6 (DMQ_6) to 5-demethyl Q_6 in the penultimate step within the biosynthetic pathway for Coenzyme Q_6 (CoQ_6) (Martin-Montalvo et al., 2011, Padilla et al., 2009, Tran et al., 2006). CoQ_6 is the yeast form of Coenzyme Q (CoQ - with 6 prenyl units; whereas humans have 10), a redox-active lipid whose primary function is to shuttle electrons from Complex I and Complex II to Complex III within the inner mitochondrial membrane (Tran and Clarke, 2007).

Intriguingly, the intron within the *PTC7* transcript lacks a premature termination codon and is 93 nucleotides long (divisible by 3), such that it can be translated in frame with the rest of the transcript and produce a longer protein product (Juneau et al., 2009). The existence of this protein ($Ptc7_{NS}$) has previously been demonstrated by us and others, and it has been reported to localize to the nuclear membrane, due to the intron encoding for a single trans-membrane helix located close to the N-terminus of the protein (Awad et al., 2017, Juneau et al., 2009). Interestingly, the read through nature of the intron is conserved across most *Saccharomycetaceae* species (Marshall et al., 2013, Juneau et al., 2009). The exception is *Tetrapisispora blattae,* a

close relative of *Saccharomyces cerevisiae* that only diverged after the ancestral whole genome duplication (WGD) event roughly 100 million years ago (Kellis et al., 2004, OhEigeartaigh et al., 2011). While *S. cerevisiae* lost one copy of the *PTC7* gene, *T. blattae* retained both copies, but each lost the functional capacity to encode two protein isoforms. Instead, one copy of the *PTC7* gene in *T. blattae* codes for a mitochondrial PP2C (Ptc7b), and the other, a nuclear envelope localized one (Ptc7a) (Marshall et al., 2013). The conservation of two *PTC7* PP2C type phosphatases in all of the examined *Saccharomycetaceae* species strongly suggests that both isoforms are functional and important for cellular fitness. While the role of the mitochondrial $Ptc7_S$ has previously been described, no function for the nuclear membrane localized $Ptc7_{NS}$ has as yet been elucidated.

We have recently shown that the SWI/SNF complex regulates the splicing of the PTC7 transcript in *S. cerevisiae*, by modulating competition for the limiting spliceosome (Awad et al., 2017). The splicing of the *PTC7* transcript improves in a SWI/SNF dependent manner upon depletion of nutrients in the surrounding media (Awad et al., 2017). We also showed that the relative ratio of the two Ptc7 isoforms changes in a Snf2 dependent manner, and that $Ptc7_{NS}$ has a repressive effect on the biosynthesis of CoQ_6 (Awad et al., 2017). Exclusive expression of $Ptc7_{NS}$ downregulates the entire CoQ_6 biosynthetic pathway, likely due to downregulation of all the components of the biosynthetic complex at the RNA level (Awad et al., 2017). However, the mechanism of this downregulation remains unknown. Here we identify potential targets for $Ptc7_{NS}$ and extend our analysis of the function of Ptc7 isoforms potentially beyond their roles in respiration, as the two proteins and their functional interaction influence the cellular response to osmotic stress.

Results

Phosphoproteomic analysis suggests that $Ptc7_{NS}$ may dephosphorylate numerous nuclear proteins: In order to elucidate the mechanism of downregulation of the CoQ synthome by $Ptc7_{NS,}$ we looked for potential nuclear targets of its phosphatase activity. Interestingly, the catalytic phosphatase domain of $Ptc7_{NS}$ is uninterrupted by the intronic transmembrane helix and remains intact and potentially active (Awad et al., 2017). The phosphatase domain has been predicted to be cytoplasmic-facing using *in silico* methods (Juneau et al., 2009). However, this remains yet to be experimentally confirmed.

A recent study identified with high confidence ($p<0.01$) numerous differentially phosphorylated proteins in a *ptc7*Δ strain (Guo et al., 2017). Notably, this proteomic analysis does not distinguish between the potential effects of the two Ptc7 isoforms globally. In fact, rescue experiments using plasmid-based expression of *PTC7* (full length) does not restore dephosphorylation levels in a significant number of nuclear proteins (two clusters indicated by black boxes in **Figure 6.1A**). In contrast, analysis of mitochondrial proteins using similar parameters showed that the increased phosphorylation shown by mitochondrial proteins upon deletion of *PTC7* is almost completely reversed by exogenous expression of Ptc7 (**Figure 6.1B**). This discrepancy suggests that nuclear protein phosphorylation may be particularly sensitive to features of Ptc7 expression that are unique to the endogenous context. For example, the plasmid-based expression of Ptc7 isoforms may not recapitulate the endogenous levels of *PTC7* unspliced RNA and/or spliced vs. unspliced ratios precisely. This leads us to hypothesize that nuclear proteins whose phosphorylation fails to decrease upon plasmid-based rescue (or decreases only slightly), might be potential targets for the nuclear membrane localized $Ptc7_{NS}$. In light of the surprisingly large number of nuclear proteins that show a change in phosphorylation in the

absence of Ptc7, we cannot rule out indirect effects. However, a closer examination of the data reveals a number of interesting functional classes of proteins. One intriguing category includes transcriptional regulators, including transcription factors such as Mig1, Xbp1, Ume6 and Gat1; chromatin remodelers like Swi5 and chromatin modifiers like Snt1 and Set3 (both members of the Set3C meiotic repressor complex). A second category is a group of proteins involved in nucleo-cytoplasmic transport. Interestingly, Nup1 and Nup60, the only two nucleoporins restricted to the nuclear face of the pore complex (Rout et al., 2000), both show increase in phosphorylation upon deletion of *PTC7* (indicated by red arrows in **Figure 6.1A**), without significant change upon plasmid rescue. This suggests that Nup1 and Nup60 could be potential targets for the activity of $Ptc7_{NS}$, perhaps suggesting that the catalytic phosphatase domain of $Ptc7_{NS}$ is likely faced towards the nucleoplasm. Intriguingly, a recent study has shown a functional connection between regulation of the nuclear pore complex and mitochondrial function in yeast (Lord et al., 2015). Hence, along with a potential role for $Ptc7_{NS}$ in regulation of nucleo-cytoplasmic transport, it may indirectly affect mitochondrial function. $Ptc7_{ns}$ also appears to affect phosphorylation of Src1, a component of the TREX complex, which associates with the inner nuclear membrane (Grund et al., 2008) (**Figure 6.1A**). The magnitude of the changes in phosphorylation of nuclear proteins appear to be less than that observed with mitochondrial proteins (**Figure 6.1**), which is not unsurprising, given that the predominant protein isoform in yeast cells is $Ptc7_s$ (Awad et al., 2017). It should also be noted that the phosphorylation of proteins within the particular functional classes discussed above show varying degrees of responsiveness to the deletion of Ptc7, and are not always the most strongly affected. However, the functional clustering of these proteins is likely to amplify the effects of changing phosphorylation via co-regulation by Ptc7, making the pathways they are involved in interesting

candidates for further study. Although indirect effects on phosphorylation cannot be ruled out, these analyses raise the provocative idea that $Ptc7_{NS}$ may actively dephosphorylate some nuclear protein or proteins. Proteomic studies with $Ptc7_{NS}$ are underway to identify direct targets of its activity.

Ptc7 isoforms are involved in the response to osmotic stress: Despite the opposing effects of Ptc7 isoforms of the biosynthesis of CoQ_6 (Awad et al., 2017), neither exclusive expression of either Ptc7 isoform, nor the absence of either isoform (*ptc7*Δ) results in a growth defect for yeast on either fermentable or non-fermentable carbon sources (**Figure 6.2A**). This result, while surprising, is nevertheless consistent with our prior observations that ~1-10% of CoQ_6 levels are sufficient for comparable growth under unstressed conditions in a phenotypic assay. One possible explanation for the residual CoQ_6 levels in the absence of $Ptc7_S$ is due to redundancies that exist between Ptc7 and other PP2C type phosphatases, such as Ptc5 and/or Ptc6. In fact, the *ptc5*Δ*ptc7*Δ double null mutant has impaired growth under conditions of temperature stress (Martin-Montalvo et al., 2013, Sharmin et al., 2014). Furthermore, as previously shown, the expression of either Ptc7 isoform exclusively, or neither isoform, shows no change in the ratio of conversion from precursors to CoQ_6 **(Figure 6.2B-E**).

Potential targets of $Ptc7_{NS}$ phosphatase activity identified in the previous segment provided clues regarding the function of the nuclear isoform of Ptc7 with respect to gene regulation that may extend its role beyond that in respiration, and hint at the need to look at other pathways it may be involved in. In addition to numerous transcription factors, components of the nuclear basket, Nup1 and Nup60 are candidates for targets of $Ptc7_{NS}$. Interestingly, components of the nuclear pore complex, and specifically the nuclear basket have been implicated in numerous steps of gene regulation in *S. cerevisiae* (reviewed in (Raices and D'Angelo, 2017)).

Upon transcriptional activation, numerous stress response genes localize to the nuclear periphery via their association with nucleoporins (Casolari et al., 2004, Cabal et al., 2006, Schmid et al., 2006, Taddei et al., 2006, Luthra et al., 2007, Brickner et al., 2007, Brickner and Walter, 2004, Ahmed et al., 2010, Menon et al., 2005, Casolari et al., 2005). It has been suggested that this association is required both for the transcription as well as export of the mRNAs synthesized from these genes, as well as transcriptional 'memory'. This NPC dependent regulation has been shown to be regulated by the SAGA and TREX complexes, Moreover, several components of the SAGA and TREX complexes are also potential targets for $Ptc7_{NS}$ (**Figure 6.1**). Additionally, the persistence of nucleoporin dependent transcriptional 'memory' (poising) of certain inducible genes like *INO1* and certain *GAL* genes has also been shown to be dependent on the Set3C, another putative target for $Ptc7_{NS}$ (Brickner et al., 2007, D'Urso et al., 2016).

In the case of response to osmotic stress, the transcription and export of stress response genes is dependent on the phosphorylation of the components of the nuclear basket (Nup1, Nup2 and Nup60) by the Hog1 stress-activated protein kinase (Regot et al., 2013). Since nucleoporins are not turned over for multiple generations, they are amongst the longest-lived proteins in the cell (Toyama et al., 2013), Changes in the phosphorylation state of these proteins may modulate their activity in response to stress conditions. In order to test this, we analyzed whether the presence of Ptc7 isoforms affected the cellular response to or recovery from osmotic stress. We performed growth assays of yeast expressing both Ptc7 isofoms ($Ptc7_G$), or only the spliced or unspliced isoforms ($Ptc7_S$ or $Ptc7_{NS}$), or neither (*ptc7Δ*), previously grown in liquid YPD (with no additional salt) onto plates that contain either no additional salt (YPD only), 1M NaCl or 0.5M LiCl. We also plated cells grown up in liquid media containing 1M NaCl onto YPD plates to monitor their recovery from osmostress. To our surprise, the strain expressing neither Ptc7

isoform (*ptc7Δ*) shows a moderate improvement in growth on 1M NaCl, and a striking increase on 0.5M LiCl **(Figure 6.3A)** even though the strains grown in YPD + 1M NaCl did not show any differences in recovery on plates regardless of the Ptc7 isoforms expressed (**Figure 6.3B**).

Transcript levels of selected candidate genes involved in resistance to LiCl stress do not vary in strains expressing exclusively one Ptc7 isoform: To elucidate the mechanism by which the deletion of both isoforms of Ptc7 results in the striking increase in tolerance to LiCl, we assayed the expression of candidate genes whose deletion or overexpression has been annotated to result in a comparable phenotype (*Saccharomyces* Genome Database). This diverse cohort includes *BCH2* and *CHS6*, parts of the exomer complex which transports certain proteins from the golgi to the plasma membrane (Rockenbauch et al., 2012); *FPR1*, a peptidyl prolyl cis-trans isomerase (Cardenas et al., 1994); kinases *HAL5* and *SAT4* (Mulet et al., 1999); inositol monophosphatases *INM1* and *INM2* ((Lopez et al., 1999); a yeast PTEN homolog, *TEP1* (Heymont et al., 2000); and a chromatin associate cell cycle regulator, *POG1* (Sasano et al., 2013). We measured the expression of these genes over 2 hours of growth in YPD + 0.25M LiCl (this is the highest experimental concentration of LiCl in liquid culture to still support growth). With the exception of a modest increase in *FPR1* expression, none of the other genes show a statistically significant change in expression in the *ptc7Δ* strain compared to the others after 2 hours of exposure to LiCl containing media **(Figure 6.4)**. Moreover, since a deletion of *FPR1* was previously shown to confer increased resistance to LiCl in yeast, the result is contradictory (Cardenas et al., 1994). However, this experiment measures only the total transcript level of each assayed gene within the yeast cell. As previously discussed, Ptc7 isoforms could potentially affect both the transcription and export of target genes, potentially via NPC phosphorylation. Any defect in the export of the assayed transcripts cannot be detected by the experimental setup

described above. Interestingly, a number of the assayed genes show a pattern of increased expression in the $Ptc7_S$ strain compared to the others at most or all time points assayed **(Figure 6.4)**. Since the $Ptc7_S$ strain demonstrates no change in growth on salt containing media from the WT, the significance of this pattern of upregulation is as yet unknown, but could provide further insight into the distinct functions of the two Ptc7 isoforms. However, the genes assayed in this experiment are by no means an exhaustive list of genes involved in the response to osmotic stress. Further experiments to more comprehensively characterize the gene expression profiles in strains expressing Ptc7 isoforms are underway and are described in later sections.

***PTC7* expression doesn't vary in LiCl stress:** Since the simultaneous absence of both Ptc7 isoforms confers increased resistance to LiCl, we examined RNA levels from the *PTC7* gene over 2 hours of growth in YPD + 0.25M LiCl. No isoform dependent changes in the expression of total *PTC7* was observed upon exposure to LiCl, although the strain expressing only the spliced isoform of Ptc7 ($Ptc7_S$) showed higher basal expression of *PTC7* **(Figure 6.5)**.

$Ptc7_{NS}$ represses increase in CoQ_6 biosynthesis upon LiCl stress: We hypothesized that the epistatic interaction observed between the two Ptc7 isoforms upon exposure to LiCl stress is due to their roles in CoQ_6 biosynthesis. In order to test this, we treated yeast cells with 0.1M LiCl and measured the synthesis of CoQ_6, as well as intermediates of the pathway DMQ_6 and HHB, in strains expressing both *PTC7* isoforms ($PTC7_G$), spliced isoform only ($PTC7_S$), unspliced isoform only ($PTC7_{NS}$) or neither isoform (*ptc7*Δ). $Ptc7_S$ promotes the conversion of DMQ_6 to CoQ_6, whereas $Ptc7_{NS}$ globally downregulates the entire pathway. We observed that strains lacking $Ptc7_{NS}$ ($PTC7_S$ and *ptc7*Δ) showed an increase in CoQ_6 synthesis upon LiCl treatment, while strains with $Ptc7_{NS}$ ($PTC7_G$ and $PTC7_{NS}$) do not demonstrate the same increase **(Figure 6.6A)**. Interestingly, the same strains also show an increase in DMQ_6 levels, but not in

HHB levels, indicating that the mechanism by which $Ptc7_{NS}$ represses increased CoQ_6 biosynthesis acts between the early precursor HHB and DMQ_6. The exact nature of this mechanism remains unknown, and is the subject of ongoing investigation.

Discussion

We have previously described distinct and opposing roles in Coenzyme Q biosynthesis for the two isoforms of Ptc7 derived from the spliced and unspliced isoforms of the *PTC7* transcript (Awad et al., 2017). While $Ptc7_S$ has previously been shown to dephosphorylate Coq7, permitting it to associate with the rest of the CoQ synthome on the mitochondrial membrane (Martin-Montalvo et al., 2013, Martin-Montalvo et al., 2011); the molecular function of $Ptc7_{NS}$ remains unknown. Here we identify potential nuclear targets for the phosphatase activity of $Ptc7_{NS}$ **(Figure 6.1)**, and demonstrate a novel epistatic interaction between the two isoforms of Ptc7 under conditions of severe osmotic stress **(Figure 6.3)**.

Crosstalk between nuclear and mitochondrial proteins has been described previously (Boukouris et al., 2016), and several mitochondrial enzymes have been described to play important roles in gene regulation (De and Chatterjee, 1962a, De and Chatterjee, 1962b, Yogev et al., 2010, Jung et al., 2015, Lee et al., 2009). However, to the best of our knowledge, this is the first described instance of a functional interaction between two differentially localized splice isoforms in *Saccharomyces cerevisiae*. Nevertheless, the nature of the functional interaction between $Ptc7_S$ and $Ptc7_{NS}$ that confers resistance to LiCl stress when both isoforms are absent, remain unknown. It also remains to be determined whether the roles of the Ptc7 isoforms in osmotolerance are distinct from their role in cellular respiration via regulation of CoQ_6 biosynthesis. Recent work has demonstrated that the prevalent metabolic mode of *S. cerevisiae*

informs the nature of the cellular response to osmostress (Babazadeh et al., 2017). When yeast are grown on a non-fermentable carbon source such as ethanol, the primary intracellular osmoprotectant utilized is trehalose, as opposed to glycerol, which is principally used when growing on a fermentable carbon source (Babazadeh et al., 2017). It has also been hypothesized that disruption of the redox balance within yeast cells renders them susceptible to osmostress. Since Coenzyme Q is a redox-active lipid with functions in multiple cellular biosynthetic pathways (Turunen et al., 2004), it is conceivable that disruption of CoQ_6 metabolism in the absence of Ptc7 isoforms is indirectly responsible for the altered osmotolerance observed **(Figure 6.3)**, via as-yet-unknown mechanisms.

We have also previously shown that exclusive expression of $Ptc7_{NS}$ downregulates the mRNA levels of the components of the CoQ_6 synthome (Awad et al., 2017). It is unclear whether the mechanism of downregulation is transcriptional or post-transcriptional. One possibility is that $Ptc7_{NS}$ directly associates with and represses membrane-associated genes of the CoQ synthome. Although membrane association is typically associated with activation and increased transcription of genes in *S. cerevisiae*, relocation to the nuclear periphery has also been shown to cause gene repression under specific conditions (Green et al., 2012). The previously described nuclear localization of CLK-1 and COQ7, the respective *C. elegans* and human homologs of Coq7, raises another intriguing possible mechanism of transcriptional regulation by $Ptc7_{NS}$ (Monaghan et al., 2015, Liu et al., 2017). Coq7 is a previously described mitochondrial target of $Ptc7_S$ (Martin-Montalvo et al., 2013), and the human homolog has been shown to directly associate with chromatin and possibly act as a transcription factor, albeit of unknown function (Monaghan et al., 2015). Potential $Ptc7_{NS}$ dependent dephosphorylation of the nucleoporins **(Figure 6.1)** could also influence transcription of CoQ synthome mRNAs. Further, $Ptc7_{NS}$

potentially dephosphorylates numerous components of the TREX complex, which could inhibit the trafficking of the mRNAs into the cytoplasm, and cause degradation by nuclear factors. Post transcriptional control of the CoQ synthome by an RNA binding protein has previously been described (Lapointe et al., 2017).

Future Directions: The function of the $Ptc7_{NS}$ isoform and the nature of the epistatic interactions between the two Ptc7 isoforms under osmostic stress remain outstanding, as yet unanswered questions. To gain a better understanding of the role of $Ptc7_{NS}$, it is crucial to draw a comprehensive picture of its direct and indirect effects on gene expression. Measurement of global transcript levels in all of the various isoform strains of Ptc7 in the presence or absence of osmotic tress, combined with a map of potential genomic association sites of $Ptc7_{NS}$ will go a long way towards parsing out the direct roles of $Ptc7_{NS}$ on gene expression. Experiments to generate these datasets using total RNA sequencing as well as ChIP-seq are currently underway. To further understand the mechanisms by which $Ptc7_{NS}$ effects the gene expression changes, it is crucial to identify, with high confidence, changes in the yeast phosphoproteome attributable to the enzymatic activity of $Ptc7_{NS}$. Mass-spectrometry experiments with each of the strains described in **Table 6.1** are in progress to determine the targets of $Ptc7_{NS}$ phosphatase activity. We hope that the combination of targets of $Ptc7_{NS}$ enzymatic activity, coupled with its genomic localization and its effects on gene expression will facilitate greater insight into the role of this conserved fungal protein in CoQ_6 biosynthesis and other cellular processes.

Overall, the work described in this chapter has demonstrated that the protein products of alternative splicing play a functional role in *Saccharomyces cerevisiae*. While the molecular mechanism of $Ptc7_{NS}$ action remains unknown, it clearly has profound phenotypic effects on the yeast cell.

Materials and Methods

Yeast strains and culture conditions: The yeast strains used in this study are listed in Table 6.1. All strains are derived from the BY background. Yeast strains were grown in YPD (1% yeast extract, 2% peptone, 2% dextrose) medium at 30 °C. The generation of the strains has been described previously (Awad et al., 2017).

TABLE 6.1: Genotype and Source of Yeast Strains

Strain Number	Name	Genotype	Source or reference
TJY7114	*PTC7$_g$HA*	*MATa his3Δ leu2Δ ura3Δ PTC7$_g$HA:KanMX*	(Awad et al., 2017)
TJY7116	*PTC7$_s$HA*	*MATa his3Δ leu2Δ ura3Δ PTC7$_s$HA:KanMX*	(Awad et al., 2017)
TJY7118	*PTC7$_{ns}$HA*	*MATa his3Δ leu2Δ ura3Δ PTC7$_{ns}$HA:KanMX*	(Awad et al., 2017)
TJY7142	*ptc7Δ*	*MATa his3Δ leu2Δ ura3Δ ptc7Δ:KanMX*	(Awad et al., 2017)

Phosphoproteome heat map: Phosphoproteome data from Guo et al. were filtered to identify proteins with significantly different phospho-isoforms ($p<0.01$) between *ptc7Δ* and *WT* yeast, and the normalized phospho-isoform abundance was represented for WT, *ptc7Δ* and *ptc7Δ+PTC7(URA)* (Guo et al., 2017). Heat maps with hierarchical clustering of changes in phospho-isoform abundance were plotted using the *gplots* package in R. In the case of multiple phosphorylated peptides from a single protein, only the peptide with the highest confidence (lowest p-value) was considered. Nuclear (nuclear periphery, nucleus or nucleolus) or mitochondrial localization was defined as positive localization to respective compartments as in (Huh et al., 2003).

Plate Dilution Assays: Strains were grown overnight in 5 mL of YPD with or without indicated salt concentrations and diluted to an A_{600} of 0.2 in YPD. A 5-fold serial dilution in YPD was performed, after which 5 µL of each dilution were spotted onto the designated plates.

Real time PCR analysis: RNA was isolated from a 10 ml aliquot of cell culture corresponding to strains and time points described in each experiment. After DNase treatment (Williams et al.), equal quantities of total RNA from each sample were used to make cDNA using cDNA synthesis kit (Fermentas). qRT-PCR was done in a 10 µl reaction volume with gene specific primers using 1 µl of cDNA diluted 1:20 using Perfecta Sybr Green Fastmix (Quanta Biosciences) and a CFX96 Touch System (BioRad). All samples were analyzed in triplicate for each independent experiment. qRT-PCR was also performed for the *scR1* RNA from each cDNA sample. Gene expression analysis was done by 2-ΔCt methods using *scR1* cytoplasmic RNA as reference. Primers for each gene assayed are listed in Table 6.2. Fold-expression of mRNA was measured compared to WT by 2-ΔΔCt methods (Livak and Schmittgen, 2001)

TABLE 6.2 Real-time PCR primers

Gene Name	Forward primer (5' to 3' sequence)	Reverse primer (5' to 3' sequence)
sCR1	TTTCTGGTGGGATGGGATAC	TTTACGACGGAGGAAAGACG
BCH2	CAAAGAGCGTCTATGCAACG	ACGGGTCATTCGTCATCAAG
CHS6	TGGTGGCGATTATACACCTG	TGGTGGCGATTATACACCTG
FPR1	AGTCATCAAGGGTTGGGATG	GGAATCAAACCTGGGAAACC
HAl5	GCGATGATGGTGACAATGAC	CTTCTTGTTGCTGCTGTTGC
INM1	GTTATTGGGATGGTGGTTGC	CCTCACAGCCAAATATGTCC

INM2	TGTTCACGGGTTCAGAAGTG	CCACCTTCCCAATAAGCATC
POG1	GATAAACGCCTCCGAACTTG	AAGTATATGCGCCTGGTTGC
SAT4	TTACTGCTTACGCACGATGG	TATATTCCTCTGGGGCGATG
TEP1	CGCCCATCAAGCTTAATCAC	GGAGGGCATTTCTATCATCG

Analysis of CoQ_6 and CoQ_6 intermediates: Lipid extraction of cell pellets was conducted as described (Allan et al., 2015) with methanol and petroleum ether and CoQ_4 as the internal standard. Lipid measurements were performed by HPLC-MS/MS and normalized to total OD. Prior to mass spectrometry analysis, all samples were treated with 1.0 mg/mL benzoquinone to oxidize hydroquinones to quinones. Mass spectrometry analyses utilized a 4000 QTRAP linear MS/MS spectrometer (Applied Biosystems), and data were acquired and analyzed using Analyst versions 1.4.2 and 1.5.2 software (Applied Biosystems). Separation of lipid quinones was performed with a binary HPLC delivery system and a Luna 5µ phenyl-hexyl column (100 × 4.6 mm, 5 µm, Phenomenex). The mobile phase consisted of a 95:5 methanol:isopropanol solution, with 2.5 mM ammonium formate as Solution A and a 100% isopropanol solution, with 2.5 mM ammonium formate as Solution B. The percent of Solution B was increased linearly from 0 to 5% over 6 min, whereby the flow rate was increased from 600 µL to 800 µL. Initial flow rate and mobile phase conditions were changed back to initial phase conditions linearly over 3.5 min. Each sample was analyzed using multiple reaction monitoring (MRM) mode. The following precursor to product ion transitions were detected, as well as the +17 *m/z* ammoniated adducts for each of the metabolic products: ^{12}C-HHB *m/z* 547.4/151.0 (ammoniated: 564.4/151.0), ^{12}C-DMQ_6 *m/z* 561.6/167.0 (ammoniated: 578.6/167.0), ^{12}C-CoQ_6

m/z 591.4/197.1 (ammoniated: 608.4/197.1), and ^{12}C-CoQ_4 *m/z* 455.4/197.0 (ammoniated: 472.4/197.0).

Acknowledgements

The work in this chapter was performed in collaboration with Agape Awad and Dr. Catherine Clarke. I am grateful for their continued intellectual and experimental support.

Figures

Figure 6.1

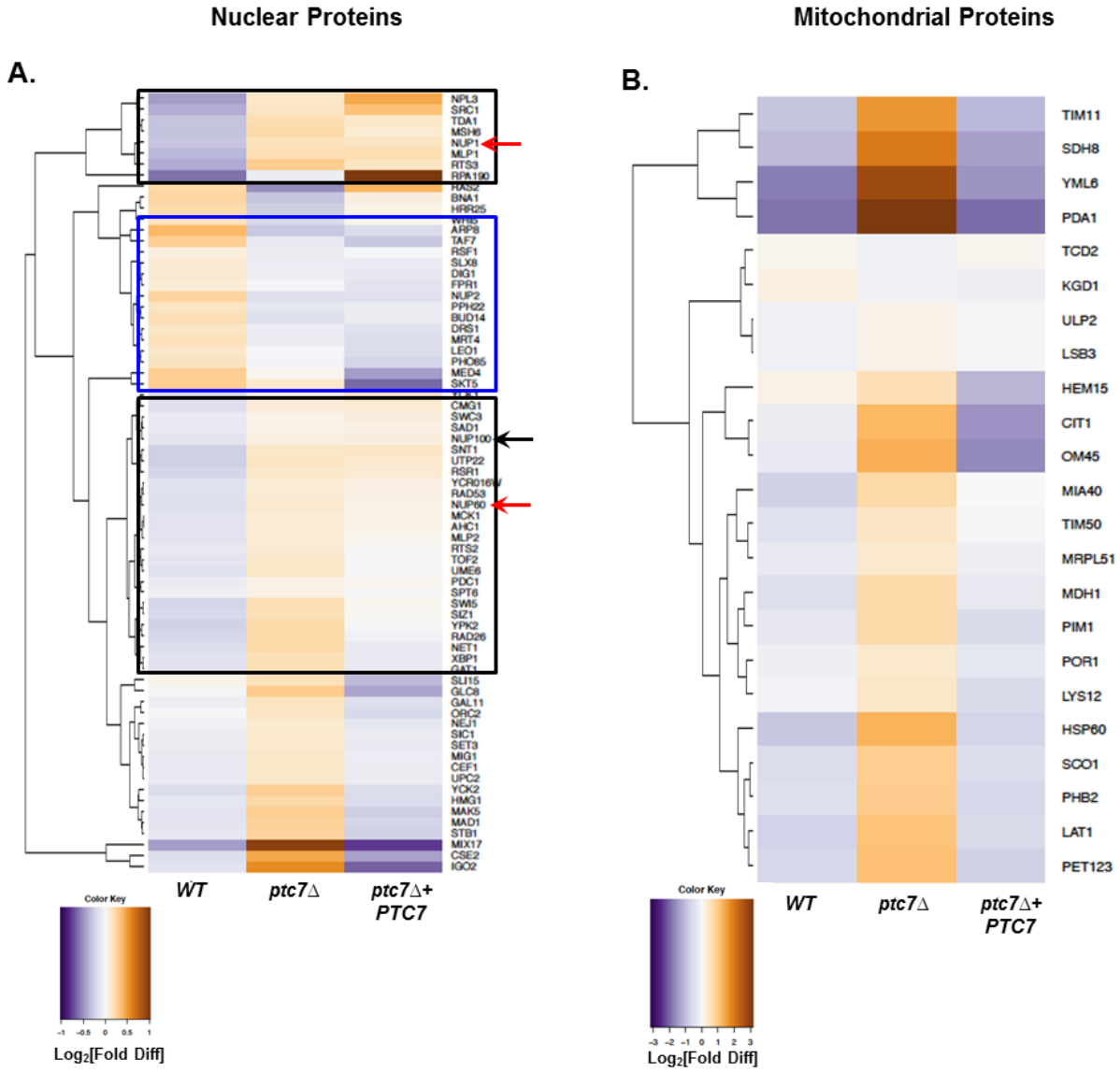

Figure 6.1: Potential nuclear roles for Ptc7$_{ns}$.

A. Heat map with hierarchical clustering of changes in phospho-isoform abundance in

nuclear proteins in ptc7Δ compared to WT and upon putative restoration of Ptc7. Nuclear proteins with significantly different phospho-isoforms ($p<0.01$) between *ptc7*Δ and WT were identified; and the normalized phospho-isoform abundance was represented for WT, *ptc7*Δ and *ptc7*Δ+*PTC7*. Proteins whose phosphorylation increase in *ptc7*Δ but are not restored to levels comparable to WT upon expression of Ptc7 are indicated by the two black boxes. Proteins whose phosphorylation decreases upon deletion of *PTC7* but is not restored to levels comparable to WT upon rescue are indicated by the blue box. Two exclusively nuclear-facing nucleoporins are indicated with red arrows. Another nucleoporin with nucleo-cytoplasmic distribution is indicated with a black arrow. Analysis of supplementary data from (Guo et al., 2017). In the case of multiple phosphorylated peptides from a single protein, only the peptide with highest confidence (lowest p-value) was considered. Nuclear localization was defined as positive localization to nuclear periphery, nucleus or nucleolus as in (Huh et al., 2003).

B. Heat map with hierarchical clustering of changes in phospho-isoform abundance in mitochondrial proteins in *ptc7*Δ compared to *WT* and upon putative restoration of Ptc7. Mitochondrial proteins with significantly different phospho-isoforms ($p<0.01$) between *ptc7*Δ and *WT* were identified*;* and the normalized phospho-isoform abundance was represented for *WT, ptc7*Δ and *ptc7*Δ+*PTC7.* In the case of multiple phosphorylated peptides from a single protein, only the peptide with highest confidence (lowest p-value) was considered. Mitochondrial localization was defined as in (Huh et al., 2003).

Figure 6.2

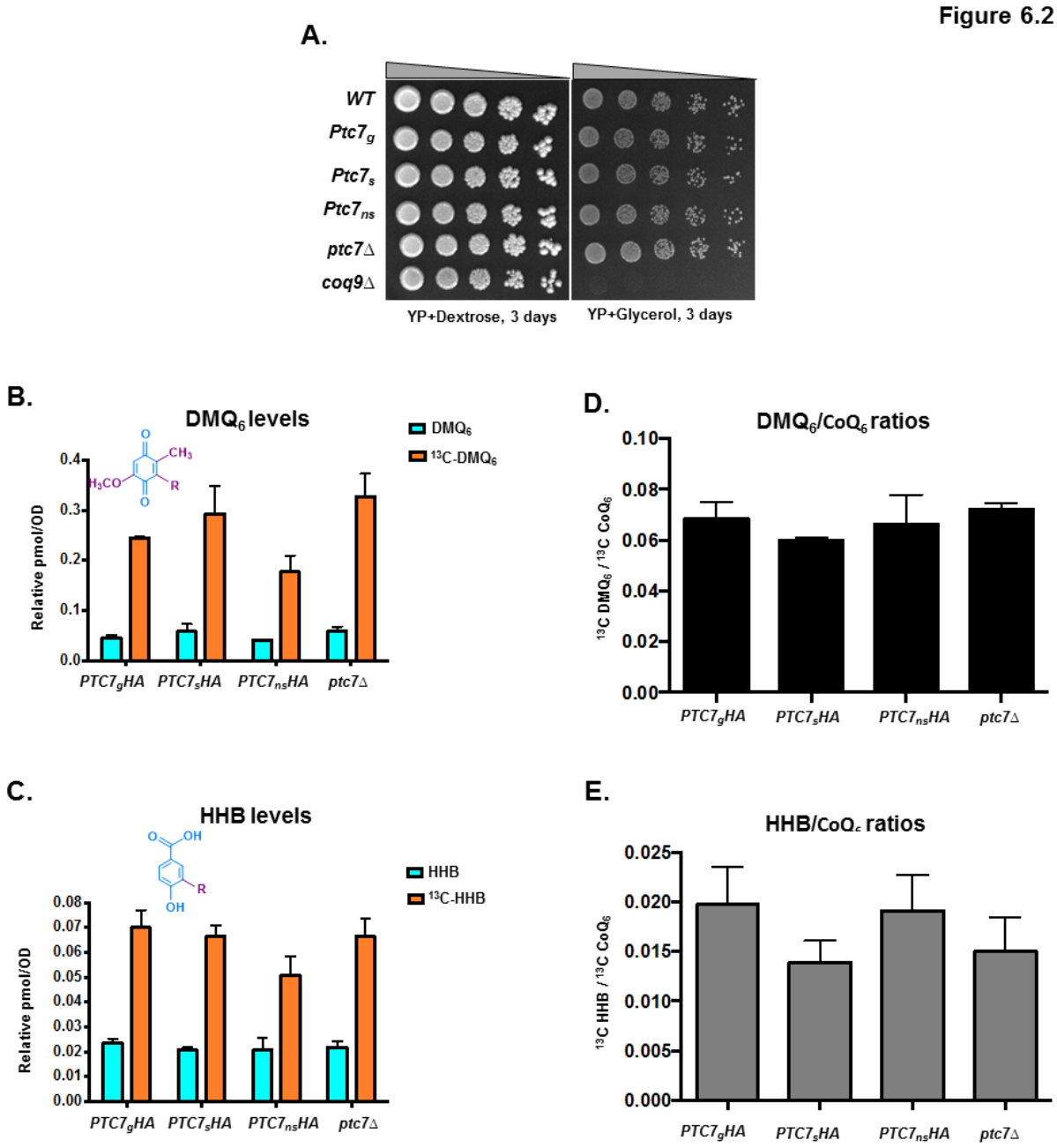

Figure 6.2: Exclusive expression of Ptc7 isoforms does not significantly affect conversions of precursors within the CoQ_6 biosynthetic pathway.

A. Serial dilutions (5-fold) of various *PTC7* isoform strains, *ptc7*Δ, and *coq9*Δ (negative

respiratory-deficient control) on YP agar plates with dextrose or glycerol as the carbon sources.

B. Levels of steady state (^{12}C-DMQ$_6$, blue bars) and *de novo* synthesized ($^{13}C_6$-DMQ$_6$, orange bars) in strains expressing different Ptc7 isoforms (*PTC7$_g$HA:* genomic, both isoforms expressed at endogenous levels; *PTC7$_s$HA:* exclusively expresses isoform from spliced mRNA; *PTC7$_{ns}$HA:* exclusively expresses isoform from nonspliced pre-mRNA) and *ptc7*Δ. Error bars represent ± 1 SD of n=3 biological replicates.

C. Levels of steady state (^{12}C-HHB, blue bars) and *de novo* synthesized ($^{13}C_6$-HHB, orange bars) in strains expressing different Ptc7 isoforms (*PTC7$_g$HA:* genomic, both isoforms expressed at endogenous levels; *PTC7$_s$HA:* exclusively expresses isoform from spliced mRNA; *PTC7$_{ns}$HA:* exclusively expresses isoform from nonspliced pre-mRNA) and *ptc7*Δ. Error bars represent ± 1 SD of n=3 biological replicates.

D. Ratio of $^{13}C_6$-(Awad et al., 2017)DMQ$_6$/$^{13}C_6$-CoQ$_6$ in strains expressing different Ptc7 isoforms (*PTC7$_g$HA:* genomic, both isoforms expressed at endogenous levels; *PTC7$_s$HA:* exclusively expresses isoform from spliced mRNA; *PTC7$_{ns}$HA:* exclusively expresses isoform from nonspliced pre-mRNA) and *ptc7*Δ. Ratios derived from levels of $^{13}C_6$-CoQ$_6$ previously reported (Awad et al., 2017). Error bars represent ± 1 SD of n=3 biological replicates.

E. Ratio of $^{13}C_6$-HHB/$^{13}C_6$-CoQ$_6$ in strains expressing different Ptc7 isoforms (*PTC7$_g$HA:* genomic, both isoforms expressed at endogenous levels; *PTC7$_s$HA:* exclusively expresses isoform from spliced mRNA; *PTC7$_{ns}$HA:* exclusively expresses isoform from nonspliced pre-mRNA) and *ptc7*Δ. Ratios derived from levels of $^{13}C_6$-CoQ$_6$ previously reported . Error bars represent ± 1 SD of n=3 biological replicates.

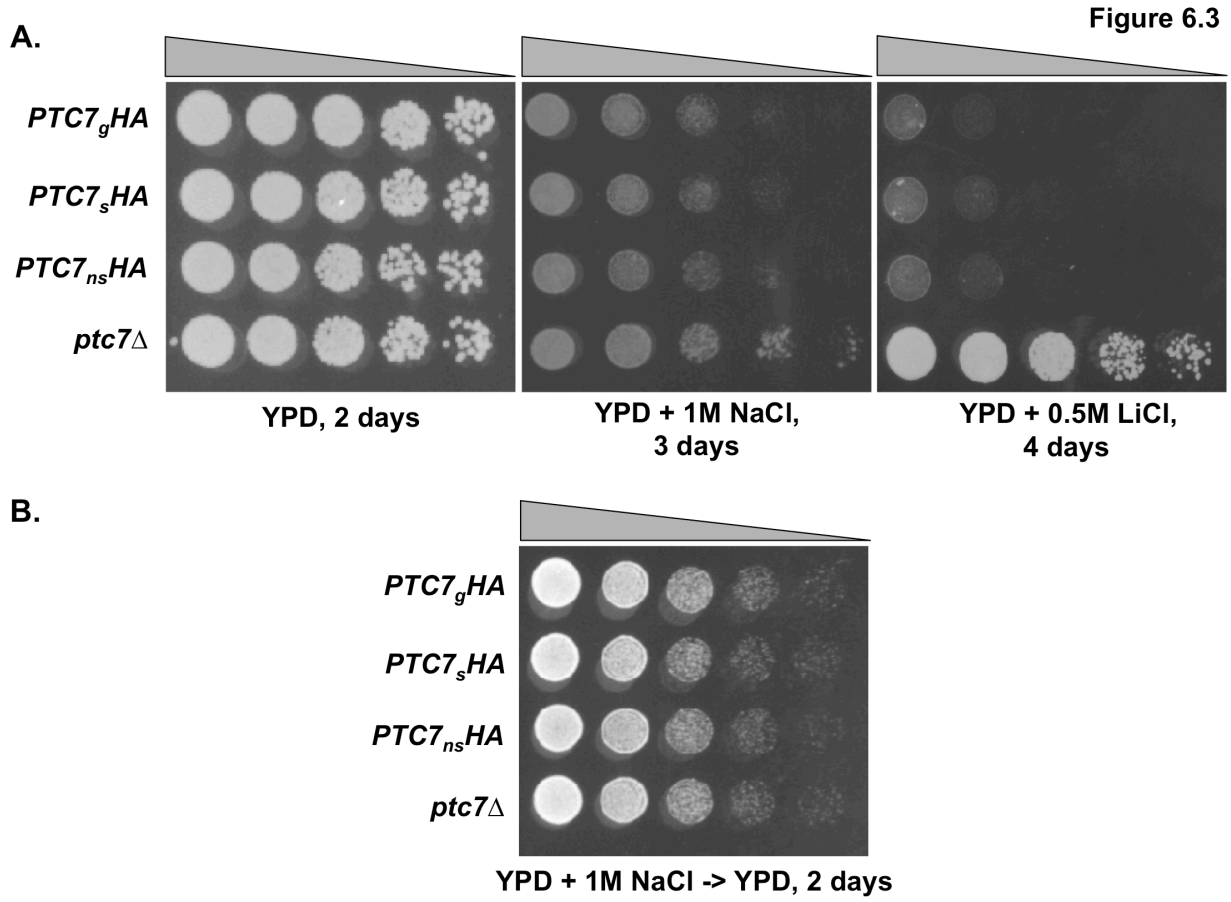

Figure 6.3: Absence of both Ptc7 isoforms, but not either one individually, causes increased resistance to osmotic stress.

A. Serial dilutions (5-fold) of various *PTC7* isoform strains and *ptc7*Δ previously grown in YPD liquid media, on YPD agar plates without salt, with 1M NaCl or 0.5M LiCl.

B. Serial dilutions (5-fold) of various *PTC7* isoform strains and *ptc7*Δ previously grown in YPD + 1M NaCl liquid media, on YPD agar plates.

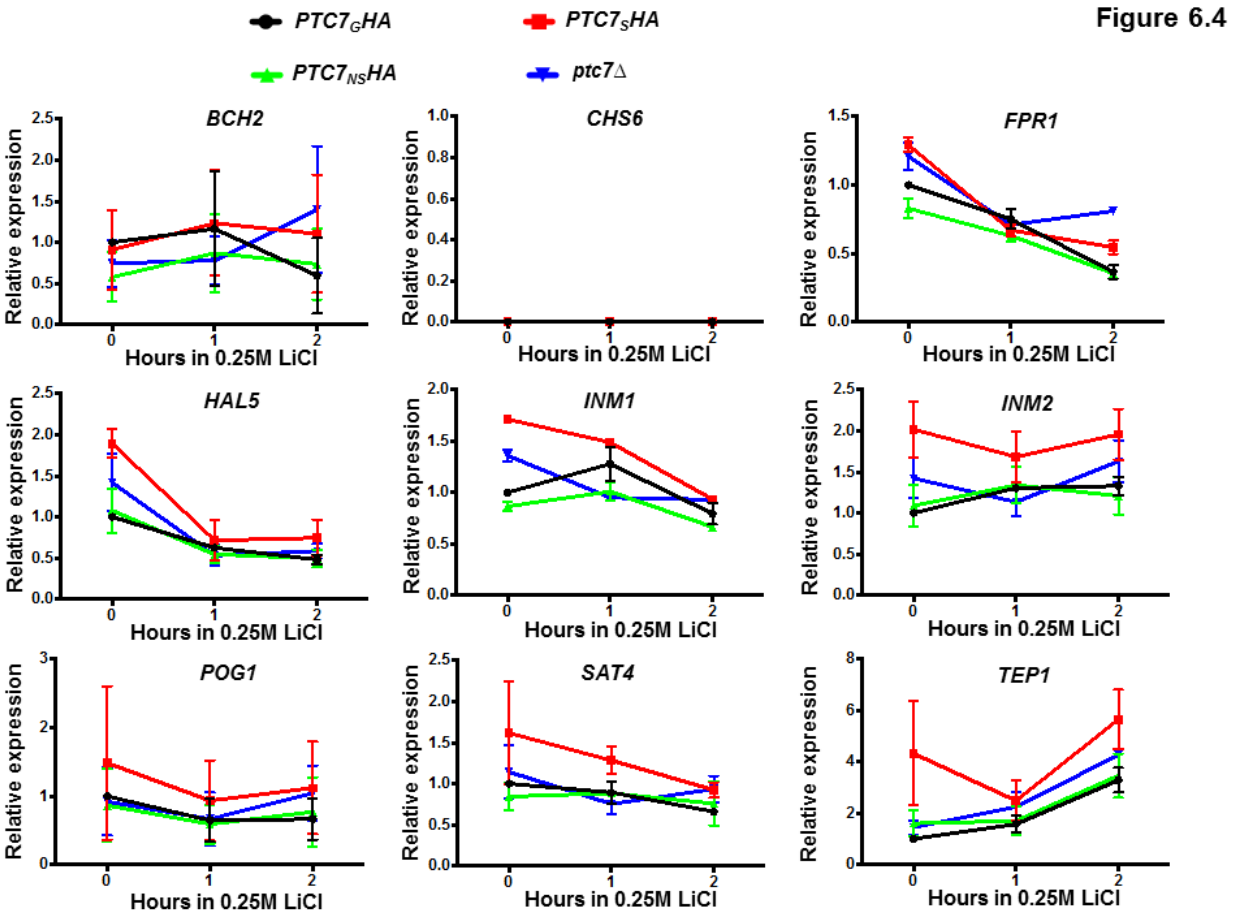

Figure 6.4: Expression of genes annotated as having a role in increased resistance to LiCl (*Saccharomyces* Genome Database), measured by qPCR in Ptc7 isoform and null strains growing in YPD + 0.25M LiCl.

Figure 6.5

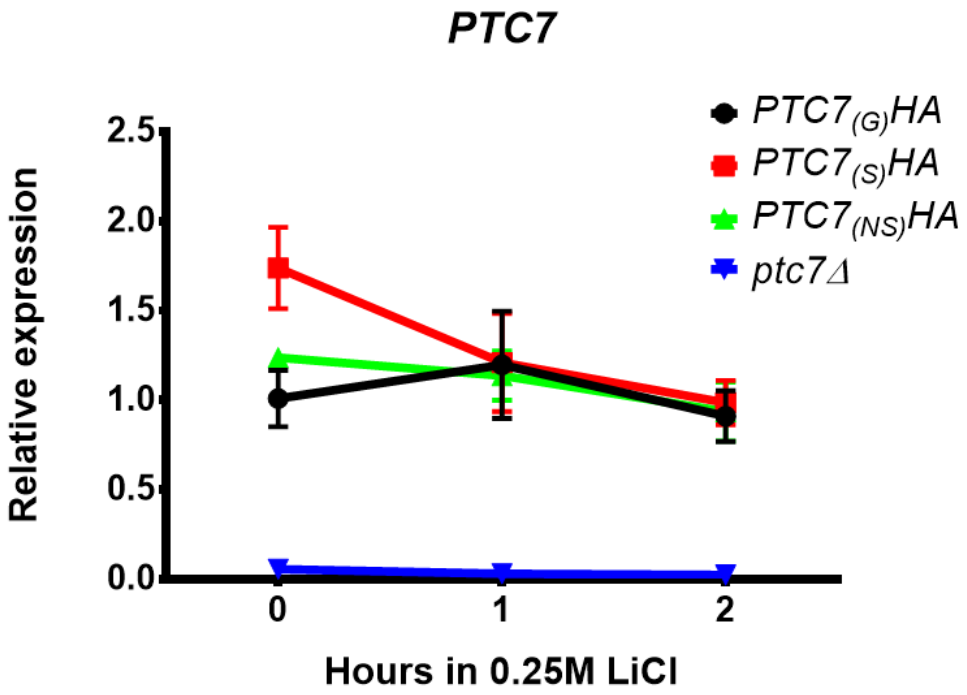

Figure 6.5: Expression of total *PTC7* measured by qPCR in Ptc7 isoform and null strains growing in YPD + 0.25M LiCl.

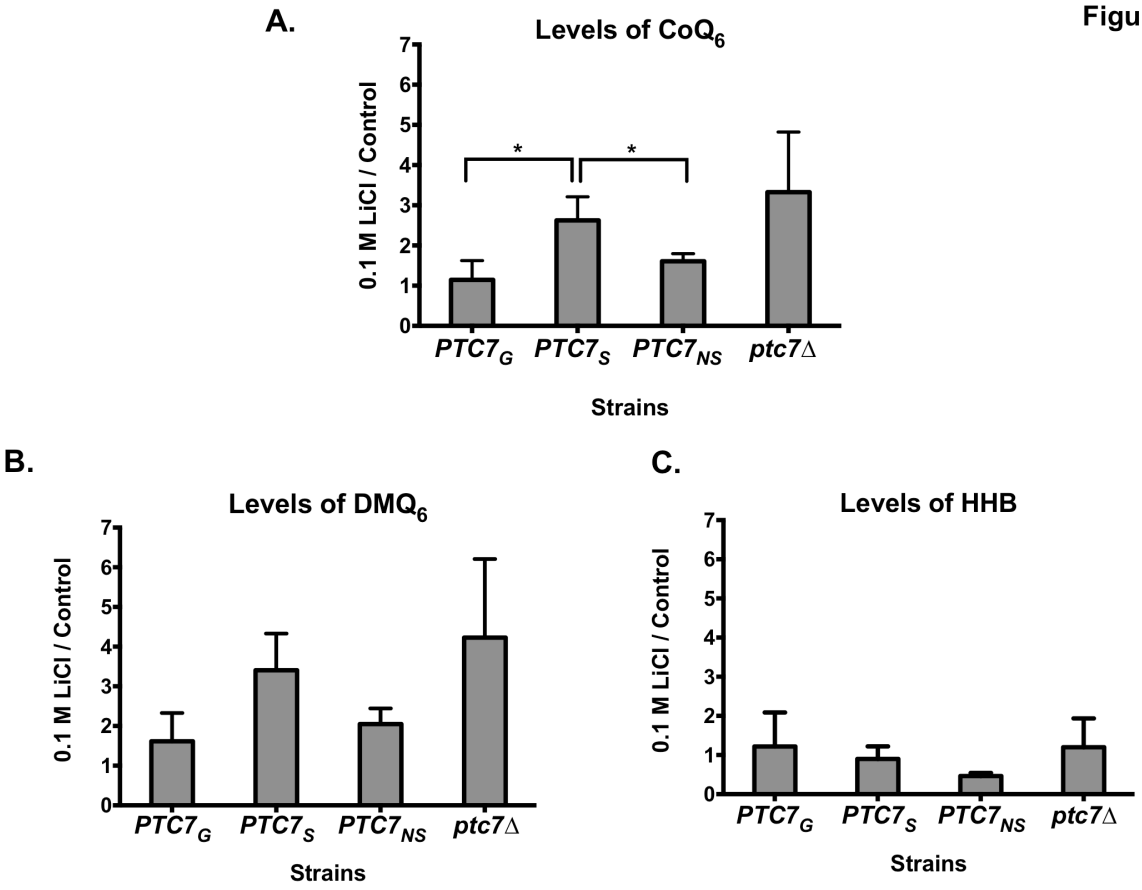

Figure 6.6: Ratio of CoQ_6 and pathway intermediates between LiCl treated and control yeast cells.

A. Ratio of total CoQ_6 during growth in YPD + 0.1M LiCl to YPD control in strains expressing different Ptc7 isoforms (*$PTC7_G$:* genomic, both isoforms expressed at endogenous levels; *$PTC7_S$:* exclusively expresses isoform from spliced mRNA; *$PTC7_{NS}$:* exclusively expresses isoform from nonspliced pre-mRNA) and *ptc7*Δ. Error bars represent ± 1 SD of n=3 biological replicates (* : $p<0.05$).

B. Ratio of total DMQ_6 during growth in YPD + 0.1M LiCl to YPD control in strains expressing different Ptc7 isoforms (*$PTC7_G$:* genomic, both isoforms expressed at endogenous levels; *$PTC7_S$:* exclusively expresses isoform from spliced mRNA; *$PTC7_{NS}$:*

exclusively expresses isoform from nonspliced pre-mRNA) and *ptc7*Δ. Error bars represent ± 1 SD of n=3 biological replicates.

C. Ratio of total HHB during growth in YPD + 0.1M LiCl to YPD control in strains expressing different Ptc7 isoforms (*PTC7*$_G$*:* genomic, both isoforms expressed at endogenous levels; *PTC7*$_S$*:* exclusively expresses isoform from spliced mRNA; *PTC7*$_{NS}$*:* exclusively expresses isoform from nonspliced pre-mRNA) and *ptc7*Δ. Error bars represent ± 1 SD of n=3 biological replicates.

References

Ahmed, S., Brickner, D. G., Light, W. H., Cajigas, I., McDonough, M., Froyshteter, A. B., Volpe, T. & Brickner, J. H. 2010. DNA zip codes control an ancient mechanism for gene targeting to the nuclear periphery. *Nature Cell Biology,* 12**,** 111-U43.

Allan, C. M., Awad, A. M., Johnson, J. S., Shirasaki, D. I., Wang, C., Blaby-Haas, C. E., Merchant, S. S., Loo, J. A. & Clarke, C. F. 2015. Identification of Coq11, a new coenzyme Q biosynthetic protein in the CoQ-synthome in Saccharomyces cerevisiae. *J Biol Chem,* 290**,** 7517-34.

Awad, A. M., Venkataramanan, S., Nag, A., Galivanche, A. R., Bradley, M. C., Neves, L., Douglass, S., Clarke, C. F. & Johnson, T. L. 2017. Chromatin-remodeling SWI/SNF complex regulates coenzyme Q6 synthesis and a metabolic shift to respiration in yeast. *Journal of Biological Chemistry*.

Babazadeh, R., Lahtvee, P. J., Adiels, C. B., Goksor, M., Nielsen, J. B. & Hohmann, S. 2017. The yeast osmostress response is carbon source dependent. *Sci Rep,* 7**,** 990.

Boukouris, A. E., Zervopoulos, S. D. & Michelakis, E. D. 2016. Metabolic Enzymes Moonlighting in the Nucleus: Metabolic Regulation of Gene Transcription. *Trends Biochem Sci,* 41**,** 712-30.

Brickner, D. G., Cajigas, I., Fondufe-Mittendorf, Y., Ahmed, S., Lee, P. C., Widom, J. & Brickner, J. H. 2007. H2A.z-mediated localization of genes at the nuclear periphery confers epigenetic memory of previous transcriptional state. *Plos Biology,* 5**,** 704-716.

Brickner, J. H. & Walter, P. 2004. Gene recruitment of the activated INO1 locus to the nuclear membrane. *Plos Biology,* 2**,** 1843-1853.

Cabal, G. G., Genovesio, A., Rodriguez-Navarro, S., Zimmer, C., Gadal, O., Lesne, A., Buc, H., Feuerbach-Fournier, F., Olivo-Marin, J. C., Hurt, E. C. & Nehrbass, U. 2006. SAGA interacting factors confine sub-diffusion of transcribed genes to the nuclear envelope. *Nature,* 441**,** 770-773.

Cardenas, M. E., Hemenway, C., Muir, R. S., Ye, R., Fiorentino, D. & Heitman, J. 1994. Immunophilins interact with calcineurin in the absence of exogenous immunosuppressive ligands. *EMBO J,* 13**,** 5944-57.

Casolari, J. M., Brown, C. R., Drubin, D. A., Rando, O. J. & Silver, P. A. 2005. Developmentally induced changes in transcriptional program alter spatial organization across chromosomes. *Genes & Development,* 19**,** 1188-1198.

Casolari, J. M., Brown, C. R., Komili, S., West, J., Hieronymus, H. & Silver, P. A. 2004. Genome-wide localization of the nuclear transport machinery couples transcriptional status and nuclear organization. *Cell,* 117**,** 427-439.

D'Urso, A., Takahashi, Y. H., Xiong, B., Marone, J., Coukos, R., Randise-Hinchliff, C., Wang, J. P., Shilatifard, A. & Brickner, J. H. 2016. Set1/COMPASS and Mediator are repurposed to promote epigenetic transcriptional memory. *Elife,* 5.

De, P. & Chatterjee, R. 1962a. Evidence of Nucleolar Succinic Dehydrogenase Activity. *Experimental Cell Research,* 27**,** 172-173.

De, P. & Chatterjee, R. 1962b. Nucleolar Localization of Succinic Dehydrogenase in Human Malignant Cells with MTT. *Experientia,* XVIII**,** 562.

Green, E. M., Jiang, Y., Joyner, R. & Weis, K. 2012. A negative feedback loop at the nuclear periphery regulates GAL gene expression. *Molecular Biology of the Cell,* 23**,** 1367-1375.

Grund, S. E., Fischer, T., Cabal, G. G., Antunez, O., Perez-Ortin, J. E. & Hurt, E. 2008. The inner nuclear membrane protein Src1 associates with subtelomeric genes and alters their regulated gene expression. *J Cell Biol,* 182**,** 897-910.

Guo, X., Niemi, N. M., Hutchins, P. D., Condon, S. G., Jochem, A., Ulbrich, A., Higbee, A. J., Russell, J. D., Senes, A., Coon, J. J. & Pagliarini, D. J. 2017. Ptc7p Dephosphorylates Select Mitochondrial Proteins to Enhance Metabolic Function. *Cell Rep,* 18**,** 307-313.

Heymont, J., Berenfeld, L., Collins, J., Kaganovich, A., Maynes, B., Moulin, A., Ratskovskaya, I., Poon, P. P., Johnston, G. C., Kamenetsky, M., DeSilva, J., Sun, H., Petsko, G. A. & Engebrecht, J. 2000. TEP1, the yeast homolog of the human tumor suppressor gene PTEN/MMAC1/TEP1, is linked to the phosphatidylinositol pathway and plays a role in the developmental process of sporulation. *Proc Natl Acad Sci U S A,* 97**,** 12672-7.

Huh, W. K., Falvo, J. V., Gerke, L. C., Carroll, A. S., Howson, R. W., Weissman, J. S. & O'Shea, E. K. 2003. Global analysis of protein localization in budding yeast. *Nature,* 425**,** 686-91.

Juneau, K., Nislow, C. & Davis, R. W. 2009. Alternative splicing of PTC7 in Saccharomyces cerevisiae determines protein localization. *Genetics,* 183**,** 185-194.

Jung, S. J., Seo, Y., Lee, K. C., Lee, D. & Roe, J. H. 2015. Essential function of Aco2, a fusion protein of aconitase and mitochondrial ribosomal protein bL21, in mitochondrial translation in fission yeast. *FEBS Lett,* 589**,** 822-8.

Kellis, M., Birren, B. W. & Lander, E. S. 2004. Proof and evolutionary analysis of ancient genome duplication in the yeast Saccharomyces cerevisiae. *Nature,* 428**,** 617-24.

Lapointe, C. P., Stefely, J. A., Jochem, A., Hutchins, P. D., Wilson, G. M., Kwiecien, N. W., Coon, J. J., Wickens, M. & Pagliarini, D. J. 2017. Post-Transcriptional Control of Coenzyme Q Biosynthesis Revealed by Transomic Analysis of the RNA-Binding Protein Puf3p. *bioRxiv*.

Lee, S. M., Kim, J. H., Cho, E. J. & Youn, H. D. 2009. A nucleocytoplasmic malate dehydrogenase regulates p53 transcriptional activity in response to metabolic stress. *Cell Death Differ,* 16**,** 738-48.

Liu, J. L., Yee, C., Wang, Y. & Hekimi, S. 2017. A single biochemical activity underlies the pleiotropy of the aging-related protein CLK-1. *Sci Rep,* 7**,** 859.

Livak, K. J. & Schmittgen, T. D. 2001. Analysis of relative gene expression data using real-time quantitative PCR and the 2(-Delta Delta C(T)) Method. *Methods,* 25**,** 402-8.

Lopez, F., Leube, M., Gil-Mascarell, R., Navarro-Avino, J. P. & Serrano, R. 1999. The yeast inositol monophosphatase is a lithium- and sodium-sensitive enzyme encoded by a non-essential gene pair. *Mol Microbiol,* 31**,** 1255-64.

Lord, C. L., Timney, B. L., Rout, M. P. & Wente, S. R. 2015. Altering nuclear pore complex function impacts longevity and mitochondrial function in S. cerevisiae. *J Cell Biol,* 208**,** 729-44.

Luthra, R., Kerr, S. C., Harreman, M. T., Apponi, L. H., Fasken, M. B., Ramineni, S., Chaurasia, S., Valentini, S. R. & Corbett, A. H. 2007. Actively transcribed GAL genes can be physically linked to the nuclear pore by the SAGA chromatin modifying complex. *Journal of Biological Chemistry,* 282**,** 3042-3049.

Marshall, A. N., Montealegre, M. C., Jimenez-Lopez, C., Lorenz, M. C. & van Hoof, A. 2013. Alternative splicing and subfunctionalization generates functional diversity in fungal proteomes. *PLoS Genet,* 9**,** e1003376.

Martin-Montalvo, A., Gonzalez-Mariscal, I., Padilla, S., Ballesteros, M., Brautigan, D. L., Navas, P. & Santos-Ocana, C. 2011. Respiratory-induced coenzyme Q biosynthesis is regulated by a phosphorylation cycle of Cat5p/Coq7p. *Biochem J,* 440**,** 107-14.

Martin-Montalvo, A., Gonzalez-Mariscal, I., Pomares-Viciana, T., Padilla-Lopez, S., Ballesteros, M., Vazquez-Fonseca, L., Gandolfo, P., Brautigan, D. L., Navas, P. & Santos-Ocana, C. 2013. The phosphatase Ptc7 induces coenzyme Q biosynthesis by activating the hydroxylase Coq7 in yeast. *J Biol Chem,* 288**,** 28126-37.

Menon, B. B., Sarma, N. J., Pasula, S., Deminoff, S. J., Willis, K. A., Barbara, K. E., Andrews, B. & Santangelo, G. M. 2005. Reverse recruitment: The Nup84 nuclear pore subcomplex mediates Rap1/Gcr1/Gcr2 transcriptional activation. *Proceedings of the National Academy of Sciences of the United States of America,* 102**,** 5749-5754.

Monaghan, R. M., Barnes, R. G., Fisher, K., Andreou, T., Rooney, N., Poulin, G. B. & Whitmarsh, A. J. 2015. A nuclear role for the respiratory enzyme CLK-1 in regulating mitochondrial stress responses and longevity. *Nat Cell Biol,* 17**,** 782-92.

Mulet, J. M., Leube, M. P., Kron, S. J., Rios, G., Fink, G. R. & Serrano, R. 1999. A novel mechanism of ion homeostasis and salt tolerance in yeast: the Hal4 and Hal5 protein kinases modulate the Trk1-Trk2 potassium transporter. *Mol Cell Biol,* 19**,** 3328-37.

OhEigeartaigh, S. S., Armisen, D., Byrne, K. P. & Wolfe, K. H. 2011. Systematic discovery of unannotated genes in 11 yeast species using a database of orthologous genomic segments. *BMC Genomics,* 12**,** 377.

Padilla, S., Tran, U. C., Jimenez-Hidalgo, M., Lopez-Martin, J. M., Martin-Montalvo, A., Clarke, C. F., Navas, P. & Santos-Ocana, C. 2009. Hydroxylation of demethoxy-Q6 constitutes a control point in yeast coenzyme Q6 biosynthesis. *Cell Mol Life Sci,* 66**,** 173-86.

Raices, M. & D'Angelo, M. A. 2017. Nuclear pore complexes and regulation of gene expression. *Current Opinion in Cell Biology,* 46**,** 26-32.

Regot, S., de Nadal, E., Rodriguez-Navarro, S., Gonzalez-Novo, A., Perez-Fernandez, J., Gadal, O., Seisenbacher, G., Ammerer, G. & Posas, F. 2013. The Hog1 stress-activated protein kinase targets nucleoporins to control mRNA export upon stress. *J Biol Chem,* 288**,** 17384-98.

Rockenbauch, U., Ritz, A. M., Sacristan, C., Roncero, C. & Spang, A. 2012. The complex interactions of Chs5p, the ChAPs, and the cargo Chs3p. *Mol Biol Cell,* 23**,** 4402-15.

Rout, M. P., Aitchison, J. D., Suprapto, A., Hjertaas, K., Zhao, Y. & Chait, B. T. 2000. The Yeast Nuclear Pore Complex: Composition, Architecture and Transport Mechanism. *The Journal of Cell Biology,* 148**,** 635-651.

Sasano, Y., Haitani, Y., Hashida, K., Oshiro, S., Shima, J. & Takagi, H. 2013. Improvement of fermentation ability under baking-associated stress conditions by altering the POG1 gene expression in baker's yeast. *Int J Food Microbiol,* 165**,** 241-5.

Schmid, M., Arib, G., Laemmli, C., Nishikawa, J., Durussel, T. & Laemmli, U. K. 2006. Nup-PI: The nucleopore-promoter interaction of genes in yeast. *Molecular Cell,* 21**,** 379-391.

Sharmin, D., Sasano, Y., Sugiyama, M. & Harashima, S. 2014. Effects of deletion of different PP2C protein phosphatase genes on stress responses in Saccharomyces cerevisiae. *Yeast,* 31**,** 393-409.

Taddei, A., Van Houwe, G., Hediger, F., Kalck, V., Cubizolles, F., Schober, H. & Gasser, S. M. 2006. Nuclear pore association confers optimal expression levels for an inducible yeast gene. *Nature,* 441**,** 774-778.

Toyama, B. H., Savas, J. N., Park, S. K., Harris, M. S., Ingolia, N. T., Yates, J. R. & Hetzer, M. W. 2013. Identification of Long-Lived Proteins Reveals Exceptional Stability of Essential Cellular Structures. *Cell,* 154**,** 971-982.

Tran, U. C. & Clarke, C. F. 2007. Endogenous synthesis of coenzyme Q in eukaryotes. *Mitochondrion,* 7 Suppl**,** S62-71.

Tran, U. C., Marbois, B., Gin, P., Gulmezian, M., Jonassen, T. & Clarke, C. F. 2006. Complementation of Saccharomyces cerevisiae coq7 mutants by mitochondrial targeting of the Escherichia coli UbiF polypeptide: two functions of yeast Coq7 polypeptide in coenzyme Q biosynthesis. *J Biol Chem,* 281**,** 16401-9.

Turunen, M., Olsson, J. & Dallner, G. 2004. Metabolism and function of coenzyme Q. *Biochim Biophys Acta,* 1660**,** 171-99.

Williams, R. M., Primig, M., Washburn, B. K., Winzeler, E. A., Bellis, M., Sarrauste de Menthiere, C., Davis, R. W. & Esposito, R. E. 2002. The Ume6 regulon coordinates metabolic and meiotic gene expression in yeast. *Proc. Natl. Acad. Sci. U. S. A.,* 99**,** 13431-13436.

Yogev, O., Yogev, O., Singer, E., Shaulian, E., Goldberg, M., Fox, T. D. & Pines, O. 2010. Fumarase: a mitochondrial metabolic enzyme and a cytosolic/nuclear component of the DNA damage response. *PLoS Biol,* 8**,** e1000328.

CHAPTER 7

Concluding remarks and perspectives.

Since the discovery of DNA as genetic material, beautiful work over the decades has brought to light the molecular detail of gene regulation reactions like transcription, pre-mRNA splicing, and translation; as well as the machineries that carry them out. However, while the mechanisms of a number of these gene regulation steps might be known, each step has traditionally been studied in isolation. Over the last few years, there is the increasing realization that gene expression processes are coupled together mechanistically (i.e. transcription is coupled to pre-mRNA splicing, which is in turn coupled to translation), and therefore, coordinated regulation of these processes must be considered. Furthermore, the advent of new and powerful technologies make it possible to study a gene expression program in the context of every other such program, giving us a more holistic and integrated view of the inner workings of a cell.

While the perspectives of its study are certainly broadening, certain aspects of gene regulation such as the stoichiometry of the key enzymatic components in relation to the substrates they act on, a molecular "accounting" of sorts, are commonly ignored. The availability of gene regulation machinery has to be considered carefully to understand the kinetics, thermodynamics and eventual consequences of a regulatory reaction. Commonly, the core machineries of gene expression such as the polymerase, the spliceosome and the ribosome are assumed to be in excess. However, recent work has shown that that is certainly not true, and competition for limiting machineries of gene regulation has functional consequences (Munding et al., 2013, Baumgartner et al., 2011). The work presented in this dissertation elucidates two examples of the biological consequences of the limiting nature of the *Saccharomyces cerevisiae* spliceosome in remodeling gene expression networks and cellular decision-making in response to environmental conditions. We lay out mechanisms by which a single chromatin remodeling factor, the SWI/SNF complex coordinately controls the availability of spliceosome by regulating

the transcription of translation-related genes, which are enriched in introns. The SWI/SNF complex lies at the nexus of transcription, splicing and translation and effects profound changes in the metabolic nature of the cell in response to environmental changes. (Venkataramanan et al., 2017, Awad et al., 2017).

We demonstrate that regulation of spliceosome availability by the SWI/SNF complex in response to environmental conditions activates the specialized developmental program of meiosis in *S. cerevisiae,* enabling survival in the absence of nutrients (Venkataramanan et al., 2017). Further, we begin to uncover novel mechanisms by which Snf2, the core ATPase component of the SWI/SNF complex is regulated. A combination of uORF mediated regulation of translation, m^6A methylation, protein deacetylation, and degradation exquisitely regulate the activity of the SWI/SNF complex to effect the developmental and metabolic changes involved in a critical cellular process. In addition, we present evidence of a novel functional role for the alternative splicing of a yeast gene, wherein protein isoforms derived from the splicing or retention of a conserved intron within a single gene have opposing effects on the biosynthesis of a key metabolite involved in the switching of metabolic modes (Awad et al., 2017).

The work described in this dissertation has implications beyond *S. cerevisiae.* Recent theoretical work has proposed that the translation of very highly expressed and efficiently translated genes (such as ribosomal protein genes themselves) serves as a ribosome sink, effectively downregulating the translation of other mRNAs in the cytoplasm (Raveh et al., 2016). The regulatory potential of this is only beginning to be explored. However, recent evidence suggests that in organisms ranging from yeast to humans, translation related genes are translationally repressed under specific conditions of stress or differentiation, perhaps to promote the translation of other, specialized transcripts (Blair et al., 2017, Arribere et al., 2011). The role

of competition for fundamental machines of gene regulation is therefore a burgeoning and potentially very fruitful area of exploration in our quest to understand the biology of the cell.

Switching metabolic modes in *Saccharomyces cerevisiae*

Responding and adapting to environmental stimuli is one of the characteristic features of life itself. *Saccharomyces cerevisiae* are unique in that they experience dramatic shifts in metabolism in response to environmental changes, and the organism's extreme utility to human civilization and long history of domestication has caused these shifts to be systematically studied. In the mid-nineteenth century, Louis Pasteur observed that *S. cerevisiae* utilized more glucose in the absence of oxygen that in its presence, likely due to the activation of anaerobic glycolysis over fermentation to meet cellular ATP requirements (Pasteur, 1861). However, the 'Pasteur Effect' is limited to conditions of carbon limitation. In fact, under glucose-rich conditions, *S. cerevisiae* primarily utilizes a fermentative mode of metabolism regardless of oxygen concentrations, likely due to a combination of glucose repression and relative activities of pyruvate dehydrogenase (which shunts carbon into the citric acid cycle and respiration) vs. pyruvate decarboxylase (which converts pyruvate to acetaldehyde, which in turn is eventually reduced into ethanol) (Crabtree, 1929, De Deken, 1966, Kappeli, 1986). This is called the 'Crabtree effect', and is thought to be consequence of the organism 'preferring' to produce ATP rapidly (fermentation) as opposed to maximize the ATP output per glucose molecule consumed in a slower, but more efficient process (respiration) (Otterstedt et al., 2004). As detailed above, the metabolic switch in yeast is controlled by both the abundance of oxygen as well as the abundance and composition of carbon sources within the medium. Furthermore, in *S. cerevisiae,* the development of gametes (meiosis, or sporulation) is also regulated by environmental

conditions, and utilizes specialized metabolic pathways (Halpern and Miller, 1956, Miller, 1957, Miller et al., 1959, Ramirez and Miller, 1964, Dickinson, 1988). Recent results have shown that the process of respiration is essential for entry into sporulation, both in terms of providing energy for the process, as well as other as yet unknown metabolites (Jambhekar and Amon, 2008). Therefore, growth and development of yeast rely on accurately sensing environmental nutrient conditions, and responding to it by switching metabolic modes as appropriate and confers greatest fitness advantage.

Since the earliest of these findings, extensive studies have been performed on the mechanism by which the yeast achieves this shift in metabolic modes (reviewed in (Conrad et al., 2014)). The presence of absence of specific nutrients is conveyed using secondary metabolites as messenger molecules within signal transduction pathways. For example, the presence of glucose activates the Ras/cAMP dependent Protein Kinase A (PKA) pathway, with cAMP functioning as the secondary messenger. Target of Rapamycin Complex I (TORC1) senses nitrogen in the environment and regulates cellular responses accordingly. Interestingly, regulation of both TORC1 and PKA have been shown to be crucial for the proper timing of sporulation (Weidberg et al., 2016). The expression of a number of genes is regulated downstream of these signal transduction pathways, and this is, in a sense, the final effector of the cellular decision making in response to nutrient conditions.

SWI/SNF in the yeast sexual cycle

We have recently shown that the chromatin remodeling complex SWI/SNF plays a previously unexplored but fundamental role in regulating meiotic splicing. We demonstrate that at the onset of meiosis, Snf2 levels are rapidly downregulated leading to a corresponding down-

regulation of expression of ribosomal protein genes (Venkataramanan et al., 2017). Since RPGs are highly enriched in introns, down-regulating this class of genes alters the splicing landscape of the cell and frees up spliceosomes to interact with intron-containing meiotic transcripts, almost of which contain splice sites that make them poor substrates of the spliceosome. In addition to its role in spliceosome redistribution, Snf2 is required to overcome Ume6-dependent repression of Mer1 expression. Hence, Snf2 is a key regulator of the central controller of meiotic splicing (Venkataramanan et al., 2017).

This idea might extend even further. Snf2 was also independently identified as Swi2, required for the "Switching" phenotype, the core process of homothallic mating in *S.cerevisiae* (Stern et al., 1984). Briefly, heterothallic mating in *S.cerevisiae* occurs when a cells encounter α cells, as a consequence of different mating factors produced by the two cell types. However, *S.cerevisiae* also have a homothallic phenotype, viz. the ability to switch mating type and undergo a self-fertile sexual cycle. Two silenced loci called *HML* and *HMR* homologous to the a and α at the *MAT* locus are normally silenced, but upon expression of the HO endonuclease, the *MAT* locus is cleaved, causing a gene conversion between the *MAT* locus and the *HML* or *HMR* locus. Thus, a cell of a single mating type can undergo mating by this process; following cell divisions, HO is activated in the mother cells, evoking a mating type switch event to result in a pair of cells of opposite mating type and thereby enabling mating between the mother and daughter cells (Haber, 1998, Haber, 2012). It has long been known that Snf2 (as well as other components of the complex) is essential for the expression of the HO endonuclease, and the fulfillment of homothallic potential in yeast (Stern et al., 1984, Nasmyth, 1993, Mitra et al., 2006). This combined with our observations that place the Swi/Snf complex at a nexus point in

the control of meiosis indicate that the entire sexual cycle of *S. cerevisiae* is potentially under the control of the SWI/SNF complex (Venkataramanan et al., 2017).

The origins of meiosis (and sexual reproduction in general) in early eukaryotic history have never been satisfactorily explained (Lenormand et al., 2016). While meiosis almost certainly evolved from the more primitive mitosis, there are numerous cytological events that occur in the meiotic cycle of even the most primitive eukaryotes, such as *S. cerevisiae,* that appear to be unique to that process (Heitman et al., 2013). We have also put forth an argument for the entire "sexual cycle" of *S. cerevisiae* to be under the control of a single protein complex, performing multiple distinct functions at different stages of the cycle. At first sight, it appears difficult to reconcile this with a sense of Darwinian gradualism in answering the question of how meiosis evolved. However, to our minds, this is a fallacy. The evolutionary intermediates in the development of meiosis, perhaps a primitive ascomycetous fungi that developed homologous pairing, or suppression of kinetochore splitting, or dual-karyokinesis, are perhaps entirely lost to us (Lenormand et al., 2016, Goodenough and Heitman, 2014, Heitman et al., 2013, Ni et al., 2011, Lee et al., 2010, Solari, 2002). The archetypal "early" sexual cycle most commonly studied remains *S. cerevisiae*, and that is a fully formed cytological process, exquisitely controlled by SWI/SNF protein complex at every step.

Many questions remain unanswered in the evolutionary intermediates. How did the genes involved in meiosis evolve? We assume they arose from largely mitotic counterparts, but when and how they diverged remains unknown. Perhaps more confoundingly, why are they enriched in introns? Even more specifically, why do almost all IC meiotic genes possess non-consensus splice sites? We assume this is to prevent their splicing except under exceptional circumstances, to prevent the a/α diploid from undergoing meiosis under favorable growth conditions. After all,

early meiosis, such as the forms seen in ascomycetous fungi appears to be a survival mechanism, induced by starvation; and not necessarily a preferred branch of the cell cycle (Lee et al., 2010). Did the poorly-spliceable introns arise as a control mechanism, a rheostat to make sure that the functional products of these genes, which cause the organism to entire a non-productive, hunker down and survive mode of existence are not formed when environmental conditions are favorable for proliferation? If so, the "rheostat" is clearly controlled by the preponderance of introns amongst the massively abundant RPGs. Which arose first? Are meiotic genes enriched in weakly-spliced introns because that was the easiest and most economical way to control their expression? Or did the highly abundant RPGs gain introns to titrate away spliceosomes from, and prevent expression of, a non-productive pathway? Where does Mer1 fit into the picture? Did evolution over-correct? In making these introns difficult to splice, so that they aren't spliced under favorable environmental conditions, perhaps a few of them were made so difficult to splice that even the large excess of spliceosomes that occur upon RPG depletion is unable to splice them, and this is was the pressure for the Mer1 splicing enhancer to evolve?

This control of SWI/SNF over sexual cycles is not limited to fungi. In fact, Swi/Snf has been known to have roles in metazoan meiosis. Previous reports have shown that Brg1, the ATPase subunit of the mammalian Swi/Snf complex, peaks in expression during the early stages of meiosis and is turned off in maturing round spermatids; and also that knocking down Brg1 results in prophase arrest during meiosis I, caused due to a failure to complete synapsis (Wang et al., 2012, Kim et al., 2012). Mammalian HFM1/Mer3 is an integral part of the ZMM group of proteins involved in this process, and has been shown to be required for the completion of synapsis during meiosis, and the deletion of Hfm1 closely resembles the phenotype of a Brg1 knockdown (Guiraldelli et al., 2013). While it is unlikely that the methods of regulation remain

exactly the same, it is conceivable that the SWI/SNF complex has retained its role in regulating meiosis through evolution. In fact, the vast global changes in splicing have been reported during male meiosis in mammals, and it is entirely possible that the SWI/SNF complex directly or indirectly contributes to the same (Schmid et al., 2013).

SWI/SNF in yeast respiration

Concurrently with its role in homothallic mating in *S. cerevisiae,* Snf2 was originally identified as being required for the expression of the glucose-repressed, signal peptide containing, longer form of the *SUC2* mRNA (Neigeborn and Carlson, 1984). This 1.9 kb mRNA encodes for the secreted form of the yeast invertase enzyme, which cleaves sucrose to give glucose and fructose, and is repressed in the presence of glucose (Carlson and Botstein, 1983, Carlson et al., 1983, Carlson and Botstein, 1982, Perlman et al., 1982). The SWI/SNF complex has been shown to be required for the induction and maintenance of expression of this gene during growth on sucrose (Trumbly, 1992, Geng and Laurent, 2004). Despite it's role in the activation of a number of glucose repressed genes required for growth on non-fermentable carbon sources, we have recently demonstrated that the levels of Snf2 protein decrease as glucose is depleted in the medium (Awad et al., 2017, Biddick et al., 2008, Geng and Laurent, 2004). This downregulation of Snf2 allows for a corresponding downregulation of RPG transcript levels and redistribution of the spliceosome, permitting the splicing of *PTC7,* a gene required for optimal CoQ_6 biosynthesis and mitochondrial activity during respiration (Awad et al., 2017). The conservation of two *PTC7* isoforms across fungal species indicates that this is an example of the utilization of alternative splicing to functionally expand the yeast proteome (Marshall et al., 2013). This implies a dual role for Snf2 in the natural diauxic shift during batch

growth, similar to its roles in the transition to sporulation media and meiosis (Venkataramanan et al., 2017, Awad et al., 2017).

SWI/SNF as a nexus of multi-layer gene regulation in response to environmental cues

The work presented within this dissertation establishes the SWI/SNF complex as a hub of gene regulation in response to environmental cues. We show that the state and abundance of Snf2, the core ATPase component of the SWI/SNF complex, is dynamically regulated in response to environmental conditions. The dynamics of the SWI/SNF complex under nutrient stress results in changes in the transcription of numerous genes, including but not limited to a decrease in the components of the ribosome (RPGs). In this manner, the translational output of the cell is reduced, conserving energy within the context of a nutrient-scarce environment. The downregulation of the RPGs also serves to render the yeast spliceosome no longer limiting, allowing for the splicing of numerous stress-responsive pre-mRNAs. Furthermore, the transcriptional activity of the SWI/SNF complex is also required to initiate the transcription of these pre-mRNAs, as well as other stress-specific genes required for their splicing, as well as the overall cellular response. The SWI/SNF complex thus modulates cellular transcription, pre-mRNA splicing, as well as translation, thereby integrating the gene regulation response at multiple steps to coordinately activate specific stress-response or developmental programs.

References

Arribere, J. A., Doudna, J. A. & Gilbert, W. V. 2011. Reconsidering movement of eukaryotic mRNAs between polysomes and P bodies. *Mol Cell,* 44**,** 745-58.

Awad, A. M., Venkataramanan, S., Nag, A., Galivanche, A. R., Bradley, M. C., Neves, L., Douglass, S., Clarke, C. F. & Johnson, T. L. 2017. Chromatin-remodeling SWI/SNF complex regulates coenzyme Q6 synthesis and a metabolic shift to respiration in yeast. *Journal of Biological Chemistry*.

Baumgartner, B. L., Bennett, M. R., Ferry, M., Johnson, T. L., Tsimring, L. S. & Hasty, J. 2011. Antagonistic gene transcripts regulate adaptation to new growth environments. *Proc Natl Acad Sci U S A,* 108**,** 21087-92.

Biddick, R. K., Law, G. L., Chin, K. K. & Young, E. T. 2008. The transcriptional coactivators SAGA, SWI/SNF, and mediator make distinct contributions to activation of glucose-repressed genes. *J Biol Chem,* 283**,** 33101-9.

Blair, J. D., Hockemeyer, D., Doudna, J. A., Bateup, H. S. & Floor, S. N. 2017. Widespread translational remodeling during human neuronal differentiation. *bioRxiv*.

Carlson, M. & Botstein, D. 1982. Two differentially regulated mRNAs with different 5' ends encode secreted with intracellular forms of yeast invertase. *Cell,* 28**,** 145-54.

Carlson, M. & Botstein, D. 1983. Organization of the SUC gene family in Saccharomyces. *Mol Cell Biol,* 3**,** 351-9.

Carlson, M., Taussig, R., Kustu, S. & Botstein, D. 1983. The secreted form of invertase in Saccharomyces cerevisiae is synthesized from mRNA encoding a signal sequence. *Mol Cell Biol,* 3**,** 439-47.

Conrad, M., Schothorst, J., Kankipati, H. N., Van Zeebroeck, G., Rubio-Texeira, M. & Thevelein, J. M. 2014. Nutrient sensing and signaling in the yeast Saccharomyces cerevisiae. *FEMS Microbiol Rev,* 38**,** 254-99.

Crabtree, H. G. 1929. Observations on the carbohydrate metabolism of tumours. *Biochem J,* 23**,** 536-45.

De Deken, R. H. 1966. The Crabtree effect: a regulatory system in yeast. *J Gen Microbiol,* 44**,** 149-56.

Dickinson, J. R. 1988. The metabolism of sporulation in yeast. *Microbiol Sci,* 5**,** 121-3.

Geng, F. & Laurent, B. C. 2004. Roles of SWI/SNF and HATs throughout the dynamic transcription of a yeast glucose-repressible gene. *EMBO J,* 23**,** 127-37.

Goodenough, U. & Heitman, J. 2014. Origins of eukaryotic sexual reproduction. *Cold Spring Harb Perspect Biol,* 6.

Guiraldelli, M. F., Eyster, C., Wilkerson, J. L., Dresser, M. E. & Pezza, R. J. 2013. Mouse HFM1/Mer3 is required for crossover formation and complete synapsis of homologous chromosomes during meiosis. *PLoS Genet,* 9**,** e1003383.

Haber, J. E. 1998. Mating-type gene switching in Saccharomyces cerevisiae. *Annu Rev Genet,* 32**,** 561-99.

Haber, J. E. 2012. Mating-type genes and MAT switching in Saccharomyces cerevisiae. *Genetics,* 191**,** 33-64.

Halpern, C. & Miller, J. J. 1956. The metabolism of yeast sporulation. I. Effect of certain metabolites and inhibitors. *Can J Microbiol,* 2**,** 519-37.

Heitman, J., Sun, S. & James, T. Y. 2013. Evolution of fungal sexual reproduction. *Mycologia,* 105**,** 1-27.

Jambhekar, A. & Amon, A. 2008. Control of meiosis by respiration. *Curr. Biol.,* 18**,** 969-975.

Kappeli, O. 1986. Regulation of carbon metabolism in Saccharomyces cerevisiae and related yeasts. *Adv Microb Physiol,* 28**,** 181-209.

Kim, Y., Fedoriw, A. M. & Magnuson, T. 2012. An essential role for a mammalian SWI/SNF chromatin-remodeling complex during male meiosis. *Development,* 139**,** 1133-1140.

Lee, S. C., Ni, M., Li, W., Shertz, C. & Heitman, J. 2010. The evolution of sex: a perspective from the fungal kingdom. *Microbiol Mol Biol Rev,* 74**,** 298-340.

Lenormand, T., Engelstadter, J., Johnston, S. E., Wijnker, E. & Haag, C. R. 2016. Evolutionary mysteries in meiosis. *Philos Trans R Soc Lond B Biol Sci,* 371.

Marshall, A. N., Montealegre, M. C., Jimenez-Lopez, C., Lorenz, M. C. & van Hoof, A. 2013. Alternative splicing and subfunctionalization generates functional diversity in fungal proteomes. *PLoS Genet,* 9**,** e1003376.

Miller, J. J. 1957. The metabolism of yeast sporulation. II. Stimulation and inhibition by monosaccharides. *Can J Microbiol,* 3**,** 81-90.

Miller, J. J., Hoffmann-Ostenhof, O., Scheiber, E. & Gabriel, O. 1959. The metabolism of yeast sporulation. III. Respiration of sporulating and growing cells. *Can J Microbiol,* 5**,** 153-9.

Mitra, D., Parnell, E. J., Landon, J. W., Yu, Y. & Stillman, D. J. 2006. SWI/SNF binding to the HO promoter requires histone acetylation and stimulates TATA-binding protein recruitment. *Mol Cell Biol,* 26**,** 4095-110.

Munding, E. M., Shiue, L., Katzman, S., Donohue, J. P. & Ares, M. 2013. Competition between Pre-mRNAs for the Splicing Machinery Drives Global Regulation of Splicing. *Mol. Cell,* 51**,** 338-348.

Nasmyth, K. 1993. Regulating the HO endonuclease in yeast. *Curr Opin Genet Dev,* 3**,** 286-94.

Neigeborn, L. & Carlson, M. 1984. Genes affecting the regulation of SUC2 gene expression by glucose repression in Saccharomyces cerevisiae. *Genetics,* 108**,** 845-58.

Ni, M., Feretzaki, M., Sun, S., Wang, X. & Heitman, J. 2011. Sex in fungi. *Annu Rev Genet,* 45**,** 405-30.

Otterstedt, K., Larsson, C., Bill, R. M., Stahlberg, A., Boles, E., Hohmann, S. & Gustafsson, L. 2004. Switching the mode of metabolism in the yeast Saccharomyces cerevisiae. *EMBO Rep,* 5**,** 532-7.

Pasteur, L. 1861. Influence de l'oxygène sur le développement de la levure et la fermentation alcoolique. *Bulletin de la Société chimique de Paris Société chimique de France***,** 79-80.

Perlman, D., Halvorson, H. O. & Cannon, L. E. 1982. Presecretory and cytoplasmic invertase polypeptides encoded by distinct mRNAs derived from the same structural gene differ by a signal sequence. *Proc Natl Acad Sci U S A,* 79**,** 781-5.

Ramirez, C. & Miller, J. J. 1964. The Metabolism of Yeast Sporulation. Vi. Changes in Amino Acid Content during Sporogenesis. *Can J Microbiol,* 10**,** 623-31.

Raveh, A., Margaliot, M., Sontag, E. D. & Tuller, T. 2016. A model for competition for ribosomes in the cell. *J R Soc Interface,* 13.

Schmid, R., Grellscheid, S. N., Ehrmann, I., Dalgliesh, C., Danilenko, M., Paronetto, M. P., Pedrotti, S., Grellscheid, D., Dixon, R. J., Sette, C., Eperon, I. C. & Elliott, D. J. 2013. The splicing landscape is globally reprogrammed during male meiosis. *Nucleic Acids Res,* 41**,** 10170-84.

Solari, A. J. 2002. Primitive forms of meiosis: the possible evolution of meiosis. *Biocell,* 26**,** 1-13.

Stern, M., Jensen, R. & Herskowitz, I. 1984. Five SWI genes are required for expression of the HO gene in yeast. *J Mol Biol,* 178**,** 853-68.

Trumbly, R. J. 1992. Glucose repression in the yeast Saccharomyces cerevisiae. *Mol Microbiol,* 6**,** 15-21.

Venkataramanan, S., Douglass, S., Galivanche, A. R. & Johnson, T. L. 2017. The chromatin remodeling complex Swi/Snf regulates splicing of meiotic transcripts in Saccharomyces cerevisiae. *Nucleic Acids Research*.

Wang, J., Gu, H., Lin, H. & Chi, T. 2012. Essential roles of the chromatin remodeling factor BRG1 in spermatogenesis in mice. *Biol Reprod,* 86**,** 186.

Weidberg, H., Moretto, F., Spedale, G., Amon, A. & van Werven, F. J. 2016. Nutrient Control of Yeast Gametogenesis Is Mediated by TORC1, PKA and Energy Availability. *PLoS Genet,* 12**,** e1006075.